MICROFUIDIC DEVICES AND OPEN ACCESS TOOL FOR LOCALIZED MICROINJECTION AND HEART MONITORING OF *DROSOPHILA MELANOGASTER*

ALIREZA ZABIHIHESARI

A Dissertation Submitted to The Faculty of Graduate Studies in
Partial Fulfillment of The Requirements for The Degree of Doctor of Philosophy

Graduate Program in
MECHANICAL ENGINEERING

York University
Toronto, Ontario
MAY 2022

Abstract

Drosophila melanogaster, the fruit fly, is a model organism that has been used to study cardiac toxicity, developmental abnormalities, and functional impairment of the heart. Among different developmental stages of fruit fly, the larval stage is privileged due to biological maturity, optical accessibility, and the myogenic nature of the heart. However, the small size of the larva, its flexibility and mobility, and having a hemolymph-floating heart tube have impeded the use of intact *Drosophila* larvae in cardiac screening studies.

Cardiac studies on intact *Drosophila* larvae require precise chemical administration via feeding, perfusion, or microinjection. Perfusion and oral administrations have been preferred in toxicity assessments due to their feasibility and affordability compared to microinjection. However, they are inaccurate due to uncertainties associated with the exact amount of chemicals taken up by the specimens. Also, enzymatic, cellular, and tissue barriers present in *Drosophila*'s saliva and digestive tract prevent the translocation of some chemicals from the digestive tract into the hemolymph. Microinjection is the only method suitable for delivering a controlled amount of both soluble and insoluble chemicals to specific intra-body sites while reducing the consumption of costly chemicals.

Several microfluidic techniques have been reported for *Drosophila* manipulation, imaging, and microinjection, mainly focused on embryonic stage or dissected tissues, which are not amenable to the larval stage. Automatic detection and accurate quantification of intact larval heart activities is another technical challenge associated with using *Drosophila* larvae for *in-vivo* cardiac toxicity assays. Conventional methods for parametric quantification of heart activities are complex and mostly done on dissected, irreversibly immobilized, or anesthetized larvae.

This thesis *aims* to *address the current research gaps associated with the use of Drosophila larvae as an in-vivo model for cardiac toxicity and cardiac gene screening*. In **objective 1**, we have developed a hybrid multi-tasking microfluidic platform that enables desired orientation, reversible immobilization, and localized microinjection of intact *Drosophila* larvae for recording heart activities upon injection of controlled dosages of different chemicals. In **objective 2**. we have

developed software for *in-vivo* quantification of essential heartbeat parameters on intact *Drosophila* larvae. Several image segmentation and signal processing algorithms were developed to detect the heart, extract the heartbeat signal, and quantify heart rate and arrhythmicity index automatically, while other heartbeat parameters were quantified semi-automatically using the M-mode. In **objective 3a**, we demonstrated the application of our microfluidic device and heartbeat quantification software for investigating the effect of different chemicals (e.g., serotonin and heavy metals) on *Drosophila* larval heart function. Also, we applied our technology to genetically modified *Drosophila* larvae to investigate the effect of metal responsive transcription factor (MTF-1) against heavy metals cardiac toxicity (**objective 3b**).

Our technology can be used to provide an alternative approach for screening intravenous drugs and toxicants *in-vivo* using a whole-animal model, with the potential to be applied to other biological models for automatic screening of drugs and alleles that affect the heart.

Dedication

… but deep within my heart lies a melody of love

written by my dearest of all,

Shahrzad, Zohreh, and Esmaeil.

Acknowledgment

The completion of this dissertation would have never been made possible without the extended support from my supervisors, committee members, colleagues, family, and friends. I would like to take this opportunity to sincerely express my appreciation to all individuals and organizations who supported me throughout this journey.

First, I would like to thank my supervisor, Professor Pouya Rezai, for his endless support, thoughtful comments, recommendations, and guidance in my Ph.D. research. He continuously provided encouragement and was always willing and enthusiastic to help me in any way he could. Dr. Rezai's extensive knowledge and expertise in mechanical engineering, biomedical engineering, and microfluidics qualified me to oversee my projects and increase my work efficiency. Dr. Rezai taught me to be not only a hardworking and dedicated researcher but also a well-organized individual, which will positively influence all aspects of my life.

I would like to thank my co-supervisor, Professor Arthur Hiller, for his great support in the biological aspects of my research and for giving me the privilege to work in his laboratory and have access to the expertise of his students. His knowledge and expertise in biology and genetics was always helpful during this research.

I am also thankful to my committee members, Professor Gerd Grau and Professor Terry Sachlos, for their advice during my annual committee meetings and comprehensive exam. I would also like to express my great appreciation to professor Hang Lu and Professor Siu N. (Sunny) Leung for accepting to be the external referee and the chair of my oral examination, respectively.

This research would not have been possible without the help of my colleagues and friends. I would like to thank Dr. Alistair B Coulthard for preparing *Drosophila* strains and their maintenance and Mr. Alexander Molnar for assisting me with PCR tests. I would like to thank Joaquin Ramirez-Medina (undergraduate researcher) for his help in data analysis and experimentation during the last year of my Ph.D. I am also grateful to my friends Dr. Morteza Javid, Dr. Milad Shakeri Bonab, Dr. Reza Emamalipour, and Mr. Mohammad Charjouei Moghadam, as well as my colleagues in the advanced center for microfluidic technology (ACµTE), Dr. Khaled Youssef, Arsalan Nikdoost, Arezoo Khalili, and Ehsan Tabesh for their continuous support and help throughout my Ph.D.

I sincerely thank York University for the financial support through the Provost Dissertation Scholarship in the last year of my Ph.D. and the department of Mechanical Engineering for several awards presented to me during my Ph.D. program.

Above all, I cannot emphasize enough the everlasting love and support received from my wife, Shahrzad; my parents, Esmaeil and Zohreh; and my siblings, Adel, Fatemeh, and Aref. I owe my deepest gratitude to Shahrzad for her enduring love, encouragement, support, and patience during my research. After all, this thesis is dedicated to my wife, my parents, and my siblings.

Table of Contents

List of Figures

List of Tables

Abbreviations

CVD	Cardiovascular disease
CHD	Congenital heart disease
OCT	Optical coherence tomography
5-HT	5-hydroxytryptamine
ECG	Electrocardiogram
EEG	Electroencephalogram
MTF-1	Metal-responsive transcription factor-1
Cic	Capicua
SVD	Singular value decomposition
3D	Three- dimensional
Bcd	Bicoid
FACS	Fluorescent-activated cell sorting
COPAS	Complex object parametric analyzer and sorter
GFP	Green fluorescent protein
TSW	Switching time
siRNA	Small interfering RNA (siRNA)
LSFM	Light-sheet fluorescent microscopy
SPIM	Selective Plane Illumination Microscopy
CNS	Central nervous system
VNC	Ventral nerve cord
CNC	Computer numerical control
IFT	Intraflagellar transport
ORN	Olfactory receptor neurons
OR	Outer brass
RING	Rapid iterative negative geotaxis
PMMA	Polymethylmethacrylate
Trh	Tryptophan hydroxylase
Ddc	Dopa decarboxylase
Tdc2	Tyrosine decarboxylase 2
NPF	Neuropeptide F
GRNs	Gustatory receptor neurons
FGF	Fibroblast growth factor
SRR	Source reservoir
SKR	Sink reservoir
SRC	Source chamber
SKC	Sink chamber
PETL	Polyethylene-terephthalate laminate
EVA	Ethylene vinyl acetate
ROI	Region of interest
CNN	Convolutional neural networks

FTIR	Frustrated total internal reflection
SOHA	Semi-automated optical heartbeat analysis
OFA	Optical flow algorithm
EMD	Empirical mode decomposition
STFT	Short-time Fourier transform
PM	Particulate matter
MT	Metallothionein
PBS	Phosphate-buffered saline
UAS	Upstream activation sequence
PCR	Polymerase chain reaction
RN	Removable needle
CPM	Capillary pressure microinjection
PDF	Pressure-driven flow
GUI	Graphical user interface
SGF	Savitzky-Golay-Filter
RE	Recall
PR	Precision
AC	Accuracy
TP	True positive
FP	False-positive
FN	False-negative
PSD	Power spectral density
HR	Heart rate
AI	Arrhythmicity index
HP	Heart Period
EDD	End-diastolic diameter
ESD	End-systolic diameter
M-mode	Motion mode
FS	Fractional shortening
SV	Shortening velocity
SEM	Standard error of the mean
VDTS	Volume determination using two standards
SPA	Smoothness priors' approach
OCM	Optical coherence microscopy
ROS	Reactive oxygen species
MREs	Metal-response elements
PDMS	Polydimethylsiloxane
OC	Open channel
SC	Sealed channel
PVA	Polyvinyl alcohol
DLW	Direct laser writing
SLA	Stereo lithography
FDM	Fused deposition modeling

Chapter 1

INTRODUCTION

1.1 Background Information and Research Direction

Fruit fly or *Drosophila melanogaster* (called *Drosophila* in this thesis) is a multi-cellular model organism with a rapid life cycle of approximately 10 days at 25℃ (Fig. 1-1). *Drosophila* development is divided into four distinct stages, i.e., egg (embryo), larva, pupa, and adult stages. Each adult female fly can lay up to ~100 eggs per day for up to 20 days [1]. It has been more than a century from the first documented use of *Drosophila* in the research laboratory [2]. Ever since, *Drosophila* has been extensively used to comprehend the role of genes in the development of embryos from a single cell to a mature multicellular organism [3]. *Drosophila* embryos are transparent and small with a length of ~0.5 mm. A day after an egg is laid, a *Drosophila* larva hatches. The larval stage consists of first instar, second instar, and third instar with approximately one-day intervals. The third instar larvae have a length of ~3 mm. At the end of 3rd larval stage, the animal stops eating and moving, and the cuticle hardens and darkens to form the puparium. During the pupal stage, metamorphosis occurs for ~ 4 days. At the end of metamorphosis, the folded wings and the pigments in the eyes are visible. Finally, the adult fly emerges from the anterior end of puparium and can live for several weeks [4–6].

Drosophila has emerged as an amenable model system for cardiovascular diseases (CVDs), including the studies of developmental abnormalities and functional impairments associated with different heart disorders [7] and cardiac toxicity of chemicals [8]. From a genetic point of view, the main reason that supports the use of *Drosophila* as a model for CVDs is its genome containing several genes associated with human heart diseases [9]. Moreover, heart-specific genetic manipulations can be done using various techniques at *Drosophila's* larval and adulthood stages, which makes functional and developmental studies feasible. Other advantages such as being easy to culture and inexpensive to maintain in labs, having short life cycles, and being transparent at embryonic and larval stages has given rise to emergence of *Drosophila* as a unique model for cardiac toxicity, development, function, and aging [1,10,11]. Among different stages of the *Drosophila* life cycle, the larval stage is privileged for cardiac toxicity and heart disease studies primarily due to the myogenic nature of the heart, biological maturity, and transparency of the animal's cuticle at this stage [7,9,11,12].

Manipulation of *Drosophila* at different stages of its life cycle including its delivery, orientation, and immobilization plays an important role in the speed, efficiency, and repeatability of the biological assays. Concerning *Drosophila* at the larval stages, complete immobilization and desired orientation of *Drosophila* larvae are crucial for visual accessibility of target cells, neurons, and organs of interest for different purposes such as neural imaging [14–16], cell ablation [17], and heart monitoring [18]. The voluntary movement of the larva overcomplicates manipulation when compared to embryonic assays. *Drosophila* larvae use a peristaltic type of motion which makes their immobilization more complex. These peristaltic motions are accompanied by strong forces that the larva can generate due to its larger size and more muscles compared to other small organisms e.g., *C. elegans* [19]. Another factor that complicates assays of *Drosophila* at the larval stage is the fact that the internal organs of the larva are suspended and hence moving in the hemolymph. These motions are more noticeable when the larva attempts to crawl [19]. However, even if the outer body is immobilized, e.g., by encapsulation [20], larval internal organs can loosely move inside the hemolymph-filled body cavity which complicates the assay [21].

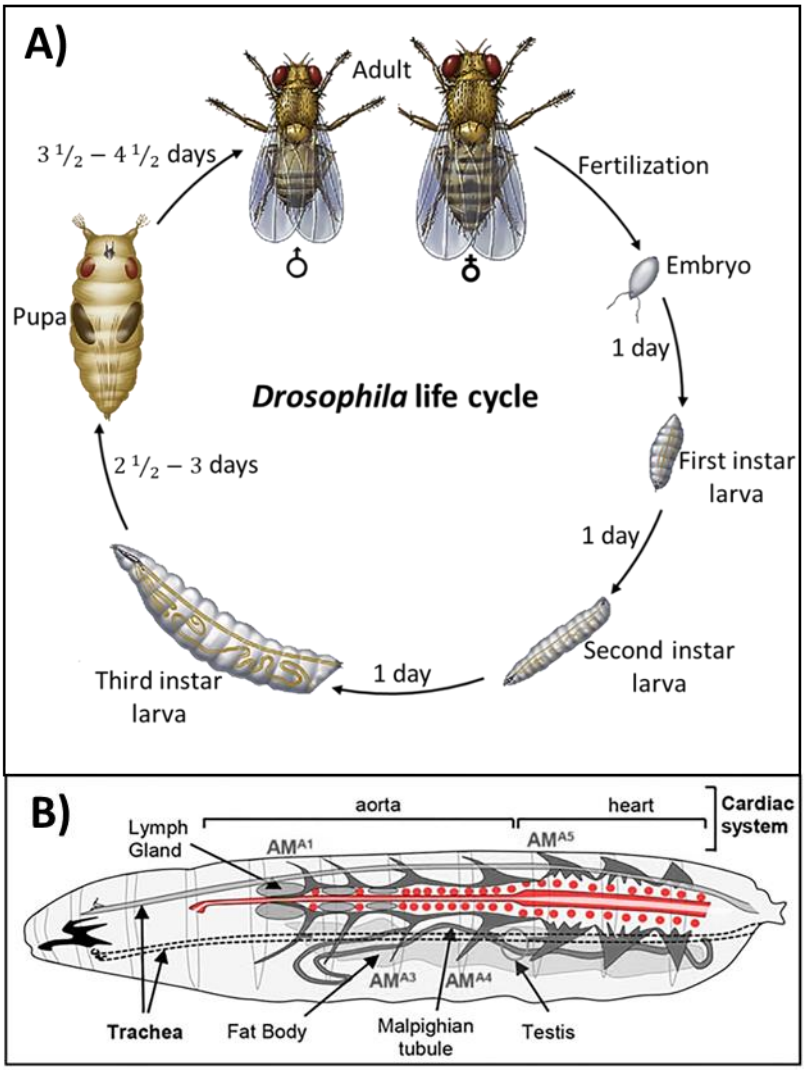

Figure 1-1: The life cycle of Drosophila melanogaster [6] which takes ~10 days at 25°C and includes embryo, larva, pupa, and adult stages (A). Drosophila embryos develop in 24 hours to the larval stage. The larval stage includes first, second, and third instars with 1-day intervals. The cuticle of 3rd instar larva hardens and darkens to form the puparium. In pupal stage, metamorphosis happens for ~ 4 days. Finally, the adult fly emerges from the anterior end of the puparium. Schematic of a 3rd instar larva showing the cardiac system surrounded by alary muscles (AMs) and other tissues [13]. Desired dorsal orientation is required for monitoring the heart and aorta. Panel A and B reproduced by permissions from TAYLOR & FRANCIS and Company of Biologists, respectively.

In conventional larvae manipulation techniques, tweezers [18] are used to orient the larvae and anesthetics [22], glue [18], double-sided tapes [18], glass plates [18], or dissection pins [18] are used for immobilization. Using tweezers for handling and orientation of delicate larvae requires technical expertise and can damage the animal if not executed with care. Using glue or tape for immobilization is mostly irreversible and possibly toxic to animals; therefore, not suitable for long-term assessments [23]. Anesthetics are reversible, but can adversely affect neural activities and

change neural physiology [24,25]. At the larval stage, many organ and sub-organ based studies were performed on dissected larvae. However, dissection of small larvae is time-consuming, requires technical skills, and is lethal; hence, not suitable for post-imaging assays [18,26].

Microfluidics is the science and technology to process and manipulate fluids and suspended matters which are geometrically constrained to sub-millimeter scales [27]. Microfluidic technology has been extensively employed to improve automation, control and quantitative analysis in biological investigations on cells [28], tissues [29], organs [30,31], and small organisms including zebrafish [32], roundworms [33], and fruit flies [14,34]. Current microfluidic devices for *Drosophila* research are mostly focused on embryos [14,34–40] while studies on larval [41] [42], pupal [43], and adult [44] stages of *Drosophila* are scarce [45]. Attention in *Drosophila* microfluidics has been mostly placed on embryonic sorting [46] and trapping [47], larval immobilization for imaging [17,48], and adult flies oviposition (egg-laying) [49]. *Drosophila* research can also benefit from microfluidic technology in different applications including the cardiac toxicity and gene screening. In this thesis, we have focused on the development of novel microfluidic devices and accessories for heart studies on *Drosophila* larvae.

1.2 Scientific and Technological Gaps

The existing research on *Drosophila* heart has been mostly focused on developmental aspects at embryonic stages for congenital heart disease (CHD) studies [50–52]. The advent of new techniques to measure the activities of adult fly heart such as optical coherence tomography (OCT) has facilitated the long-term investigation of factors such as diet, exercise and aging [53,54]. At the larval stage, the isolated heart tubes from dissected larvae have been used as a testing platform to investigate the effect of biological processes such as genes and pharmacological compounds such as neurotransmitters and chemical contaminants on the cardiac activity [18,55]. Research on intact *Drosophila* larva's heart still has a lot of technological and scientific gaps, with some targeted and filled in this thesis as described below.

Cardiac studies on intact *Drosophila* larvae for the purpose of chemical and gene screening require precise chemical administration to the heart. The main approaches for chemical exposure include feeding, perfusion, or microinjection. Moreover, desired orientation and reversible immobilization

are needed for precise monitoring of the heart activities over extended periods and or multiple animal generations [56–58]. The feeding and perfusion administration pathways are inaccurate due to uncertainties associated with the exact amount of chemicals taken up by the specimens. For instance, it has been shown that the food composition and the digestive enzymes and drug transporters in the insect's saliva and gut play key roles in the feeding behavior and absorption of chemicals into the hemolymph of the *Drosophila* larvae, subsequently affecting the heart activities [59–61]. Moreover, feeding the animal is not feasible when the food contains unstable compounds which can decompose rapidly if treated improperly. For instance, the stability of neurotransmitter serotonin (5-hydroxytryptamine, or 5-HT) is highly influenced by different factors such as light, PH and temperature [57,62]. Therefore, for a precise chemical screening in cardiac toxicity assays, the heart of *Drosophila* should be directly exposed to the tested chemical.

Microinjection is the only method suitable for delivering a controlled amount of both soluble and insoluble chemicals to specific intra-body sites while reducing the consumption of costly chemicals [63,64]. Microinjection of *Drosophila* pupae is easier than larvae because of its immobility during pupation. Fluorescent dye injection into *Drosophila* pre-pupae and pupae has been used for dye angiography to characterize the hemolymph circulation and to investigate heart physiological defects [65]. Yet, microinjection of *Drosophila* larvae is technologically challenging because they are highly flexible and motile, and need to be completely immobilized for microneedle piercing and heart monitoring. Desired orientation is also needed for physical and optical access to the heart tube located at the dorsal vessel [18]. Developing an integrated microfluidic platform which enables orientation, immobilization, and reversible microinjection of intact *Drosophila* larvae still remains a challenge. Addressing this challenge will facilitate capturing immediate and acute changes in the cardiac activities, right after injection of controlled doses of rapid-acting chemicals such as neurotransmitters (e.g., serotonin) and chemical toxicants (e.g., zinc and cadmium heavy metals), as investigated in this thesis.

Automatic detection and accurate quantification of intact larval heart activities is another technical challenge associated with the use of *Drosophila* larvae for *in-vivo* cardiac toxicity assays. Conventional methods for parametric quantification of heart activities on intact larvae are complex and require implementing external components (e.g., using photodiodes and phototransistors [57,66–69]), while being limited by only providing the heart rate as a quantitative measure. Other

techniques which enable measuring several heartbeat parameters of *Drosophila* larvae are either expensive (e.g., OCT [70–72]) or require fluorescent labeling [73] or dissection [74,75] to have a clear picture of the heart. Yet, automatic detection and accurate quantification of intact larval heart activities using optical microscopy without the need for dissection or fluorescent labeling remain challenging. Small movements associated with the organisms' flexibility, loose immobilization for reversibility, and suspended internal organs lead to non-stationaries like intense noises and undesired low-frequency trends in heartbeat signals. Non-stationarities can distort the signal in time- and frequency-domains [76]. In this regards, we asked a) whether image segmentation algorithms which previously used for pupa (which no longer eats or moves) for automatic detection of the heart [77] are effective for intact larvae immobilized in our microfluidic device (with some modifications) and b) whether intense noises and undesired low-frequency trends in heartbeat signals of an intact larvae can be removed using those signal processing algorithms used for electrocardiogram (ECG) and electroencephalogram (EEG) signals [78,79].

In terms of scientific gaps, *Drosophila* larva's heart responses to many chemicals (e.g., neurotransmitters) and pollutants (e.g., heavy metals), as well as the role of genes (e.g., MTF-1[†]) in cardiac toxicity have not been investigated on the intact (not dissected) larvae. Specifically, previous toxicity assessments of heavy metals on *Drosophila* are limited to investigating the survival, development rate, and climbing behaviour by oral administration while cardiac toxicity of these elements has not been investigated [80,81]. In this area, questions that we have asked are a) what is the acute effect of zinc and cadmium on heartbeat parameters such as heart rate and arrhythmicity? and b) is there any effect on survival of larvae to pupal and adulthood stages and flies' lifespan after injection of larvae with controlled doses of zinc and cadmium? Moreover, *Drosophila* heart response to neurotransmitters (e.g., serotonin) and peptides was investigated at pre-pupal, pupal, and adult stages [66,67]. However, a pupa undergoes metamorphosis, and the animal experiences hormonal changes, fluctuating biogenic amines, and heart structural transformation, all giving rise to difficulties in controlling variables during investigation of myocytes [82]. During metamorphosis, neuronal innervations form in the heart tube. Therefore, the heart in adult flies is neurogenic, unlike vertebrates [83]. On the other hand, *Drosophila* heart at larval stage is myogenic, which makes it comparable to a mammalian heart, including the human

[†] Metal-responsive transcription factor-1 is a pluripotent transcriptional regulator involved in cellular adaptation to various stress conditions, primarily exposure to heavy metals but also to hypoxia or oxidative stress [319].

heart, and suitable for *in-vivo* investigations [18]. The questions asked in this thesis in terms of cardiac neurotransmitters toxicity were a) what is the acute effect of serotonin on the heart rate of intact *Drosophila* larvae? and b) is this effect consistent in different larval stages (i.e., 2nd and 3rd instar larvae)? From a genetic point of view, tissue-specific overexpression of MTF-1 was previously done in *Drosophila* peripheral nervous system, motor neurons, gut, and hemocytes to study the role of MTF-1 against heavy metal toxicity [80,81]. Yet, the role of MTF-1 in defense against heavy metal toxicity, when expressed specifically in the heart, has not been investigated. The questions asked in this thesis from a genetic perspective are a) whether heart-specific overexpression of MTF-1 can change the heart response to zinc and cadmium injection or not?, and b) whether MTF-1 overexpression in the heart affects the survival of larvae to other stages and flies' longevity after injection of zinc and cadmium.

1.3 Thesis Goals and Objectives

Given the abovementioned scientific and technological gaps, this thesis aimed to address current challenges associated with the use of *Drosophila* larvae as an *in-vivo* model for cardiac toxicity and cardiac gene screening.

In terms of technical gaps, our research aimed to address the challenges which stem from the small size of *Drosophila* larvae, mobility of the intact larvae, floating internal organs, and the necessity of positioning and orienting the larvae for microinjection and monitoring the heart. We focused on developing a hybrid microfluidic device for desired orientation, reversible immobilization, and localized microinjection and heart monitoring, as well as a MATLAB-based software for automatic non-invasive heartbeat quantification of *Drosophila* larvae in response to various stimuli such as neurotransmitters and heavy metals. Considering the limitations associated with the adoption of microfluidic devices in biological laboratories and data analysis in biological tests, the proposed device and software were designed with cost-efficiency and operational simplicity in mind.

In terms of addressing scientific gaps, the cardiotoxicity of two heavy metals (zinc and cadmium) and one neurotransmitter (serotonin) were investigated by direct exposure of intact (not dissected) *Drosophila* larval heart to controlled doses of these chemicals. Moreover, transgenic *Drosophila*

models were developed by collaborators and a set of genetic studies were conducted to characterize the cardioprotective role of metal-responsive transcription factor (MTF-1) gene against cardiac toxicity of heavy metals in *Drosophila* larvae.

To achieve our goals above, the following objectives were pursued

1. Localized microinjection of intact *Drosophila* larvae with controlled amounts of injectants using a microfluidic device.
2. Phenotypic quantification of heartbeat parameters for *in-vivo* cardiac toxicity and cardiac gene screening studies using a MATLAB-based software.
3. Application of our microfluidic device and heartbeat quantification software for investigating the effects of:
    a. neurotransmitter chemicals like serotonin and heavy metals like zinc and cadmium on *Drosophila* larval heart function.
    b. metal responsive transcription factor (MTF-1) gene effect against heavy metals cardiac toxicity.

1.4 Contributions

My thesis contributions to the general body of knowledge can be divided into fundamental and applied categories. At the applied level, an innovative low-cost technique has been developed to accurately control the microinjection site and the amount of chemical delivered into the intact *Drosophila* larva's body through capillary pressure microinjection (CPM). This has been achieved by integrating several components into a microfluidic platform, i.e., glass capillaries for loading and orientation, suction channels for pneumatic immobilization, a one degree-of-freedom microneedle, and a custom-made pressure driven reagent delivery system for microinjection. The microinjection unit was characterized and the effect of several parameters (e.g., the amplitude of the pressure pulse, the duration of the pressure pulse, and the size of the needle) were investigated. Moreover, an image processing algorithm was developed for extraction of heartbeat signal and phenotypic quantification of several heartbeat parameters *in-vivo*. The microfluidic microinjection and heartbeat quantification techniques, achieved at this stage of the thesis, were utilized to

develop a variety of cardiac toxicity and gene screening assays using wild type and genetically modified *Drosophila* larvae as *in-vivo* models of the heart.

At a fundamental level, the effect of controlled doses of chemicals (serotonin, zinc, and cadmium) on the heart function and the role of heart-specific overexpression of MTF-1 against cardiac toxicity of heavy metals were investigated on intact *Drosophila* larvae. Moreover, eight heartbeat parameters, i.e., heart rate (HR), cardiac arrhythmicity (AI), end-diastolic diameter (EDD), end-systolic diameter (ESD), shortening distance (SD), shortening time (ST), shortening velocity (SV), and fractional shortening (FS) were quantified on wild type intact larvae.

The following describes my contributions to the articles constituting Chapters 2-6. A large portion of Chapter 2 was published as a review paper [45] with contents on microfluidics for *Drosophila* research. I wrote the original draft and the initial responses to reviewers. The revisions were provided by Dr. Pouya Rezai and Dr. Arthur Hilliker. A microfluidic device was previously developed in our group by Ramtin Ardeshiri and Dr. Pouya Rezai for manipulation and multi-directional imaging of *Drosophila* larvae [23]. I have modified the device design and added new modules to the previous device to expand it for microinjection. Chapter 3-6 (mostly published [19,84–90]) consisted of idea development, device design and fabrication, software development, experimentation, data analysis, writing original drafts, writing review and editing, and initial response to reviewers' comments, which was done by me.

Dr. Pouya Rezai contributed to conceptualization, idea development, and device design enhancement. He also supervised the research, revised the manuscripts, and provided funding and resources in years 1-5. Dr. Arthur Hilliker co-supervised the research, provided partial funding and all the fly models (in years 1-5), and contributed to paper revisions. Dr. Alistair B Coulthard contributed to fly culture, maintenance, and developing transgenic fly models in years 1-5. I have worked with and mentored several undergraduate students during my Ph.D. During this mentorship, I taught them how to perform microfabrication (i.e., soft lithography and photolithography), microscopy, microfluidic testing, and data analysis. They also learned how to use the MATLAB-based heartbeat quantification software to measure heartbeat parameters and analyze the results. Two undergraduate research assistants, Shahrzad Parand and Joaquin Ramirez-Medina, assisted me with data analysis and writing review and editing in years 4 and 5. Joaquin was also involved in device fabrication and testing. Also, Ellen van Wijngaarden (undergraduate

student) contributed to data analysis for one conference paper in year 4. I was financially supported by the Provost Dissertation Scholarship and the Academic Excellence Fund from York University in year 5 of my research, the Mechanical Engineering Excellence awards in all categories (*i.e.*, graduate research, graduate teaching assistantship, conference travel, and PhD best seminar presentation) and the Parya Trillium Foundation Scholarship in years 2-5 of my PhD.

1.4.1 Publications Related to the Thesis

Peer-reviewed journal papers:

1) **A. Zabihihesari**, S. Parand, A. B. Coulthard, A. Molnar, A.J. Hilliker, P. Rezai, An In-Vivo Microfluidic Assay Reveals Cardiac Toxicity of Heavy Metals and the Protective Effect of Metal Responsive Transcription Factor (MTF-1) in Drosophila Model, *Available at SSRN 4028275. (2022)*. http://dx.doi.org/10.2139/ssrn.4028275
2) **A. Zabihihesari**, S. Parand, P. Rezai, Microfluidic Capillary Pressure-Driven Viscometry of Drosophila melanogaster's Hemolymph, *Journal of Experimental Biology*. Under review
3) **A. Zabihihesari**, A. Khalili, A.J. Hilliker, P. Rezai, Open access tool and microfluidic devices for phenotypic quantification of heart function of intact fruit fly and zebrafish larvae, *Computers in Biology and Medicine*. 132 (2021) 104314. https://doi.org/10.1016/J.COMPBIOMED.2021.104314
4) **A. Zabihihesari**, A.J. Hilliker, P. Rezai, Localized Microinjection of Intact Drosophila melanogaster Larva to Investigate the Effect of Serotonin on Heart Rate, *Lab on a Chip*. (2020) 343–355. https://doi.org/10.1039/C9LC00963A
5) **A. Zabihihesari**, A.J. Hilliker, P. Rezai, Fly-on-a-Chip: Microfluidics for Drosophila melanogaster Studies, *Integrative Biol*ogy. 11 (2020) 425–443. https://doi.org/10.1093/intbio/zyz037

Conference proceedings

1) **A. Zabihihesari**, S. Parand, A. B. Coulthard, E. van Wijngaarden, A.J. Hilliker, P. Rezai, MICROFLUIDIC-BASED CARDIAC TOXICITY ASSAY TO INVESTIGATE THE ROLE OF METAL RESPONSIVE TRANSCRIPTION FACTOR (MTF-1) IN A DROSOPHILA HEART MODEL, *The 25th International Conference on Miniaturized Systems for Chemistry and Life Sciences (µTAS 2021)*, October 10 – 14, 2021, Virtual, PP. 377-378.
2) **A. Zabihihesari**, S. Parand, A.J. Hilliker, P. Rezai, MICROFLUIDICS FOR MEASURING DROSOPHILA HEMOLYMPH VISCOSITY, *The 25th International Conference on Miniaturized Systems for Chemistry and Life Sciences (µTAS 2021)*, October 10 – 14, 2021, Virtual, PP. 1637-1638.

3) **A. Zabihihesari**, A. J. Hilliker, P. Rezai, IN-VIVO QUANTIFICATION OF DROSOPHILA LARVA HEART FUNCTIONS, *The 24th International Conference on Miniaturized Systems for Chemistry and Life Sciences (µTAS 2020)*, October 4 – 9, 2020, Virtual, PP. 396-397.
4) **A. Zabihihesari**, A. J. Hilliker, P. Rezai, Microfluidic-based Anesthetic-free Microinjection of Intact Drosophila Larva to Investigate the Effect of Serotonin on Heartrate, *The 23rd International Conference on Miniaturized Systems for Chemistry and Life Sciences (µTAS 2019)*, October 27 – 31, 2019, Basel, Switzerland, PP. 396-397.
5) **A. Zabihihesari**, T. Akbar, A. J. Hilliker, P. Rezai, In-vivo Cardiovascular Screening Model Using a Microfluidic Device for Localized Microinjection into Intact Drosophila melanogaster Larval Heart Tube, *The 22nd International Conference on Miniaturized Systems for Chemistry and Life Sciences (µTAS 2018)*, November 11 – 15, 2018, Kaohsiung, Taiwan. PP. 1546-1549.
6) **A. Zabihihesari**, P. Rezai, A Microfluidic Device for Localized Microinjection into Intact Drosophila melanogaster Larval Heart Tube, *Ontario-on-a-Chip and TOeP Symposium*, May 24 – 25, 2018, Toronto, Canada.

1.4.2 Publications Beyond the Thesis

Peer-reviewed journal papers:

1) **A. Zabihihesari**, J. Ramirez-Medina, L. Thorat, J. Paluzzi, P. Rezai, An In-vivo Microfluidic Approach to Assess Cardiac Sequela Associated with SARS-COV-2 ORF3a Protein Expression in Drosophila Larval Heart. (Under preparation)
2) **A. Zabihihesari**, J. Ramirez-Medina, P. Rezai, High-throughput Acoustofluidic Rotational Manipulation of Drosophila embryos Using Oscillating Bubbles in a Microfluidic Device. (Under preparation)
3) **A. Zabihihesari**, A. Khalili, M. J. Farshchi Heydari, A. Eilaghi, P. Rezai, Developing a Low-cost Double-bridge Microfluidic Device for Microplastics Identification Using Electrical Resistance Measurements. (Under preparation)

1.4.3 Grant Writing

1) Co-wrote the **NSERC Alliance Grant** titled "Microfluidic Devices for In-vivo Toxicity Studies of Antimicrobial Coatings Using Small Model Organisms" ($214,285, to work on the project co-sponsored by NSERC and VivaVax Inc.)
2) Co-wrote the **Mitacs Accelerate Grant** titled "Integration of Microfluidics, Raman Spectroscopy and Electric Sensing for the Detection of Microplastics" ($60,000, to work on the project co-sponsored by MITACS and Ocean Diagnostics Inc.)

1.5 Thesis Outline

Chapter 1: Introduction

In this chapter, I provide the background information and research direction, scientific and technological gaps, research goals and objectives, and my contributions to the general body of knowledge.

Chapter 2: Literature survey

In this chapter, we review the existing literature in the field of *Drosophila* research considering both technical and scientific aspects. From a technical point of view, different microfluidic devices that have been developed for *Drosophila* research at different stages of the animal's life cycle are reviewed. The application of these technologies in a set of unit operations, such as sorting, immobilizing, imaging, and chemical/drug screening are described to highlight the technical challenges associated with microinjection and heart monitoring. Moreover, methods for quantifying the cardiac functions of small model organisms with a focus on *Drosophila* are presented. From a scientific point of view, the use of *Drosophila* as a model organism for toxicity assessment of different chemicals and genes are reviewed with a focus on chemicals and genes investigated in our study to highlight the limitations associates with performing cardiac toxicity on *Drosophila* larvae.

Chapter 3: Designs, Methods and Experimental Procedures

In this chapter, the microfluidic device design and fabrication techniques are described. Different steps in developing experimental setups including the custom-made CPM microinjection and heart monitoring units are presented. Different image and signal processing techniques used to develop the heartbeat quantification software are also explained. Moreover, experimental procedures, data analysis, animal preparation and genetic manipulation methods used for different cardiac toxicity and gene screening assays of this research are described.

Chapter 4: Results

The first section of this chapter mainly focuses on the techniques developed for localized microinjection, heart monitoring, and phenotypic quantification of heartbeat parameters to perform *in-vivo* cardiac toxicity and gene screening on *Drosophila* larvae (Obj. 1-2). Then, the developed technology was applied in Obj. 3 to determine the cardiotoxicity of two heavy metals (i.e., Zn and Cd) and one neurotransmitter (i.e., serotonin) through quantifying heart functional impairments and analyzing the survival of *Drosophila* larvae to higher stages. Moreover, a genetic study has been conducted to characterize the cardioprotective role of MTF-1 against cardiac toxicity of heavy metals.

Chapter 5: Conclusions and Recommendations for the Future Work

This chapter provides an overview of the conclusions and discussions presented in the previous chapters of this thesis, followed by recommendations for the future work.

Appendices

This chapter provides more in-depth theoretical and experimental facts relevant to the thesis. This includes details of data analysis and instructions on installation and use of the heartbeat quantification software. Moreover, a microfluidic device and experimental methodology is offered for measuring *Drosophila* hemolymph viscosity, as the main fluidic component of *Drosophila*'s circulatory system.

Chapter 2

LITERATURE SURVEY[‡]

Drosophila has been used as a promising model organism in genetics, developmental and behavioral studies as well as in the fields of neuroscience, pharmacology, and toxicology [1,91,92]. Not only all the developmental stages of *Drosophila*, including embryonic, larval, and adulthood stages (Fig. 1-1), have been used in experimental *in-vivo* biology, but also the organs, tissues and cells extracted from this model have found applications in *in-vitro* assays [93,94]. However, the manual manipulation, cellular investigation and behavioural phenotyping techniques utilized in conventional *Drosophila*-based *in-vivo* and *in-vitro* assays are mostly time-consuming, labor-intensive, and low in throughput [93,94]. Moreover, stimulation of the organism with external

[‡] Contents of this chapter have been collected from a review paper and the introduction sections of the published journal articles (permissions acquired and presented in the following):

- A. Zabihihesari, A.J. Hilliker, P. Rezai, Fly-on-a-Chip: Microfluidics for Drosophila melanogaster Studies, *Integr. Biol*. 11 (2020) 425–443.
- A. Zabihihesari, A. Khalili, A.J. Hilliker, P. Rezai, Open access tool and microfluidic devices for phenotypic quantification of heart function of intact fruit fly and zebrafish larvae, *Comput. Biol. Med*. 132 (2021) 104314.
- A. Zabihihesari, A.J. Hilliker, P. Rezai, Localized microinjection of intact Drosophila melanogaster larva to investigate the effect of serotonin on heart rate, *Lab Chip*. (2020) 343–355.
- A. Zabihihesari, S. Parand, A.B. Coulthard, A. Molnar, A.J. Hilliker, P. Rezai, An In-Vivo Microfluidic Assay Reveals Cardiac Toxicity of Heavy Metals and the Protective Effect of Metal Responsive Transcription Factor (Mtf-1) in Drosophila Model, *SSRN Electron. J*. (2022) 1–33.

biological, chemical or physical signals requires precision in signal delivery, while quantification of neural and behavioral phenotypes necessitates optical and physical accessibility to *Drosophila*. Recently, microfluidic and lab-on-a-chip devices have emerged as powerful tools to overcome these challenges. This chapter demonstrates the role of microfluidic technology in *Drosophila* studies with a focus on both *in-vivo* and *in-vitro* investigations. The reviewed microfluidic devices are categorized based on their applications to various stages of *Drosophila* development. We have emphasized technologies that were utilized for tissue- and behavior-based investigations. Furthermore, the challenges and future directions in *Drosophila*-on-a-chip research, and its integration with other advanced technologies, will be discussed to highlight the technical gaps related to cardiac screening using *Drosophila* larvae.

2.1 Microfluidic Devices for *Drosophila* Embryonic Studies

2.1.1 High-Throughput Arraying and Parallelized Imaging

Drosophila embryo has been widely used as a whole-biological model for developmental genetics [95]. The distribution of morphogens governs cell differentiation and tissue development in the process of morphogenesis, one of the most crucial processes of developmental biology. *In-vivo* live imaging of this highly dynamic developmental process in combination with recent advances in fluorescent microscopy have been utilized to investigate the fundamental principles governing embryogenesis [96–99]. Inherent endogenous variability of embryos and technical laboriousness associated with imaging the anterioposterior, and more challenging, dorsoventral patterning of the proteins and transcripts lead to low-throughput assays [100,101]. However, meaningful data from large sample sizes is needed for drawing confident conclusions in biological experiments. In this regard, microfluidic technology has been utilized to effectively array and orient a large number of embryos for high-throughput embryogenesis studies.

Chung et al. [102] developed a microfluidic embryo-trap array which enabled high-throughput imaging of the dorsoventral distribution of morphogens in *Drosophila* embryos (Fig. 2-1a). The device was fabricated by polydimethylsiloxane (PDMS) casting on a master mold which was made by the photolithography process. With this device, ~700 cylindrical embryo traps were replicated

and arrayed in a compact area of ~50×17 mm^2. The device included a serpentine channel and an array of cross-flow channels which hydrodynamically guided the embryos individually into the traps. The secondary Dean flow, due to the curved shape of the serpentine channel, and the converging and diverging flow through the cross-flow channels helped pushing the embryos toward the traps. With this design, embryo loading efficiency was greatly enhanced up to 90%. The trap design provided an end-on orientation in which embryos were placed vertically (Fig. 2-1b). Using this microfluidic device, the distribution of Dorsal (D1), an NF − κB transcription factor which initiates the dorsoventral patterning of *Drosophila* embryos, was investigated. The ventral-to-dorsal distribution of nuclear DI was quantified, and the lowest level of nuclear DI was observed at the most-dorsal point of the embryo.

The above device was then redesigned to enable lateral orientation of embryos (Fig.2-1c and 2-1d) [103]. The modified device had a central serpentine manifold with dozens of modified trap channels which allowed anterior-posterior imaging of embryos. Finite element modeling was performed to maximize the embryo trapping efficiency. The device was used for live imaging of the spatiotemporal pattern of a DNA-binding transcriptional repressor Capicua (Cic)[§] which could be harnessed for functional studies of the Ras signaling pathway in *Drosophila* embryo. Although live imaging of Cic had been done before at a level of single-embryo [104], quantitative analysis of the Cic dynamics across mutant backgrounds required live imaging of multiple embryos in parallel. Results demonstrated that at the early embryonic stage, the Cic pattern is distributed along the anterior-posterior axis in such a way that its level is low at the poles while increasing toward the embryo midbody. In addition, the spatiotemporal Cic pattern was approximated by decomposing the individual movies of Cic dynamics into one dominant spatial mode and one time-dependent amplitude using singular value decomposition (SVD) method.

[§] *Capicua (Cic)* is a protein which regulates gene transcription in both fruit fly and mammals. It plays a key role in developmental processes including embryonic patterning during *Drosophila* embryogenesis [320].

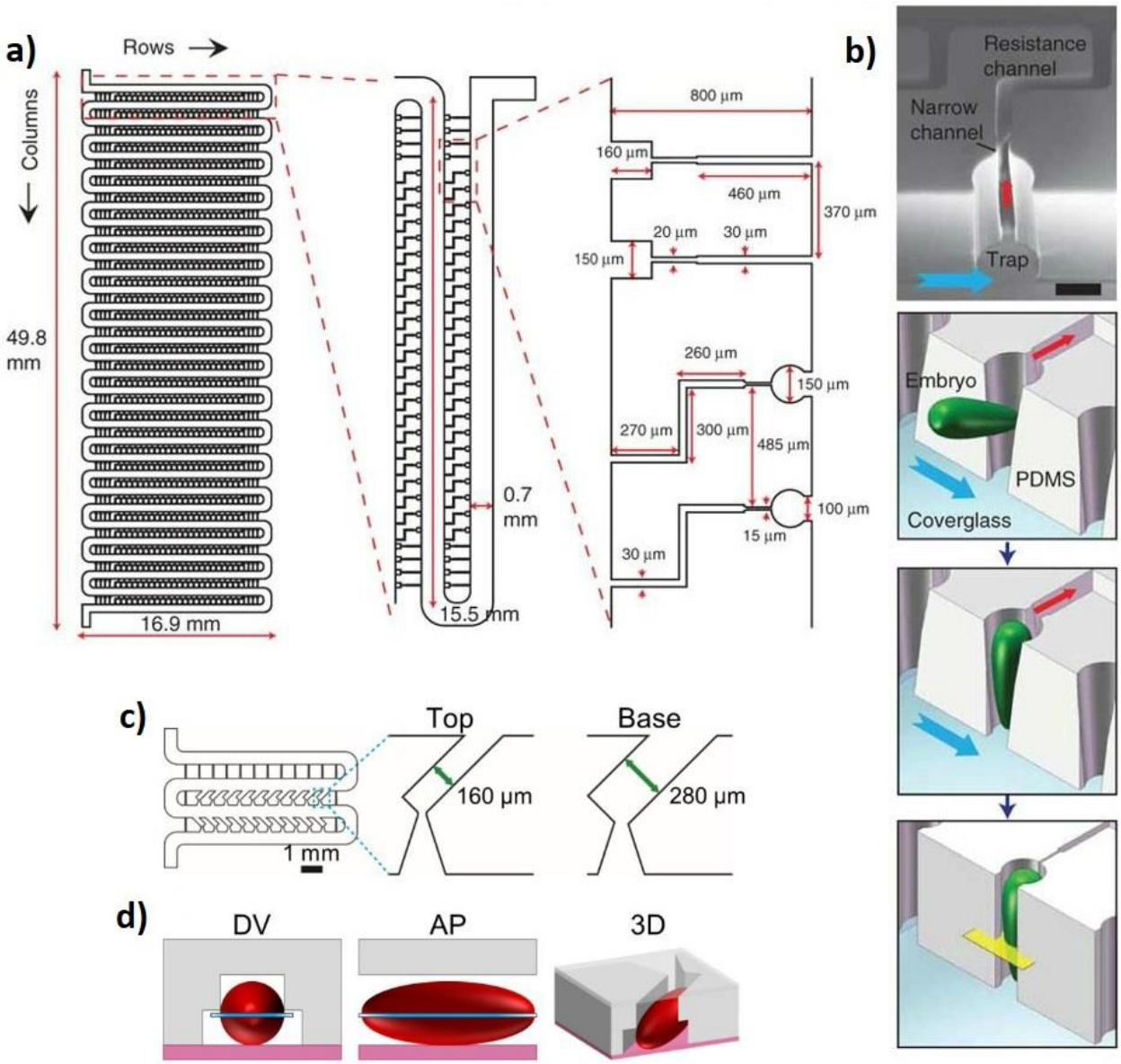

Figure 2-1: Microfluidic device for high-throughput arraying and parallelized imaging of Drosophila embryos. (a) Schematic of the top view of the embryo trap array for end-on imaging developed by Chung et al. [102]*. (b) Scanning electron micrograph of the trap region (scale bar, 100 µm) and the embryo trapping process. (c) schematic of the microfluidic chip developed by Goya et al.* [103] *with close-up views of a trap region in two different layers. (d) Dorsal-ventral (DV) and anterior-posterior (AP) cross sections, and three- dimensional (3D) view of the trapped embryo. Figures reproduced by permissions from Springer Nature (a and b) and Company of Biologists (c and d).*

2.1.2 Controlled Spatiotemporal Perturbation of Microenvironments During Embryogenesis

Conventional approaches to investigate biochemical gradients *in-vivo* include perturbing native molecule gradients by genetic manipulations such as knockdown and overexpression experiments or exogenously supplying molecules through microinjection to change an existing gradient or introduce a new gradient [38]. Disturbance of the microenvironment around developing embryos is a complementary approach to perturb the biochemical networks during embryogenesis [38]. Due to the laminar flow field in microchannels, diffusion plays the dominant role in mass and heat transfer, enabling precise spatiotemporal control of the microenvironment. Accordingly, microfluidic technology has offered the opportunity to introduce local changes around individual embryos to control the temperature or chemical composition gradients with a spatial resolution smaller than the size of the embryo. This unique advantage of microfluidic platforms aided the study of diffusible morphogens (e.g. Bicoid) and pair-rule genes (e.g. even skipped) which induce spatial patterning in *Drosophila* embryos.

Lucchetta et al. [105] reported a microfluidic device to generate a sharp temperature gradient along the anterior-posterior axis of a single *Drosophila* embryo. This device consisted of a Y-shaped channel with two inlets for co-flowing cold and warm fluids over an embryo (Fig. 2-2a). The device contained two PDMS layers fabricated by replica molding on machine-milled brass masters. An embryo was placed on a double-sided tape at the converging point of the two inlets in the bottom PDMS layer. Then, the second PDMS layer was inverted over the embryo and clamped to the first layer for fluidic sealing. Cold (17℃ or 20℃) and warm (27℃) fluids were supplied through the inlets. A higher nuclear density was observed in the warmer half of the embryo, confirming that it was developing faster. Although temperature changed the temporal order in which even-skipped stripes were formed, it was reported that it did not affect the pattern spatially, showing that the embryo compensated for the abnormal temperature conditions.

The device above was used later to identify the conditions for creating a sharper temperature gradient over the embryo [106]. The fluid flow and heat transport inside the device were characterized both experimentally and numerically to estimate the temperature distribution around and within the embryo. The effect of embryo position on temperature distribution across the main

channel was also investigated by numerical simulation. The characterized device was validated by observing the expression of Paired protein in *Drosophila* embryos. The Paired stripes formed out of order with stripes forming more rapidly in the warm half of the embryo. However, the final position of the stripes were not affected, showing that the embryos were able to compensate for the consequences of temperature disturbance. Using the same device and thermal stepping, Lucchetta et al. [107] were able to modulate the Bicoid (Bcd)** gradient and found that the stability of Bcd gradient before cellularization is not necessary for normal development.

Despite many advantages, there are three drawbacks associated with the microfluidic platform developed above. First, manual mounting of single embryos inside the chip is time-consuming and prone to misalignment and damage to the embryo. Second, the embryo should be removed from the device for further fluorescent immunostaining and imaging. Therefore, the data acquisition process is limited and discontinuous. Third, the inlet fluids must be heated off-chip which could lead to a huge temperature loss at the entrance of the device. Thus, a large temperature gradient may not be generated at the junction of the two branched channels where the embryo is located. As a possible solution, the experiment could be performed inside a large incubator with a controlled temperature to decrease the heat loss which complicates the experiment.

To address some of these challenges, Dagani et al. [108] utilized surface modification for self-assembly of the embryo inside the Y-shaped microfluidic channel. They used oil adhesive pads as minimal potential-energy wells to immobilize the embryo inside the channel (Fig. 2-2b). An alcohol-based surfactant was used as the carrier fluid. When the embryo was attached to the oil pad, the alcohol surfactant was removed and the embryo-oil adhesion increased by three times since water has a higher interfacial tension with oil.

Bai et al. [109] developed another Y-shaped PMMA-PDMS microfluidic platform and used it to investigate *Drosophila* embryo's early cleavage cycles under exposure to a temperature gradient across the anterior-posterior axis (Fig. 2-2c). Double-sided tape was used to seal the chip and immobilize the embryo. They generated temperature gradients using water tanks of different temperatures located right under the Y-shaped microchannel to resolve issues with thermal loss and temperature drop between reservoirs and the embryo. There was only a layer of double-sided

** *Bicoid (Bcd)* is a gene whose protein concentration gradient controls the development of the anterior-posterior axis of *Drosophila* embryos[321].

tape between the water tanks and the fluid flow in the PDMS channel, hence, heat loss was minimized, and a stable temperature gradient was achieved. Real-time image acquisition was made in-situ under a confocal microscope. Results showed that upon applying a temperature gradient, early nuclear cycle division was disrupted, leading to an asynchronous development which depended on the orientation of the thermal gradient.

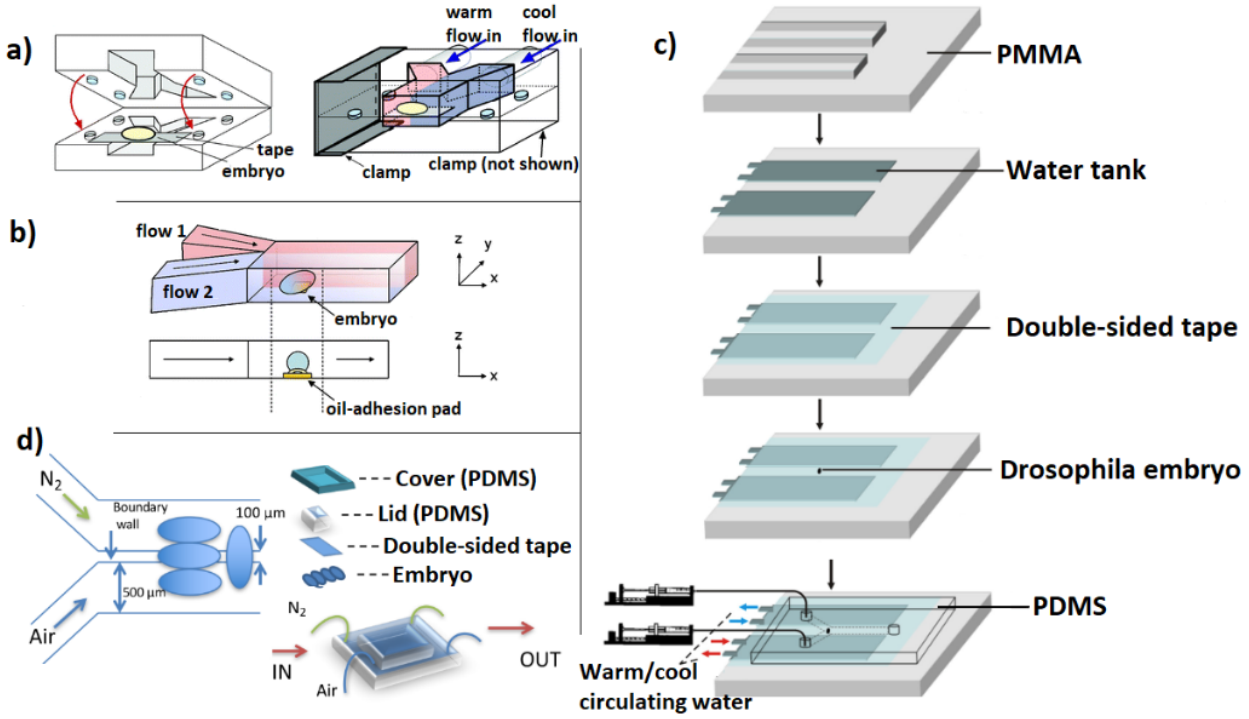

Figure 2-2: Microfluidic platforms for spatiotemporal perturbation of Drosophila embryogenesis. (a) (i) Embryo was placed on a double sided-tape over the bottom channel. (ii) Temperature gradient was generated by cold and warm laminar flows surrounding the embryo [105]. *(b) Microfluidic device equipped with an oil-adhesion pad for self-assembly of Drosophila embryo* [108]. *(c) Microfluidic device for generating temperature gradient around the Drosophila embryo with thermal reservoirs brought closer to the embryo trapping region* [109]. *(d) (i) Microfluidic channels with different infused gases and various embryo positions inside the microfluidic device. (ii) Various components of the microfluidic chip designed to establish an oxygen concentration gradient* [110]. *Figures reproduced by permissions from Springer Nature (a and b, Elsevier (c), and Public Library of Science (d).*

A similar mechanism was used to expose embryos to different gas compositions. Wang et al. [110] investigated the effect of localized hypoxia on *Drosophila* embryo development using a microfluidic device which could impose a controllable oxygen gradient on developing embryos. The device consisted of a membrane, a microchannel, and an embryo culture medium (Fig. 2-2d). The gas-permeable membrane was made by spin coating of PDMS on top of a silicon wafer and bonding it to other device components using a plasma-exposure technique. The embryos were placed on top of the membrane and immobilized using a double-sided tape with a PDMS lid. The

infused gas in the microchannel below the embryo created a concentration gradient in the embryo culture medium due to the permeability of the PDMS membrane. Results using this device indicated that the pole cell movement and tail retraction of developing embryos are strongly affected by oxygen concentration.

The abovementioned devices in this section could create a reliable temperature or chemical gradient over individual embryos. However, they cannot be used for high-throughput applications in which perturbation of microenvironment is required for a larger number of embryos. The microfluidic embryo-trap array by Chung et al. [111] was further modified to provide high-throughput live imaging of developing embryos which were exposed to short-term oxygen deprivation (anoxia) [112]. The extended length of the serpentine channel in the previous design led to an undesired oxygen concentration gradient due to PDMS permeability. In addition, considering the optimum imaging frequency and magnification, only ~20 embryos per experiment could be imaged using laser scanning confocal microscopy. Therefore, the device was miniaturized to twenty-two traps to minimize the variability of the microenvironment along the serpentine channel and the strain applied to the embryos, while maintaining the highest possible throughput. Exposure to anoxia was performed by pulsating humidified nitrogen gas through the serpentine channel. Using this system, anoxia-induced delay in development and resumption of embryonic development after anoxia was reported. Short-term anoxia in nuclear cycle 13 caused ~11.1 ± 2.3 minutes prolongation in this stage. After anoxia exposure, a delay of ~14.1 ± 4.2 minutes was seen in ventral furrow formation in stage 4. However, anoxia did not affect the recovered embryos during stage 5 and the next phases of development, which indicated an immediate but short-term effect of anoxia on developmental arrest.

2.1.3 Sorting

Sorting embryos based on fluorescent reporter expression from a larger population of embryos is an important step in *Drosophila* genetic studies. Manual sorting of *Drosophila* embryos is time-consuming and laborious; however, the basic principles of embryo sorting is close to that of cell sorting [113]. For instance, fluorescent-activated cell sorting (FACS) is a common approach for separating groups of cells based on fluorescent labeling [114]. The Complex Object Parametric Analyzer and Sorter (COPAS) from Union Biometrica utilized principles of the FACS technique for sorting multicellular organisms [115]. This system has been commercialized to sort small

objects ranging from 250-2000μm including *Drosophila* embryos based on physical parameters of animal length, optical density, and the intensity of fluorescent markers [116]. In this system, a pneumatic manifold removes particles not meeting the sorting criteria by short bursts of compressed air. This device has been successfully used to sort *Drosophila* embryos with nearly 100% sorting accuracy [117,118]. However, the technology is costly and not accessible by many researchers in the field.

Using microfluidic technology, the FACS technique has been miniaturized on chip and adapted for sorting *Drosophila* embryos based on the expression of GFP. For instance, Furlong et al. [119] adopted the concept of the conventional FACS for sorting *Drosophila* embryos. In this system, a solution containing embryos was flown through a narrow channel so that embryos were passed individually through an optical cuvette and illuminated by an argon laser. A photomultiplier tube was used to detect the emitted light filtered at 510±5nm wavelength (i.e., GFP). If the GFP peak was below or above a defined threshold, a signal was sent to an electromagnetic switch which was utilized to direct the embryos either to a “save” or a “waste” bin. This system was able to sort 15 embryos per second with more than 99% accuracy.

Instead of using a mechanical valve in the channel, Chen et al. [46] proposed a microfluidic chip for sorting *Drosophila* embryos based on the pressure change in the microchannels. This device consisted of a channel for loading embryos, two control inlets, and two outlets all fabricated by standard photolithography on a silicon layer, then sandwiched between two pyrex (glass) wafers by anodic bonding (Fig. 2-3a and 2-3b). An off-chip pressure driven system was used to control the pressure of the two control inlets, thereby switching the main flow and embryo streamlines between the two outlets. The effects of control pressure, chamber length, and entrance length on the switching time were investigated to optimize sorting of the embryos. The results demonstrated that the switching time (TSW) decreases if the control pressure increases and the functional relation between them can be expressed as $TSW=98381P-0.5307$ ($10kPa<P<40kPa$). Using numerical simulations, the optimum chamber length was found to be 500μm which led to the shortest switching time of 357μs with a control pressure of 20kPa. The switching time dropped linearly by increasing the entrance length in the range of 1500-4500μm. One deficiency of this setup is the dependency of switching time on the response time of the electro-magnetic three-way valve (5ms) that was used to control the pressures of the inlet flows.

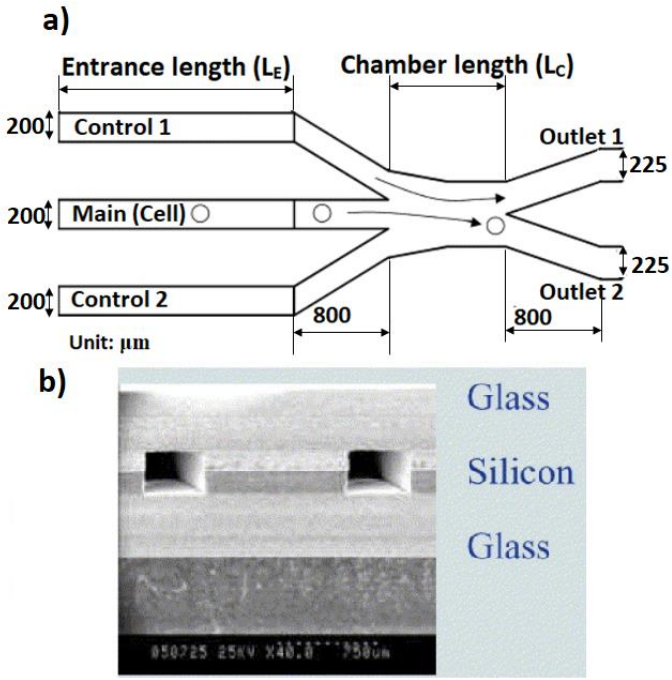

Figure 2-3: The microfluidic embryo switch proposed by Chen et al. [46]. *(a) Schematic of the microfluidic chip. (b) SEM of the fabricated microfluidic chip. Figures reproduced by permission from Elsevier.*

2.1.4 Microinjection

Microinjection is a technique to deliver controlled amounts of chemicals into specific intra-body sites. It is a favorable method especially for water-insoluble materials which cannot be provided by perfusion or feeding [63]. Furthermore, microinjection of foreign substances, such as DNA, RNAi, sperm, and protein into individual cells, embryos, tissues and organs of small organisms plays a decisive role in genetics, transgenics, and reproductive studies [120]. Pressure-based microinjection is the common approach for injection into cells and embryos which involves immobilizing the sample and injecting them using a pressurized injection pipette controlled by a manual or motorized manipulator. This technique requires relatively expensive equipment and injection throughput is limited by the operator's level of expertise [121,122]. Microfluidic technology has offered advantages to make the injection process easier, faster, and more precise and cost-effective.

The microfluidic devices which have been developed for microinjection of *Drosophila* embryos can be categorized based on their embryo-needle actuation method. In these systems, either embryos are pushed towards a fixed needle [123] or the needle is moved to penetrate the embryo

[124]. A fixed needle enables high-throughput injection while a moveable needle provides more control during the penetration and is appropriate for localized injection.

Delubac et al. [123] reported a microfluidic injector based on a Pyrex-silicon-Pyrex sandwich structure with an integrated surface-micromachined silicon nitride microneedle (Fig. 2-4a). This device was able to separate clustered embryos and flow them individually towards the fixed microneedle using a sheath flow mechanism. This controlling flow aligned the embryos close to the needle and prevented them from tilting. Using an external camera and image processing technique, the embryo at the inlet and the reagent injection were detected to automatically control the subsequent embryo ejection. The authors demonstrated the reliability of their system by injecting embryos that expressed an enhanced GFP (eGFP) with small interfering RNA (siRNA) against eGFP. The injection process for each embryo took 3-4s and 90% of the embryos showed silencing of eGFP after injection. However, this system was not able to distinguish the anterior side from the posterior end of the oriented embryos; while the microneedle should preferably penetrate the posterior part of the embryo.

Ghaemi et al. [124] developed a microfluidic injector with a movable needle which could inject controlled volumes as low as 30 ±10 pL at various positions inside the *Drosophila* embryo (Fig. 2-4b). This microfluidic device consisted of a compliant mechanism, a needle channel, top and bottom needle aligners, a microneedle, and an embryo chamber. Soft lithography technique was utilized to fabricate the PDMS chip. A microneedle made of fused silica microcapillaries was glued to the compliant mechanism which consisted of a moveable block and two posts. A manual micropositioner was attached to the compliant mechanism to control the position of the needle tip with 5µm resolution. Top and bottom aligners were used to control the motion of the needle in the vertical direction. This microfluidic injector was used to investigate the effect of sodium azide (NaN3) on the migration velocity of cardioblast cells and the dose sensitive effect of the toxin on heart assembly of *Drosophila* embryos. Results showed that injection of NaN3 with concentrations more than 10mM led to a dose-dependent reduction in the migration velocity of cardioblast cells. At least 50 embryos could be easily injected with the above device. One of the challenges associated with the microfluidic microinjectors is the integration of microneedles with the PDMS chip. In the above device, the microneedle was glued into the microfluidic chip using a droplet of PDMS. In addition, the back end of microneedle was attached to a tube (the reagent chamber)

using epoxy. In order to use the same chip for another chemical, the microneedle should be replaced with a new one which is not easy because of the PDMS glue and the epoxy being irreversible.

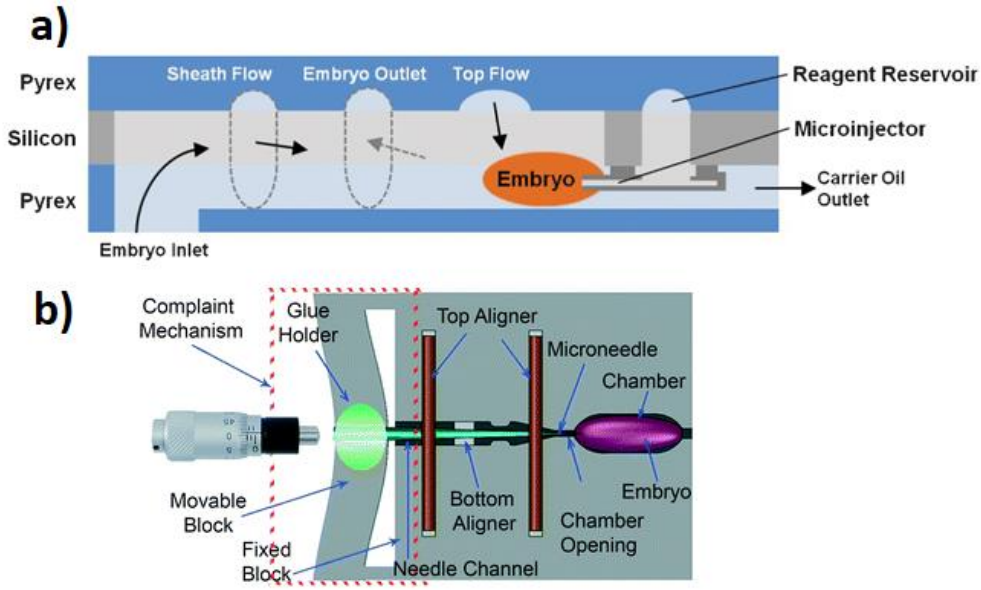

Figure 2-4: Microfluidic devices for microinjection of Drosophila embryos using (a) a fixed microneedle developed by Delubac et al. [123] *and (b) a moveable needle developed by Ghaemi et al.* [124]. *Figures reproduced by permission from Royal Society of Chemistry.*

2.1.5 Mechanotransduction

Mechanotransduction is the mechanism by which cells sense and respond to mechanical stimulation by converting them into electrochemical signals [125]. An emerging theory in embryonic development is that mechanical forces can affect the expression of certain genes such as twist [126]. Conventional techniques for applying mechanical stimulation such as needle indentation and coverslip actuation are low-throughput and require manual alignment. Recently, microfluidic technology has been utilized to automatically align, immobilize, and compress hundreds of *Drosophila* embryos [127]. Embryos were loaded into three straight channels with thin flexible sidewalls surrounded by closed gas channels (Fig. 2-5a and 2-5b). The sidewalls could be deflected by applying pressurized air through gas channels, thereby compressing the embryos (Fig. 2-5c). The device was fabricated by photolithography and PDMS replica molding. The authors developed analytical and numerical models to predict the deflection of sidewalls. They

used this device to measure embryos' stiffness and to show that dose and duration of compression affect the mechanical induction of twist using twist:eGFP embryos. Microfluidic devices have been used previously to study mechanotransduction on cells and tissue constructs [128]. However, less attention has been given to the application of microfluidics for *Drosophila* embryo mechanotransduction studies and this filed is yet to be matured.

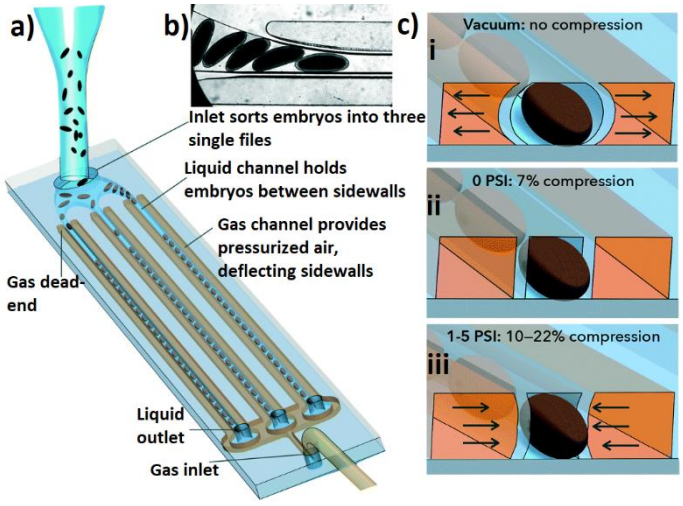

Figure 2-5: Microfluidic device for high-throughput mechanotransduction studies on Drosophila embryos [127]. *(a) The schematic of the microfluidic device. The embryos were loaded into the device through liquid channels (blue channels). (b) The inlet of the device which sorted hundreds of embryos into three single files. (c) Schematic showing sidewall deflection. (i) Vacuum was applied to expand the channels for loading embryos. (ii) At rest, the embryos were arrayed and immobilized. (iii) Upon applying pressurized air through the air channels, the sidewall was deflected, compressing embryos. Figures reproduced by permission from the Royal Society of Chemistry.*

2.1.6 Light-sheet microscopy

The advent of new imaging techniques in recent years enables researchers to perform volumetric (3D) microscopic analysis deeper into small multicellular organisms with high spatiotemporal resolution. Light-sheet fluorescent microscopy (LSFM) is an imaging technique which has been used to image cellular dynamics of intact *Drosophila* embryos expressing fluorescent markers [129]. In LSFM a light sheet illuminates the sample while a lens which is located perpendicular with respect to the light sheet detects the fluorescence. In this approach only a single plane of focus is illuminated; therefore, phototoxicity and bleaching is minimized. In addition, in LSFM, the imaging speed is faster and the signal to noise ratio is higher than confocal microscopy [39,129]. Selective Plane Illumination Microscopy (SPIM) is the commonly used modality of LSFM for *Drosophila* embryos [129]. In SPIM, the sample is embedded in a agarose column inside a glass capillary and imaged from different angles over time [129–131]. One of the important challenges

in microfluidics is the integration of microfluidic chips with light sheet microscopy. Microfluidic chips usually utilize a glass cover slip for the imaging side of the chip which causes significant optical aberration during light sheet microscopy. Recently, the integration of microfluidic platforms with new imaging modalities including SPIM has enabled high-throughput real-time parallel imaging of multiple embryos for a long time under controllable exposures.

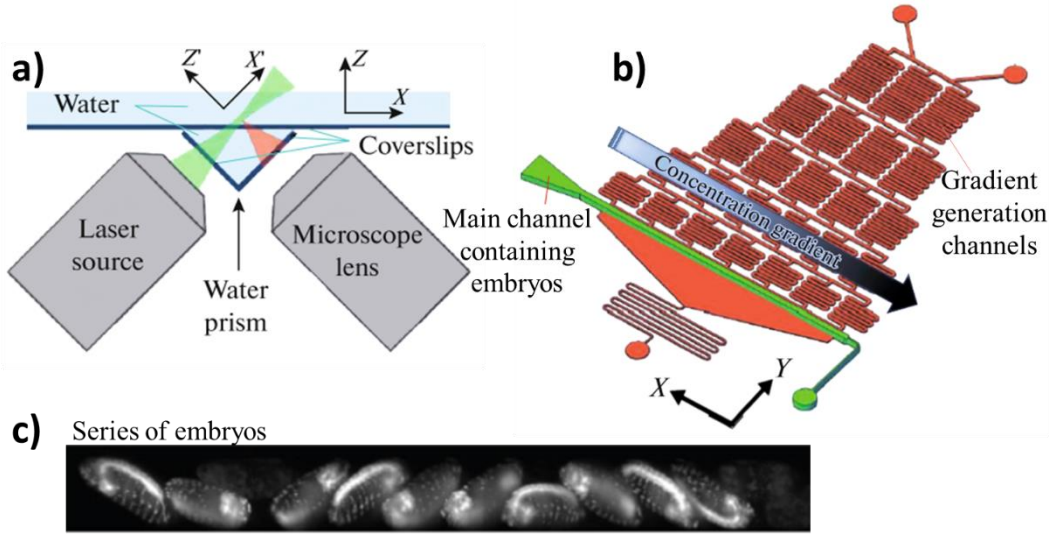

Figure 2-6: The integration of microfluidic technology with a plane illumination microscopy system [132]. *(a) The schematic of the open-top SPIM with illumination and detection objectives beneath the sample stage and a water prism used to compensate the optical aberrations. (b) Schematic of the microfluidic device consisting of an embryo-containing channel and gradient generation channels. (c) A series of developing embryos which were imaged using SPIM inside the microfluidic device. Figures reproduced by permission from the Optical Society of America.*

McGorty et al. [132] developed a novel open-top SPIM which is compatible with microfluidic platforms (Fig. 2-6). In this design, both illumination and detection objectives were placed beneath the sample stage at 45 degrees to the sample stage. The key component of this configuration was a water prism used to compensate the optical aberrations caused when imaging at 45 degrees through a coverslip (Fig. 2-6a). The microfluidic device was fabricated by standard soft lithography and consisted of a single, snake-like channel with multiple 14-mm long straight sections allowing 32 embryos to line up in each straight section with anterior-posterior axis along the channel. The whole channel with all embryos was scanned by SPIM technique providing a single 3D data set of all embryos. A more complicated microfluidic device was fabricated which maintained a 0 to 200μM linear gradient of methylmercury chloride along a straight channel using another network of microchannels (Fig. 2-6b and 2-6c). Using this device, the dose-dependent effect of methylmercury chloride on the development of central nervous system (CNS) was

investigated in a single imaging experiment over 36 hours. The condensation in the embryonic *Drosophila* ventral nerve cord (VNC) which normally occurs at stage 16 of the embryogenesis was observed in only 6 embryos at the lowest end of the gradient.

2.2 Microfluidic Devices for *Drosophila* Studies at Larval, Pupal, and Adult Stages

2.2.1 *In-vivo* Neuron and Organ Assays

Drosophila at the larval stage is a promising model for neuronal, developmental, learning, and behavioral studies [1]. Imaging and monitoring of biological processes such as CNS activities and heart function can be performed owing to the semi-transparent cuticle of *Drosophila* larvae; however, complete immobilization is required for these purposes because of the continuous locomotion of the larvae. The conventional immobilization techniques include using dissection [133], glue [134], and anesthetization [135,136]. Dissection technique is lethal; hence, not suitable for post-imaging assays. Glue-based immobilization is irreversible and potentially toxic to the animal; in addition, it is laborious and difficult to implement for young, small animals because each animal should be glued individually [42,137]. Anesthetics such as cold temperature, carbon dioxide (CO_2) [138], isoflurane [24] and desflurane [139] can be used for multiple organisms in parallel assays. However, they are known to influence the animal's neurophysiology, neural activity, and heartrate [24,25,42,138]. For instance, exposure to CO2 blocks synaptic transmission at the neuromuscular junction and causes cardiac arrest while isoflurane reduces presynaptic excitability in *Drosophila* larvae [24,138]. In addition, cold and CO2 anesthetization of adult *Drosophila* significantly affects the animal’s sensitivity to low and high temperature, starvation, and desiccation as well as locomotor activity and fecundity of female flies [140]. Moreover, anesthetics are regulated chemicals which can threaten the user’s safety; therefore, relevant training and installation of safety component are needed before using them [137]. Microfluidic technology has been utilized as a tool to physically confine *Drosophila* larvae to facilitate biological investigations on intact specimens.

Yan et al. [41] developed a mechanical microcompressor which could be equipped with different microfluidic platforms to trap single cells and multicellular organisms and immobilize them by flattening the specimen (Fig. 2-7a). This device could be used for high-resolution bright field and fluorescence microscopy for both short-term and long-term observations. It could be integrated with microfabricated channels on a glass slide, allowing on-chip chemical perfusion. In addition to soft lithography, computer numerical control (CNC), and laser techniques were needed for this device, thereby making it more complicated and expensive to fabricate. The authors utilized the device for *in-vivo* imaging of the eye imaginal disk of third instar *Drosophila* larvae labeled with ubiquitous E-cadherin GFP. It was mentioned that the larvae could not survive until the next day after the experiment which limits the application of this device in developmental studies.

Mondal et al. [42] developed a microfluidic platform for subcellular imaging of organelle transport processes in unanesthetized intact C. elegans worms and *Drosophila* larvae. The device consisted of two main PDMS layers plasma bonded together. The first layer included the animal chamber and a flexible membrane used for immobilization. The second layer composed of a control channel used to deflect the flexible membrane upon applying pressurized nitrogen gas through a liquid column. Standard lithography of SU8 was used to fabricate the molds required for replica molding of PDMS. The device was used to image pre-synaptic vesicle transport, intraflagellar transport (IFT), dendritic transport and the migration of neuroblasts in C. elegans, and the mitochondrial transport in intact *Drosophila* larvae. They compared the microfluidic-based immobilization with anesthetized-based immobilization and reported the adverse effect of anesthetization on some neuronal transport processes *in-vivo* (e.g., the cessation of pre-synaptic vesicle transport in C. elegans under exposure to specific anesthetic concentrations). The same device was used later to measure the heartbeat of zebrafish larvae using time-lapse imaging [141].

Ghannad-Rezaie et al. [17,48] proposed two microfluidic chips for short-term (up to 1 hour) and long-term (up to 10 hours) immobilization of *Drosophila* larvae (Fig. 2-7b). They used the chip for live imaging of the subcellular responses to neural injury caused by laser axotomy or pinching the segmental nerves using forceps. They investigated the calcium dynamics and axonal transport after axotomy. The short-term immobilization device comprised a microchamber which snugly fit a 3rd instar larva. The long-term immobilization chip employed both mechanical forces and the supply of carbon dioxide (CO_2) gas for temporary immobilization. The chip consisted of two main

layers. The first layer had a larva microchamber for immobilization and two food supply microchannels to avoid starvation. The second layer included a CO2 supply channel. CO2 diffused into the larva microchamber through the PDMS membrane to enhance immobilization. CO2 gas minimized the stress on larva's body and facilitated repetitive live imaging over a long period. In both the short-term and long-term immobilization devices, the larva chamber was surrounded by a microfluidic network held under a stable vacuum to provide a reliable seal between the PDMS, oil, and coverslip. Chaudhury et al. [137] utilized the same technique for on-chip cryo-anesthesia of *Drosophila* larvae. Instead of CO2 in the second layer, they used a concentrated saltwater solution as a coolant to create a low-temperature microenvironment and immobilize the larvae using pressure/cooling techniques. The advantage of on-chip cooling-based immobilization is that the movement of internal organs inside the hemolymph filled body cavity is sufficiently minimized. Additionally, the authors modified the device design so that different developmental stages of *Drosophila* larvae could be tested using their chip. They used this microfluidic device to image the mitochondrial trafficking in neurons and monitor the developmental growth of synapses *in-vivo*.

Ghaemi et al. [21,142] constructed two microfluidic chips to immobilize and image *Drosophila* 3rd instar larva's CNS in response to auditory stimuli (Fig. 2-7c). The first chip was designed for automatic pneumatic loading and unloading with a tapered larva immobilization channel, while the second device was a flexible PDMS chip for manual loading and unloading of the larva. Using tapered traps in the pneumatic chip and a clamping mechanism in the flexible chip the larva was immobilized. Auxiliary 3D narrowing contractions in the trap enabled segmenting the body to improve immobilization. Therefore, the CNS capsule was stabilized with respect to the larva's movement and hemolymph flow. Using genetically encoded calcium indicator GCaMP5, the authors demonstrated that the CNS response to an acoustic stimulus is amplitude-dependent and peaks at 200Hz frequency. Indirect access of the larva to sound stimulation in the pneumatic chip was mentioned as a drawback. However, the flexible chip enabled direct access to both acoustic vibrations for stimulation and air for respiration.

Studying the primary olfactory receptor neurons (ORNs) in *Drosophila* requires exposure to different odors at different concentrations and imaging the responses of ORNs with a cellular resolution at the same time. Si et al. [143] have used a microfluidic device consisting of 24 fluid

delivery channels and a gradually tapering channel for immobilization of a first instar larva. The device was fabricated by standard soft lithography approach. They used air pressure for stimulus delivery with a switching time of approximately 20ms and water was used as a washing liquid. The results demonstrated that the ORNs activities increase with odorant concentrations but with different sensitivities.

Ardeshiri et al. [23,144] constructed a microfluidic device to monitor the heart activity of 3rd instar *Drosophila* larvae under exposure to aqueous and gaseous chemicals (Fig. 2-7d). Replica molding of PDMS on 3D-printed master molds was used to fabricate the device. The proposed device was capable of loading, orienting, and reversibly immobilizing the larva. After loading the larva via a loading glass capillary into the trap region of the device, the head of the larva was grabbed by a negative pressure applied to the orientation glass capillary. The larva was positioned in the desired orientation and then pneumatically immobilized by applying negative pressure to the suction channels. Using chemical infusion channels, different chemicals could be introduced to the anterior or posterior sides of the larva's body. They used their devices to investigate the transient effect of different concentrations of sodium azide, carbon dioxide, and oxygen on the cardiac activity of *Drosophila* larvae. The larval heartrate decreased under exposure to sodium azide, carbon dioxide, and lack of oxygen (anoxia) and increased under exposure to excess oxygen (hyperoxia). Inducing hyper or hypo cardiac activities depended on the concentration of these chemicals. Except for exposure to sodium azide, larvae could recover to the normal heartrate after removing the chemicals.

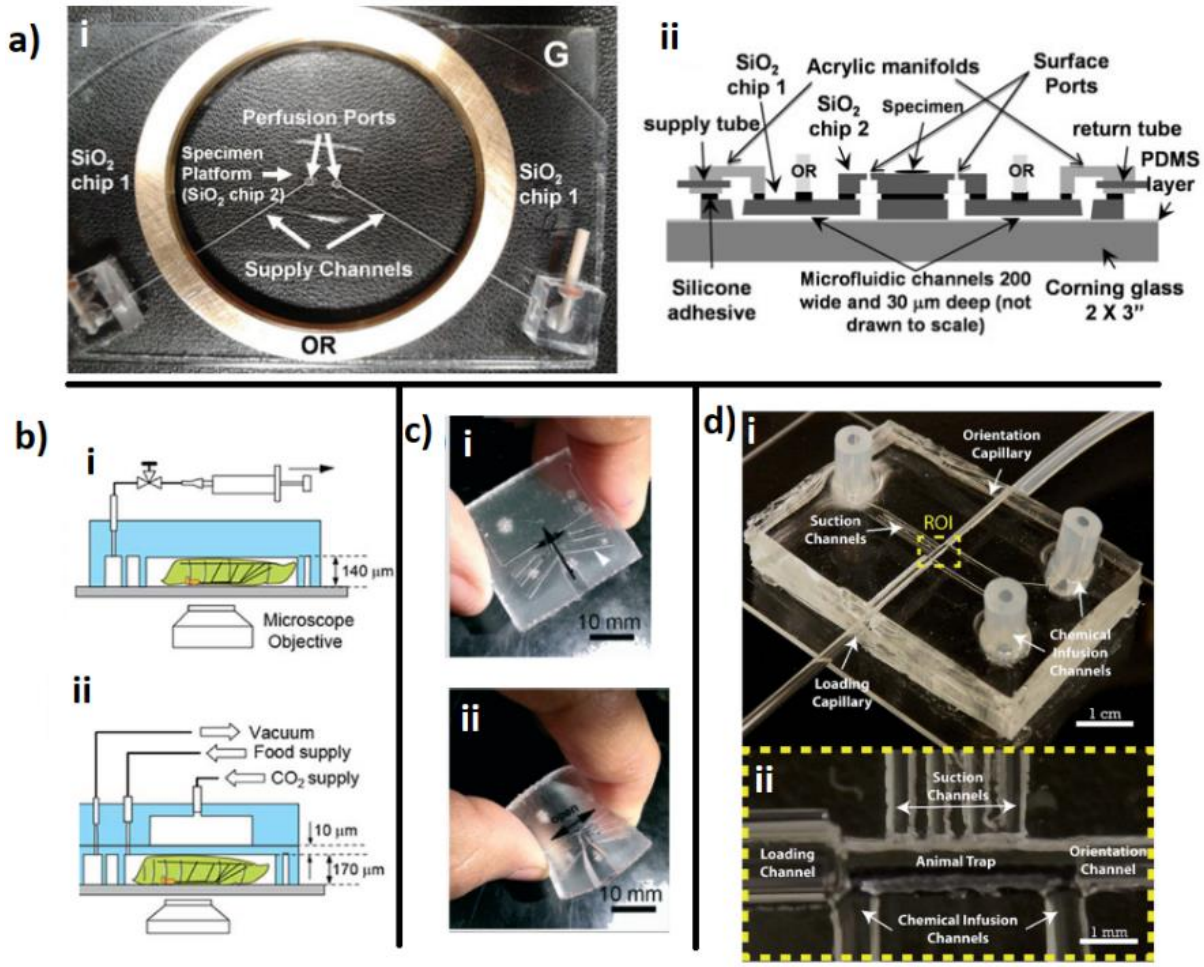

Figure 2-7: Microfluidic devices for intact Drosophila larvae studies. (a) (i) Mechanical microcompressor for immobilization of biological samples including Drosophila larvae [41]. *The outer brass ring (OR) is cemented to the glass slide (G). (ii) Schematic of the device from the side view. (b) Short-term (i) and long-term (ii) immobilization microfluidic devices developed by Ghannad-Rezaie et al.* [17]. *(c) Flexible chip developed by Ghaemi et al.* [142]. *The chip (i) is bent (ii) for animal loading. (d) Microfluidic device for orientation, immobilization, and cardiac screening of Drosophila larvae developed by Ardeshiri et al.* [23]. *Figures reproduced by permissions from Cambridge University Press (a), Public Library of Science (b), and Royal Society of Chemistry (c and d).*

2.2.2 *In-vivo* Behavioral Assays

Drosophila behavioral assays are used to determine the role of genetic and environmental factors as well as drugs on different behaviors such as larval crawling, adult climbing, oviposition and courtship [145]. For instance, groups of larvae or adult flies are fed with drugs dissolved in their food. Then, larval crawling is quantified by counting the number of grid lines crossed on a graph paper [145] and adult climbing is quantified using rapid iterative negative geotaxis (RING) technique in which flies ascending the wall of a cylinder are monitored after being tapped to the bottom of the cylinder [146]. Courtship and oviposition assays include observing male and female

flies' mating under a dissection microscope [145] and quantification of the number of eggs laid on various substrates [59]. These conventional techniques are time-consuming and laborious. They cannot resemble the natural habitat of fruit flies in which the larvae can perform digging and diving into the food in addition to crawling. Lack of control over behavior stimulation and difficulties with rapid monitoring of the behavioral phenotypes are other challenges in conventional behavioral assays. Micro-scale chemical delivery has a crucial role in food-seeking and oviposition assays but none of the conventional *Drosophila* food seeking studies enabled dynamic food delivery at the micro-scale [147,148]. Many of these limitations have recently been resolved by microfluidic devices.

Navawongse et al. [44] used a microfluidic chip to deliver a minuscule meal size of liquid food to *Drosophila* adult flies. The chip consisted of two main layers of transparent thermoplastic polymethylmethacrylate (PMMA) which were patterned by CNC milling. The first layer contained a food delivery channel and enabled delivering 80nl of liquid food. The second channel included a feeding alcove and a larger chamber called the behavior chamber. Food foraging behavior of the fly was investigated inside this chamber upon multiple food deliveries with intervals. The results showed that repeated presentation of food in a fixed position improves flies' path choice implying that food foraging is a learned behavior. Using the same device, Erikson et al. [149] investigated the effect of silencing neuromodulatory systems on food discovery and food intake. Results demonstrated that silencing Tryptophan hydroxylase (Trh) neurons enhances food intake while silencing Dopa decarboxylase (Ddc), Tyrosine decarboxylase 2 (Tdc2), and neuropeptide F (NPF) neuronal cells reduces food intake in *Drosophila* adult flies. The drawback of the device was that only one fly could be tested at a time and each device required one pump for liquid delivery.

Kim et al. [150] investigated the food search behavior of *Drosophila* larvae in a microfluidic device which resembled their natural habitats (Fig. 2-8a). The device was fabricated by PDMS casting in a micro-milled mold and consisted of three main regions, i.e. a closable channel for loading the larva, an air chamber which provided air for larva's breathing, and a long and narrow rectangular agarose chamber in which larva could dive to find food. The digging and diving investigations using the microfluidic device uncovered three main behavioral modes of 1) resting at the surface of the gel, 2) digging while larva forages with at least half of its body embedded in the gel, and 3) diving in depth to explore the medium. Using different percentages of agarose mixed in water, the

authors investigated the effect of substrate hardness on diving behavior. They also studied the effect of respiration on dig-and-dive behavior by blocking the posterior spiracles using thermoplastic glue. Results of this assay showed that spiracle obstruction leads to a significant decrease in the time of dig and dive phases while the time spent on surfacing phase increases. By injecting a small amount of odor at the bottom of the diving chamber, the authors concluded that the olfactory stimulation promotes food search behavior. Furthermore, a significant difference in the dig-and-dive behavior was observed between *Drosophila* and D. suzukii, another family of fruit fly which uses different food resources [151].

Another important behavioral readout metric in the fruit fly is oviposition (egg laying) which can be used for assessment of biological fitness and behavioral responses of the fly including fly's sensory system performance, survival rate, and reproduction. Environmental stimuli such as chemicals, physical conditions of the substrate, humidity, light, electromagnetic radiation, and temperature can influence the egg laying process as well as the viability of the fly [152–154]. Conventional assessments on agar-juice plates as the standard substrates are time-consuming and labor intensive, have large footprints due to oversized oviposition sites, and are prone to chemical evaporation thereby, undesired changes in chemical concentrations [49]. Microfluidic technology has been used to overcome these challenges.

Leung et al. [155] constructed a microfluidic platform to investigate the effect of substrate properties including exposure area, sugar content, and stiffness on oviposition and viability of *Drosophila* adult flies. The device consisted of a patterned PDMS membrane with different sizes of holes (i.e. exposure areas) which was assembled on top of an oviposition agar juice substrate. The effect of sugar content and stiffness were investigated by altering the amount of sugar and agarose in the agar-juice recipe. Results indicated that flies avoid laying eggs on pure PDMS and are more likely to lay eggs inside the agar-exposed holes larger than 0.5mm diameter, along the edge of the PDMS agar interface of the membrane. The amount of agar exposure primarily influenced the flies' viability while the spacing between access holes did not have any effect. Additionally, the amount of sugar in agar juice substrate affected neither the oviposition rate nor the site selection; however, flies were more likely to lay eggs on softer agar substrates.

Afterward, Leung et al. [49] modified their on-chip oviposition screening device to make it capable of single and multi concentration chemical infusion into the agar-juice substrate (Fig. 2-8b). The

device integrated the above agar substrate and top-patterned PDMS layer with chemical delivery microchannels at the bottom of the agar substrate. The microchannels were fabricated in-situ using ice as a sacrificial layer. Chemicals were hydrostatically infused into the agar substrate through the microchannels and their effects on the oviposition behavior of adult flies in the stock bottle installed on top of the substrate were investigated. The authors fabricated two different chemical delivery devices for toxicity assays with one oviposition site and multiple-choice preference chemical screening with three oviposition sites. They investigated the effect of zinc and acetic acid at different concentrations, reporting that 70mM of zinc is repulsive while 2-20 mM zinc attracts the flies and increases the egg laying. Similarly, acetic acid had both attractive and repellant effects at 5% and 15% concentrations, respectively.

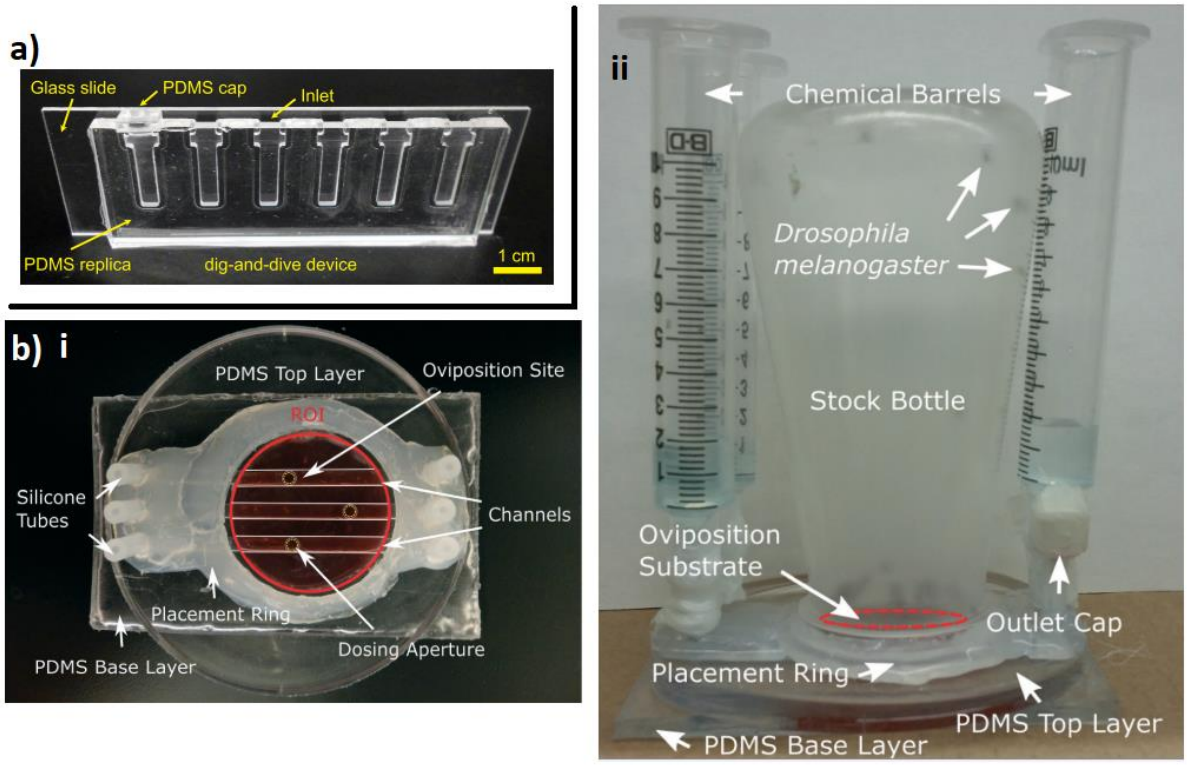

Figure 2-8: Microfluidic devices for behavioral assays. (a) The dig-and-dive microfluidic device developed by Kim et al. [150] *for investigation of food search behavior on Drosophila larvae. (b) (i) Top view of the hybrid agar-PDMS microfluidic device for oviposition- based chemical screening of Drosophila adult flies* [49]. *(ii) Experimental setup including chemical barrels and fly stock bottle which is installed on top of the microfluidic chip. Figures reproduced by permissions from ELife Sciences Publications (a) and Royal Society of Chemistry (b).*

2.2.3 *In-vitro* Cell and Tissue Assays

In-vitro studies using biological cells, tissues and organs isolated from parental animals and organisms are widely used in cellular biology and neuroscience. Cell and tissue cultures are powerful tools for investigation of cell growth, survival, and cell-cell interactions, as well as the toxicity or therapeutic mechanisms of different chemicals [156–158]. However, *in-vitro* approaches require dissociation techniques for separating cells from intact tissues. In addition, precisely controllable culture media and chemical exposure environments are required for cell survival, growth and chemical screening [159].

Traditional dissociation techniques include the dissection of target tissues followed by empirically determined enzyme treatment and mechanical trituration. Mechanical trituration mechanisms typically include chopping, flushing through pipette tips, applying mechanical vibrations, and using filters [160,161]. During these processes the tissue becomes invisible; therefore, operator cannot control and troubleshoot the process properly. In addition, the level of mechanical stress on the tissue cannot be measured or controlled. Different microfluidic platforms have been developed which facilitates the dissociation process and cell culturing for mammalian and insect cells [162–164]. However, a few of them are dedicated to cell- and tissue-based *Drosophila* assays.

Jiang et al. [165] developed a microfluidic device to dissociate *Drosophila* larval CNS into viable single neurons. The device had a single microchannel with a constriction at its center to enhance shear and normal stress gradients on the loaded tissue. The brain tissue of a 3rd instar *Drosophila* larva was loaded into the device and exposed to a flow-induced oscillating stress field. The loaded tissue was driven back and forth through the constriction zone until it broke into individual neurons. The channel dimensions, the amplitude, and frequency of the oscillating flow rate were determined based on several outcomes including the initial cell yield, neuronal survival, and neurite-arbor size. Microfluidic devices such as the one developed by Jiang et al. [165] can offer impressive advantages during the dissociation process such as controlling the stress level and enhancing the throughput. This direction of research has not been extensively explored and offers numerous opportunities for technological innovation in *Drosophila* and other model organism-based studies.

Another benefit of microfluidic technology is related to controlling the physical and chemical properties of the microculture medium during optical and fluorescent microscopy. Giesen et al. [166] utilized a microfluidic device to measure physiological responses of gustatory receptor neurons (GRNs) of 3rd instar *Drosophila* larvae by delivering precise and temporally controlled taste-provoking stimuli (Fig. 2-9a). The PDMS chip was a V-shaped channel with a tissue chamber located at the junction of the inlet and outlet branches. Chemicals with different tastes such as sucrose (sweet) and denatonium (bitter) were added into water, the baseline solution, to stimulate the larva's chemosensory organs. The head of the larva was dissected and introduced into the tissue chamber ensuring that the fluid flow directly exposed the chemosensory organs through the channel. A drop of diluted agarose was poured on top of the brain tissue to seal the chip. Adult fruit fly and mammals have unimodal sensory neurons which means each gustatory neuron is tuned to a specific taste modality [167]. However, using this device, Giesen and colleagues analyzed the properties of different GRNs expressing the calcium sensor GCaMP5 and demonstrated the existence of multimodal GRNs in *Drosophila* larvae with different degrees of multimodality. The same chip was used to measure the neuronal activity at single-cell resolution in the GRNs of adult proboscis and leg [94]. Using an off-chip tubing system containing eight (or more) input channels, the authors were able to stimulate the same animal with different chemicals or combinations of chemicals. According to the authors, although the semi-intact preparation of the animal eliminated the problem of peristaltic movements, it limited the imaging time to 1 hour. Additionally, the chip fits only the 3rd instar larvae and for other larval stages, the chip dimensions should be modified.

Beck et al. [168] employed a previously developed microfluidic device called the bridged μlane [169] to investigate the effect of fibroblast growth factor (FGF) concentration on the migration of *Drosophila* vision-critical glia cells. The device was a two-layer PDMS chip which could establish a controlled concentration gradient over time by relying on convection and diffusion. The first layer contained a microchannel with a hydraulic diameter of 95μm connecting two 95μl reservoirs called source reservoir (SRR) and sink reservoir (SKR). The second layer was a user interface layer consisting of two cylindrical chambers known as source chamber (SRC) and sink chambers (SKC), vertically connected to the SRR and SKR. The source and sink chambers were connected by an open bridge channel. The bridge channel was used to adjust the liquid levels in SRR and SKR and eliminate the hydrostatic pressure differences between the two chambers. Results showed that the gilia cells motility increases with increasing the FGF concentration.

In addition to chemical stimulation, microfluidic devices can be used to control mechanical perturbation of cells and tissues. Narciso et al. [170] developed a two-layer microfluidic chip to apply controllable mechanical and chemical perturbations to *Drosophila* wing disc (Fig. 2-9b). The first layer of the device consisted of fluidic channels and culture chambers for loading the tissue and chemical delivery. The second layer consisted of air channels for pneumatically controlling the deformation of a flexible membrane. Both layers were made from PDMS using standard soft lithography. This microfluidic chip was used to investigate the regulation of Ca2+ signaling under chemical and mechanical perturbations. The authors reported that not the initial application but instead the release of mechanical stimulation initiated the intracellular calcium waves in *Drosophila* wing disc.

Although cell culturing inside microchannels is widely used, it is associated with some problems such as channel clogging. In addition, culture conditions such as gaseous and nutriment exchange should be precisely adjusted using controlled flow rates. To overcome these challenges, Morel et al. [171] developed microfluidic stickers using a UV-polymerizable material which could firmly adhere onto cells, tissues, or explants cultured on a coverslip using standard cell culture protocols Microfluidic stickers were made by soft imprint lithography of a UV curable resin on a PDMS stamp. The stamp was fabricated by PDMS casting on a photolithogriphied-SU8 master mold. The patterned sticker was immersed in culture media containing cells or tissues and sealed with either gentle mechanical pressure for low-pressure applications or UV exposure for high-pressure applications. They used the device to image the dissected wing imaginal disk of *Drosophila* pupae expressing GFP-tagged myosin II. The microfluidic device had no adverse effect on the multicellular organization of the tissue. Since the cells and tissues were cultured off the chip, before placing the microfluidic stickers on the coverslip, the growth of cells and neurons were not confined by the geometry of the microchannels. The chance of clogging was also less than microfluidic devices in which cells were cultured inside the closed channels. Moreover, off-chip culturing the cells and tissues enables implementing different biological techniques such as immunolabeling, RNA slicing, microinjection, and transfection before placing the specimen in the microchambers.

Traditional microfabrication techniques such as standard soft lithography are usually expensive and require expertise. However, rapid design and validation of microfluidic devices are essential

for new applications. Recently, researchers have developed microfabrication techniques which are cheaper, faster, and easily customizable for different multicellular systems. For instance, Levis et al. [172] used the hybrid-polyethylene-terephthalate laminate (PETL) as a quick fabrication method to create hybrid microfluidic platforms for various applications including *Drosophila* cell and organ culture and mechanobiology studies (Fig. 2-9c and 2-9d). These devices consisted of layers of PET films bonded with the thermal adhesive ethylene vinyl acetate (EVA). They used a complex network of channels to form a chemical gradient across a population of *Drosophila* wing imaginal disc cells (Fig. 2-9c). By adding a PVC layer as a flexible membrane, they were able to apply mechanical forces to *Drosophila* wing imaginal disk as a micro-organ (Fig. 2-9d). They used this device to measure mechanical properties, including strain, Poisson's ratio, and elastic modulus of the wing imaginal disc.

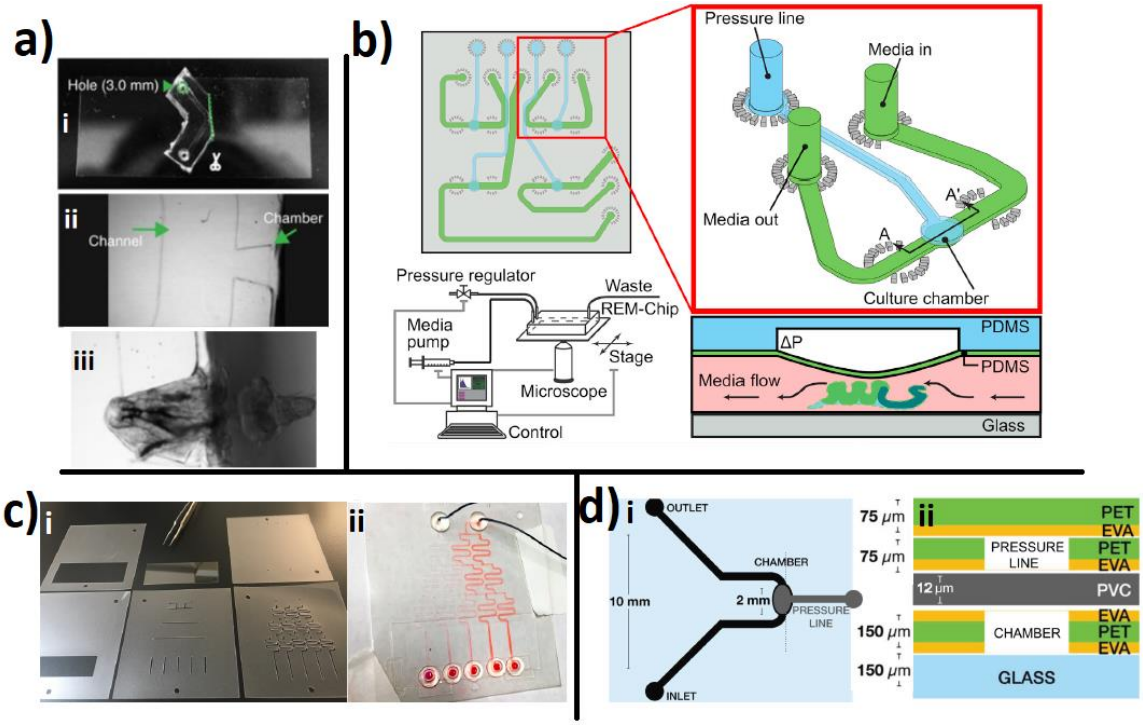

Figure 2-9: Microfluidic devices for Drosophila tissue-based assays. (a) (i) Microfluidic chip for measuring neuronal activities in chemosensory neurons of Drosophila larva. (ii) Empty chip under the microscope. (iii) Dissected larva's head inside the chip [94]. *(b) Regulated environment for micro-organs chip (REM-Chip) which was used to apply mechanical and chemical perturbations to Drosophila wing disc* [170]. *(c) Cell gradient PETL (CG-PETL) device for generating a chemical gradient across Drosophila wing imaginal disc cells using a complex network of channels. (i) The PET-EVA films before assembly. (ii) The final CG-PETL device. (d) Mechano-PETL (M-PETL) device for applying mechanical forces* [172]. *(i) The schematic showing the top view of the device. (ii) The schematic showing the cross-section of the device including different layers of PET, EVA, PVC, and glass substrate. Figures reproduced by permissions from Springer Nature (a), Elsevier (b), and AIP Publishing (c and d).*

2.3 Current gaps in the Field of *Drosophila* Microfluidics

Microfluidic technology has offered clear benefits for *Drosophila* research in all stages of its life cycle. According to substantial differences in the shape, size, stiffness and behavior of this organism at different stages of its life cycle (embryonic, larval, pupal, and adult), different designs and fabrication techniques have been proposed. However, there are many needs and unexplored scientific and technological areas in this field of research. **The effectiveness of these microfluidic devices can be enhanced by developing multi-tasking and high-content multi-phenotypic screening devices via integration with other advanced technologies**. The microfluidic chip invented recently by Shorr et al. [127] is a good example of such a device, at an embryonic level, which is capable of high-throughput alignment, immobilization, compression, real-time imaging, and recovery of hundreds of embryos. Lessons learned from embryonic devices and other small organism chips can be directly applied to enhance the throughput of post-embryonic devices, especially for behavioural screening and organ function analysis (e.g., heart function) due to organ maturity at larval and adult stages. One of biological processes that was remarkably enhanced by the advent of microfluidics is precise chemical administration using microinjection. However, **the microfluidic-based microinjection platforms for *Drosophila* are limited to the embryonic stage** [123,124]. The flexibility and mobility of the animal at larval stage as well as having floating internal organs (e.g., heart tube) makes the microinjection a challenging task in this stage. **Having a microfluidic technology capable of providing reversible immobilization, desired orientation, and localized microinjection of larvae still remains a challenge** (Obj. 1).

Such multi-tasking *Drosophila* microfluidic devices at larval stages can be integrated with microvalves and computer-based control modules to enable automatic loading, orientation, injection, and other manipulation treatments; thereby enhancing the throughput of the assays in post-embryonic stages.

Moreover, the combination of microfluidic devices with high-speed image acquisition and processing techniques can significantly boost the throughput of experiments. Because there is always a trade-off between the quality of the images and the speed of image acquisition, microfluidic devices may need to be adapted based on the imaging system to meet the throughput and the quality at the same time. Recent advances in different imaging techniques such as confocal

microscopy, light-sheet fluorescent microscopy, and multi-photon fluorescent microscopy and the advent of new label-free methods such as harmonic generation microscopy and micro-computed tomography (Micro-CT) may change the design criteria of *Drosophila* microfluidic systems [39]. Moreover, image and video analysis methods have been developed that enhance phenotypic analysis of fly's behaviour at larval and adult stages and can easily be applied for microfluidic-based screening platforms. Examples include tracking software for analyzing fly's movement or heartbeat quantification methods which are reviewed in details in the next section.

New microfluidic devices can be designed and integrated with various electronic and optical features to investigate multiple phenotypes in behavioral and neurobiological assays of larval and adult flies. This can be used to facilitate chemotaxis, thermotaxis, phototaxis and electrotaxis studies using *Drosophila* at different stages.

2.4 Methods for Phenotypic Quantification of Heart Function in Small Model Organisms

Several methods have been proposed to quantify the cardiac functions of small model organisms; Examples include stopwatch counting, laser doppler microscopy, and electrocardiography methods applied to *Drosophila* and zebrafish [74,77,173–182] (reviewed thoroughly in Table 1). **Despite many advantages, these manual methods are labor-intensive and time-consuming; in most of these methods the region of interest (ROI), i.e. heart, should be manually selected to obtain satisfying results.** Moreover, these methods **are limited by only providing the heart rate as a quantitative measure** and not being accurate in measuring high-frequency beats over a long time.

Automated detection of light intensity fluctuations due to heart contractions using a set of photodiodes or phototransistors was proposed to measure the heart rate of fruit fly larvae, pupae, or adult flies [57,66–69]. The heart rate is again the only output of these methods and they are not applicable for higher content phenotypic assessments. Measuring the electrical activity of the isolated heart of *Drosophila* larvae and adult flies using microelectrodes has also been used to

obtain heart rate information [183,184]. **The implementation of electrodes requires dissection and is technically challenging for long-term measurements.**

Optical coherence tomography (OCT) is a noninvasive imaging technique that enabled the measurement of different heartbeat parameters on immobilized zebrafish and flies [75,185,186]. Researchers applied different image segmentation algorithms along with convolutional neural networks (CNN) on OCT images which enabled semiautomatic [70] and automatic [71,72] segmentation of the heart chamber to facilitate heartbeat counting. However, the **OCT technique requires highly specialized equipment with a limited spatial resolution as the imaging depth of OCT impedes access to the inner organs of the larva. Moreover, live recording duration with OCT is limited to short periods, which can be inadequate if symptoms are infrequent** [70,71,186].

Various digital image analysis tools have been proposed to partially or fully automate cardiac screening in fruit fly and zebrafish [74,75,77,178,187–195]. Berh et al. [77] introduced an automated *in-vivo* heartbeat detection algorithm for *Drosophila* pupae based on frustrated total internal reflection (FTIR). In this method, the contraction of the pupal heart in a video was detected from the movement of the surrounding fat body tissue which results in intensity variation. Although the FTIR-based imaging method enables high-throughput imaging of *Drosophila* pupae, it only provides heart rate and was not tested on *Drosophila* larvae. Semi-automated optical heartbeat analysis (SOHA) was proposed by Fink and Cammarato [74,75]; a method in which functional parameters of *Drosophila* heart can be determined from high-speed video files. SOHA was tested on close-up movies of dissected adult fly hearts and could measure heart rate, diastolic and systolic intervals, systolic and diastolic diameters, percent fractional shortening, contraction wave velocity, cardiac arrhythmicity, and contraction and relaxation phases. Using the optical flow algorithm (OFA), Mönck et al. [178] proposed an extension of SOHA to extract other features including lateral and axial direction and amplitude of movements of the dissected heart tube. The accuracy of SOHA and OFA depends on the quality, magnification, and speed of the recorded videos. In these methods, **a dissection phase is required before recording the videos**. In addition, manually marking the heart wall positions at systolic and diastolic states and selecting a ROI may affect the results. These approaches have not been tested for *in-vivo* monitoring of intact

Drosophila heart which is needed in long-term investigations of the heart function after certain treatments.

Some software have been developed for zebrafish analysis that may be applicable to *Drosophila* as well. De Luca et al. [187] proposed the ZebraBeat software for evaluation of heart rhythm in transgenic zebrafish embryos. In this method, a resonant laser-scanning confocal microscope was used to record sequential images and the heart function was quantified by tracking the movement of the heart edges and/or counting the blood cell content in heart chambers during cardiac cycles. Although the method allowed flexibility, reproducibility, and high throughput, an expensive confocal microscope was required to measure the heart rate of zebrafish. Lin et al. [189] used an image processing technique to analyze the heart rate of zebrafish larvae. Fluorescent images of larvae laterally trapped in a microfluidic device were used for automated detection of the heart area. The fluctuation of the heart area was quantified to derive the heartbeats. **Their algorithm was only applicable for fluorescently labeled hearts.** In another work, image analysis was used to detect the living status of a zebrafish embryo. To achieve this goal, the area around the heart was identified and periodic grey-level variations in this area, corresponding to a heartbeat, were determined**. However, the video analysis was only performed on anesthetized embryos** [191]. There is still a need for a method that enables automatic detection of the heart and phenotypic measurement of heartbeat parameters in intact zebrafish larvae without the need for anesthetization or fluorescent labeling.

Multiple microfluidic devices have been proposed to enhance manipulation and reversible immobilization of intact fruit flies and zebrafish larvae on a chip [45,84,196,197]. However, heart rate analysis in most of these devices remains manual. **Automatic detection and accurate quantification of intact larval heart activities using microfluidics and optical microscopy remain challenging** (Obj. 2). This is mostly due to small movements associated with the organisms' flexibility, loose immobilization for reversibility, and suspended internal organs which lead to non-stationaries like intense noises and undesired low-frequency trends in heartbeat signals. Non-stationarities can distort the signal in time- and frequency-domains [76]. Different signal processing methods were proposed to remove the undesired trends and noises from biomedical signals such as electrocardiogram (ECG) and electroencephalogram (EEG) signals [78,79], which may also be applicable to organism-based heartbeat signals.

Table 2-1. Overview of Open-Source Software, algorithms, and methods for the analysis of Drosophila and zebrafish heart function

Software/ Authors name	Animal stage	Preparation Prerequisite	Operative system/program	Types of analyses	Noise reduction methods	Analyzable files	Measured parameter	Level of Automation	Accuracy in heartbeat detection	Webpage	Reference
Johnson et al., Zornik et al, White et al., Nikoh et al., Wasserthal et al.	Drosophila pupae (P1) and adult fly	Phototransistors	Windows	Using phototransistor to monitor changes in light intensity. Resulting voltage changes were amplified and recorded digitally	-	-	HR	Automated	-	https://link.springer.com/article/10.1007/s00360005005 1	[66–69,198]
Papaefthimiou et al., Ocorr et al.	Drosophila adult fly	Dissection	Windows	Measuring the electrical activity of the isolated heart using microelectrodes	-	-	HR	Automated	-	https://pubmed.ncbi.nlm.nih.gov/11573820/	[183,184]
Guo et al., Lee et al., FlyNet 2.0/ Dong et al.	Drosophila adult fly [70,71][72], early pupae, and larvae [72]	OCT system and anesthesia for adult flies	Windows/MATLAB	OCT images were analyzed using image segmentation algorithms [70–72], histogram-based thresholding algorithms [70], a supervised learning method [71] and neural network analysis [72] to detect the heart chamber	Threshold setting	OCT image sequences	- HR, HP [70–72] - EDD, ESD [70,72] - DI, SI, EDA, ESA, AI, FS [70];	Semi-automated, the inner margin of the heart chamber should be marked manually [70]; Automatic [71,72];	Not reported [70,71]; 92% [72]	_____	[70–72]
Paternostro et al.	Drosophila adult fly	Anesthesia	Not reported	Intensity variation analysis along a line segment of pixels crossing the heart tube	Low-pass filter	Image sequences (format is not reported)	HR	Semi-automated, Manual selection of a line across the ventricular lumen is required	-	https://www.ahajournals.org/doi/10.1161/hh1001.090857	[177]
Berh et al.	Drosophila pupae	FIM imaging device [199]	Windows/ C++, MATLAB	Intensity variation analysis from the automatically detected most contractile heartbeat region	Extraction of the heartbeat signal from the most salient heartbeat region only, the one-dimensional AF and SGF	Image sequences (format is not reported)	HR	Automatic	~95%	https://www.uni-muenster.de/PRIA/en/forschung/index.shtml	[77]

Mönck et al.	*5- to 7-day-old flies*	*Dissection*	*Windows/ MATLAB*	*Measuring the direction and magnitude of movements of a dissected heart tube using the optical flow algorithm (OFA)*	*Threshold setting, Manual ROI selection*	*AVI video files*	*HR, FS, CV, SV, CO, DI, SI, CP, IP, RP, velocity of the peristaltic wave*	*Semi-automated, Manual selection of ROI, shortening and lengthening times, and heart wall positions for diameter measurements is required*	-	*https://github.com/hmoenck/OFAnalysis_supplementary*	[178]
SOHA/Fink et.al.	*Drosophila adult fly, 2–3-day old zebrafish larvae*	*Dissection for Drosophila and immobilization for zebrafish*	*Windows/ Stand-alone MATLAB-based application*	*Intensity variation analysis of frames and individual pixels and manual marking of the heart wall positions*	*Threshold setting, High- and low-pass filter, manual ROI selection*	*Black and white AVI and CXD files*	*HR, DI, SI, EDD, ESD, FS, contraction wave velocity, and AI*	*Semi-automated, Manual selection of ROI, shortening and lengthening times, and heart wall positions for diameter measurements is required*	-	*http://www.sohasoftware.com/download-soha.html*	[74,193]
HeartBeat/ Gierten et al.	*unhatched zebrafish embryos (24-72 hpf)*	*A stationary plate holder combined with moving optics*	*Windows, MATLAB*	*Segmentation, feature extraction by calculating the standard deviation in identified segments over time, spectral analysis and classification of heart regions*	-	*Image sequences (format is not reported)*	*HR and rhythm*	*Automatic*	-	*https://osf.io/kygd4/*	[200]
Kang et al.	*Zebrafish embryos and larvae*	-	*Not reported*	*generate a mask and extract the brightness intensity of each video frame inside the half-heart mask to form heartbeat-signal and calculate the HR*	*High-pass filter (Empirical Mode Decomposition (EMD))*	*Video files (format is not reported)*	*HR*	*Automatic*	*~99%*	*https://github.com/mbilab/zebrafish.*	[201]
ZebraBeat/ De Luca et al.	*Zebrafish embryos*	*Embryos should be anesthetized; the heart of the double fluorescent transgenic zebrafish embryos should be imaged using a confocal*	*MATLAB*	*Image segmentation for the identification of the cardiac chamber wall, Calculation of (a) the area enclosed within the segmented region at each time frame and extraction of the time history of the enclosed area, or of (b) the blood pool content at each time frame, Extraction of the time history along with the cardiac phases*	-	*Sequential images acquired with a resonant laser-scanning confocal microscope*	*HR*	*Semi-automatic*	-	*Available upon request*	[187]

		resonant scanner									
Lin et al.	*5-8 dpf zebrafish larvae*	*Transgenic zebrafish lines*	*Image processing*	*Acquisition of fluorescence images, application of a threshold to generate a binary template, quantification of the fluctuation for ROIs to derive heartbeat counting*	-	*Sequential fluorescent images*	*HR*	*Automatic*	-	-	[189]
Pylatiuk et al.	*36–120 hpf zebrafish embryos*	*Treatment of embryos with 0.003% PTU (1-phenyl-2-thiourea) to prevent pigment formation*	*MATLAB*	*Intensity variation analysis to acquire a unique region of the heart*	-	*Video files (format is not reported)*	*HR and beat to beat variability*	*Automatic*	*>97%*	-	[190]
Puybareau et al.	*7-9 dpf zebrafish larvae*	*Anesthetized larvae*	*Python 2.7 environment under Windows 7*	*Intensity variation analysis*	-	*Video files (format is not reported)*	*Cardiac arrest*	*Automatic*	-	-	[202]
Malone et al.	*30 hpf zebrafish embryos*	*Anesthetized fish embryos*	-	*Laser-scanning velocimetry*	-	*High-quality images captured using an Olympus Fluoview FV1000 laser scanning microscope with an Olympus PlanApo N lens using DIC optics*	*HR and Stroke volume*	*Automatic*	-	-	[194]

Chan dt al.	*52 hpf zebrafish embryos*	*anesthetization, followed by mounting embryos in agarose of low concentration*	*C# language*	*Power spectral analysis and Short-time Fourier Transform (STFT) analysis*	-	*RGB colored video frame*	*HR, rhythmicity index, beat to beat interval variability*	*Automatic image analysis and data analysis*	-	-	[188]
SmallHeart / Zabihihesari et al.	*Drosophila and zebrafish larvae*	*Immobilization using microfluidic devices*	*Windows/ Stand-alone MATLAB-based application*	*Intensity variation analysis from the automatically detected most contractile heartbeat region and Manual marking the heart wall positions on the M-mode*	*Threshold setting, High- and low-pass filter, manual ROI selection, SGF, SPA*	*AVI, MP4, 3gp, MOV, and MKV video files*	*HR, HP, EDD, ESD, FS, AI, SD, and ST of Drosophila larvae and HR, HP, and AI of Zebrafish*	*Semi-automated, Manual selection of heart wall positions for diameter measurements is required on the M-mode, selectable ROI is optional*	*94.5% for 20 fps videos and 98.86% for 100 fps videos*		

FIM, FTIR-based Imaging Method; AF, average filter; SGF, Savitzky-Golay-Filter; HR, heart rate; HP, heart period; EDA, end-diastolic area; ESA, end-systolic area; DI, diastolic interval; SI, systolic interval; AI, arrhythmicity index; FS, fractional shortening; CV, Cardiac volume; SV, Stroke volume; CO, Cardiac output; CP, Contraction phase; IP, isometric phase; RP, Relaxation phase; SD, shortening distance; ST, shortening time; SPA, smoothness priors approach

2.5 Chemical and Gene Screening Studies in *Drosophila*

Our first two objectives of in this thesis were develop a microinjection tool and a software for *Drosophila* larvae cardiac studies. In Obj. 3, we aimed to apply these tools to chemical and gene screening. For this, we selected surrogates of neurotransmitters and heavy metals to be serotonin, zinc and cadmium, respectively. The existing literature on the effect of these reagents on *Drosophila* is reviewed in the following sections, and the gaps are bolded.

2.5.1 Effect of Serotonin on *Drosophila* Heart Function

Serotonin is a neurotransmitter found primarily in the brain, enterochromaffin tissue and blood platelets and is involved in the nervous system cells communication[203]. It has been shown that serotonin has a decisive role in psychiatric and nonpsychiatric states such as depression, anxiety, aggression, pain, sleep, and migraine [204]. Taking some medicines such as antidepressants may change the body's level of serotonin and cause a group of symptoms which is known as serotonin syndrome. Studies on vertebrates have shown that serotonin has various cardiophysiological effects [203]. For instance, a dose-dependent increase in pulmonary artery pressure, pulmonary vascular resistance, cardiac contractility, and stroke volume was observed in dogs [205] and arterial thrombus and regulation of heart rate was reported in rats [206] and humans [207].

Previous attempts to reveal the possible effect of neural transmitters (e.g. serotonin, octopamine) and peptides on the heart rate of *Drosophila* were performed on pre-pupal, pupal, and adulthood stages [12,67]. In adulthood stage, **the animal was anesthetized for injection** and heart monitoring *in-vivo* **or was dissected** to study the innervation of the adult abdominal heart *in-vitro* [12,67]. **The results demonstrated that the heart in adult flies is neurogenic due to a pair of nerves innervating cardiac chambers and alary muscles**, which connect the heart tube to the cuticle in a flexible manner and support the heart tube in the body cavity [9]. These nerves are formed during metamorphosis in pupal stage. The injection and observation of heart in pupal stage is easier compared to motile larvae; **however, because of the dramatic morphologic and physiologic changes of the heart which occur during pupation, the heart activity in pupal stage**

is not representative of larval cardiac physiology. Yet, the effect of serotonin on the heart rate of intact *Drosophila* larvae has not been investigated (Obj. 3a).

2.5.2 Heavy Metals Toxicity and the Effect of MTF-1 on *Drosophila*

Heavy metals are a group of materials that possess a relatively high density of more than 5 g/cm3 [208]. Some heavy metals are highly toxic with no established biological function, e.g., cadmium (Cd), lead (Pb), and mercury (Hg) [80,209]. Some other heavy metals like zinc (Zn), iron (Fe), and magnesium (Mg) are essential elements of many biochemical and physiological processes at low concentrations while posing cellular and tissue damage when exceeding a threshold concentration [80,209].

Integration of epidemiologic, toxicologic, and clinical evidence has proved that Cd is a potential risk factor of cardiovascular diseases (CVDs), the leading cause of death globally [210–213]. Measurements of Cd concentration in blood and urine has demonstrated a positive association between Cd concentration with CVDs such as hypertension, myocardial infarction, coronary heart disease (CHD), heart failure, atherosclerosis, and peripheral artery disease (PAD) [210–212,214].

In human, exposure to high levels of Zn could cause several cardiovascular symptoms including premature atrial beats, hypertension secondary to intravascular volume, hypovolemic shock (pulse over 120 beats per minute) and hypertension [215]. Excessive and chronic Zn supplementation can lead to copper (Cu) deficiency, a risk factor for cardiomyopathy [216–218]. Measurements of Zn concentration in cardiac and skeletal muscles of dystrophic hamsters with advanced hypertrophic cardiomyopathy has revealed the possible pathogenetic involvement of Zn in muscular dystrophy [219]. Moreover, human exposure to airborne particulate matter (PM) can cause adverse cardiovascular effects, and water-soluble Zn is a major element detected in PM [220]. Kodavanti et al. [221] demonstrated that water-soluble Zn is one of the causative PM components causing several cardiac injuries in rats.

Metallothioneins (MTs) are a family of intracellular, low molecular weight, cysteine-rich proteins with a remarkable ability to bind essential and non-essential metals. MTs are considered one of the metal-homeostatic mechanisms in living organisms that diminish heavy metal toxicity by regulating cellular metabolism and storage of metal ions. Metal responsive transcription factor (MTF-1) protein is the primary activator of metallothionine genes [222]. MTF-1 is evolutionarily conserved between

insects and mammals and controls the transcription induction of MTs in response to various stress conditions, primarily exposure to heavy metals but also hypoxia or oxidative stress [222,223]. Significant efforts have been made to understand how the metal-dependent activity of MTF-1 is regulated. Developing transgenic animal models in which the MTF-1 is knockout or overexpressed in different parts of the body significantly helped scientists understand the tissue-specific role of MTF-1 under various conditions. However, genetic manipulation of MTF-1 in mammalian models such as mice is challenging and may cause mortality. For instance, MTF-1 knockout mice die at the embryonic stage due to liver degeneration, while knockout of MTF-1 in *Drosophila* is not lethal [81,224].

By developing transgenic fly lines, heavy metal toxicity and the role of MTF-1 was investigated in the fruit fly [80,81]. *Drosophila* lacking MTF-1 survive well under normal conditions while are considerably sensitive to elevated concentrations of heavy metals [81]. Tissue-specific overexpression of MTF-1 was previously done in *Drosophila* peripheral nervous system, motor neurons, gut, and hemocytes. MTF-1 overexpression in these tissues increased the lifespan on Cu, Fe, and Cd-supplemented media while sensitizing flies to Zn supplementation [80]. **Yet, the cardiac toxicity of heavy metals on intact animals and the role of MTF-1 in defense against heavy metal toxicity, specifically in the heart, has not been investigated** (Obj. 3a and Obj. 3b). Moreover, **Toxicity assessments using *Drosophila* are mostly based on oral administrations due to the feasibility and affordability of the feeding assay compared to microinjection**. **The exact amount of chemicals taken up by the animal in feeding and perfusion administration pathways is not well controlled**. **Moreover, the enzymatic, cellular, and tissue barriers present in the saliva and digestive tract of *Drosophila* prevent the translocation of heavy metals from the digestive tract into the hemolymph, thereby limiting the systematic exposure of the internal organs, including the heart tube** (Obj. 3a and Obj. 3b). [60,61,225,226]. Microinjection following with heart monitoring of larvae can be used to investigate the acute cardiac toxicity of heavy metals and the role of MTF-1 against cardiac toxicity in genetically modified flies (Obj. 3a and Obj. 3b).

Chapter 3

MATERIALS AND METHODS[*]

We aimed to design a low cost, multi-tasking, and easy to use device that allows a) delivering controlled dosages of chemicals into specific sites of *Drosophila* larva's body and b) high quality imaging/monitoring the heart function to perform precise cardiac toxicity and cardiac gene screening assessments by quantifying several heartbeat parameters *in-vivo*. This was achieved by integrating several components into one microfluidic chip. The loading, orientation, and immobilization of the larvae were performed pneumatically, and CPM was considered as the injection method. All the components can be integrated with microvalves and computer-based control modules to enable automatic loading, orientation, injection, heart monitoring, and other manipulation treatments if needed.

[*] Contents of this chapter have been collected from the published journal articles (permissions acquired and presented in the following):

- A. Zabihihesari, A.J. Hilliker, P. Rezai, Localized microinjection of intact Drosophila melanogaster larva to investigate the effect of serotonin on heart rate, *Lab Chip*. (2020) 343–355.
- A. Zabihihesari, A. Khalili, A.J. Hilliker, P. Rezai, Open access tool and microfluidic devices for phenotypic quantification of heart function of intact fruit fly and zebrafish larvae, *Comput. Biol. Med*. 132 (2021) 104314.
- A. Zabihihesari, S. Parand, A.B. Coulthard, A. Molnar, A.J. Hilliker, P. Rezai, An In-Vivo Microfluidic Assay Reveals Cardiac Toxicity of Heavy Metals and the Protective Effect of Metal Responsive Transcription Factor (Mtf-1) in Drosophila Model, *SSRN Electron. J*. (2022) 1–33.

Moreover, to reduce the cost of the experimental setup, the microinjection module was custom designed based on the most common laboratory component, including solenoid valve, function generator, regular pressure gages, etc., which can be assembled effortlessly while preserving the accuracy and precision in the process.

Our heartbeat quantification software has been developed as an open-access user-friendly tool to quantify several heartbeat parameters *in-vivo*. The amenability of the software to be used for small organisms (i.e., *Drosophila* and zebrafish) trapped in microfluidic chips have been tested.

3.1 Materials

3.1.1 Fly culture and Maintenance

Drosophila melanogaster were cultured in plastic fly stock bottles under uncrowded conditions at room temperature (22 ℃) on a 12 h:12 h light:dark photoperiod. The standard *Drosophila* yeast media was prepared as described in [80] and contained 100 g of sugar, 50 g of dry yeast, 18 g of agar, 8 g of sodium potassium tartrate tetrahydrate, 1 g of potassium phosphate monobasic, 0.5 g of sodium chloride, 0.5 g of calcium chloride dihydrate, 0.5 g of magnesium chloride hexahydrate, 0.5 g of iron (III) sulfate hydrate, 5ml of propionic acid and 2 g of methyl 4-hydroxy benzoate (2 g dissolved in 20 ml of 95% ethanol) dissolved in 1 L of tap water. Before conducting the experiments, adult flies were removed from the bottle and an individual 2nd or 3rd instar larva was transferred into a Petri dish containing phosphate-buffered saline (PBS). Then, a loading glass capillary was used to load the larva into the microfluidic chip for microinjection and heart monitoring.

3.1.2 Fly Stocks and Strains

Both wild-type rosy+5 and heart-specific MTF-1 overexpressing larvae (Fig. 3-1) were used in our experiments. We used the GAL4-UAS binary expression system to induce the expression of MTF-1 transgene in the heart of wild-type *Drosophila* larvae. This system consists of the GAL4 gene encoding the yeast transcription activator protein GAL4 and the UAS (Upstream Activation Sequence), an enhancer where GAL4 specifically binds to activate gene transcription. The target gene is silent in the absence of GAL4. To activate the target gene in a cell- or tissue-specific pattern,

flies carrying the target (UAS-Gene X) should be crossed to flies expressing GAL4. The GAL4 line used in this study was NP1029-GAL4 driver expressed in the larval heart [48]. The NP1029-GAL4 line was obtained from the Kyoto Stock Center (stock number 112459). The UAS-MTF-1 and UAS-GFP flies were obtained from Dr. Arthur Hilliker's laboratory at York University and created by Bahadorani et al. [80].

Green fluorescent protein (GFP) expression was used to assess the tissue specific overexpression of MTF-1 using the NP1029-GAL4 driver. Fig. 3-1A shows the non-expressing-GFP cardiac tube in wild type larvae. On the other hand, Fig. 3-1B demonstrate that the cardiac tube was properly labeled with NP1029-GAL4-driven membrane bound GFP. To quantify the GFP expression, the mean GFP intensity of the background ($I_{background}$) was subtracted from the mean intensity of a region of interest (ROI) around the heart (I_{ROI}) and normalized to the mean GFP intensity of the background ($\frac{I_{ROI}-I_{background}}{I\_background} \times 100$). The heart-specific MTF-1 overexpressing larvae (NP1029-GAL4:MTF-1) will be briefly called MTF-1 larvae in this thesis.

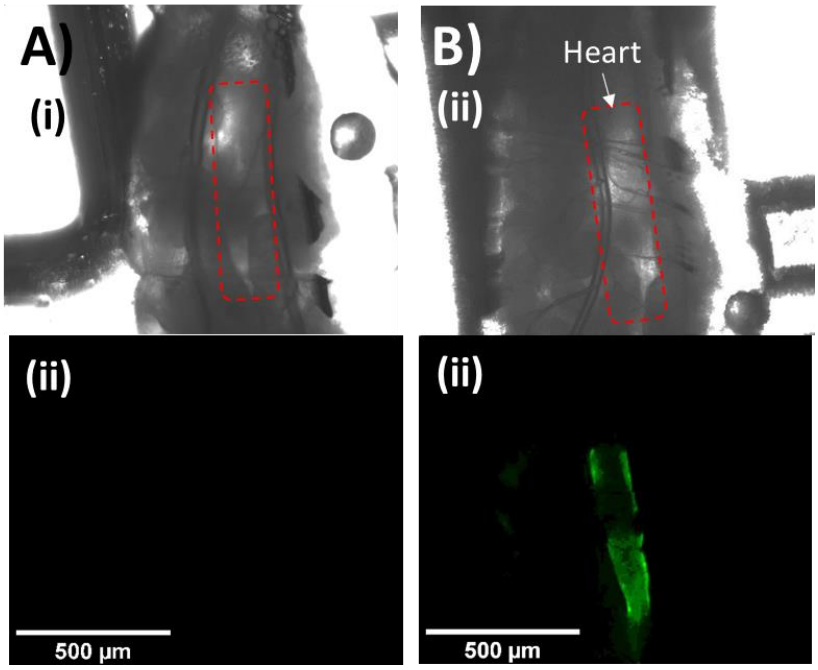

Figure 3-1: Qualitative GFP expression in the heart of 3rd instar Drosophila larvae. A) The wild type larva under bright field microscope (i) and the non-expressing-GFP cardiac tube under fluorescent microscope (ii) are shown. B) The heart-specific GFP overexpressing larva under (i) bright field microscope and (ii) the GFP expressing heart under fluorescent microscope. The heart tube was properly labelled with NP1029-Gal4-driven membrane bound GFP.

3.1.3 Chemicals and Reagents

Cyanoacrylates glue (LePage Ultra Gel, Henkel, Canada) was used for glue-based immobilization as the control experiment while the effect of microfluidic-based immobilization on cardiac activity of larvae was being investigated. Corn oil was used for characterization of the reagent delivery system.

A modified physiological saline was made as the drug carrier solution that contained 4 mM $MgCl_2$, 2 mM KCl, 1.8 mM $CaCl_2$, 128 mM NaCl, 36 mM sucrose, 5 mM Hepes, and 0.01% BSA, with a pH of 7.2.

Serotonin (P#14927-25MG, Sigma Aldrich, USA), $CdCl_2$ (Part #655198-100G, Sigma Aldrich, USA), and $ZnCl_2$ (Part #208086-100G, Sigma Aldrich, USA) were dissolved in the drug carrier solution to prepare the serotonin solution with concentrations of 0.001 mM, 0.01 mM, 0.1 mM, and 1mM, the Cd solution with a concentration of 10 mM and the Zn solution with concentrations of 10 mM and 100 mM (Table 3-1).

Table 3-1: The list of chemicals and concentrations used in microinjection assay

Chemicals	Compound	Concentrations
Serotonin	$C_{10}H_{12}N_2O$	0.001 mM, 0.01 mM, 0.1 mM, 1 mM
Zinc	$ZnCl_2$	10 mM and 100 mM
Cadmium	$CdCl_2$	10 mM

A small dose of 0.1% sulforhodamine B sodium salt (Part #S1402-1G, Sigma Aldrich, USA) was always added to the final control, serotonin, and heavy metal solutions as a fluorescent tracer to visualize the injection under a fluorescent microscope.

3.1.4 Quantitative Real-Time PCR to Develop MTF-1 Strain

This work was done by Dr. Hilliker's lab, and is included here solely for the sake of thesis completion. RNA was purified from 3-day old male flies using the TRIzol protocol. 5 entire flies were used for the collection of 1 RNA sample. The quantitative polymerase chain reaction (PCR) was done with iTaq Universal SYBR Green One-Step Kit and Rotor-Gene Q. Kit instructions were

followed, except tubes were not centrifuged prior to being placed in Rotor-Gene Q and tubes were not sealed with optically transparent film. Each tube had a 20 µL reaction volume. The primers listed in Table 1 were used:

Table 3-2: The list of primers that were used for quantitative real-time PCR

Forward MTF-1 primer	5'-AAAGACGCAGCAGACCAAGT-3'
Reverse MTF-1 primer	5'-TGGGAATGATGGGCTTAGAG-3'
β-Tubulin L primer	5'-AACATCTGCTGGGTCAGCTC-3'
β-Tubulin R primer	5'-CCAACTGAACGCTGATCTCC-3'

A total of 4 replicates were done for each gene x RNA sample combination. Concentrations were calculated as $2^{\text{Ct of first β-Tubulin replicate} - \text{Ct of sample}}$. Relative gene expression was calculated as concentration/average β-Tubulin concentration from the same RNA sample. Statistical significance was assessed using a 2-tailed Student's t-test with unequal variance.

3.2 Microfluidic Device Design

The microfluidic chip (Fig.3-2A and 3-2B) consisted of a larva trapping channel which was surrounded by loading and orientation glass capillaries, side immobilization suction channels, and a microneedle insertion channel. The loading glass capillary (1.1 mm inner diameter) was used to load a single larva from a petri dish containing PBS into the trapping channel. The trapping channel (4 mm-long, 0.8 mm-wide, 0.8 mm-thick) loosely fitted a 3rd instar *Drosophila* larva (~0.6 mm diameter). The orientation glass capillary (0.4 mm inner diameter) was used to grab the head of the larva by applying a gentle suction and to adjust the position and orientation of the larva inside the trapping channel. The side suction channels (250 µm×250 µm cross-section) were designed to immobilize the larva pneumatically by applying a negative pressure. This design was inspired from another microfluidic device which was previously developed in our group for rotational manipulation of small organisms [23]. The chemical infusion channels in the previous design were replaced with a needle channel. The needle channel (1 mm diameter) provided a one-degree of freedom control of the microneedle during actuation.

3.3 Microfluidic Device Fabrication and Assembly

The microfluidic device was fabricated by replica molding of two PDMS layers, containing the network of above mentioned microchannels onto 3D-printed plastic master molds. In our previous device[23], one layer of PDMS containing the channel networks was bonded to a flat PDMS layer. In the new design, the channels were half-embedded in each PDMS layer to align the microneedle with the larva. The thickness of the microchannels were equal on both molds, such that the anterior-posterior axis of the larva and the needle axis were perpendicular and located on the same plane. Such a design allowed the microneedle to easily penetrate the larva while in our previous design, it could pass the larva without penetration, specially for early stage samples. PDMS base monomer was mixed with the curing agent (Sylgard 184 elastomer, Dow Silicon Co., USA) with a weight ratio of 10:1 and degassed in a vacuum chamber for 10 minutes. A plastic tube (P#96400-14, Cole-Parmer, Canada), as the outlet of side-suction channels, was placed on the top master mold layer. Then, the degassed PDMS pre-polymer was poured over the master molds and cured at 75°C. After 4 hours, the plastic tube firmly adhered to the solidified PDMS and the PDMS layers were peeled off from the molds. The top and bottom PDMS layers were bonded to each other, and then to a supporting glass slide (35×50 mm2, Fisher Scientific, USA) using oxygen plasma (Plasma Flo PCD-FMS and plasma cleaner PDC-001-HP, Harrick Plasma, USA). Finally, the loading (P#22-260-943, 1.1 mm inner diameter, Fisher Scientific) and orientation (P#1-000- 800, 0.4 mm inner diameter, Fisher Scientific, USA) glass capillaries were installed into the device.

Borosilicate glass capillaries (P#1B100F-4, 1mm outer and 0.58mm inner diameters, WPI, USA) with an initial length of 10 cm were pulled on a needle puller (KOPF Model 730, Tujunca, CA, USA) to fabricate microneedles with tip sizes in the range of 0.5-3μm, taper angles of ~10 degrees, and an overall length of 35 cm.

As shown in Fig. 3-2C, a 3D-printted (ProJet HD 3000, 3D Systems, USA) plastic fixture was designed and fabricated with three main modules, i.e., a needle holder, a movable block needle actuator, and a device holding module. The needle holder consisted of a dual removable needle (RN) coupler (P#55752-01, Hamilton, Nevada, USA) which was connected to a PEEK tubing (P#51085K44, McMaster-Carr, USA) using a set of RN compression fitting (P#55751-01, Hamilton, Reno, Nevada, USA). The PEEK tubing was connected to a solenoid valve, a pressure regulator,

and an air compressor. The needle holder was installed onto a designated hole inside the moveable block needle actuator. This assembly was installed onto the device holding module using a spring guide rod assembly which enabled a reversible axial movement of the needle. The microneedle was connected to the needle holder using another set of RN compression fitting (P#55750-01, Hamilton, Nevada, USA). Then, the microfluidic chip which was previously bonded to a glass slide was installed onto the device holding module through the designated groove and tongue joints, such that the microneedle was positioned inside the needle channel. The fixture was equipped with a micropositioner (P#8578A72, McMaster-Carr, USA) to actuate the moveable block with a ~5 µm resolution.

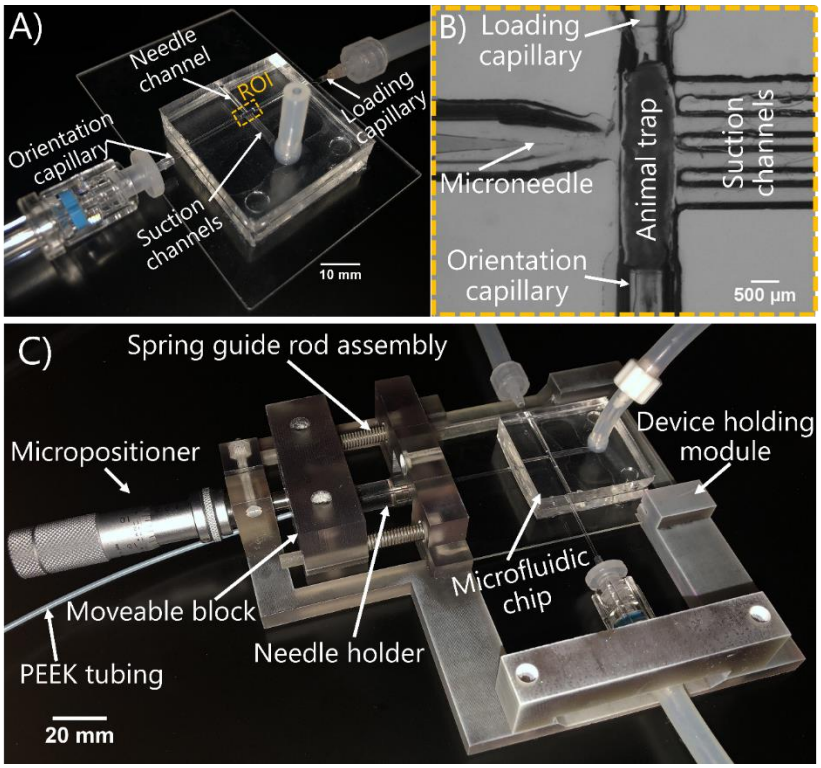

Figure 3-2: Microfluidic chip and setup for Drosophila melanogaster larvae microinjection. A) Microfluidic chip consisting of loading and orientation glass capillaries, a larva trapping channel, side immobilization suction channels and a needle insertion channel. B) Magnified region of interest (ROI) of the device. C) A 3D printed fixture equipped with a micropositioner for axial actuation of the injection microneedle. Figures reproduced by permission from the Royal Society of Chemistry.

3.4 Experimental Setup and Procedure

The experimental setup shown in Fig. 3-3A consisted of three main components, i.e., an animal manipulation unit, an injection unit, and a video acquisition and processing unit.

The animal manipulation unit comprised of two syringes connected to the loading and orientation glass capillaries, and a vacuum system providing a negative pressure at the side suction channels of the microfluidic chip. The vacuum system consisted of a vacuum pump (P# UN86KTP, KNF, USA), a vacuum gauge (0-30 inHg vac, Ashcroft Inc., Brazil), and a waste reservoir.

CPM technique was used for chemical delivery, where the microneedle penetrated the larva's cuticle and the injection substance was delivered from the microneedle into the larva's body upon a pressure pulse. The custom-made injection unit consisted of a pressure regulator (P# PR4021-200, Ingersoll Rand, Canada), a solenoid valve (P# 01540-11, Cole-Parmer, Canada), a power supply (SN B900655, Good Will Instrument Co., LTD. Taiwan), a function generator (SN AFG3022C, Tektronix, USA), and a custom-made MOSFET amplifier circuit (Fig. 3-3B). The microneedle was connected to the solenoid valve using the PEEK tubing. The solenoid valve was connected to the pressure regulator which reduced the input pressure of the air compressor to a desired value. A step function was generated using the function generator with the desired duration, an offset of 2.5 V, and a maximum amplitude of 5 VPP (peak-to-peak voltage). Signal amplification was used to enhance the voltage to 12 VPP, using the MOSFET switch, as needed for the solenoid valve.

The video acquisition unit consisted of an inverted microscope (BIM-500FLD, Bio- imager Inc., Canada), a camera (SN 14120187, Point Gray Research Inc. Canada), and a computer where the recorded videos were saved for further analysis. Animal manipulation was monitored under bright field microscopy at 2.5× magnification until the animal was immobilized. Then, the magnification was changed to 10× (to zoom on the heart tube), if necessary, and bright field microscopy was changed to fluorescent microscopy to track the distribution of the injectant which contained fluorescent dye. Recorded videos were analyzed for heart rate quantification using the heartbeat quantification software. Monitoring of the heart activity began 5 minutes after immobilization to eliminate the effect of stress. For each larva the heart rates were normalized based on the average heart rate one minute prior to injection which is called baseline heart rate.

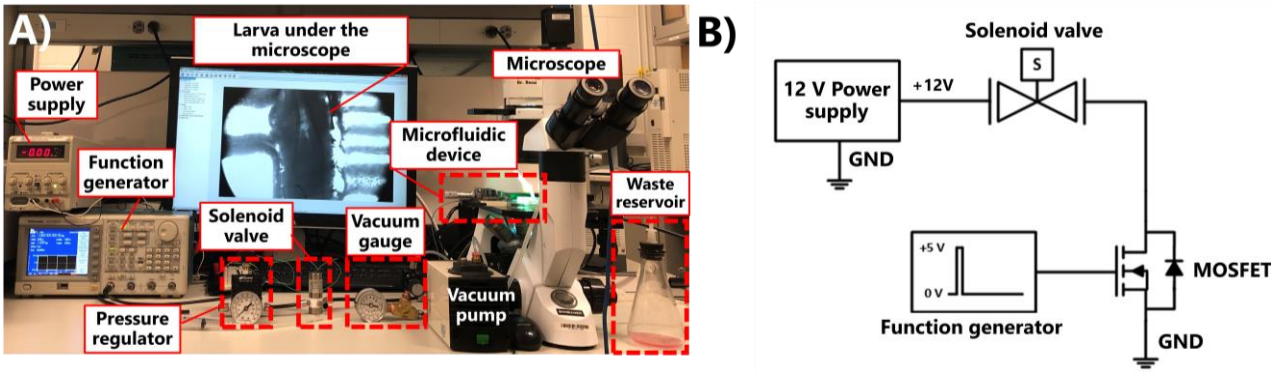

Figure 3-3: A) Experimental setup consisting of various components to inject and video-record the heart activities of Drosophila melanogaster larvae inside the microfluidic chip. A vacuum system including vacuum pump and waste reservoir was used for applying negative pressure to immobilize the larva inside the microfluidic chip. The power supply, function generator, pressure regulator, and solenoid valve were used to generate pressure pulses for the reagent delivery system. The microscope equipped with a camera was used for video recording the heart activity of the larva. B) Schematic of the custom-made MOSFET amplifier circuit, which connected the solenoid valve to the function generator and power supply. Figures reproduced by permission from the Royal Society of Chemistry.

When filling the microneedles with the injection substance, even small bubbles inside the microneedle could stop the injection. In order to fill the microneedles without air bubble formation, we used glass capillaries that had an internal filament for needle fabrication. After pulling the glass capillaries, the blunt end of the microneedle was placed into the injection liquid. The liquid was drawn up into the tip of the microneedle via capillary action in ~3 minutes. Then the rest of the needle was backfilled using a MicroFil (P# CMF90U, WPI, Sarasota, USA), a fused silica capillary coated with polyimide (Fig. 3-4). The filled microneedle was installed onto the needle holder and then coupled with the movable block and assembled with the custom-made fixture as described before.

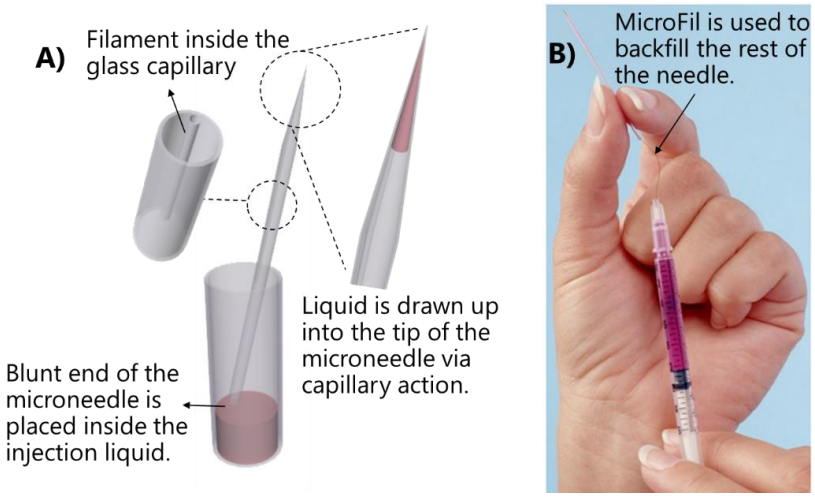

Figure 3-4: Illustration of the microneedle filling technique. A) The glass capillary with an internal filament was pulled and its blunt end was placed inside the injection liquid. After few minutes, the liquid was drawn up through the filament via capillary action and filled the tip of the microneedle. B) A MicroFil made up of a flexible fused silica capillary coated with polyimide was connected to a syringe containing the injection liquid and used to backfill the rest of the microneedle. Figures reproduced by permission from the Royal Society of Chemistry.

3.4.1 Characterization of the Reagent Delivery System

Capillary pressure microinjection (CPM) was used for reagent transport in the microneedle, which is based on a pressure-driven flow (PDF) using a controlled pressure pulse at the microneedle inlet. The delivered volume could be controlled with parameters such as the amplitude of the pressure pulse, the duration of the pressure pulse, and the size of the needle. Ideally, for a particular size of the needle, if the pressure amplitude and time stayed the same, all larvae were expected to receive the same amount of sample. However, after pulling the glass capillaries with controlled temperature and pulling rate, breaking the tip of the needles resulted in different tip sizes (0.5-3 µm inner-diameter). Therefore, characterization of the reagent delivery system with respect to the volume of the delivered reagent was normalized based on the needle size. To characterize the system, we injected the drug carrier solution into a petri dish containing corn oil and measured the diameter of the injected droplet using ImageJ [227]. The injected volume (V) in such a system was assumed to be a function of the pressure amplitude (P), pulse duration (t), needle tip diameter (d), injected liquid viscosity (μ_1), oil viscosity (μ_2), interfacial tension between the injected liquid and oil (σ_1), interfacial tension between air and injected liquid (σ_2), and the taper angle of the needle tip (α).

$$V = f(P, t, d, \mu_1, \mu_2, \sigma_1, \sigma_2, \alpha) \tag{3-1}$$

The Buckingham Π theory was used to find a correlation which could predict the volume of the injected droplet, V. Hence, Eq. 3-1 was written as.

$$\frac{V}{d^3} = f\left(\frac{Pd}{\sigma_1}, \frac{\mu_1 d}{t\sigma_1}, \frac{\sigma_2}{\sigma_1}, \frac{\mu_1}{\mu_2}, \alpha\right) \tag{3-2}$$

In this study, we investigated the effects of pressure amplitude, pulse duration, and inner diameter of the needles. Since the properties of air, water, and oil were constant, the Π groups $\frac{\sigma_2}{\sigma_1}$, $\frac{\mu_1}{\mu_2}$, and α were assumed to remain constant in our experiments, reducing the Π groups in Eq. (3-2) to $\frac{V}{d^3}$, $\frac{Pd}{\sigma_1}$ and $\frac{\mu_1 d}{t\sigma_1}$. The general power correlation in Eq. (3-3) with constants c1, c2 and c3 was considered for the dimensionless injected volume. The experimental data points representing the dimensionless injected volume are shown in Fig. 3-5.

$$\frac{V}{d^3} = c_1 \left(\frac{Pd}{\sigma_1}\right)^{c_2} \left(\frac{\mu_1 d}{t\sigma_1}\right)^{c_3} \tag{3-3}$$

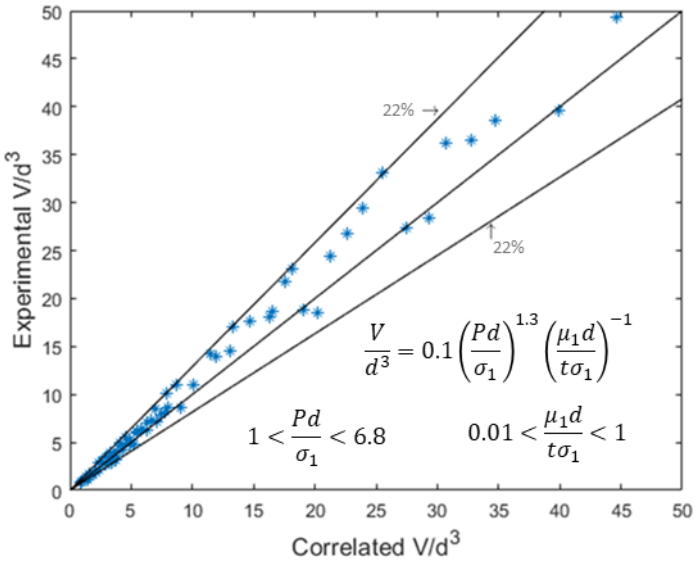

Figure 3-5: Comparison between the correlated dimensionless injected volume and the experimental results. P is pressure, t is pulse duration, d is needle tip diameter, σ_1 is interfacial tension between oil and injected liquid, and μ_1 is the viscosity of injected liquid. Figures reproduced by permission from the Royal Society of Chemistry.

The nonlinear least squares method was used to determine the constants c1, c2, and c3 in Eq. (3-3) based on the experimental data points. As a result, the following correlation was obtained for the dimensionless injected volume.

$$\frac{V}{d^3} = 0.1\left(\frac{Pd}{\sigma_1}\right)^{1.3}\left(\frac{\mu_1 d}{t\sigma_1}\right)^{-1} \tag{3-4}$$

Where the interfacial tension between oil and water and the dynamic viscosity of water were considered to be $\sigma_1 = 26.3\ \frac{\mathrm{mN}}{\mathrm{m}}$ and $\mu_1 = 1\ \mathrm{mPa.s}$, respectively [228,229]. This correlation corresponded reasonably with the experimental data. Based on this correlation and the diameter of the pulled needles, the pressure amplitude and pulse duration required to deliver 40 nL of the reagent were determined in various experiments.

We injected 40 nL of each solution close to the heart chamber of larvae using the microfluidic setup described in sections 3-2 to 3-4. We characterized the volume of injection such that it was large enough to be traceable under fluorescent microscopy and small enough to prevent possible damages to the heart tissue [84,89]. It is noteworthy that injection of higher volumes could cause long bradycardia followed by the mortality of larvae [84,89]. We pooled 10 randomly selected larvae and weighed them collectively on a scale. The measurement was done 4 times for 40 larvae. Individual larva's weight was 1.95 ± 0.02 mg which is consistent with values reported by other researchers [230]. Considering the injection volume (40 nL) and the larva's body weight (1.95 mg), we injected 10 mM and 100 mM $ZnCl_2$ and 10 mM $CdCl_2$, which are equivalent to 13.5 mg/kg and 135 mg/kg of Zn and 23 mg/kg of Cd per larval body-weight, respectively. This is in the range of the dose used by other researchers to assess the toxicity of heavy metals by injection in vertebrates [231–235] and large invertebrates [236].

3.5 Phenotypic Quantification of Heart Function of Intact *Drosophila* larvae

3.5.1 Automatic Detection of the Heart Region

After immobilizing the larva inside the microfluidic device, the heart activity was video recorded as described in previous sections (3.2 to 3.4). The recorded videos were analyzed using our MATLAB-based software which is was made available as an open-access user-friendly software called SmallHeart [19]. Detailed instructions for software installation are provided in Appendix A. In the graphical user interface (GUI) of the software, the user can select the video file, adjust the time period for analysis, define a scale for video frames, activate the M-mode option, and select a ROI manually, if desired (Fig. 3-6). *Drosophila* heart tube which is also called dorsal vessel is located underneath the dorsal epidermis and is surrounded by a pair of trachea and fat body (Fig. 3-7a). If the larva is rotated in the right direction and is properly immobilized, recording videos with 10x magnification provides a close-up view of the heart in which the heart edges are visible (Fig. 3-7b). In this case, the heart contraction results in a pixel intensity variation at the heart edges, and extraction of M-mode is possible. Otherwise, if the quality or magnification of the video does not provide a clear view of the heart edges, the movement of adjacent organs like the trachea or the fat body can be used for indirect quantification of heart rate and arrhythmicity.

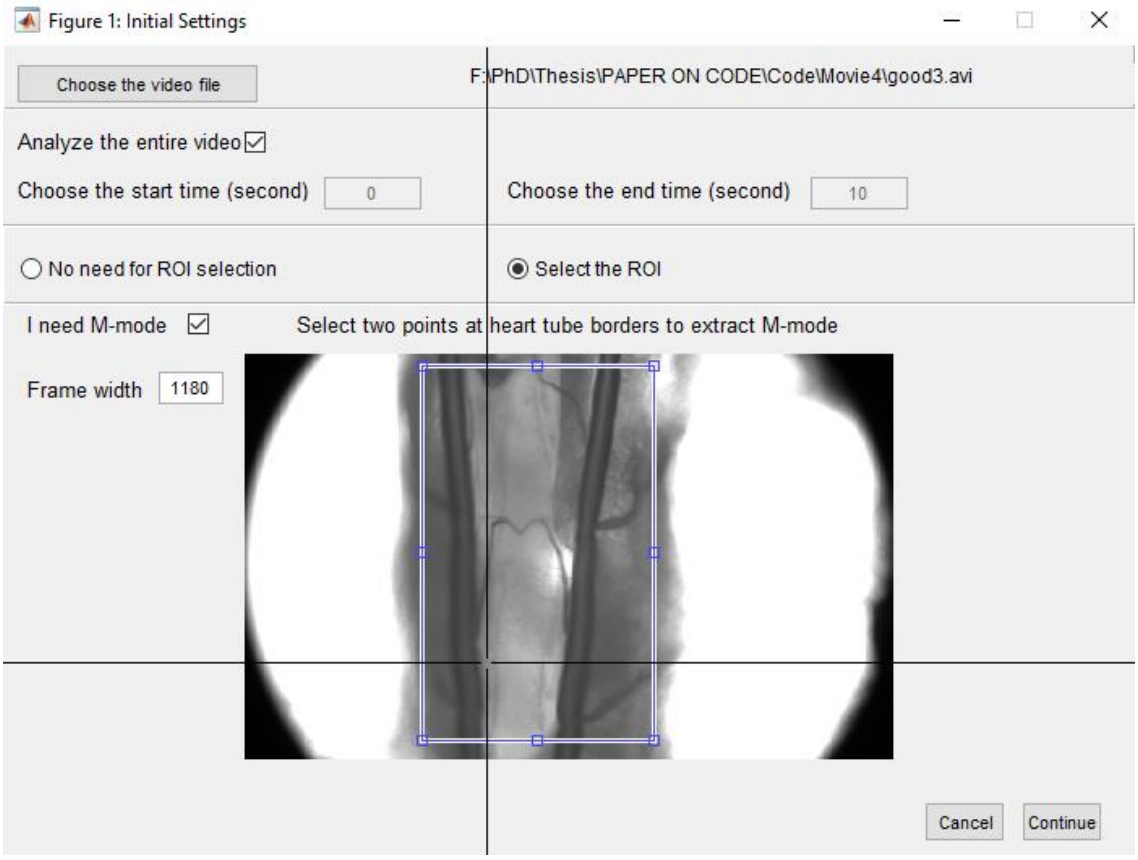

Figure 3-6: The GUI of the software showing the initial settings module after selecting the video. The user can analyze the entire video or adjust the time period for analysis. If needed, the user can select the ROI manually. If the M-mode is required, the user can check "I need M-mode" and select two points across the heart borders. Also, the frame width can be entered for calibration. Figures reproduced by permission from Elsevier.

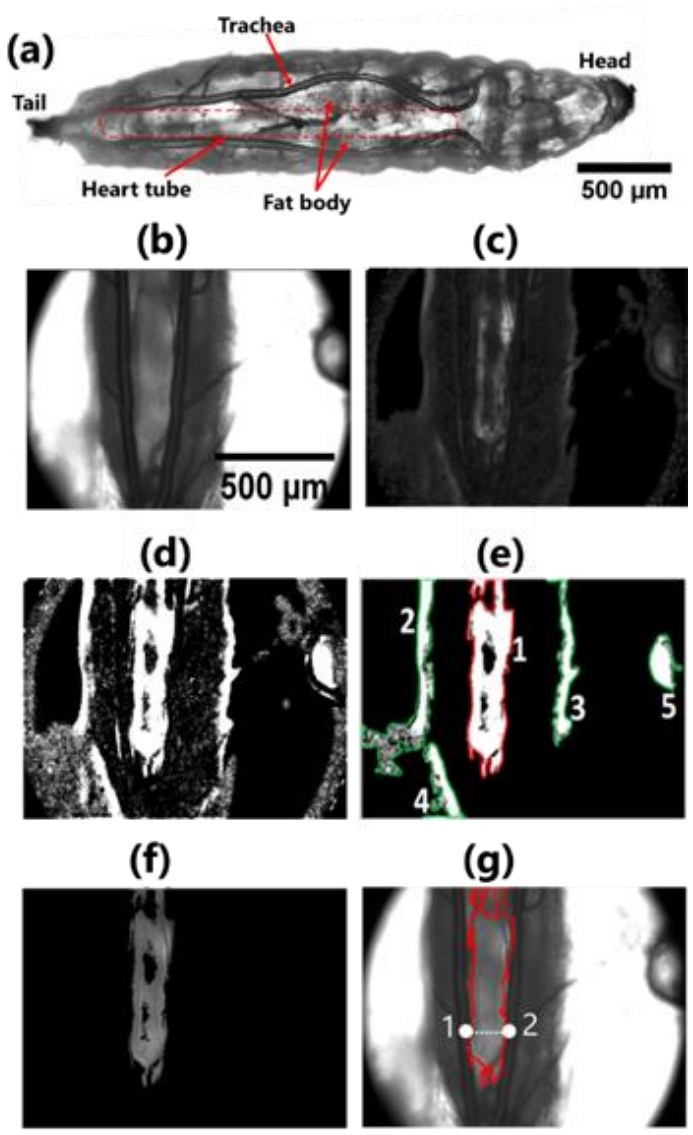

Figure 3-7: Automatic detection of the most contractile region of a 3rd instar Drosophila and 7 dpf D. rerio heart using our MATLAB-based SmallHeart software. The dorsal view of a transparent Drosophila larva under the microscope is shown at (a) 2.5x and (b) 10x magnifications. (c) The accumulated frame difference image for a 60 s video recorded with 100 fps. (d) The binary mask after performing thresholding (ζ=0.15) on the accumulated frame difference image shown in (c). (e) The connected components of the binary image with an area above the threshold ($\epsilon = 100$ pixels) which represents regions with the most significant moving parts of the video and are distinguished with different indices. (f) The larval heart tube masked by region #1 which represents the most contractile region of the heart tube. (g) The border of the most contractile region of the heart tube shown in the results menu of the software. Figures reproduced by permission from Elsevier.

To automatically extract the heartbeat signal with high accuracy, it is necessary to find the most contractile region of the heart. For this purpose, we adopted a method previously described by Berh et al. [77]. The accumulated frame difference image ($\bar{F}$) was calculated by summing up the absolute pixel intensity differences of two consecutive frames of the first three seconds of each video.

$$\bar{\mathrm{F}} = \sum_{n=1}^{N} |G(f_{n-1}) - G(f_n)| \tag{3-5}$$

where f_{n-1} and f_n are pixel intensity matrices of two consecutive frames, N is the total number of frames, and G is the two-dimensional Gaussian filter function used to blur edges and reduce the contrast of each frame. Fig. 3-7c shows the $\bar{\mathrm{F}}$ contour representing the accumulated pixel intensity changes for *Drosophila* larva. The bright regions indicate a frequent change in pixel intensity and reflect the most significant moving parts of the video.

A binary mask $\mathcal{M}$ (Fig. 3-7d) was produced by binarizing the grayscale image $\bar{\mathrm{F}}$ with a level ζ as:

$$\mathcal{M}(x, y) = \begin{cases} 1 & if \quad \bar{\mathrm{F}}(x, y) > \zeta \\ 0 & else \end{cases} \tag{3-6}$$

This split the image into separate black and white regions with different areas (Fig. 3-7d). Then, only those white regions having an area above the threshold ϵ were maintained and the rest were removed automatically (Fig. 3-7e). Afterward, an index was assigned to the remaining regions based on the value of $\bar{\mathrm{F}}$ calculated previously. The region with the highest pixel intensity changes was selected as the final mask and applied over the entire video (Fig .3-7f). This region represents the most contractile part of the video which is the heart of the organism (Fig. 3-7g).

3.5.2 Signal Processing: Detrending and Smoothing the Heartbeat Signal

The mean pixel intensity (mean gray value) of the most contractile region of the heart was calculated over time. To obtain a comparable value we normalized this signal to the interval of [0, 1] using Eq. (3-7).

$$Z = \frac{S_t - \min(S)}{\max(S) - \min(S)} \tag{3-7}$$

where S_t is the mean pixel intensity at time t. When recording the videos, small movements of the animal, movement of internal organs, or changes in environmental light led to undesired low-frequency trends presented in the raw heartbeat signal. The SPA method was used to remove the undesired trends in the raw signal. This method was used previously for human ECG signals [76] and has never been tested on small model organisms. In this approach, the raw heartbeat signal (Z) was considered to have two components as

$$Z = Z_{stat} + Z_{trend} \tag{3-8}$$

where Z_{stat} referred to the stationary component and Z_{trend} was the undesired aperiodic trend.

The stationary component of the heartbeat signal can be written as

$$Z_{stat} = Z - H\hat{\theta}_{\lambda} = (I - (I + \lambda^2 D_2^T D_2)^{-1})Z \tag{3-9}$$

where H is called the observation matrix. A trivial choice of identity matrix was used for the observation matrix (i.e., $H = I$). $\hat{\theta}_{\lambda}$ represents the estimate of regression parameters obtained by regularized least squares method with λ as the regularization parameter. D_2 is the second-order difference matrix. Eq. 3-9 can be written as $Z_{stat} = KZ$ in which $K = (I - (I + \lambda^2 D_2^T D_2)^{-1})$ is a time-varying finite impulse (FIR) filter with more details found in [76].

After detrending the signal, we used Savitzky-Golay-Filter (SGF) to smoothen the signal. This filter fits successive subsets of adjacent data points with a polynomial by the method of linear least squares in a specific window. This method can smoothen the signal without flattening or shifting the local maxima and minima of the signal. To implement this filter, the polynomial order k and the window size $\bar{\omega}$ should be determined such that $k < \bar{\omega}$ and k is odd. Both static bandpass filter and SPA detrending methods have been implemented in our software. The user can easily adjust the passband of the filter and the smoothing parameter (λ) of the SPA method in the result module of the software and check the results in both time and frequency domains (Fig. 3-8).

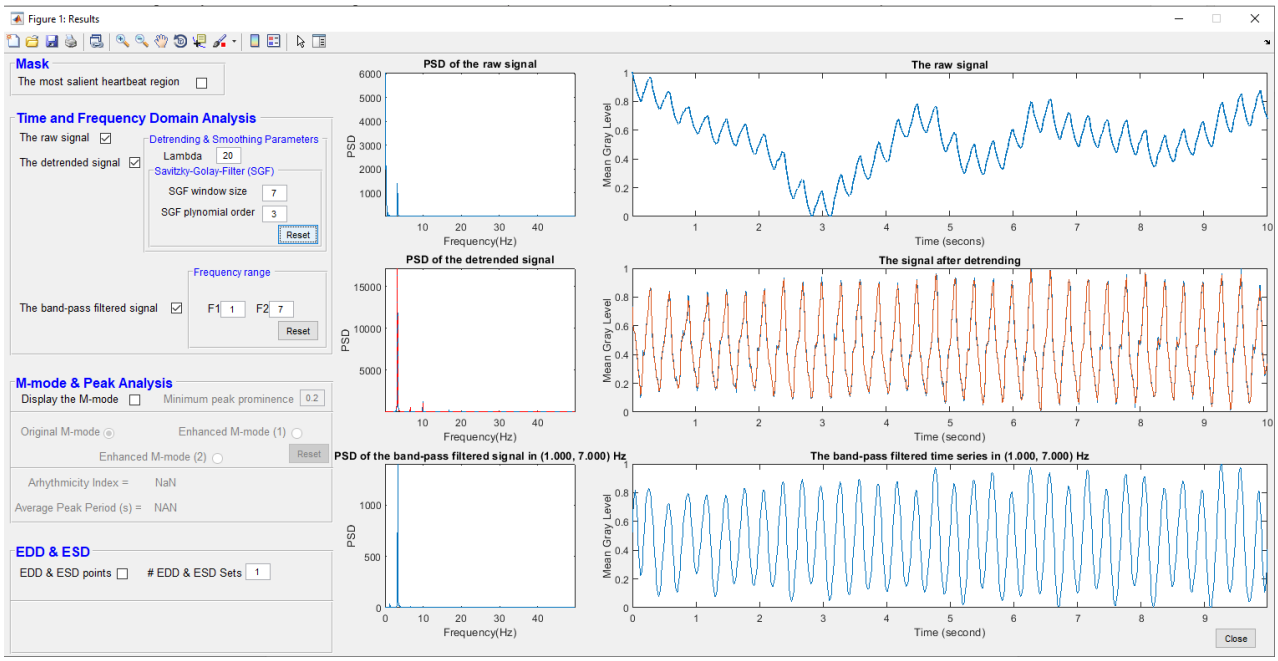

Figure 3-8: The results module of the software, for a 3rd instar Drosophila larvae, showing different heartbeat signal processing options in time (right) and frequency (left) domains. This includes the raw signal (top), the signal after detrending and smoothing (middle), and the signal after applying the bandpass filter (bottom). Figures reproduced by permission from Elsevier.

3.5.3 Peak Analysis and Extraction of M-mode

The heartbeat signal after detrending and smoothing still had multiple local peaks and valleys. Not all of these peaks represent a beat, i.e. only distinct peaks in the signal may refer to heartbeats. It should be noted that a small isolated peak may be more prominent than one that is higher but is surrounded by a range of tall peaks. Therefore, we needed to determine which peaks stood out and represented a heartbeat, based on the peak's intrinsic height and location relative to other peaks. For this purpose, we used the MATLAB implementation of a measurement called prominence which determines the dominance of each peak by measuring its height relative to other peaks. The prominence was calculated by the software as follows; First, all local peaks of the signal were selected (Fig. 3-9a). The neighborhood of each peak was determined by extending a horizontal line from the peak to the left and right. This line either crosses the signal because there is a higher peak or reaches the left or right ends of the signal. The minimum of the signal in the left and right sides of the peak in this neighborhood was found. The higher of the two minima was selected as the reference level. The height of the associated peak above this level was defined as the peak

prominence. In Fig. 3-9a, the small triangles show the local peaks, each pattern represents a neighborhood and the peak prominence for each peak is shown by a red arrow. By determining a minimum acceptable prominence p, we can remove the outliers and only keep the prominent peaks referring to heartbeats (those peaks surrounded by a circle).

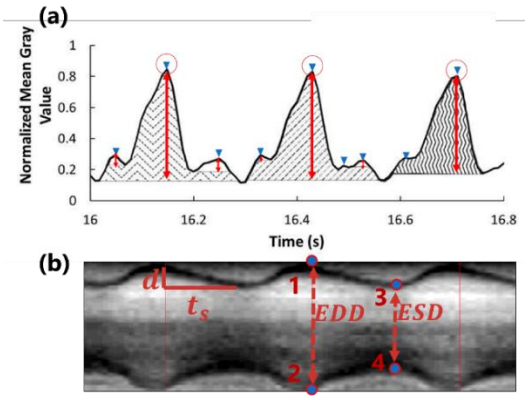

Figure 3-9: (a) Peak prominence calculation of the heartbeat signal. Arrows show the peak prominence and different patterns indicate the associated peak neighborhood. (b) The M-mode provides further information to check the accuracy of peak analysis and calculate the percent fractional shortening and shortening velocity. Figures reproduced by permission from Elsevier.

The user can also obtain the M-mode from the proposed MATLAB software, provided that the quality and magnification of the video allows extraction of the M-mode. In doing so, the user is asked to select two different points across the heart borders (Figs. 3-7g). These two points can be along a horizontal or vertical line, according to the direction of the animal in the video. Although the M-mode is not required for determination of the heart rate and cardiac arrhythmicity, it is required for calculation of percent fractional shortening and shortening velocity. Besides, M-mode can be used to check the accuracy of the peak analysis as shown in Fig. 3-9.

To increase the quality of the M-mode, we implemented two image enhancement techniques in the software which allow the user to increase the contrast of the original M-mode when needed (Fig. 3-10). In the enhanced M-modes, the borders of the heart are more visible which results in more accuracy in marking the diastole and systole phases. The first enhancement technique increased the contrast of the original M-mode by mapping the values of the original M-mode intensity image to new values such that 1% of the data became saturated at low and high intensities of the input data. The second enhancement technique was to perform histogram equalization on the intensity values of the original M-mode such that the histogram of the output intensity image was uniformly distributed.

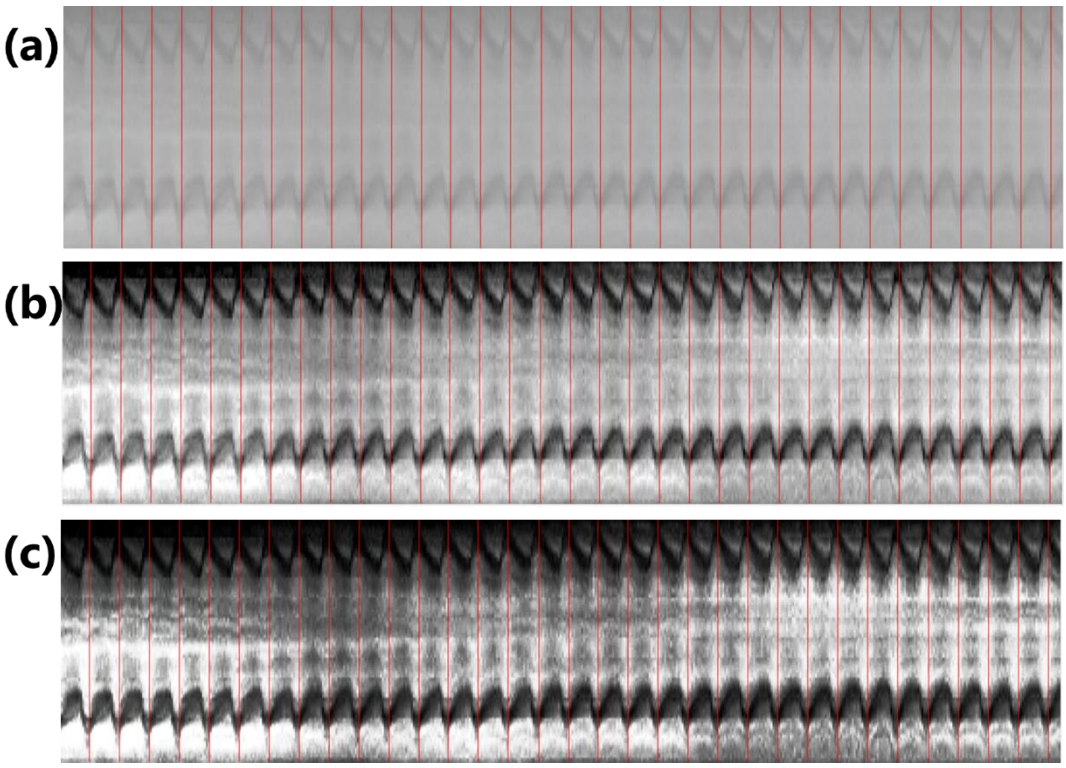

Figure 3-10: Different ways of displaying the M-mode for a 3rd instar Drosophila larva. (a) The original M-mode. (b) The first enhancement technique increases the contrast of the original M-mode by mapping the values of the original M-mode intensity image to new values, such that 1% of the data become saturated at low and high intensities of the input data. (c) The second enhancement technique performs histogram equalization on the intensity values of the original M-mode such that the histogram of the output intensity image is uniformly distributed. Figures reproduced by permission from Elsevier.

3.5.4 Performance Characterization of the MATLAB-based Software

To evaluate the performance of the software, we used a previously described method which is based on four metrics i.e., Recall (RE), Precision (PR), Accuracy (AC), and F-measure (F) used in binary detection and segmentation algorithms [71,72]. First, the ground truth (g) was determined by manually counting peaks from recorded videos. Then, the number of true positive (TP) was determined as the number of correctly detected peaks by the software. Consequently, the number of false-positive (FP) was determined as the number of detected peaks for which there is no label in g, and false-negative (FN) was determined as the number of labels in g for which no peak was detected by the software. Finally, RC, PR, AC, and F were calculated as

$$RC = \frac{TP}{TP+FP} \qquad (3\text{-}10)$$

$$PR = \frac{TP}{TP+FN} \quad (3\text{-}11)$$

$$AC = \frac{TP}{TP+FP+FN} \quad (3\text{-}12)$$

$$F = 2\frac{PR.RC}{PR+RC} \quad (3\text{-}13)$$

3.5.5 Quantification of Heartbeat Parameters

The heartbeat frequency (f) was measured as the peak frequency in the power spectral density (PSD) of the signal. The heart rate (HR) was defined as the number of beats per minute ($HR = \frac{60}{f}$). Cardiac arrhythmicity was quantified using the arrhythmicity index as $AI = \frac{\sigma(HP)}{\widehat{HP}}$, where HP is the heart period and $\widehat{HP}$ is the median of the heart period. HP was measured as the time interval between two consecutive peaks in the heartbeat signal.

To measure the end-diastolic diameter (EDD) and end-systolic diameter (ESD), the M-mode option had to be selected in the first GUI of the software. After loading the video, the user inserts the frame width in μm as a calibration parameter (Fig. 3-6). After processing the video, the diastole and systole phases were clearly shown in the M-mode and the user could measure the EDD and ESD by selecting two points for each parameter as shown in Fig. 3-9b. To reduce the error caused by manual selection of the points, the user could measure several EDD and ESD on the M-mode, and the software reported the average value (Fig. 3-11).

Percent fractional shortening (FS) is defined as the percent change in heart diameter during contraction of the heart and was measured as:

$$FS = \frac{EDD-ESD}{EDD} \times 100 \quad (3\text{-}14)$$

Shortening velocity (SV) can be calculated as $SV = \frac{d}{t_s}$, based on the shortening distance d and the shortening time t_s, obtained from the M-mode (Fig. 3-8b and Fig. 3-11).

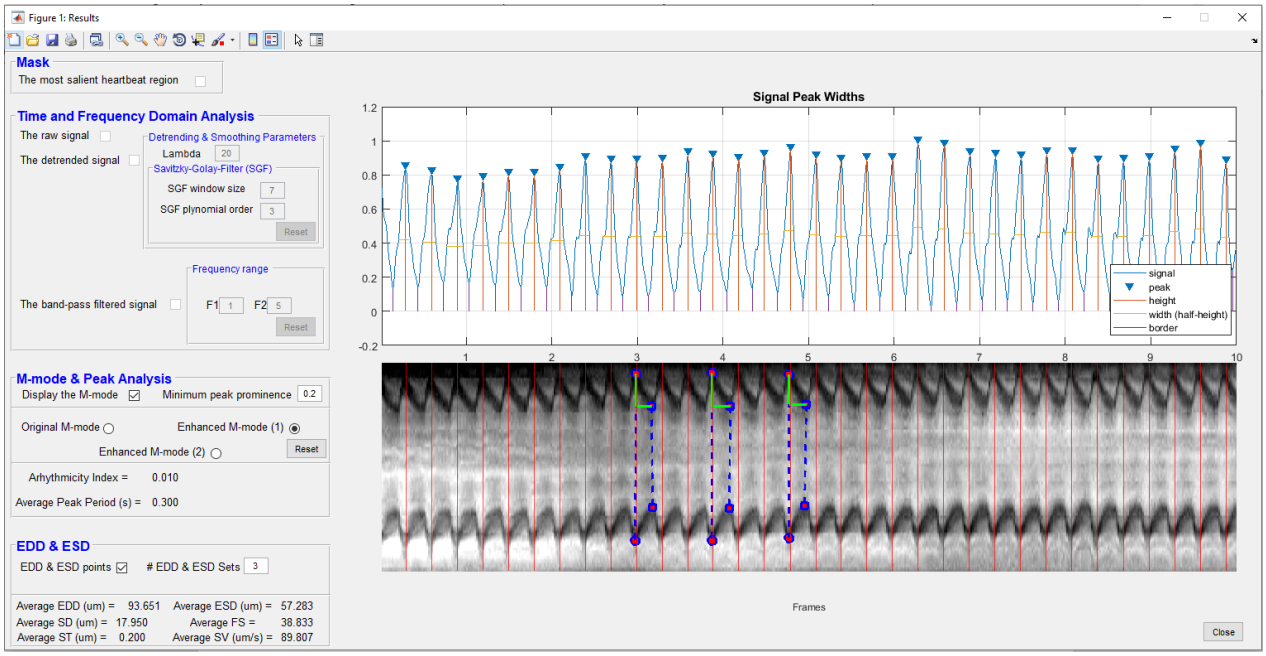

Figure 3-11: The results module of the software for a 3rd instar Drosophila larva, showing how the user can mark diastolic and systolic phases on the M-mode. The user can change the number of EDD and ESD sets to take more than one measurement and the software reports the average value for different parameters. Figures reproduced by permission from Elsevier.

3.6 Data Analysis and Statistics

All data were expressed as mean ± standard error of the mean (SEM). To analyze the significance of the difference between any two groups, we used 2-tailed Student's t-test with unequal variance. When comparing more than two groups, we used one way ANOVA test. Spearman's correlation coefficient was used to quantify the strength and direction of the relationship between the heart rate and arrhythmicity index. Also, the significance of the difference between *Drosophila* survival curves was analyzed using the Kaplan-Meier log-rank test. The median age in the survivorship study was defined as the age dividing the population into two parts of equal size.

Chapter 4

RESULTS

4.1 Manipulation and Injection of *Drosophila* Larvae in the Microfluidic Device[†]

A third or second instar *Drosophila* larva was loaded into the trap channel via the loading capillary (Fig. 4-1A). Then, the larva's head was manually grabbed by negative pressure inside the rotatable orientation glass capillary to adjust the position and the orientation of the larva (Fig. 4-1B). Preliminary studies showed that injection location highly affected the diffusion of the injectant in the hemolymph and resulted in damages to the cardiac tissues and the central nervous system (CNS).

[†] Contents of this section have been collected from the published journal articles (permissions acquired and presented in the following):

- A. Zabihihesari, A.J. Hilliker, P. Rezai, Localized microinjection of intact Drosophila melanogaster larva to investigate the effect of serotonin on heart rate, *Lab Chip*. (2020) 343–355.
- A. Zabihihesari, S. Parand, A.B. Coulthard, A. Molnar, A.J. Hilliker, P. Rezai, An In-Vivo Microfluidic Assay Reveals Cardiac Toxicity of Heavy Metals and the Protective Effect of Metal Responsive Transcription Factor (Mtf-1) in Drosophila Model, *SSRN Electron. J*. (2022) 1–33.
- A. Zabihihesari, S. Parand, P. Rezai, Microfluidic Capillary Pressure-Driven Viscometry of Drosophila melanogaster's Hemolymph, *Journal of Experimental Biology*. Under review

Ideally, the injected liquid should quickly enter the heart through ostia cells (inflow tracts) to get distributed around the larva's body via the pumping mechanism of the heart. Therefore, the position of the larva along the trapping channel was adjusted so that the needle could be inserted at the junction of the heart and aorta, close to the ostia cells. While the larva was still grabbed by the orientation glass capillary, it was axially rotated with heart tube downwards to maximize the optical accessibility for heart monitoring under the inverted microscope. Then, the oriented larva was pneumatically immobilized by applying a 5-10 psi negative pressure at the side suction channels (Fig. 4-1C). Microneedle was actuated by the micropositioner and inserted into the body, then the delivery system was pulsed at an amplitude of 50-200 kPa and a duration of 0.1-1 s (depending on the needle size) to inject 40 nL of injection substance (Fig. 4-1D). Preliminary studies were performed to determine the injection volume so that the injection and distribution of liquid in larva's body could be seen without affecting the heart rate and viability. This injection volume was also consistent with the previous injection assays for pre-pupae and pupae [67]. Volume determination using two standards (VDTS) method was used to determine the hemolymph volume in 3rd instar *Drosophila* larvae. The results demonstrated that the hemolymph volume depends on dietary conditions. The total hemolymph volume for larvae raised on normal food ranged from ~400 to 690 nL [237]. The manipulation and injection steps on the microfluidic chip took 3-4 minutes for each larva.

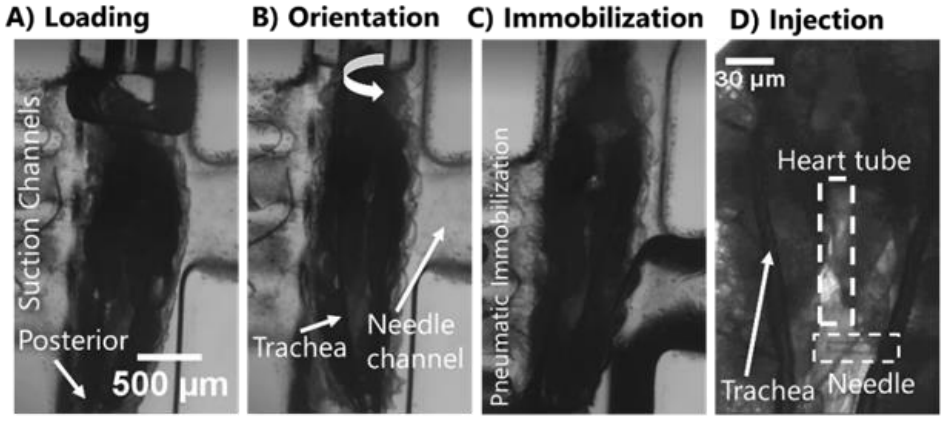

Figure 4-1: Manipulation and injection of a 3rd instar Drosophila larva in the trap region of the microfluidic device. The animal was (A) loaded into the microfluidic device via a loading glass capillary, then (B) larva's head was grabbed by applying suction through the rotatable orientation glass capillary. After desired orientation, the larva was (C) pneumatically immobilized by applying negative pressure in the side suction channels. (D) The needle was inserted at the junction of the heart and aorta, close to the ostia cells inside the larva's body cavity. Figures reproduced by permission from the Royal Society of Chemistry.

4.1.1 Effect of Microfluidic-Based Manipulation on 3rd Instar *Drosophila* Larva's Cardiac Activity

To understand whether the microfluidic manipulation has any effect on the heart rate, animal's heart activity in the chip without any injection was investigated after loading and the results were compared with an off-chip glue-based immobilization approach [134]. Ten, larvae were loaded individually, dorsally oriented and then immobilized in the chip. The heart rate of immobilized larvae inside the microfluidic chip was measured in the first 5 minutes post immobilization with 1-minute intervals. Right after immobilization, the average heart rate was 201±8 (SEM). The average heart rate gradually decreased in the next 4 minutes post-immobilization and stabilized around 180±4 (SEM). Therefore, monitoring the heart activity began 5 minutes after immobilization to eliminate the deceptive results caused by stress. The heartbeats were then recorded for a period of 30 minutes in 5-minute intervals. Another group of ten 3rd instar *Drosophila* larvae were conventionally oriented using tweezers and immobilized on a glass slide using double-sided tape and their heart activity was recorded under the microscope in a similar way. As shown in Fig. 4-2, the heart rates in both methods were consistent with previous reports for intact *Drosophila* larva [134,238]. To compare the microfluidic-based technique with the glue-based technique, a two-tail t-test was done which resulted in p-values of 0.583, 0.663, 0.589, 0.453, 0.961, and 0.635 at 5, 10, 15, 20, 25, and 30-minute intervals, respectively. These results demonstrate that there is no statistically significant difference between the two methods, proving that the microfluidic device does not have a negative impact on larva's heart rate activity. However, the heart rate of *Drosophila* larvae in the microfluidic device was significantly more stable (lower errors in Fig. 4-2) and manipulation of a larva using the microfluidic platform was easier, faster, and most importantly reversible when compared to the glue-based approach.

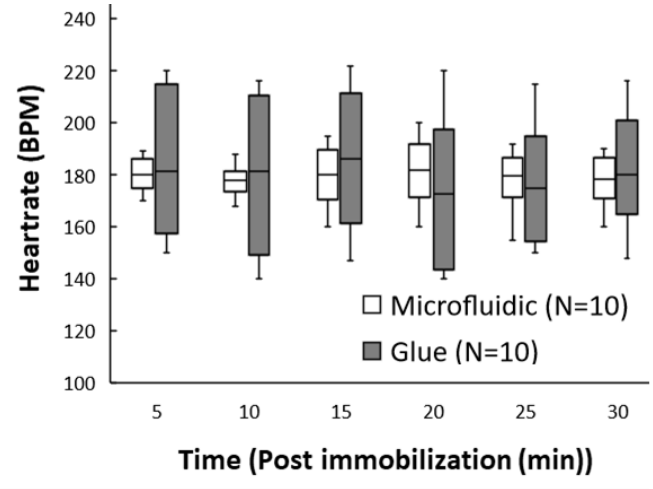

Figure 4-2: Heart rate of 3rd instar Drosophila larvae immobilized using the microfluidic chip (N =10, negative pressure for immobilization= 35 kPa) and the conventional glue-based method (N= 10). There is no statistically significant difference between the two groups. In the box plot, the lower limit shows the first quartile, the horizontal line shows the median, and the upper limit shows the third quartile of the data. The whiskers connect each quartile to the minimum and maximum data points. Figures reproduced by permission from the Royal Society of Chemistry.

4.1.2 Localized Microinjection into Intact 3rd Instar *Drosophila* Larvae

We used a method called dye angiography [65] to show the suitability of our device for microinjection of reagents with spatial precision and investigating the hemolymph circulation in larva's body. In this method, a fluorescent dye was injected into the larva's body and the dye distribution was monitored under fluorescent microscopy. For rapid distribution of chemicals around the larva's body via hemolymph flow, we needed to inject the dye into the body cavity, adjacent to the heart chamber. Ostia cells are inflow tracts of *Drosophila* larval heart which are located at the posterior compartment of the heart tube. There are three pairs of these openings in each side of the posterior heart chamber [83,239]. Since the diameter of the aorta is smaller than heart chamber, injection along the aorta is less likely to damage the heart; however, the needle should be close enough to the ostia cells so that the injected substance can enter the heart chamber easily through ostia. Moreover, anterior injection may damage the larva's CNS. To satisfy the above conditions, the needle was inserted close to the junction of the heart chamber and aorta. After injection in this location, the injected substance could easily enter the heart chamber through ostia and was rapidly pumped towards the outflow tract at the anterior part of the larva's body, close to the head (Fig. 4-3A).

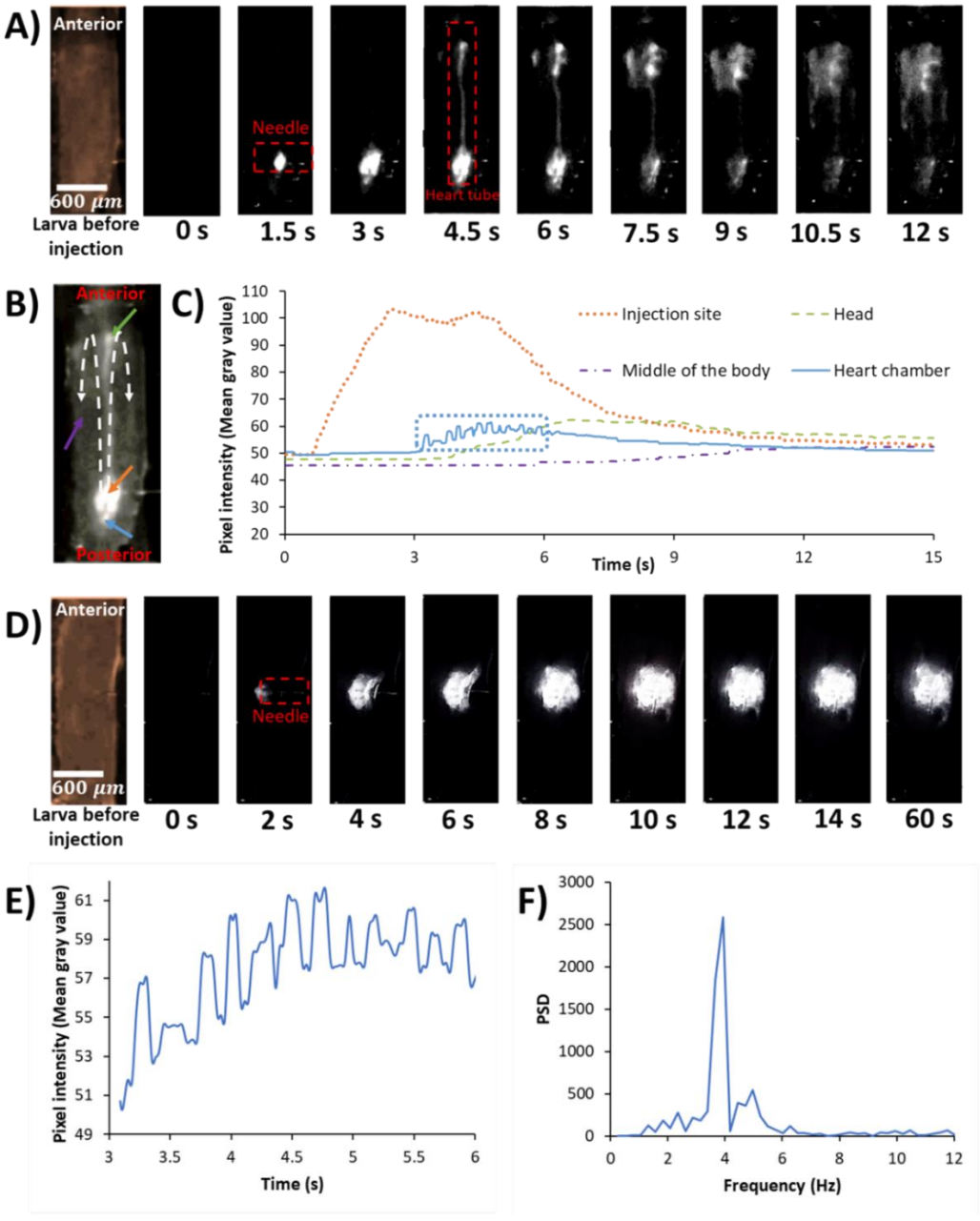

Figure 4-3: Fluorescent imaging during dye angiography of intact 3rd instar Drosophila larvae. (A) Injection into the body cavity close to the heart openings (ostia). The injected substance could easily enter the heart chamber and was rapidly pumped towards the outflow tract at the anterior part of the larva's body, close to the head. (B) White dashed arrows showing the flow direction and color-coded sites along the larva's body at which the pixel intensity signals were calculated. (C) Time-varying pixel intensities at the color-coded body sites in B. (D) Injection into the fat body. Absence of hemolymph flow in this organ led to the slow distribution of injected substance, which depended only on diffusion. (E) Oscillatory part of the pixel intensity signal (dashed rectangle in C) at the heart chamber after applying cubic spline interpolation. (F) PSD of the pixel intensity signal in D. Figures reproduced by permission from the Royal Society of Chemistry.

We did not observe a reverse flow from aorta to the heart chamber providing evidence that the hemolymph flow is unidirectional in larval heart tube and ostia function as hemodynamic valves, not simple openings which were previously reported in the pupal stage [240]. The time-varying pixel intensities at different locations in Fig. 4-3B were measured to quantify the dye distribution and hemolymph circulation around the larva's body (Fig. 4-3C). During injection, the dye was accumulated in the injection site which increased the local pixel intensity rapidly in the first few seconds. Then, the injected dye was transported away from the injection site by convective transport during the cardiac cycle. After exiting from the anterior aorta, the dye returned from the anterior side of the body towards the posterior heart which led to an increase in the pixel intensity at locations away from the injection site (the purple curve in Fig. 4-3C). To demonstrate the capability of our microfluidic device for localized microinjection, we injected the same amount of reagent (40 nL) into the larval fat body (Fig. 4-3D). The absence of hemolymph flow in this organ led to the slow distribution of injected substance only based on the diffusion of the chemical inside the fat body. Upon injection inside the fat body, the injected substance remained in the injection location and was not distributed around the body even after 1 minute. Success rates of 90% and 70%, out of N=10 tested larvae, for injection close to the ostia cells and into the fat body were achieved, respectively.

On-chip fluorescent dye angiography also allowed us to observe the cardiac systole and diastole periods, two physiological processes of the larval cardiac cycle which are comparable to the mammalian cardiac system. Systole was distinguished by the ejection of hemolymph from the heart chamber to the aorta and diastole was distinguished by heart filling through the ostia. The dynamic accumulation (diastole) and clearance (systole) of the heart is clearly seen in the time-varying pixel intensities of the heart chamber in Fig. 4-3C (dashed rectangular area) and Fig. 4-3E. Moreover, the peak frequency in the PSD of the pixel intensity signal in Fig. 4-3F perfectly corresponded with the heart rate of the tested larva.

The dye angiography technique presented here provided useful insights into intracardiac, aortic and extracellular-extravascular hemolymph flow in the open circulatory system of *Drosophila* larvae. However, further investigation is required to characterize the physiology of *Drosophila* cardiovascular system. This includes characterization of biophysical properties of hemolymph, the main cardiovascular fluid of *Drosophila*. In Appendix B, we presented a microfluidic device and

experimental procedure to measure *Drosophila* hemolymph viscosity (1.34 cP ± 0.07) and estimated the amount of shear stress in the heart of *Drosophila* larvae (~0.5–1 dyne/cm^2).

4.1.3 Effect of Microfluidic-Based Microinjection on Viability of 3rd Instar *Drosophila* Larvae

Viability test was done to investigate the effect of microneedle penetration and dye injection on the survival rate of 3rd instar *Drosophila* larvae. This experiment was done on three groups of larvae. The first group (N=16) was only loaded into a petri dish containing PBS as the preparation process for loading them into the device. The second group (N=18) was loaded into the device, oriented, immobilized, and penetrated by the needle. The needle was inserted at the posterior part of the body close to the heart tube without injection. The third group (N=15) was loaded into the device and injected by 40 nL of the drug carrier solution containing 0.1% sulforhodamine B sodium salt (Acid-Red). After the above experiments, the larvae were transferred into normal food vials and monitored for 13 days. Fig. 4-4A shows the results of the viability test.

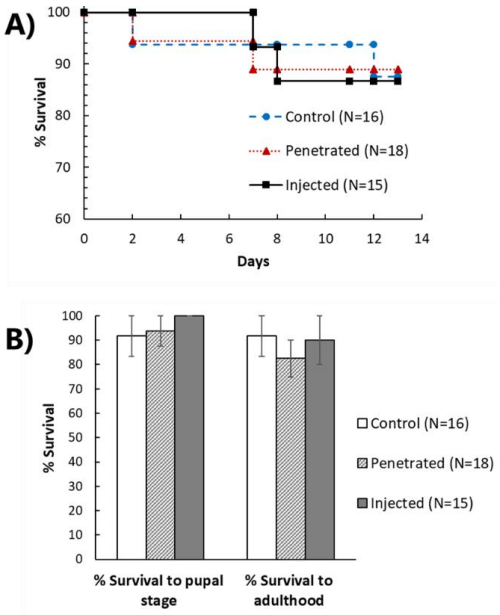

Figure 4-4: Effect of microfluidic injection on the viability of 3rd instar Drosophila larvae. A) Life span of three groups of larvae. The first group (control) were only loaded into a petri dish containing PBS. The second group was penetrated by the needle (without injection). The third group were injected by 40 nL of carrier solution. The significance of the difference between survival curves (control versus penetrated and injected groups) was analyzed using the Kaplan–Meier log-rank test (Both P-values > 0.05). B) Survival of larvae to pupal and adult stages. The significance of the difference between survival curves (control versus penetrated and injected groups) was analyzed using the t-test (P-values > 0.05). Figures reproduced by permission from the Royal Society of Chemistry.

The survival rate analysis was done using the Kaplan-Meier log-rank statistical test [241]. Fig. 4-4B shows the survival rate of the three groups of larvae to pupal and adulthood stages. The results of penetrated and injected groups were compared with the control group. Both P-values were more than 0.05 showing no statistically-significant difference between the survival rate of these groups and the control larvae. We also did not observe any significant delay in pupariation of the two groups in comparison with the control larvae. Therefore, it was concluded that needle insertion and microinjection of the carrier solution did not affect the viability of larvae in our device.

4.2 Phenotypic Quantification of Heart Function of Intact Fruit Fly Larvae Using SmallHeart Software[‡]

4.2.1 Effect of Thresholding Parameter ζ on the Most Contractile Region of the Heart Tube

When binarizing the grayscale image $\bar{F}$ with a level ζ, all the pixels in the input image with luminance greater than level ζ will be replaced with value 1 (white) and all other pixels will be replaced with value 0 (black). The effect of thresholding parameter ζ had to be investigated to obtain the optimum area for the most contractile region of the heart. For this purpose, several *Drosophila* videos were analyzed using our software with different ζ values ranging from 0.05 to 0.25 (Fig. 4-5). When ζ increases, the area of the mask decreases. ζ=0.05 resulted in a large mask that covered almost the whole larva's body and the signal generated with this mask had a high level of noise. When ζ was too large, the area of the mask was too small failing to cover enough pixels as shown for ζ=0.25. A mask with ζ=0.15 covered the heart properly and worked well for all the *Drosophila* larva videos (N=23) which were analyzed in our experiments. Therefore, ζ=0.15 was set as default in the software. If needed, the user can easily adjust this value manually using a slider (Fig. 4-5).

[‡] Contents of this section have been collected from the published journal article (permissions acquired and presented in the following):

- A. Zabihihesari, A. Khalili, A.J. Hilliker, P. Rezai, Open access tool and microfluidic devices for phenotypic quantification of heart function of intact fruit fly and zebrafish larvae, *Comput. Biol. Med*. 132 (2021) 104314.

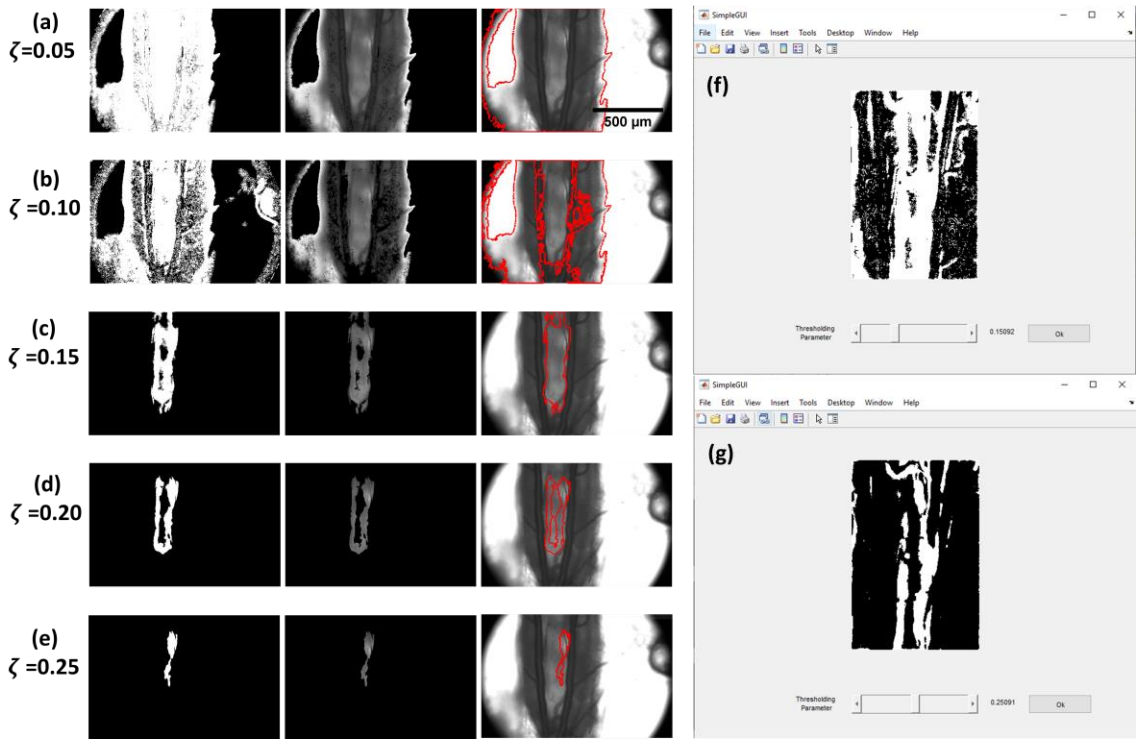

Figure 4-5: Effect of thresholding parameter ζ on the area of the most contractile heart tube region of a 3rd instar Drosophila larva (a-e). The default value on the software was set as ζ=0.15 and worked well at 10x magnification; however, the user can change it manually based on the magnification and the quality of videos (f-g). Figures reproduced by permission from Elsevier.

4.2.2 Parameter Settings for Signal Processing

The raw heartbeat signal (Z), calculated using Eq. 3-7, is shown by the blue line in Figs. 4-6a and 4-6b for *Drosophila* larvae. The black dashed lines in these figures show the undesired low-frequency trend caused by small movements of the animal, movement of internal organs, or changes in environmental light which should be eliminated using the detrending method. We used the smoothness priors' approach (SPA) to remove the undesired low-frequency trends in the raw signal. In this method, the smoothing parameter λ should be selected such that the frequency components of interest are not significantly affected. After testing different values for λ, a default choice of λ=15 was set in the software; however, in the result module of the software, the user can assign different values to λ and observe the changes in time and frequency domain representations of the signal. The detrended signals of Fig. 4-6a and 4-6b are respectively shown in Figs. 4-6c and 4-6d. The performance of the SGF smoothing method applied to the red-shaded regions in Figs. 4-6d is shown in Figs. 4-6e. The default value for the polynomial order k and the window size ϖ were set as k=3

and $\bar{\omega}$ =7 and worked well for all the videos in our experiments (N=23). However, the user can easily change these parameters in the result module of the software and track the changes in the time and frequency domains of the signal.

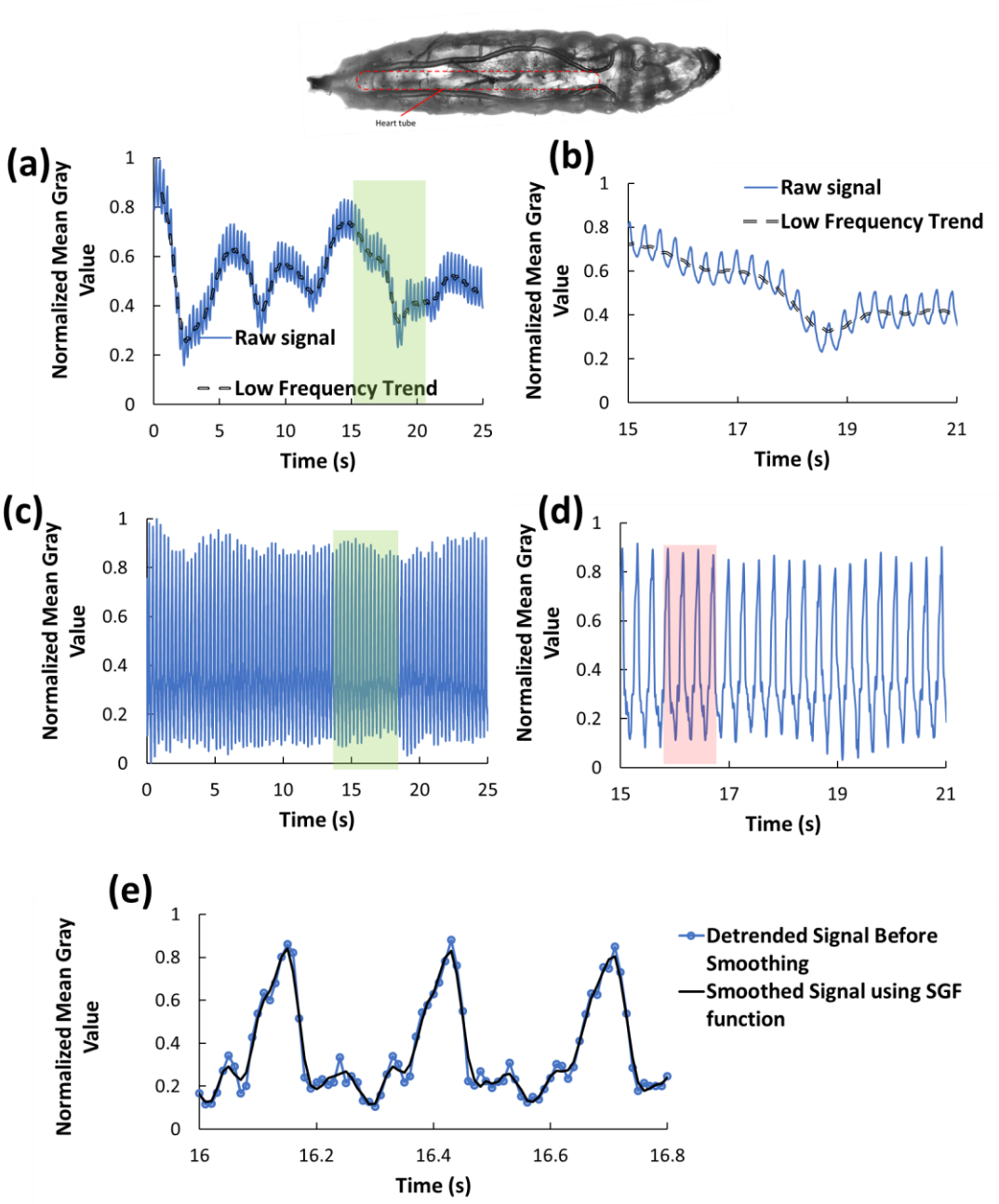

Figure 4-6: Heartbeat signal processing for a 3rd instar Drosophila larva. (a) The raw signal (blue line) and the low-frequency trend (dashed black line) extracted from the most contractile region of the Drosophila heart tube. (b) Close-up of the green highlighted area in (a). (c) Drosophila heartbeat signal after detrending with λ=15. (d) Close-up of the green highlighted area in (c) showing the signal after detrending. (e) Close-up of the red highlighted areas in (d), showing the detrended Drosophila heartbeat signal, before smoothing (dotted blue line) and the smoothed signal using the SGF method (black line) with k=3 and $\bar{\omega}$=7. Figures reproduced by permission from Elsevier.

4.2.3 Performance of the MATLAB-Based SmallHeart Software

To examine the execution time of the software, we ran the program three times for each video and measured the average processing time on a computer with a CPU of Intel Core i7, 2.2 GHz with 4 GB RAM. We analyzed 12 videos with a length of 60 s. The average processing times for detection of the most contractile regions of the heart were 47 s. The average processing times for calculation of the heartbeats were 80 s for *Drosophila* larvae. Other steps for calculation of heartbeat parameters using the M-mode images required ~1 minute. These processing times are significantly faster than manual video analysis methods that are amenable to user-based errors.

After processing a video, the user can easily match the detected peaks with the M-mode as shown in Fig. 4-7a and 4-7b. The default value for the minimum peak prominence was set to p=0.2 while the user can change this value and observe the outcomes in the result module of the software. If for some heartbeats in the M-mode, there is no peak detected in the signal, the user should decrease the p-value. If the number of peaks in the signal exceeds the number of heartbeats in the M-mode, the p-value should be increased. Misdiagnosis of peaks will lead to incorrect *HP* and *AI* parameters.

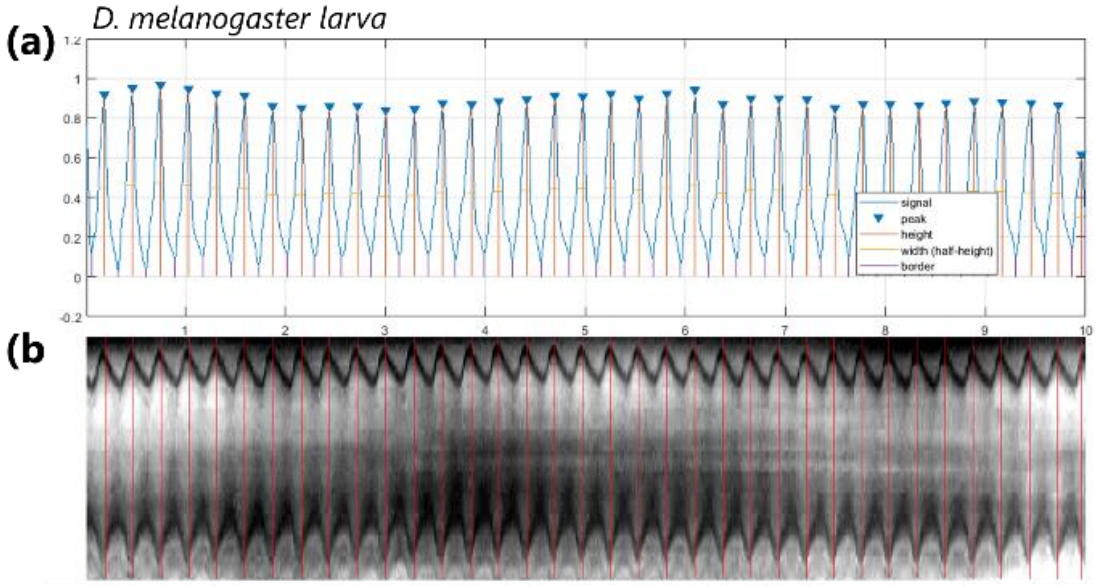

Figure 4-7: Comparison between the peak analysis and the M-mode. (a) peaks were detected automatically with p=0.2 for Drosophila larva, and are shown as blue triangles in the signal. (b) is the M-modes extracted by selecting two points across the heart borders of Drosophila larva. The contraction and expansion of the heart chamber are clearly visible in the M-mode and match with the detected peaks. Figures reproduced by permission from Elsevier.

Table 4-1 shows the performance of the proposed software for the detection of peaks in *Drosophila* heartbeat signals extracted from 34,480 frames of 12 videos. When the measurement of heartbeat parameters from the M-mode is needed, the video must have enough frames between each diastolic and systolic phase, enabling precise partitioning of the shortening and lengthening periods. This required recording the videos with a frame rate of 100 fps which enabled capturing at least 15 frames during a single systolic interval and resulted in accurate measurements. However, if only the measurement of heart rate and rhythmicity are required, videos can be recorded with a lower frame rate. Here, we investigated the performance of our software for the detection of heartbeats from videos recorded with two different speeds of 100 fps and 20 fps. The lower number of FP in 20 fps videos led to a slightly higher *PR* value compared to 100 fps videos, however, the accuracy of peak analysis (*AC*) was slightly higher for 100 fps videos. According to the *RC* values, 98.86% of peaks were classified correctly in 100 fps videos. The number of correctly detected peaks decreased to 94.66 % for 20 fps videos. Still, an F-measure > 0.97 demonstrate that the software yields an acceptable *performance* at both video speeds. These results indicate that our MATLAB-based software can be used for phenotypic heart activity monitoring of *Drosophila* larvae that are intact and reversibly immobilized in a microfluidic chip.

Table 4-1: Performance of the MATLAB-based software for detection of the peaks in Drosophila heartbeat signal for videos recorded at 100 and 20 fps.

	TP	FP	FN	PR	RC	AC	F-measure
100 fps	935	23	11	0.979	0.9886	0.96801	0.9828
20 fps	605	1	35	0.9983	0.9466	0.945	0.9706

4.2.4 Comparison of SPA and a Conventional Filtering Method

Previously, static high-pass and low-pass filters were used to remove the noises in videos obtained from dissected adult fly hearts [74,75]. The level of noise in immobilized intact larvae is much higher due to the movement of the internal organs. For instance, the time and frequency domains of the heartbeat signal of a 3rd instar *Drosophila* larva is shown in Fig. 4-8. The original signal had very-low-frequency components (<0.4 Hz) with intensity prominence in the PSD of the original signal (Fig. 4-8a). As a result, the heartbeat frequency (~2.8Hz) was not visible in the PSD of the original

signal. After applying a bandpass filter with a passband of 0.4 Hz < f < 5 Hz and as shown in Fig. 4-8b, the heartbeat frequency became visible while the low-frequency components were still prominent. *Drosophila* larval heart rate changes in the wide range of ~1-6 Hz as the animal grows from the 1st instar to the 3rd instar stage. Also, exposure to different chemicals and genetic mutations may change the heart rate significantly. If the heart rate is lower than normal due to any of the above conditions, it may be shielded by the low-frequency noise components, thereby making it difficult to correctly distinguish the heartbeat from the noise by static bandpass filters. The SPA method as a time-varying high-pass filter could attenuate undesired low-frequency components without affecting the heartbeat frequency (Fig. 4-8c).

Both static bandpass filter and SPA detrending methods have been implemented in our software. The user can easily adjust the passband of the filter and the smoothing parameter (λ) of the SPA method in the result module of the software and check the results in both time and frequency domains (Fig. 4-8 and Fig. 3-8).

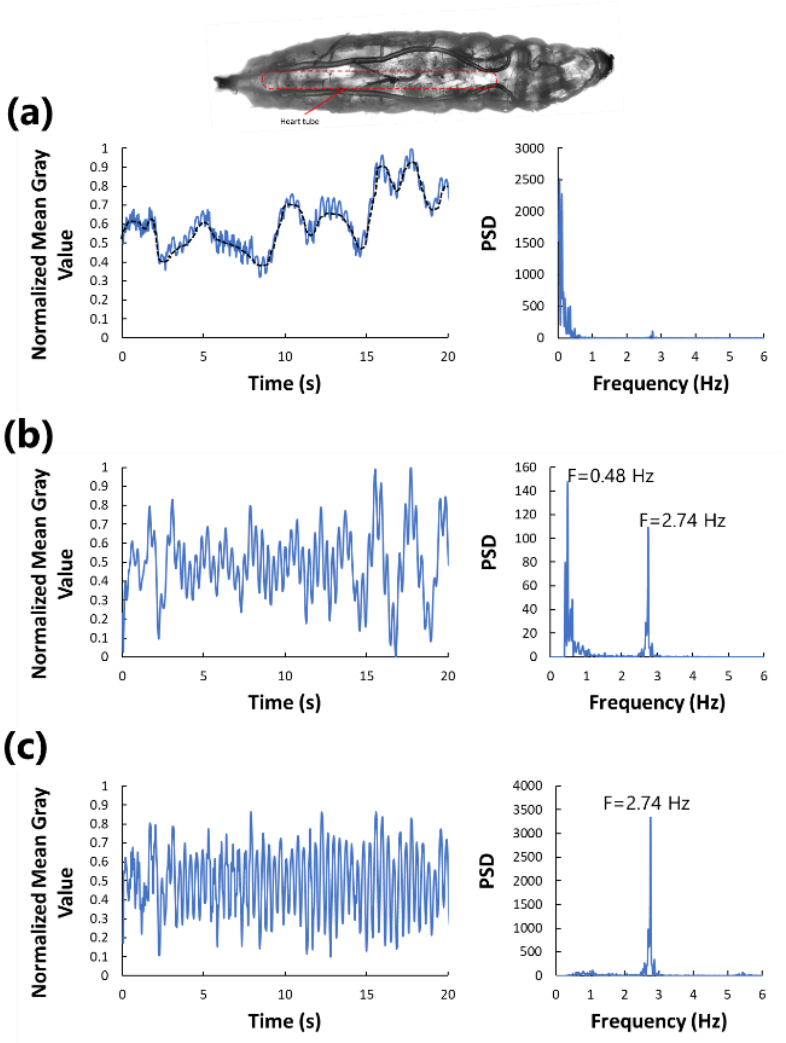

Figure 4-8: Comparison between the conventional static bandpass filtering with the SPA method for a 3rd instar Drosophila larva. (a) The raw heartbeat signal in time (left) and frequency (right) domains. (b) The heartbeat signal after applying a bandpass filter with a passband of 0.4 Hz < f < 5 Hz. (c) The heartbeat signal after applying the SPA detrending method. Figures reproduced by permission from Elsevier.

4.2.5 Detection of Cardiac Arrest

The cardiac system of intact *Drosophila* larvae senses and responds to mechanical stimulation by regulating the heart activity [73]. The heart tube is firmly attached to the epidermis by alary muscles. When the larva attempts to crawl, strong muscle contraction leads to changes in mechanical forces exerted on cardiomyocytes. This muscle contraction leads to transient cardiac arrests in intact larvae. This phenotype was also observed in immobilized larvae in our device which still attempt to crawl but are not able to advance. We investigated the capability of our software in detecting this phenotype and observed that the software could correctly detect cardiac arrests as shown in Fig. 4-

9. There was not a specific trend in the frequency and duration of cardiac arrest in wild type larvae. However, it happened whenever the larvae attempted to crawl. This phenomenon can be investigated in more quantitative detail in the future applications of the proposed software.

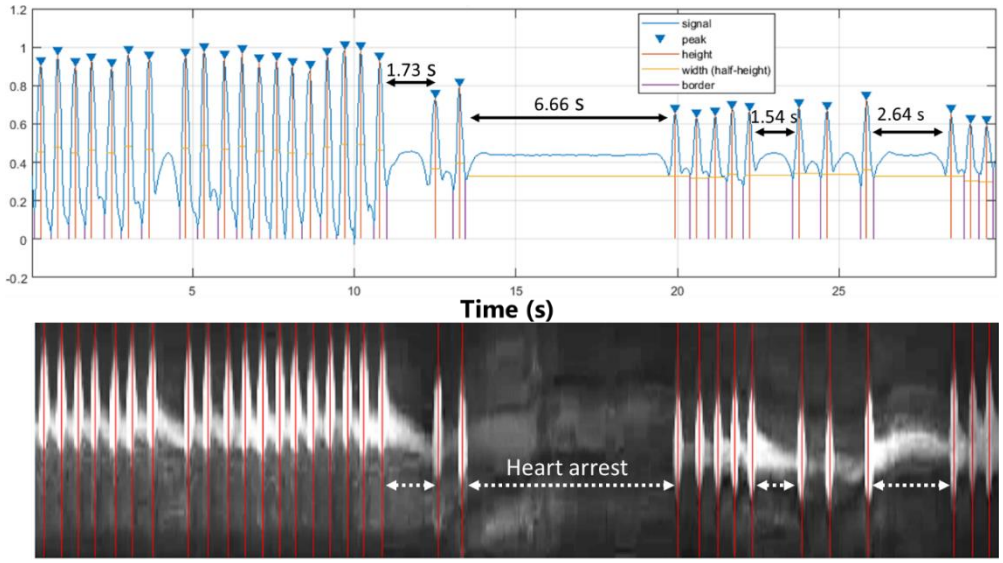

Figure 4-9: In-vivo detection of cardiac arrests on an intact 3rd instar Drosophila larva immobilized in our microfluidic chip. Figures reproduced by permission from Elsevier.

4.2.6 Heartbeat Parameters for Intact Wild Type *Drosophila* Larvae

Third instar *Drosophila* larvae (N=22) were immobilized in the microfluidic chip and their heartbeat parameters were measured as described before. The results are shown in Table 4-2. All videos were analyzed when the larvae were in the resting status and did not attempt to crawl, i.e., with no cardiac arrests. As mentioned before, the heart rate of *Drosophila* larva varies during larval development. It also depends on different environmental conditions such as temperature [198,242]. The heart rate of intact *Drosophila* larvae in our experiments was similar to what was reported previously by our group and other researchers [84,198,242]. Although the heart rate is the most widely used parameter in the field, it cannot thoroughly represent the heart function. Previously, other heartbeat parameters which require optical accessibility to the heart edges have been measured on dissected *Drosophila* [74,75]. However, the primary disadvantage of dissection is that it is not applicable for long-term investigation of factors such as diet, exercise, and aging. Optical coherence microscopy (OCM) has been used to measure EDD, ESD, and FS in intact fly [243,244]. Nevertheless, this technique

requires highly specialized equipment. Moreover, both dissection and OCM methods are time-consuming and require a high level of expertise. *In-vivo* measurement of heartbeat parameters under bright field microscopy has been limited due to the challenges associated with the floating internal organs and the cardiac interruptions occurring in intact animals. Our microfluidic device minimizes these disruptive factors by providing desired orientation and reversible immobilization required for optical accessibility to the intact heart. Our software enabled measurement of other heartbeat parameters including EDD, ESD, SD, ST, FS, and SV that are being reported for the first time for intact larvae using bright field microscopy.

Table 4-2: Heartbeat parameters for intact 3rd instar Drosophila larvae measured using the proposed software.

	HR (Hz)	AI	EDD (μm)	ESD (μm)	d (μm)	t_s (s)	FS (%)	SV (μm/s)
Average	2.83	0.06	120	54	32	0.17	54	193
SEM	0.12	0.01	4	2	2	0.01	2	11

The previous measurement of arrhythmicity on dissected adult flies showed that AI increases by age from ~0.1 in 1-week old to ~0.4 in 5-weeks old adult flies [74]. However, the reported value for AI in Table 4-2 shows that the level of arrhythmicity in 3rd instar larvae is significantly lower than in the dissected adult flies. EDD, ESD, and FS measured for 3rd instar larvae in our experiments were similar and within the range of previous measurements using the complex OCT technique [243,244]. Moreover, these three parameters in intact 3rd instar larvae (our work) are higher than what was reported for dissected 1-5-weeks old adult flies (~60 < EDD < ~80 μm, ~40 < ESD < ~48 μm, and ~32% < FS < ~40%) [74]. Also, the SV of intact 3rd instar larvae in our experiments was significantly lower than that of dissected adult flies (~ 475 μm/s) [75].

4.3 Effect of Serotonin Injection on *Drosophila* Heart Rate[§]

4.3.1 Effect of Serotonin on 3rd Instar *Drosophila* Larval Heart Rate

Here, we used our microfluidic platform as the first reversible and viable on-chip injection assay to investigate the effect of serotonin on the heart rate of intact 3rd instar *Drosophila* larvae. This device provides control for localized microinjection and heart monitoring without the need for larva dissection or immobilization using anesthetics or glue.

Serotonin at 0.001 mM, 0.01 mM, 0.1 mM and 1 mM was prepared in the drug carrier solution and injected (V=40 nL) on-chip into N=16 larvae per group. The control group was only injected with 40 nL of the drug carrier fluid. Larvae's heart was monitored for 1 minute prior to injection to obtain the baseline heart rate. Then, injection was performed and the heart rate was monitored for 10 minutes after injection. Here, we reported the values for 2 min, 6 min, and 10 min post-injection (Fig.4-10).

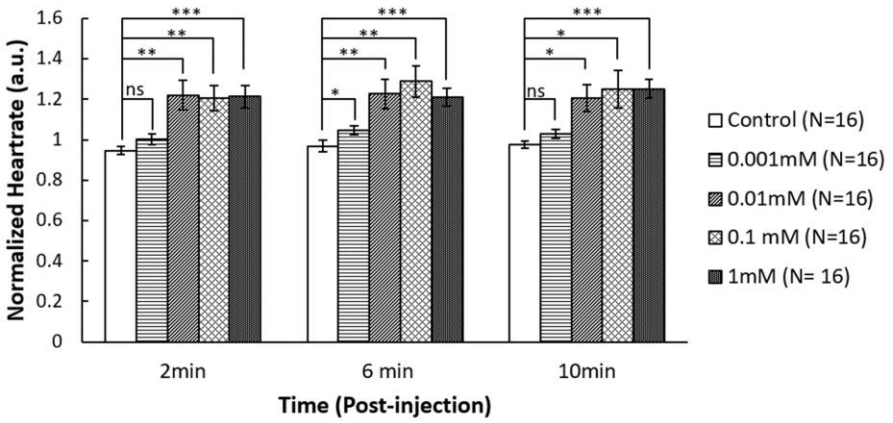

Figure 4-10: Normalized heart rate activities of 3rd instar Drosophila larvae injected with 40 nL of only drug carrier solution (control) and 0.001, 0.01, 0.1, and 1 mM serotonin dissolved in the drug carrier solution (N=16 for each group). Heart rates were monitored for a minute prior to injection to obtain the baseline value for normalizing the data. Then the heart rates were counted 2, 6, and 10 minutes after injection and normalized. An increase in heart rate was statistically identified after injection of serotonin with concentrations equal or more than 0.01 mM (: P<0.05, **: P<0.01, ***: P<0.001). Figures reproduced by permission from the Royal Society of Chemistry.*

[§] Contents of this chapter have been collected from the published journal article (permissions acquired and presented in the following):

- A. Zabihihesari, A.J. Hilliker, P. Rezai, Localized microinjection of intact Drosophila melanogaster larva to investigate the effect of serotonin on heart rate, *Lab Chip*. (2020) 343–355.

After injection of the drug carrier solution as the control group, the heart rate was not changed and remained similar to its baseline value (one minute before injection). Two minutes after injection, a slight increase in larvae's heart rate was observed for a concentration of 0.001 mM compared to control group; however, this change was not statistically significant (p-value > 0.05). By increasing the concentration of serotonin to 0.01 mM, heart rate significantly increased to 121±7% (SEM) of the pre-injection heart rate ($P < 0.01$). Further increase in serotonin concentration to 0.1 and 1 mM, increased the heart rate to the same extent as 0.01 mM resulting in a plateau state. The ANOVA test was used to determine significance between 0.01 mM, 0.1 mM, and 1 mM groups. The resulted *p*-values were 0.65, 0.75, and 0.99 for 2 min, 6 min, and 10 min post-injection which showed that there was no statistical difference between these groups. So, all these concentrations resulted in the same level of increase in heart rate. Moving further forward in time for each concentration, the increased heart rate did not change significantly. Comparing serotonin with control group, our results demonstrate that the increase in larval heart rate is the direct influence of serotonin, not stress. These results are consistent with previously reported assays on intact prepupae [66] and dissected larvae [57] providing an anesthetic and glue-free tool for screening intact larvae that can be recovered for post-injection assays.

4.3.2 Effect of Serotonin on 2nd Instar *Drosophila* Larval Heart Rate

To demonstrate the versatility of the proposed device for developmental studies, we used our chip for injection of younger stage larvae. Larvae's size increases significantly from the 1st instar to the 3rd instar stage. The size of a 1st instar larva is close to an embryo with a length of ~0.5 mm and a diameter of ~0.2 mm. The larva grows rapidly in few days such that the length and diameter of the 3rd instar larva reaches to ~3 mm and ~0.6 mm, respectively [1,40]. Accordingly, our device could not be used for the 1st instar samples. A modification in dimensions is required for this purpose. However, we showed that the proposed device can be used for injection of 2nd instar *Drosophila* larvae (Fig. 4-11). The baseline heart rate of 2nd and 3rd instar larvae immobilized in our microfluidic chip were 240±6.6 (SEM) and 180±4 (SEM), respectively. A two-tail t-test demonstrated a significant decrease in heart rate during *Drosophila* larval development (*p*-value $=1.4\times10^{-5}$). This decrease in heart rate during development was previously reported by Sla´ma et al. [245].

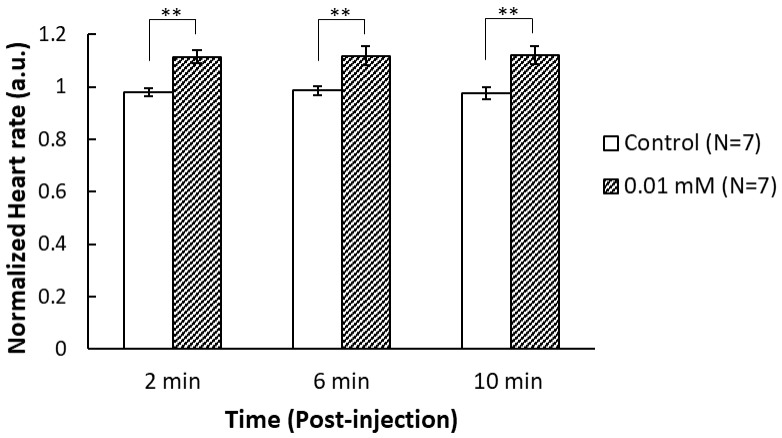

*Figure 4-11: Normalized heart rate activities of 2nd instar Drosophila larvae injected with 5 nL of only drug carrier solution (control) and 0.01 mM serotonin dissolved in the drug carrier solution (N=7 for each group). Heart rates were monitored for a minute prior to injection to obtain the baseline value for normalizing the data. Then the heart rates were counted 2, 6, and 10 minutes after injection and normalized. An increase in heart rate was statistically identified after injection of 0.01 mM serotonin (**: P<0.01). Figures reproduced by permission from the Royal Society of Chemistry.*

The length and diameter of a 2nd instar larva is approximately half of a 3rd instar. Assuming larva's body as a cylinder, the volume of a 2nd instar can be estimated as 1/8th of the volume of a 3rd instar. Therefore, we reduced the volume of the injected liquid from 40 nL to 5 nL for the 2nd instar larvae. Serotonin at 0.01 mM was prepared in the drug carrier solution and injected on-chip into N=7 2nd instar larvae per group (Fig. 4-11). The control group was only injected with 5 nL of the drug carrier fluid. Two minutes after injection of 0.01 mM serotonin, the heart rate of 2nd instar larvae significantly increased to 112±3% (SEM) of the pre-injection heart rate (p-value $=1.33\times10^{-3}$). The increased heart rate did not significantly change over time after 6 and 10 minutes post-injection (Fig. 4-11). In addition to versatility of our device for injection and drug screening of *Drosophila* at different developmental stages, these results prove that serotonin has a hyperactivity effect on the heart rate of 2nd instar larvae, making the technique suitable for developmental cardiac drug screening purposes.

4.4 Cardiac Toxicity of Heavy Metals and the Protective Effect of MTF-1 in *Drosophila* Larvae[**]

The cardiac toxicity of Zn and Cd in the *Drosophila* model has not been investigated. Important questions need to be answered, including a) the acute effect of Zn and Cd on heartbeat parameters such as heart rate and arrhythmicity, and b) the effect of MTF-1 overexpression in the heart against cardiac toxicity of Zn and Cd. We aimed to address both questions in this study. To avoid limited systemic exposure due to the enzymatic, cellular, and tissue barriers present in the saliva and digestive tract of *Drosophila* [226,246], we used our microfluidic platform to inject heavy metal solutions into the larva's body cavity and directly exposed the heart through hemolymph circulation.

4.4.1 Cardiac Toxicity of Zn and the Effect of Heart-Specific Overexpression of MTF-1

The baseline heart rates of the wild type *Drosophila* larvae, tested within our microfluidic device one minute before injection of the drug carrier solution (control solution) and the 10 or 100 mM $ZnCl_2$ solutions were 2.87 ± 0.1 Hz, 2.9 ± 0.12 Hz, and 2.89 ± 0.11 Hz, respectively, with no significant difference among these groups. These heart rates were within the range of previously reported heart rates for 3rd instar *Drosophila* larvae by our group and other researchers [84,198,242,247].

Upon injection of the control solution into the wild-type larvae, the heart rate did not change (Fig. 4-12A) as compared to the baseline value. It remained constant during the 15 min observation time in the device. Similarly, injection of 10 mM $ZnCl_2$ into the wild-type larvae had no significant effect on the heart rate compared to the wild-type control group. However, increasing the concentration of $ZnCl_2$ to 100 mM significantly decreased the average heart rate of wild type larvae by 14.3%, only

[**] Contents of this chapter have been collected from the published journal articles (permissions acquired and presented in the following):

- A. Zabihihesari, S. Parand, A.B. Coulthard, A. Molnar, A.J. Hilliker, P. Rezai, An In-Vivo Microfluidic Assay Reveals Cardiac Toxicity of Heavy Metals and the Protective Effect of Metal Responsive Transcription Factor (Mtf-1) in Drosophila Model, *SSRN Electron. J.* (2022) 1–33.

2 min after injection. This effect continued over time such that the average heart rate gradually decreased from the baseline heart rate by 20.6%, 25.3 %, and 24.8% at 6, 10, and 15 min post-injection, respectively (Fig. 4-12A).

Similar to wild type group, the heart rate of the MTF-1 larvae was monitored one minute prior to injection to obtain the baseline heart rate for each larva. The baseline heart rates of the MTF-1 overexpressing larvae before injection of the control solution and 100 mM Zn were 3.01 ± 0.08 Hz and 3.09 ± 0.09 Hz, respectively, with no significant difference among these groups and also compared to wild type larvae. After injection of the control solution into the MTF-1 larvae, the heart rate was not changed compared to its baseline value (Fig. 4-12B). Injection of 100 mM Zn to MTF-1 larvae slightly decreased the heart rate. However, the change in the heart rate was only significant at 2 min post-injection, with this effect being ameliorated gradually such that at 6min, 10 min, and 15 min post-injection there was no significant difference in the heart rate of MTF-1 larvae injected with the control solution and 100 mM Zn.

A comparison between the wild-type and MTF-1 larvae, both injected with 100 mM $ZnCl_2$, demonstrated that the wild-type group had significantly lower heart rates compared to MTF-1 larvae at 6 min, 10 min, and 15 min post-injection with *p*-values equal to 0.0217 and 0.00391, and 0.0041 respectively. On the other hand, there was no significant difference between these two groups when injected with the control solution.

The arrhythmicity index was also measured for each larva one minute before injection and 2-15 min post-injection (Fig. 4-12C and 4-12D). The arrhythmicity index of wild type larvae before injection of the control solution and 100 mM $ZnCl_2$ was 0.062 ± 0.005 and 0.065 ± 0.005, with no significant difference between two groups (Fig. 4-12C). These values are within the range of previously reported data by our group and other researchers [74,247]. Similar to what was observed for heart rate, injection of drug carrier solution into wild-type larvae did not change the average arrhythmicity index over time compared to its value before injection. However, injection of 100 mM $ZnCl_2$ significantly increased the arrhythmicity index by 35.8%, 49.4%, and 58.2% at 6, 10, and 15 min post-injection, respectively. Also, there was a significant difference in the arrhythmicity index between wild-type larvae injected with the control solution and those injected with $ZnCl_2$ at 10 min and 15 min post-injection such that the control group had a lower arrhythmicity index.

There was no significant difference between the arrhythmicity index of wild type and MTF-1 larvae before injection. Injection of the control solution and 100 mM $ZnCl_2$ into MTF-1 larvae had no significant effect on the arrhythmicity index (Fig. 4-12D).

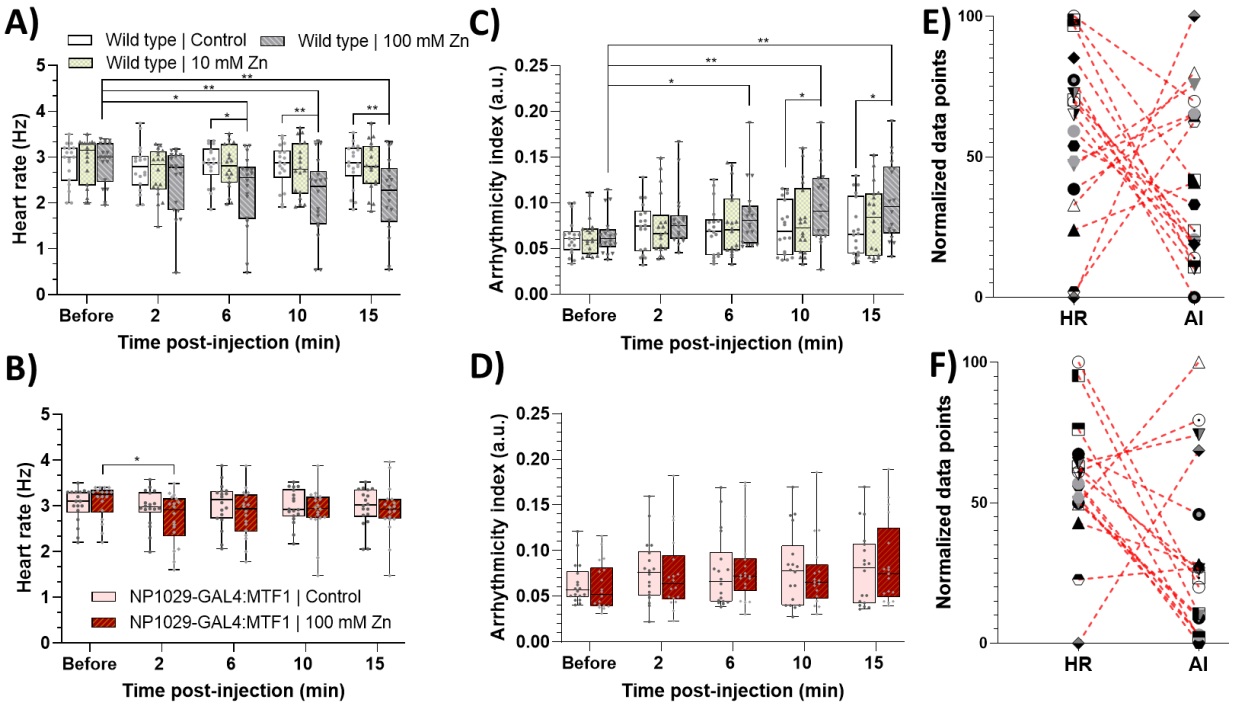

*Figure 4-12: The effect of $ZnCl_2$ injection on Drosophila heart rate and arrhythmicity index. A) Heart rate of wild type 3rd instar Drosophila larvae injected with 40 nL of only drug carrier solution (control), and 10 mM and 100 mM $ZnCl_2$ dissolved in the drug carrier solution. B) Heart rate of the MTF-1 larvae injected with 40 nL of only drug carrier solution (control) and 100 mM $ZnCl_2$ dissolved in the drug carrier solution. C) Arrhythmicity index of wild type larvae. D) Arrhythmicity index of the MTF-1 larvae. Normalized individual responses of heart rate and arrhythmicity index of wild type (E) and MTF-1 (F) larvae at 15 min post-injection. The level of significance between two groups was analyzed using t-test (N = 18 for each group, *: P < 0.05, **: P < 0.01). Figures reproduced by permission from Elsevier.*

To understand the correlation between the heart rate and arrhythmicity index in each larva, both parameters were normalized to the same scale (0-100) for comparison. Then, normalized parameters were plotted while preserving the identity of individual larvae by connecting dash-lines (Fig. 4-12E and 4-12F). The Spearman's correlation was calculated to measure the strength and direction of correlation between the heart rate and arrhythmicity index (Appendix C, Table C-1). As shown in Fig. 4-12E and Table C-1, the heart rate and arrhythmicity index in wild type larvae were inversely proportional. In other words, those larvae with lower heart rate after injection of 100 mM Zn, had higher arrhythmicity index. This trend was significant in wild type larvae at 10 min and 15 min post

injection. However, in MTF-1 larvae, the correlation between the heart rate and arrhythmicity index after injection of 100 mM Zn was not significant.

These results demonstrated that exposure to a high dosage of Zn can change the heartbeat parameters including heart rate and arrhythmicity, and the MTF-1 overexpression in the heart can ameliorate the acute response of the heart to Zn toxicity.

4.4.2 Cardiac Toxicity of Cd and the Effect of Heart-Specific Overexpression of MTF-1

The baseline heart rates of wild type and MTF-1 larvae before injection of 10 mM $CdCl_2$ were 2.98 ± 0.10 Hz and 3.04 ± 0.08 Hz, respectively, with no significant difference among these groups. Injection of 10 mM $CdCl_2$ into wild-type *Drosophila* larvae resulted in a significantly higher heart rate compared to the control solution (Fig. 4-13A). The heart rate of wild-type larvae gradually increased by 2.4%, 6.3%, 8.9%, and 11.9% at 2, 6, 10, and 15 min post-injection, respectively. On the other hand, injection of 10 mM $CdCl_2$ into MTF-1 larvae slightly decreased the heart rate; however, the difference was not significant compared to the same group of larvae injected with control solution (Fig.4-13B).

Statistical analysis between the wild-type and MTF-1 larvae, both injected with 10 mM $CdCl_2$, revealed that the wild-type larvae had significantly higher heart rate compared to MTF-1 larvae, with *p*-values equal to 0.0200, 0.0097, and 0.0057 at 6, 10, and 15 min post-injection, respectively.

There was a significant difference in arrhythmicity index between wild-type larvae injected with control solution and those injected with 10 mM $CdCl_2$ at 2, 6, 10, and 15 min post-injection (Fig. 4-13C). The arrhythmicity index of wild-type larvae increased significantly from 0.062 ± 0.005 before injection by 61.4 %, 66.16 %, 74%, and 76.8 2% at 2, 6, 10, and 15 min post-injection, respectively. Conversely, in MTF-1 larvae, the arrhythmicity index remained unchanged after injection of 10 mM $CdCl_2$ with no significant difference compared to control solution at all the times post-injection (Fig. 4-13D). Moreover, there was no obvious pattern between the heart rate and arrhythmicity index in both wild type and MTF-1 larvae injected with 10 mM $CdCl_2$ (Fig. 4-13E and 4-13F and Table C-1).

Our results demonstrated that the injection of $CdCl_2$ had an acute toxic effect that could be quantified through heart rate and arrhythmicity measurement. Also, the heart-specific overexpression of the MTF-1 could ameliorate the effect of $CdCl_2$ on the heart rate and arrhythmicity index.

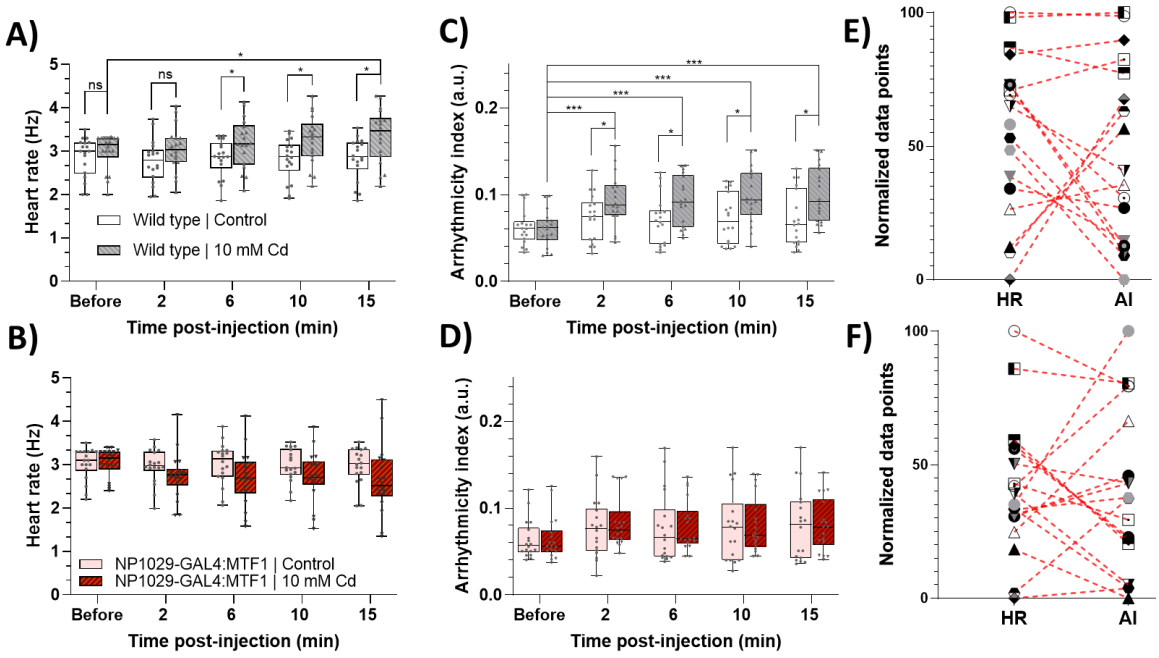

*Figure 4-13: The effect of $CdCl_2$ injection on Drosophila heart rate and arrhythmicity index. A) Heart rate of wild type 3rd instar Drosophila larvae injected with 40 nL of only drug carrier solution (control) and 10 mM $CdCl_2$ dissolved in the drug carrier solution. B) Heart rate of MTF-1 larvae injected with 40 nL of only drug carrier solution (control) and 10 mM $CdCl_2$ dissolved in the drug carrier solution. C) Arrhythmicity index of wild type larvae. D) Arrhythmicity index of MTF-1 larvae. Normalized individual responses of heart rate and arrhythmicity index of wild type (E) and MTF-1 (F) larvae at 15 min post-injection. The level of significance between two groups was analyzed using t-test (N = 18 for each group, *: P < 0.05, **: P < 0.01, ***: P < 0.001). Figures reproduced by permission from Elsevier.*

4.4.3 Effect of Heart-Specific Overexpression of MTF-1 on Lifespan Reductions Associated with Zn and Cd Toxicity

To investigate the effect of heart-specific overexpression of MTF-1 on *Drosophila* development under Zn and Cd stress, we tested the pupation (survival of pupae to adulthood) and flies' lifespan after injection of control and heavy metal solutions (Fig. 4-14). Individual larvae were transferred to the normal food after injection and heart monitoring and their viability was monitored until all flies died. We used Kaplan-Meier log-rank test to analyze the significance of the difference between

survival curves. After injection of the control solution, both wild-type and MTF-1 flies remained alive until they reached to pupal and adulthood stages with no significant difference in their lifespan (Fig. 4-14A and 4-14B). Injecting 100 mM $ZnCl_2$ in wild-type flies significantly shortened the lifespan with 40% of the population dying at the larval stage (Fig. 4-14A and 4-14B). The median age of wild type flies injected with 100 mM $ZnCl_2$ decreased by 70% compared to those injected with the control solution (Fig. 4-14A). Overexpression of MTF-1 in the heart remarkably extended the lifespan such that the median age of MTF-1 larvae injected with 100 mM $ZnCl_2$ was 100% higher than the wild type flies (Fig. 4-14A). As opposed to wild-type group, there was no mortality at the larval stage in MTF-1 larvae after injection of 100 mM Zn (Fig. 4-14Bi). However, 39% of MTF-1 overexpressing flies died at the pupal stage before reaching to adulthood (Fig. 4-14Bii).

Injection of 10 mM $CdCl_2$ caused severe mortality in wild-type flies (Fig. 4-14C and 4-14D). The lifespan of wild-type flies injected with 10 mM $CdCl_2$ shortened with 22% of flies dying at larval stage, 16% of the population dying at pupal stage, and the rest dying at adulthood stage (Fig. 4-14C and 4-14D). The median age of wild type flies injected with 10 mM $CdCl_2$ decreased by 75% compared to those injected with the control solution. The heart-specific overexpression of MTF-1 significantly increased the lifespan such that the median age of MTF-1 larvae injected with 10 mM $CdCl_2$ was 66% higher than the wild type flies injected with the same solution. As opposed to wild-type larvae, all MTF-1 larvae remained alive until reaching to the pupal stage (Fig. 4-14Di). 25% of MTF-1 pupae died before reaching to adulthood stage, and the rest of the population died in the adulthood stage (Fig. 4-14Dii).

These results illustrate that direct exposure of internal organs including the heart tube to Cd and Zn via injection can adversely affect the development and the lifespan of *Drosophila*.

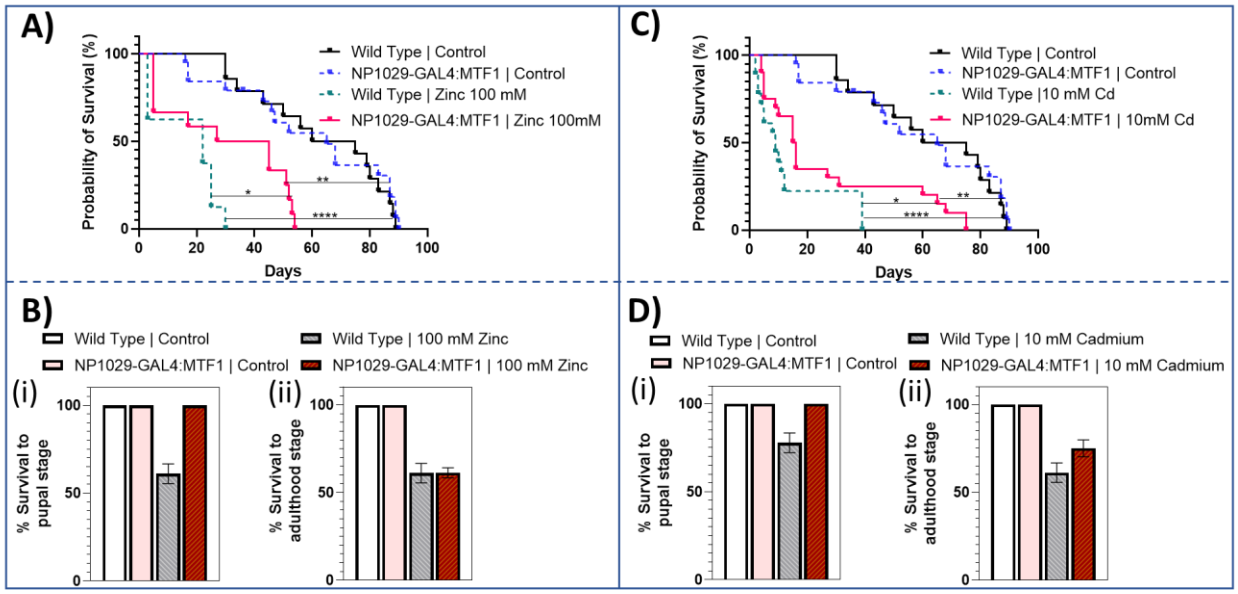

*Figure 4-14: Survival analysis of larvae after injection of heavy metal solutions. Effect of Zn (A-B) and Cd (C-D) on life span and larval growth to (i) pupal and (ii) adulthood stages in wild type and MTF-1 flies. Survival curves were analyzed using the Kaplan–Meier log-rank test, *: P < 0.05, **: P < 0.01, ***: P < 0.001, ****: P < 0.0001). Figures reproduced by permission from Elsevier.*

4.4.4 Discussion on Zn and Cd Cardiac Toxicity and Heart-Specific Overexpression of MTF-1 in *Drosophila* larvae

The cardiac toxicity of heavy metals (i.e., Zn and Cd) on *Drosophila* is being reported in our study for the first time. A significant decrease in heart rate was observed in wild type *Drosophila* larvae injected with 100 mM $ZnCl_2$ (Fig. 4-12A). Injection of 100 mM $ZnCl_2$ also resulted in a significant increase in arrhythmicity index, another heartbeat parameter that can be used to investigate the cardiotoxicity of small model organisms, including *Drosophila* larvae (Fig. 4-12C). Also, there was a significant negative correlation between the heart rate and arrhythmicity index in wild type larvae injected with 100 mM $ZnCl_2$ (Fig. 4-12E).

Zn cardiac toxicity in other model organisms, primarily aquatic animals, has been reported. For instance, studies on zebrafish larvae [248,249] and limpet Patella vulgata L [250] have shown that Zn has a cardiotoxic effect such that those animals exposed to Zn had significantly lower heart rate compared to the control group. This is consistent with the bradycardia observed in wild type *Drosophila* larvae injected with $ZnCl_2$ in our study (Fig. 4-12A). Of note, zebrafish and limpet Patella vulgata L. exposure to Zn was done over a long period (a week) and by dissolving the

chemical in animal culture medium while we used microinjection as the exposure route and investigated the acute cardiac toxicity. Our method is advantageous in shortening the time of the assay and in being precise in terms of the volume of injected drug.

Regarding cardiac toxicity of Cd in the present study, both heart rate and arrhythmicity index of 3rd instar wild type *Drosophila* larvae significantly increased after injection of 10 mM $CdCl_2$ (Fig. 4-13A and 4-13C) with no significant correlation between heart rate and arrhythmicity index (Fig. 4-13E). Cardiotoxicity of Cd was investigated on other model organisms via injection or oral administration [235,251–253]. In rats, intravenous injection of Cd acetate resulted in dose-dependent acute cardiovascular effects with a high mortality rate at higher concentrations [235]. A significant reduction in heart rate with a progressive decline toward zero was observed 3 minutes after 8 mg/kg Cd injection. In contrast, injection of 4 mg/kg Cd slightly increased the heart rate of rats with no mortality effect [235], which is consistent with what we observed after injection of 23 mg/kg Cd in wild type *Drosophila* larvae (Fig. 4-13A). In zebrafish, the cardiotoxic effects of Cd depend on different parameters such as the animal's developmental stage, Cd concentration, and exposure time [251–253]. Dissolving $CdCl_2$ in fish water during embryonic development resulted in a significant increase in zebrafish embryos' heart rate while decreasing the heart rate in adulthood [251].

In our study, the overexpression of MTF-1 in the *Drosophila* heart significantly ameliorated the changes in heart rate and arrhythmicity index that were observed after injection of $ZnCl_2$ and $CdCl_2$ in wild type larvae (Figs. 4-12 and 4-13). Unlike the wild type group, MTF-1 larvae showed no significant change in their heart rate and arrhythmicity index after injection of $ZnCl_2$ and $CdCl_2$. Also, there was no significant correlation between the heart rate and arrhythmicity index in MTF-1 larvae after injection of $ZnCl_2$ and $CdCl_2$ (Figs. 4-12 and 4-13). We speculate that insignificant changes in heartbeat parameters of MTF-1 larvae, compared to wild type group, was associated with MTF-1-induced overexpression of MT genes in the heart. Upon investigation, we found out that the normalized GFP intensity was significantly higher in NP1029-Gal4:GFP larvae than the wild type group (Fig. 4-15A), demonstrating that the NP1029-Gal4 driver resulted in heart-specific overexpression of target genes, GFP and MTF-1 in our study. The level of MTF-1 expression in NP1029-Gal4:MTF-1 flies was quantified using quantitative real-time PCR (Fig. 4-15B). As shown

in Fig. 4-15, the MTF-1 expression level was significantly higher in MTF-1 flies compared to wild type group.

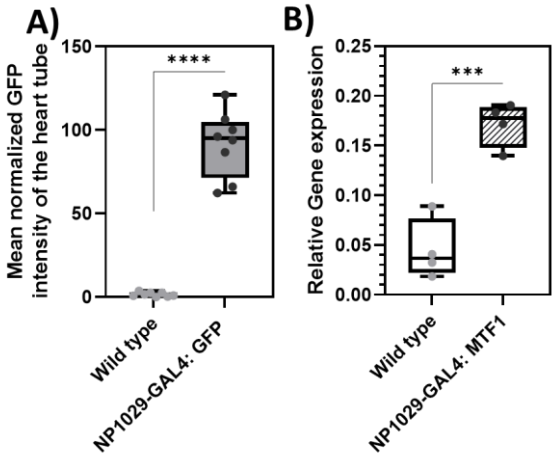

*Figure 4-15: Quantitative gene expression in Drosophila larvae. A) The normalized GFP intensity in the heart of wild type and NP1029-Gal4:GFP larvae. B) The level of MTF-1 expression measured by quantitative real-time PCR in wild type and MTF-1 larvae (NP1029-Gal4:MTF-1). The level of significance between two groups was analyzed using t-test (***: P < 0.001, ****: P < 0.0001). Figures reproduced by permission from Elsevier.*

The toxicity of heavy metals may result from different molecular mechanisms, including the production of reactive oxygen species (ROS), such as the generation of extremely toxic hydroxyl radical from hydrogen peroxide and superoxide anion [254]. Moreover, heavy metals can interact with proteins or ligand groups of enzymes; thereby, disrupting protein structure or inhibiting enzymatic activity [255,256]. Metal-homeostatic genes, including MTs play a key role in heavy metal homeostasis. MTs are the most abundant intracellular, metal-binding proteins. In both mammals and *Drosophila*, transcriptional induction of MT genes is controlled by MTF-1. Under heavy metal load and oxidative stress, MTF-1 binds to specific DNA motifs known as metal-response elements (MREs) and activates the expression of metallothionein genes [81,257]. Previous *in-vitro* studies also support our explanation and illustrate a cardioprotective effect for MT genes. The cardioprotective effect of MT overexpression against Cd toxicity and oxidative stress was investigated *in-vitro* using rat cardiac cell lines [258]. MT overexpressing cardiac cells showed a marked reduction in reactive oxygen species production and significant cellular resistance when exposed to hydrogen peroxide and Cd, respectively.

Our study also demonstrated that injection of $ZnCl_2$ and $CdCl_2$ adversely affects the survival of larvae to pupal and adulthood stages and shortens the lifespan while overexpression of MTF-1 in

the heart of *Drosophila* significantly ameliorates these effects (Fig. 4-14). Previously, the effects of different Zn and Cd concentrations on *Drosophila* growth, development, gustation, oviposition, pupation-site selection, and climbing behavior have been investigated via oral administration [259–264]. Administration of Zn and Cd with concentrations equal to or higher than 500 ppm significantly reduced larval growth, development, and lifespan in both first and second generations [262,265]. Both larvae and adult flies responded behaviourally to the presence of high concentrations of heavy metals. Both Zn and Cd acted as repellents to *Drosophila* at high concentrations, with the feeding and egg-laying of *Drosophila* significantly decreasing [263]. Moreover, the role of Zn transporters, MTF-1, and Metallothioneins in heavy metal homeostasis, excretion, and reabsorption in certain tissues, including Malpighian tubules, gut, nervous system, and hemocyte, has been investigated [80,266].

Researchers illustrated that unlike the situation in the mouse, knockout of MTF-1 in *Drosophila* is not lethal. However, MTF-1 mutants with abolished expression of MTs were significantly sensitive to Zn, Cd, and Cu with a remarkably lower lifespan than wild-type flies when exposed to heavy metals. The failure of MTF-1 knockout flies to induce MT genes was the most likely explanation for *Drosophila* sensitivity to heavy metal load [81]. On the other hand, overexpression of MTF-1 in a tissue-specific manner illustrated that MTF-1-induced changes in lifespan is highly dependent upon its expression pattern and the tissue in which overexpression occurs and can be both protective and toxic [80]. For instance, overexpression of MTF-1 in *Drosophila* gut, hemocytes, and motorneurons resulted in resistant flies with extended lifespan on Fe or Cd but also shortened lifespan on Zn supplemented media. Moreover, Bahadorani et al. [80] illustrated that tissue-specific overexpression of MTF-1 can be more protective than ubiquitous overexpression.

The protective effect of heart-specific overexpression of MTF-1 against Cd in our study is consistent with what was reported by Bahadorani et al. [80] for MTF-1 overexpression in *Drosophila* gut, hemocytes and motorneurons. However, the phenotype arising from the heart-specific overexpression of MTF-1 upon Zn injection in our study was not similar to what was reported by Bahadorani et al. [80] for an oral administration assay of Zn toxicity. The heart-specific MTF-1 overexpression in our study enhanced the resistance of larvae to injection of $ZnCl_2$ while ubiquitous and tissue-specific overexpression of MTF-1 in the gut, hemocytes, and motorneurons enhanced the sensitivity to Zn and shortened lifespan of adult flies on Zn-supplemented medium. We speculate

that the enhanced resistance to Cd and Zn fluctuations in heart-specific MTF-1 overexpressing larvae may be attributed to MTF-1-induced overexpression of MT genes in our study (Figs. 4-14 and 4-15). However, in addition to MT genes, the Zn exporter ZnT35C is also expressed under the transcriptional control of MTF-1 in the digestive tract of *Drosophila*. Bahadorani et al. [80] suggested that MTF-1-induced overexpression of ZnT35C may be responsible for the excretion of Zn and the consequent reduction of Zn pool in tissues where MTF-1 is overexpressed. Reduction of Zn pool in MTF-1 overexpressing tissues was followed by the accumulation of Zn ions in other tissues and consequently higher risk of mortality. However, ZnT35C is predominantly expressed in the malpighian tubules and other parts of the digestive tract of *Drosophila* larvae rather than the heart. In light of the expression pattern of ZnT35C in *Drosophila* digestive tracts, we speculate that MTF-1-induced expression of ZnT35C was more likely to be expressed while heavy metals were administered orally in [80] compared to our study where microinjection was used as the exposure route. Therefore, MTF-1 overexpression in our study may not result in sever expression of ZnT35C; thereby, enhancing the resistance of flies to Zn injection. Another possible reason explaining the protective effect of heart-specific overexpression of MTF-1 in the heart upon exposure to Zn is that the Zn pool in the *Drosophila* heart may be sufficiently large that it is not as severely affected by MTF-1-induced expression of ZnT35C [267]. This speculation is indirectly supported by studies on the importance of Zn in heart development and function in humans and other organisms [267–269]. In fact, Zn is an important element present in the heart that plays a crucial role in the functional integrity of this organ. Zn deficiency was considered a risk factor for cardiac oxidative damage and cardiovascular disorders in humans and other vertebrates [267–269].

Our study is the first *in-vivo* acute toxicity assay in which both wild-type and MTF-1 larvae were directly exposed to heavy metals via injection. For the first time, we used arrhythmicity index, in addition to heart rate, as a parameter that can be used to study cardiotoxic and cardioprotective genes and compounds in small organisms.

The chronic and acute toxic effects of Zn and Cd may significantly change in combination with other heavy metals and toxic compounds such as microplastics [251,270]. In the future, researchers may investigate the effect of MTF-1 against the combined toxicity of Zn and Cd using similar techniques proposed in our research.

Chapter 5

CONCLUSION AND RECOMMENDATION FOR THE FUTURE WORK

5.1 Summary of the Thesis

Drosophila melanogaster larva is one of the most widely used small-scale model organisms for cardiac toxicity and cardiac gene screening. This organism offers many advantages including but not limited to cellular and neuronal simplicity, genetic homology to humans, rapid and low-cost growth and maintenance in labs, body transparency for imaging, and amenability to genetic manipulation. However, *Drosophila* mobility at larval stage, having a small and flexible body, and a floating heart tube with a spatial position underneath the dorsal epidermis have impeded the use of intact *Drosophila* larvae in heart screening studies. Conventional *Drosophila* larva manipulation, chemical administration, and behavioural phenotyping techniques are time-consuming and labor intensive. Recently, microfluidic technology has been used widely in experimental biology using Drosophila. Microfluidic devices in this field have been developed for different purposes, including

manipulation, immobilization, stimulation, and imaging. According to the type of the assay and substantial differences in the shape, size, stiffness, and behavior of this organism at different developmental stages (embryonic, larval, pupal, and adulthood), different designs and fabrication techniques have been proposed.

In-vivo cardiac toxicity assessment on intact *Drosophila* larvae requires precise chemical delivery into the body cavity for direct exposure of the heart, proper orientation for heart monitoring, and complete immobilization of the larva, all addressed by our proposed microfluidic device (**Obj. 1**). After loading the larva via loading glass capillary, the larva's position could be adjusted by orientation glass capillary. Reversible immobilization of the larva was also achieved by side suction channels without negative effect on heart rate. A needle channel provided a one degree-of-freedom control of the microneedle during microinjection. The viability of the injected larvae using the proposed microfluidic device was not affected after injection. A single chip can be used for multiple reagents since the needle can be easily replaced. A custom-made pressure-driven flow was characterized based on the needle size to deliver a controlled amount of injection substances by controlling the amplitude and the duration of the pressure pulse. We used our technology to investigate the hemolymph circulation in *Drosophila* larval open circulatory system. The fluorescent dye angiography demonstrated that (1) the hemolymph flow is unidirectional and ostia functions as a hemodynamic valve, (2) the systole and diastole of *Drosophila* larval cardiac cycles are characterized as those in vertebrates, and (3) the hemolymph flow is a cardiac-dependent, convective bulk mass transport in *Drosophila* larvae.

Moreover, we have developed an open access tool for phenotypic quantification of heart function of Intact larvae (**Obj. 2**). In-vivo quantification of heartbeat parameters for intact larvae is challenging due to (i) the movement of internal organs which are present even when the animal is completely immobilized, resulting in high noise levels, and (ii) cardiac interruptions such as elevated arrhythmicity, bradycardia, and tachycardia. Our software enables automatic detection of the most contractile region of the heart in a video and extracts the heartbeat signal based on the mean pixel intensity in a fast and automatic manner. A strong advantage of our software is its user-friendliness which allows the user to select the desired time interval in a long video for analysis, select the ROI if needed, calibrate the video frames (define a scale for the frames), and extract the M-mode. Moreover, all the processing steps including the extraction of the most contractile region of the heart

as well as signal processing steps (*i.e.*, detrending, smoothing, and peak analysis) are inspectable which allows the user to be involved in each step and change the effective parameters if needed.

To remove the undesired low-frequency trends from the raw signal, we used the SPA method as a time-varying high-pass filter. A comparison between the SPA method and the conventional bandpass filtering demonstrated that the SPA method is more robust and less user-dependent. The peak prominence analysis followed by smoothing the detrended signal allowed us to precisely detect more than 94% of the peaks and calculate heart period and cardiac arrhythmicity. The heart rate and cardiac arrhythmicity could be quantified automatically even if the video was not magnified or did not have good quality. Using the proposed software, we successfully detected the cardiac arrests that occurred when the immobilized *Drosophila* larvae attempted to crawl. Moreover, the integration of microfluidic-based immobilization and the proposed MATLAB-based software enabled the measurement of other heartbeat parameters including EDD, ESD, SD, ST, FS, and SV on the intact larva. This could be done in a semi-automatic manner by marking the diastole and systole phases on the M-mode. Also, comparing the peak analysis with the M-mode provided a straightforward interpretation and enabled the user to validate the accuracy of the signal processing and peak analysis.

We demonstrated the application of our microfluidic device and heartbeat quantification software for investigating the effect of different chemicals (e.g., serotonin and heavy metals) (**Obj. 3a**) and genes (e.g., MTF-1) (**Obj. 3b**) on *Drosophila* larval heart function in both wild type and genetically modified larvae. A significant increase in heart rate was observed two minutes after injection of 40 nL serotonin with concentrations equal to or higher than 0.01 mM in 3rd instar larvae. In addition, the heart rate of 2nd instar larvae significantly increased after injection of 5 nL serotonin with a concentration of 0.01 mM. Previous intact *Drosophila* injection assays for the study of neurotransmitters have been done on prepupal or pupal stages in which animals experience hormone changing due to metamorphosis and no longer eat or move. However, our study is the first reversible and viable on-chip serotonin injection assay on 2nd and 3rd instar motile *Drosophila* larvae. Also, both wild-type and MTF-1 3rd instar larvae were injected with 10 mM and 100 mM $ZnCl_2$ as well as 10 mM $CdCl_2$, dissolved in drug carrier solution as the control chemical. Upon 100 mM $ZnCl_2$ injection into wild-type larvae, heart rate was significantly decreased and arrhythmicity was increased considerably 6 min post-injection. There was a significant negative correlation between

the heart rate and arrhythmicity index of individual larvae when injected with 100 mM $ZnCl_2$. Also, after 10 mM $CdCl_2$ injection into wild-type larvae, heart rate and arrhythmicity index were significantly increased 15 min and 2 min post-injection, respectively. Overexpression of MTF-1 in the heart remarkably ameliorated these effects such that there was no significant change in the heart rate and arrhythmicity index of MTF-1 larvae. The survival rate of wild-type larvae to pupal and adulthood stages, as well as flies' lifespan, were significantly decreased after injection of $ZnCl_2$ and $CdCl_2$. However, heart-specific overexpression of MTF-1 prolonged the longevity of larvae to pupal and adulthood stages and increased the overall lifespan of the flies injected with heavy metals solution. Thus, the heart function is influenced after exposure to Zn and Cd, with heart rate and arrhythmicity index as promising biomarkers for acute toxicity measurement. Moreover, overexpression of MTF-1 in the heart can ameliorate cardiac toxicity and lifespan reduction when exposed to heavy metal loads.

The application of our microfluidic injection and heartbeat quantification techniques were successfully demonstrated for dye angiography, cardiac toxicity, and gene screening on intact *Drosophila* larva as an *in-vivo* model of the heart.

5.2. Recommendations for Future Works

Despite many advantages offered by our microfluidic device and heartbeat quantification technique, we acknowledge that they may not be thoroughly ready for adoption by the end user scientists to supplement or even replace their time-consuming and labor-intensive techniques. Here, we discuss some challenges and limitations of our device and software that need to be tackled to make them more affordable and available for end-users with no engineering background.

Our microfluidic microinjection system was successfully used for 2nd and 3rd instar larvae. However, we could not use this device for 1st instar larvae due to significantly smaller size of the animal at this stage. The microneedle channel, side immobilization suction channels, loading and orientation glass capillaries were oversized such that the larva could move entirely into the immobilization channels or orientation glass capillary. Therefore, the design needs to be significantly downsized. 3D printing may not be useful for smaller dimensions; therefore, the photolithography technique is proposed for

fabricating the master molds for 1st instar larvae. Also, smaller glass capillaries must be used for fabrication of microneedles and for orientation and loading of the larva.

Although our microfluidic device enables localized microinjection and heart monitoring, the loading, orientation, and microneedle actuation are still done manually. The user needs to have a prior knowledge on *Drosophila* anatomy and some skills in animal's handling to be able to work with our device. To increase the speed of the process and decrease operator's input, loading, immobilization, microneedle actuation, and unloading should be automated. Loading and unloading can be automated by integrating solenoid actuators and deformable membrane valves which was used previously for other small organisms (e.g., *C. elegans* and zebrafish) [63,271]. The orientation glass capillary can be connected to a step motor to automate the orientation of the larvae. Machine learning algorithms can be trained based on input from camera to detect the heart tube and trachea. A feedback controller can be designed to measures the output of real-time image processing and then manipulates the input as needed to drive the step motor toward the desired angle which provides a clear picture of the heart. Using real time imaging and feedback controllers, the microneedle can be actuated too. Different injection steps including needle insertion, chemical release and needle removal can be controlled according to input from real time imaging and image processing [123]. Recently, a multiscale, multi-respective imaging technique was used to develop a computer-guided robot for off-chip microinjection of *Drosophila* embryos [272] which can be applied to our microfluidic technology for injection and heart monitoring of intact larvae. These implementations are necessary for developing fully automated microinjection and heart monitoring microsystems, capable of performing assays and gathering results without the continuous involvement of an operator.

Regarding our heartbeat quantification software, detection of the most-contractile region of the heart, extraction of the heartbeat signal, and heart rate and arrhythmicity index calculation can be done automatically. However, for parameters that are measured from the M-mode (e.g., EDD, ESD, FS), the user's involvement is required to mark the diastolic and systolic phases. Machine learning algorithms can be developed and trained to analyze the M-mode automatically and reduce the operator's input. A similar idea have been applied to OCT images to detect the heart diastolic and systolic phases [72] which can be modified for bright field microscopy.

There are several challenges associated with microneedle fabrication, integration into the PDMS chips, and using it during microinjection process. Some of these technical challenges were addressed in our work. For instance, our 3D printed fixture with several modules including a device holding module with designated groove and tongue joints, needle holder module, and moveable block for microneedle actuation facilitates the integration of microneedle into the PDMS chip and actuating it with acceptable resolution. Also, the use of glass capillaries with internal filaments for microneedle fabrication significantly facilitated the microneedle filling process. The capillary filling of microneedle tip through the narrow filament reduced the chance of trapping air inside the needle. Yet, there are other challenges in using glass capillaries for microneedle fabrication and microinjection. This includes but not limited to

Calibration: After pulling the glass capillaries with controlled temperature and pulling rate, breaking the tip of the needles resulted in different tip sizes. Manual creation of each needle-tip introduces undesired variability; because each needle tip is opened manually, an inherent variability exists in the volume of chemicals that will be injected into the organism from different needles. Therefore, characterization of the reagent delivery system with respect to the volume of the delivered reagent was required, as described in this thesis. Simillar needles are needed so calibration time and variability are greatly reduced. In this regard, instead of conventional pulling technique, microneedles with desired tip sizes may be fabricated by any suitable 3D printing technology/additive manufacturing technique, such as direct laser writing (DLW) [273]. DLW uses tightly focused femtosecond laser pulses to initiate spatially controlled polymerization (i.e., solidification) of a liquid - phase photoreactive material via two – photon (or multi – photon) absorption phenomena. By precisely positioning the focal point of the laser with a point- by- point, layer-by-layer manner, 3D structures comprising cured photomaterial can be additively manufactured with resolutions on the order of 100 nm [273]. There are other additive manufacturing techniques that have the potential to be used for microneedle fabrication including but not limited to stereo lithography (SLA) [274], fused deposition modeling (FDM) [275], etc. In general, these techniques are suitable for preparing microneedles that are made of materials other than glass, such as different types of silica [276].

Susceptibility to adherence and clogging: cytoplasmic material presents in cells and tissues of the target animal, or residuals and particles inside the injection solution can adhere to the glass surface.

Protein and lipid adhesion/adsorption can clog the needle-tip opening. Also, small air bubbles can be trapped inside the microneedle if the filling process is not executed with care. In these cases, the injection process cannot be done, and the needle is useless. The binding affinity of macromolecules (e.g., proteins, lipids, etc.) to a surface is governed by electrostatic interactions and hydrophobic interactions [277]. To enhance anti-clogging capabilities of the microneedle, the surface of the microcapillary needle may be coated with anti-adhesive and anti-clogging substances. In some aspects, microneedles fabricated by new additive manufacturing techniques (e.g., DLW, SLA, etc.) may not need an anti-clogging/anti-adhesive coating, as mechanical features (e.g., one or more side openings, microstructures, etc.) may be considered in the design of the needle tip to limit clogging as recently offered by Kinneret Rand (Fig. 5-1) [276].

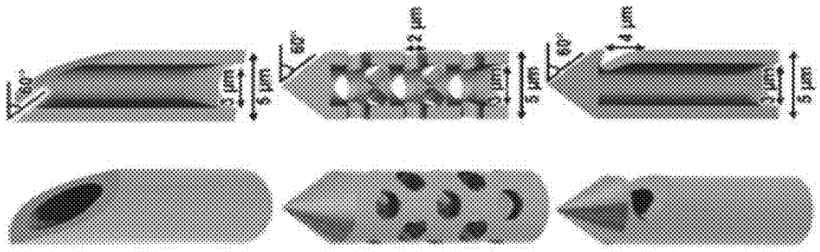

Figure 5-1: Possible designs of microneedles using additive manufacturing [276].

Low contrast visibility: the glass capillary microneedles are transparent. This creates low contrast visibility when tracking the penetrating needle-tip in PDMS chip and inside the animal's body, leading to missed-injection targets. One possible solution to this challenge, is to dissolve small amounts of fluorescent dye to the injection solution to increase the visibility of the needle and injected solution, as described in this thesis and also presented by other researchers [124]. Yet, fluorescent and bright field microscopy needs to be done simultaneously to be able to see the small concentration of dye. As an alternative solution, color marked microneedles or micropipettes may be generated using gold nanoparticles (AuNPs) or gold-silver alloy nanoparticles (AuAgNPs) to produce a broad range of colors.

Of note, the anti-adhesive, anti-clogging, and color marking reagents must be heat resistant (if exposed to pipette pullers), stable after attachment to the microneedle, non-cytotoxic, and preferably approved by a regulatory agency for *in-vivo* and *in-vitro* use [276]. Recently, SeeTrue Technology,

a Startup company is lunched to produce color marked/tinted anti-adhesive/anti-clogging microneedles. However, their product was not ready during the course of this research.

In the future, our microfluidic microinjection system and heartbeat quantification technique, can be improved by implementing abovementioned technologies to address above-mentioned technical challenges and increase the automation in chemical screening and heart monitoring. The applications of such automated platforms are extremely broad as discussed in this thesis. We already demonstrated the application of our microfluidic and heartbeat quantification software for cardiac toxicity and cardiac gene screening. The effect of other chemicals such as neurotransmitters and peptides that can regulate the heart function [278] as well as ecotoxicity of other pollutants e.g., heavy metals, microplastics, and nano- and micro-particle toxicants can be investigated on different transgenic *Drosophila* models.

Another exciting application for our *Drosophila* microfluidic technology is to use them to study infectious diseases (e.g., SARS-COV-2). SARS-COV-2 caused the coronavirus disease (COVID-19) pandemic in 2019 [279] and adversely affected many aspects of humans' life from health to economy. Our research was also influenced as we experienced several months of lab closures due to COVID-19 quarantine and isolation policies. Numerous studies aimed to stem the spread of SARS-CoV-2, control the COVID-19 pandemic, and develop vaccines and therapeutics [280]. Several forms of cardiovascular complications have been reported in patients acutely during COVID-19 and/or after apparent recovery [281]. This includes myocardial/pericardial inflammation, arrythmias, heart failure and sudden cardiac death in the acute phase (before recovery) [281]. These syndromes are more likely to occur with increasing severity of COVID-19 as well as older patients or those with existing co-morbidities. Moreover, an increased risk of clinical and subclinical cardiac sequelae has been demonstrated in patients who have recovered from COVID-19.

Due to a high degree of genetic homology and physiological similarities to humans, mammalian models played a key role in COVID-19 related studies. Invertebrates e.g., *Drosophila*, have been relatively overlooked in COVID-19 research while they offer many advantageous, as discussed in this thesis. Recently, few research groups have utilized Drosophila to investigate SARS-CoV-2-host interactions and pathogenicity [92,282–284]. Yet, the pathogenicity of SARS-COV-2 proteins in the heart of Drosophila has not been investigated. The feasibility of genetic manipulations using a

variety of methods e.g., the fly UAS-GAL4 gene expression system used in this thesis, makes this animal suitable for rapid functional investigation of virus proteins, genetic screening, and pharmacological studies in a tissue specific manner. Using heart-specific GAL4 drivers researchers can express SARS-COV-2 proteins in the heart of *Drosophila* larvae, measure the changes in heart function using our software and test potential therapeutics against them using our microinjection system.

APPENDICES

A. SmallHeart Installation Instructions

To install this software you need to download and install the Windows version of the MATLAB Runtime for R2018b. You can download it from the following link on the MathWorks website: http://www.mathworks.com/products/compiler/mcr/index.html

1. Download the SmallHeart.exe supplementary file.
2. Run the software as an administrator by right-clicking on the SmallHeart.exe file and choosing "Run as administrator" or by double-clicking the file.
3. After running the file, the software icon appears for a few seconds; then, it will disappear. The installation may take a few minutes when running the software for the first time. Finally, the first GUI of the software will appear on the screen and the user can upload the video.

B. Microfluidic Capillary Pressure-Driven Viscometry of *Drosophila melanogaster*'s Hemolymph[††]

B.1 Introduction

The main fluidic component of *Drosophila*'s circulatory system is hemolymph, an extracellular fluid representing the insect's blood. Hemolymph directly supplies different organs with nutrients, signal peptides, metabolites, hormones, and macrophages responsible for wound healing [9]. Studies on the biochemical properties of hemolymph such as amino acids, peptides, and ion homeostasis has provided new insights for different diseases such as diabetes [285–287]. The physiological homology between *Drosophila* and the mammalian circulatory system has been demonstrated to some extend by quantifying several measures of *Drosophila*'s cardiovascular function, including cardiac output, aortic hemolymph velocity and intracardiac hemolymph velocity [84,247,288].

Despite the above advancements, the physiological and rheological properties of *Drosophila* hemolymph, such as its viscosity and interfacial tension, have not been characterized. Measuring the viscosity of *Drosophila* hemolymph enables performing hemorheology studies on this model organism which can demonstrate the degree of rheological homology between *Drosophila* and vertebrates. Moreover, there is a need for studying the impact of insects' residue (hemolymph, red fluid, and exoskeleton) on aerodynamic surfaces [289–291]. Insect fouling from coagulated hemolymph and other residues was studied using *Drosophila* and other insects, demonstrating that it can increase the drag force and fuel consumption for aircrafts by causing a boundary layer transition from laminar to turbulent flow [289,292]. Knowing the physical properties of hemolymph will be necessary for studying the effect of surface wetting characteristics and dynamics resulting from a hemolymph drop impact on aircraft wings [292].

[††] Contents of this section have been collected from the journal article (permissions acquired and presented in the following):

- A. Zabihihesari, S. Parand, P. Rezai, Microfluidic Capillary Pressure-Driven Viscometry of Drosophila melanogaster's Hemolymph, *Journal of Experimental Biology*. Under review

Drosophila's mobility at larval and adulthood stages as well as its small size and relatively low hemolymph volume impose a substantial challenge to the reliable measurement of biophysical properties of hemolymph, e.g., viscosity [1]. Different techniques have been introduced for hemolymph sampling from *Drosophila* larvae and adult flies, enabling the collection of up to 300 nL hemolymph from these organisms [293,294]. However, standard viscometers (e.g., capillary tube or rotational viscometers) require a large amount of sample, typically several milliliters or more [295]. Therefore, attempts to measure the viscosity of insects' hemolymph are limited to larger ones such as hornworms and the butterfly [296].

With the advent of microfluidics, researchers have developed different devices to overcome the technical limitations of conventional viscometers, including requiring large volumes of samples, being inefficient, and being time-consuming [297–299]. Among different microfluidic viscometers [297], those relying on capillary pressure and surface wetting properties can passively draw fluids into microchannels without the need for cumbersome or expensive instrumentation (e.g., syringe pumps). This type of microfluidic viscometer has a relatively simple operation without the need for active or moving parts. A droplet of the sample placed at the inlet of the microchannel is drawn inside the device due to surface tension while the growth of the liquid column inside the channel is quantified using video recording and image analysis. An important parameter which affects the wettability of the sample is the material of the microchannels. A hydrophilic material is required for this type of viscometer. Therefore, glass has been dominantly used for fabrication of capillary pressure-driven viscometers with small micrometer-scaled channels; however, it dictates a complex and relatively expensive fabrication procedure which requires annealing at high temperature (550℃), chrome and gold layer deposition, photolithography, chemical etching using gold and chrome etchants, and bonding the patterned glass to a silicon substrate using optical adhesives [300].

Polydimethylsiloxane (PDMS) is a widely used material for microfluidic device fabrication which is low cost, chemically inert, non-toxic, and transparent [301,302]. PDMS soft lithography on 3D-printted or photolithographically patterned molds enables creating features in the micrometer range which is simpler, cheaper, and less time consuming than other competing techniques developed for less desirable materials (e.g., glass, silicon, or plastics) [303]. Nevertheless, the unique properties of PDMS such as hydrophobicity and gas permeability have hindered its use in the fabrication of microfluidic capillary pressure-driven viscometers.

Here, we first applied a previously developed PVA coating technique [303] and characterized the capillary filling process in open and sealed microchannels to addressed the technological gap of PDMS hydrophobicity and gas permeability, respectively, and used this material for fabricating a microfluidic capillary pressure-driven viscometer. This viscometer was then applied to measure the viscosity of 3rd instar *Drosophila* larval hemolymph for the first time. The reported value for *Drosophila*'s hemolymph viscosity may be used in hemorheology and physiology studies as well as other engineering applications such as modeling the hemolymph drop impact on airfoils in aerospace engineering.

B.2 Theory of Microfluidic Capillary Pressure-Driven Viscometers

A technique based on capillary pressure driven flow inside microchannels was adopted and modified in this paper for measuring the hemolymph viscosity [300]. The microfluidic device has two pairs of open channels (OC1 and OC2) and sealed channels (SC1 and SC2), as shown in Fig. A-1. The liquid viscosity in a microchannel can be calculated using the Hagen-Poiseuille equation for pressure-driven laminar flow.

$$\mu = \left(\frac{d^2}{S}\right)\left(\frac{\Delta P}{vL}\right) \tag{B-1}$$

where μ is the dynamic viscosity, d is depth of the channel, L is length of the liquid column inside the channel, ΔP is the pressure drop across the liquid column inside the channel, v is the liquid mean velocity inside the channel, and S is a constant specific to the channel geometry.

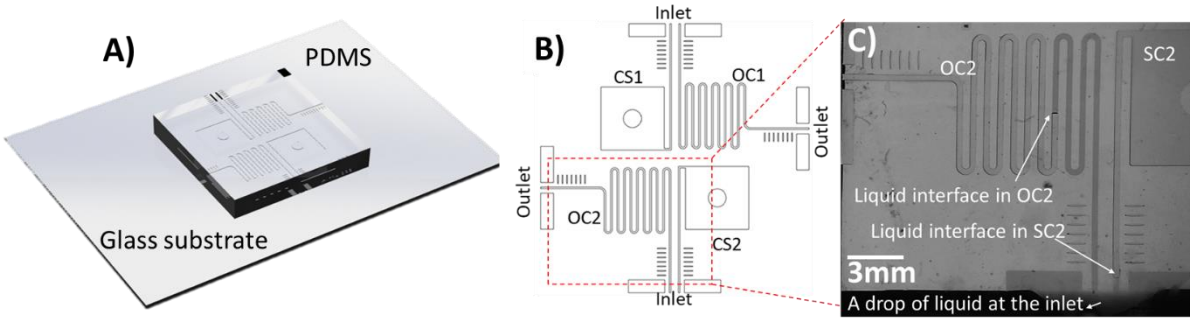

Figure B-1: The microfluidic device for Drosophila hemolymph viscosity measurement. A) The PDMS layer containing the microchannel network bonded to the glass slide. B) The schematic of the microfluidic device design. C) The capillary filling process in the open (OC) and sealed (SC) microchannels.

In the device shown in Fig. B-1, ΔP is generated due to the capillary pressure. As a result of capillary action, a drop of liquid placed at the inlet of an open hydrophilic microchannel is spontaneously drawn into the channel and continues to flow until it reaches the outlet. The capillary filling in an open channel can be understood using the Lucas Washburn equations [304,305], providing a solution for a fully developed Poiseuille flow with $x \propto \sqrt{t}$, where x is the distance of the advancing meniscus from the channel inlet.

If the microchannel is sealed at one end, the liquid is spontaneously drawn into the channel and compresses the trapped air inside the channel such that the air pressure inside the sealed channel increases as the liquid column advances. Eventually, the air pressure inside the channel reaches to a value equal to the atmospheric pressure plus the capillary pressure. At this moment, if the microchannel material is gas impermeable (e.g., glass), the liquid partially fills the sealed channel and stops at the equilibrium position as the air has no way to exit the sealed channel [300]. Otherwise, if the channel is made of a gas permeable material (e.g., PDMS in this paper), the compressed air starts to exit the sealed channel through the porous PDMS, and liquid continues to move forward and replace the air, but perhaps with a lowered velocity compared to the initial filling phase. The capillary pressure can be calculated using the ideal gas law in a sealed channel as:

$$P_{capillary} = \Delta P = P_{atm}(\frac{V_1}{V_2} - 1) \quad \text{(B-2)}$$

where, $P_{capillary}$ is the capillary pressure, P_{atm} is the atmospheric pressure, and V_1 and V_2 represent the volume of air inside the sealed channel before and after compression by the liquid, respectively. In case of PDMS, V_2 is calculated from the position of the air/liquid meniscus inside the sealed channel right after the air is compressed in the channel and liquid velocity decreases to a constant low value. Such measurement of the capillary pressure using a sealed channel does not require prior knowledge of the channel geometry, surface tension, and contact angle [300]. Hence, the microfluidic viscometer in this study has both open channels (OC) and sealed channels (SC) used to measure the product vL and ΔP, respectively (Fig. B-1B and B-1C).

The parameter $\frac{d^2}{S}$ in Eq. 1 depends on channel geometry. However, it also can be calculated using a calibration liquid of known viscosity (e.g., water) on one pair of open and sealed channels (i.e., OC1 and SC1 in Fig. B-1) as

$$\frac{d^2}{S} = \mu_{calib}\left(\frac{vL_{calib}}{P_{capillary,calib}}\right) \quad \text{(B-3)}$$

where μ_{calib} is the viscosity of the calibration liquid. vL_{calib} is the product of liquid velocity and the liquid column length calculated from the OC1. $P_{capillary,calib}$ is the capillary pressure calculated from the SC1 using Eq. B-2.

Because both OC1 and OC2 channels on the microfluidic viscometer are of identical geometry, the calculated value of $\frac{d^2}{S}$ also applies for the sample in the second open channel (OC2) and the viscosity is calculated as

$$\mu_{sample} = \mu_{calib}\left(\frac{vL_{calib}}{P_{capillay,calib}}\right)\frac{P_{capillay,sample}}{vL_{sample}} \quad \text{(B-4)}$$

B.3 Materials and methods

B.3.1 Chemicals and reagents

PDMS prepolymer base and the curing agent kit (Sylgard 184 silicone elastomer kit) were obtained from Dow Corning (Midland, USA). Polyvinyl alcohol (PVA, 87–90% and 99+% hydrolysis degree, Product# 563900), 5 cSt silicone oil (Product# 563900), and 20 cSt silicone oil (Product# 378348) were purchased from Sigma-Aldrich (St. Louis, USA). DI water was obtained using a Milli-Q system (Millipore Ltd., Canada). SU-8 2075 photoresist and silicone wafers were purchased from MicroChem Corp. (Westborough, USA) and Wafer World Inc. (West Palm Beach, USA), respectively.

B.3.2 Fly culture and maintenance

We used 3rd instar wild-type rosy^{+5} *Drosophila* melanogaster larvae in this study. Adult flies were cultured in plastic fly stock bottles under uncrowded conditions at room temperature (approximately 22°C). The standard *Drosophila* yeast media was prepared as described in [85,306] and contained 100 g sugar, 50 g dry yeast, 18 g agar, 8 g sodium potassium tartrate tetrahydrate, 1 g potassium

phosphate monobasic, 0.5 g sodium chloride, 0.5 g calcium chloride dihydrate, 0.5 g magnesium chloride hexahydrate, 0.5 g iron (III) sulfate hydrate, 5ml propionic acid and 2 g methyl 4-hydroxy benzoate (2 g dissolved in 20 ml of 95% ethanol) dissolved in 1 L of tap water. Before conducting the experiments, adult flies were removed from the bottle and 3rd instar larvae were transferred into a Petri dish containing phosphate-buffered saline (PBS) to be used for hemolymph sampling.

B.3.3 Hemolymph sampling

To extract *Drosophila*'s hemolymph, 3rd instar larvae were washed in PBS solution to remove any remaining food or waste from the cuticle. Then, larvae were placed on top of a Kimwipe tissue to dry. Larvae were placed collectively into a 1.5 mL microcentrifuge tube while being pierced near the mouth hook using a forceps tip. The hemolymph started to seep out at this stage. The bottom of the tube was cut using a laser blade and placed into a larger one (5 mL) for collecting hemolymph during centrifugation. Then, dissected larvae were centrifuged at 5000 rpm for 2 minutes and hemolymph was collected in the bottom tube. Another round of centrifugation was repeated to remove the residuals, e.g., tissues, from the sample. Hemolymph was collected from the top level of the centrifuge tube using a micropipette.

B.3.4 Microfluidic chip design and fabrication

Our PDMS microfluidic device design was inspired by the glass device reported by Srivastava et al. [300] and consisted of two open microchannels (OC1 and OC2, $d{\sim}45\,\mu m$, $w{\sim}300\,\mu m$, and $L{\sim}9\,cm$) and two sealed microchannels (SC1 and SC2, $d{\sim}45\,\mu m$, $w{\sim}300\,\mu m$) (Fig. B-1). One set of the open and sealed channels (OC1 and SC1) were used for infusing a calibration liquid into the device while the other set was used for testing the hemolymph liquid sample (OC2 and SC2).

The device was fabricated using PDMS soft lithography on photolithographically patterned master mold. The master mold was fabricated using SU-8 2075 photoresist patterned on a silicone wafer. Initially, photoresist was spin coated on a 4-inch diameter wafer at 4000 rpm followed by pre-baking at 65 °C and 95 °C. Then, UV light exposure was done with a dose of 215 mJ cm−2 using a photomask containing the microchannel patterns in Fig. B-1B on an ultraviolet exposure system

(UV-KUB 2, KLOE, France). The master mold was then post baked at 65 °C and 95 °C, developed in SU8 developer, and hard baked at 200 °C.

PDMS base monomer was mixed with the curing agent at a ratio of 10: 1 and degassed in a vacuum chamber for 10 minutes. Then, the degassed PDMS pre-polymer was poured over the master mold and cured at 75 °C in an oven.

Capillary pressure driven flow should happen in hydrophilic channels. However, PDMS is hydrophobic. Thus, polyvinyl alcohol (PVA) deposition following plasma treatment was used to make hydrophilic channels [303]. Briefly, PVA was added to DI water and stirred at room temperature and 100℃ for 40 min and 1 hour, respectively. Then, the temperature was reduced to 65℃ and the solution was stirred over night. PDMS pieces containing the microchannel networks were thoroughly degreased in IPA for 1 min and completely dried with air and dehydrated on a hot plate at 100°C for 40 minutes. PDMS pieces were then plasma oxidized using a plasma cleaner (PDC-001-HP Harrick Plasma, USA) at 870 mTorr pressure at 30 W for 1 min. Plasma treated PDMS pieces were immediately placed into the PVA solution for 10 minutes at room temperature, blown dried with air, and dehydrated on a hot plate at 100°C. Finally, the PVA-coated PDMS pieces were plasma bonded to a glass slide to form the microchannels.

B.3.5 Contact angle measurement

The contact angle measurement was done to study the surface wettability of PDMS at three conditions including a) after plasma oxidization, b) after PVA coating, and c) after plasma oxidization of PVA-coated PDMS. We used a Drop Shape Analyzer DSA100 (Hamburg, Germany) to measure the static contact angle of DI water-air on PDMS surfaces. Three different samples were used for each condition. 8 μL DI water droplets were placed on top of PDMS surfaces, far away from the edges. We measured the contact angles immediately and up to two days after PVA coating of PDMS. All measurements were carried out at room temperature (22℃).

B.3.6 Experimental procedure and data analysis for viscosity measurement

The experimental setup (Fig. B-2) consisted of the microfluidic device in Fig. B-1 and an upright microscope (Stereomicroscope Leica MZ10F, Singapore) equipped with a camera (SN 14120187, FLIR Systems Inc., Canada). Using a micropipette (Product# UZ-24505-22, Cole-Parmer, Vernon Hills, USA), one droplet of the liquid sample (~2 μL) was placed at the inlet of each channel to wick into the channels. The capillary flow of the liquid inside the microchannels was video recorded at 45 fps. This measurement was repeated four times for each liquid sample on PVA-coated PDMS devices.

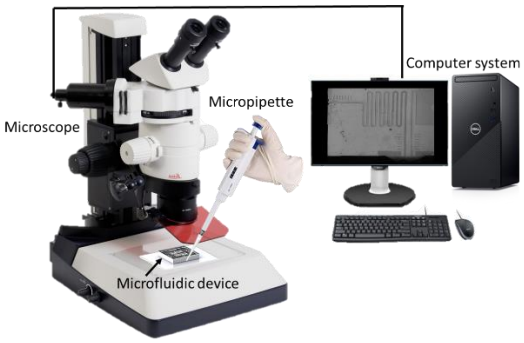

Figure B-2: The experimental setup containing an upright microscope, a micropipette, the microfluidic device, and a camera connected to a computer system.

A MATLAB code was developed to analyze the videos of liquid motion in microchannels. The code determined the location of the advancing meniscus in each video frame and measured the advancing length of the liquid column (L), defined as the distance along the channel between the advancing meniscus and the inlet of the microchannel. The incremental increase in the length (ΔL) over short times (Δt) was used to calculate the transient liquid velocity (v) in the channel. Then, the product of liquid velocity and liquid column length, vL, was calculated and used in Eq. 4 to calculate the viscosity. All data were expressed as mean ± standard deviation (SD).

B.4 Results and Discussion

B.4.1 Surface wettability of PVA-treated PDMS

PDMS hydrophobicity hinders its use to create capillary pressure driven flow in microchannels (Fig. B-3A). One approach to create hydrophilic PDMS is to use plasma or UV irradiation to oxidise the polymer surface [307]. Nevertheless, these techniques have a transient effect because the unpolymerized bulk monomers migrate to the PDMS surface only a few minutes after plasma or UV exposure [303,307]. This transient effect was also demonstrated in our experiments as the contact angle of water-air on the PDMS surface after plasma treatment (30W, 1 min) continuously increased from less than three degrees immediately after plasma treatment to 92.8 ± 3.3 one day after treatment (Fig. B-3B and B-3E). This is also consistent with what was reported by other researchers for quantifying hydrophilicity of plasma treated PDMS [307–312].

The continuous hydrophobic recovery of plasma treated PDMS hinders its use for creating stable capillary pressure driven flow, thereby causing inaccuracy in viscosity measurement using surface tension viscometers (Fig. B-3B and B-3E). On the other hand, combined plasma oxidation and PVA coating has been shown to result in more stable and sustained hydrophilicity which could be used to create capillary pressure driven flow in microchannels for different applications including viscosity measurement (Fig. B-3C and B-3E). The contact angle of water-air on PVA-coated PDMS was 34 ± 2.6, fifteen minutes post treatment. It was more stable compared to plasma treated ones such that the water-air contact angle remained almost unchanged from 15 min up to 2 hours post treatment. The PVA-coated PDMS remained hydrophilic for a long time such that the water-air contact angle increased gradually up to 57.8 ± 2, two days after treatment. The surface wettability of PVA-coated PDMS in our study is consistent with what was reported by Trantidou et al. who used PVA for hydrophilic surface modification of PDMS for droplet generation in microfluidic devices [303].

In our device, the PVA-coated PDMS must be plasma bonded to a glass slide to form the microchannels. So, the effect of the second plasma treatment (30W, 25s) on the water-air contact angle was investigated (Fig. B-3D and B-3E). The contact angle of PVA-coated PDMS 15 minutes after plasma treatment was 18.6 ± 3.1 which increased only by 5 degrees in one hour post treatment. This gave us enough time to complete the viscosity measurement between 30 minutes to 45 minutes

after bonding the PDMS layer to glass substrate. The viscosity measurement started 30 min after plasma bonding of PVA-coated PDMS when the contact angle is stable (with only ~6% increase from 30 min to 45 min post-treatment) and small enough (~19.9-21.1) to induce capillary filling process. Thirty minutes interval between PDMS bonding and viscosity measurement was also necessary for hemolymph sampling and introducing it to the device before hemolymph melanisation. The contact angle of PVA-coated PDMS after the second plasma treatment reached to 57.3 ± 2.5, same as PVA-coated PDMS before the second plasma treatment.

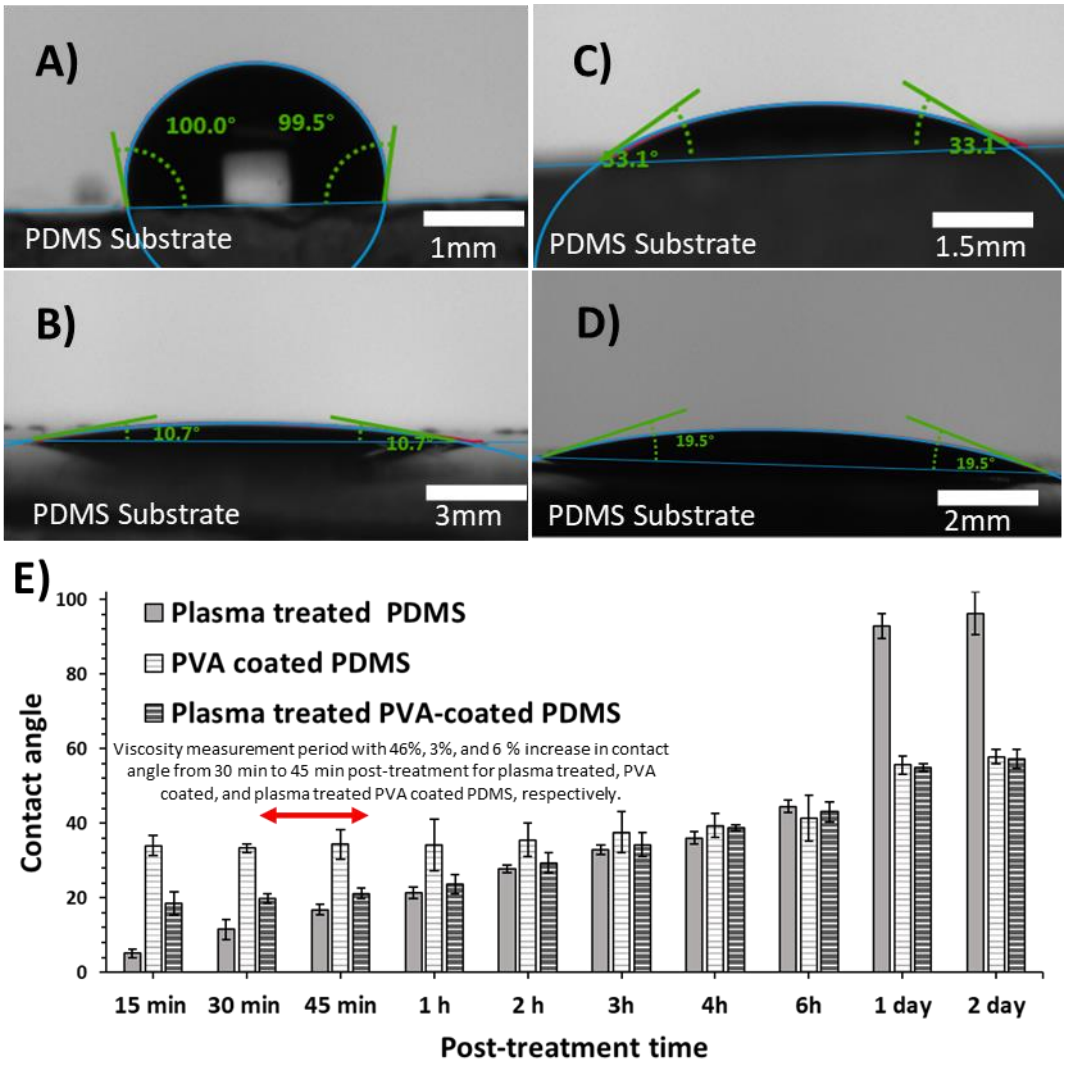

Figure B-3: Surface wettability study of PDMS under different treatments. The contact angles of water-air on PDMS surfaces are shown (A) without any PDMS treatment, (B) 30 minutes after PDMS plasma treatment, (C) 30 minutes after PVA coating of PDMS, and (D) 30 minutes after the second plasma treatment on PVA-coated PDMS. E) The contact angle measurement was done at different times post-treatment. Error bars represent standard deviation (SD). The red double arrow shows the longest viscosity measurement interval that took about 15 minutes for 20 cSt silicone oil, with no significant change in the wettability of the plasma treated PVA-coated PDMS.

B.4.2 Capillary filling of PVA-coated PDMS microchannels

Open Microchannels (OC)

The capillary filling process in plasma treated PVA-coated gas permeable PDMS microchannels was characterized to compare it with existing literature for gas impermeable (e.g., glass) microchannels [304,305]; then, used for viscosity measurement. Thirty minutes after plasma bonding of the device, a drop of liquid sample was placed at the inlet of the device and capillary-drawn into the open microchannel as shown in Fig. B-1C. In the open microchannels, the liquid moved forward with a high velocity at the beginning. As the fluid moved forward, the length of the liquid column (L) increased while the liquid velocity (v) gradually decreased due to the time-lapse increase in the channel hydraulic resistance (Fig. B-4Ai−4Ci and B-4Aii−4Cii). The average liquid velocity ($\hat{v}$) inside the open microchannel was calculated by dividing the overall channel length by the time that the sample filled the microchannel. $\hat{v}$ for water, 5 cSt silicone oil, and 20 cSt silicone oil was 14.3 ± 0.91 mm/s, 2.5 ± 0.04 mm/s, 0.18 ± 0.02 mm/s, respectively. As expected, $\hat{v}$ in the open microchannel had a negative correlation with the liquid viscosity.

The product of liquid column length and velocity (vL) was relatively constant throughout the channel, deviating mainly at the inlet and the outlet (Fig. B-4Aiii−4Ciii). This was previously explained by Srivastava et al [300]. Briefly, the deviation at the inlet is associated with the sudden reservoir contraction, error in calculating $\Delta L/\Delta t$, and a fully developed Poiseuille flow which has not been achieved yet. At the exit, the deformation of the advancing meniscus with a nonuniform radius of curvature while the flow creeps along the microchannel walls was explained as the possible reason for deviation in the mean velocity. Therefore, we neglected the value of vL at the first and the last 20% of the flow and calculated the average vL based on its value at the mid-60% time interval (transparent rectangles in Fig. B-4Aiii−4Ciii). The average vL for water, 5 cSt silicone oil, and 20 cSt silicone oil was 667 ± 87 mm2/s 108.5 ± 5.1 mm2/s, and 8.3 ± 0.9 mm2/s, respectively, with a negative correlation with the liquid viscosity. The capillary filling process in our study was similar to what was previously reported for open microchannels following the Lucas Washburn equations [304,305].

As shown in Fig. B-3E, PDMS hydrophilicity is more stable and sustained for plasma treated PVA-coated PDMS than plasma treated PDMS; however, contact angle may increase significantly over a

long period of time. Therefore, the viscosity measurement should be finished without significant changes in contact angle. The longest open microchannel filling process took ~480 s (~8 min) for 20 cSt silicone oil (Fig. B-4C). During the experiments, the longest viscosity measurement interval took less than 15 minutes for 20 cSt silicone oil and its calibration fluid (DI water), with no significant change in the wettability of the plasma treated PVA-coated PDMS (Fig. B-3E).

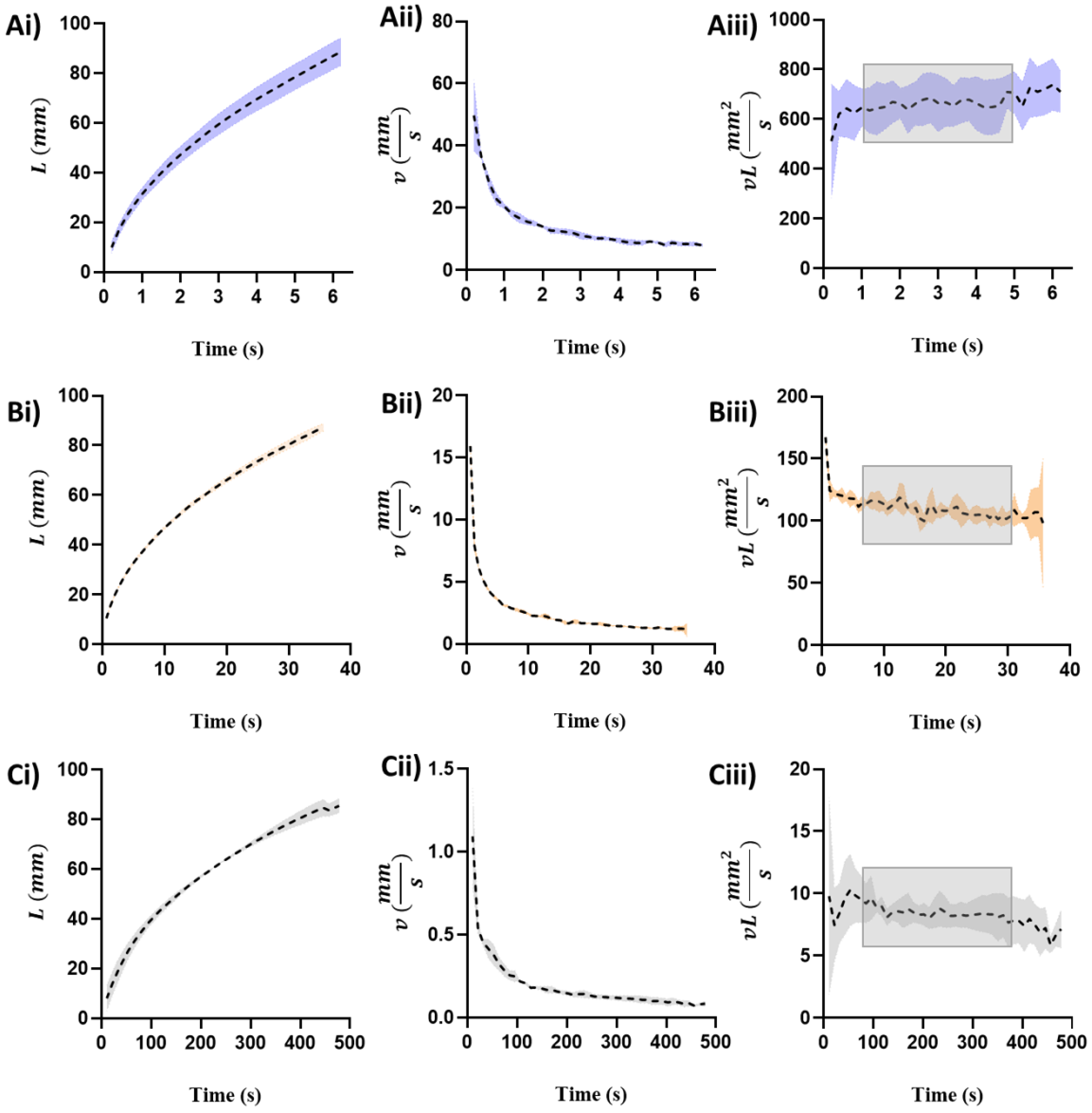

Figure B-4: Capillary filling process in the open microchannels (OC2) of the PVA-coated PDMS viscometer. The changes in the liquid column length (i), velocity (ii), and the product of velocity and liquid column length (iii) are shown for (A) water, (B) 5cSt silicone oil, and (C) 20 cSt silicone oil. The transparent rectangles in panels (iii) show the mid-60% time interval considered for averaging the vL product.

Sealed Microchannels (SC)

In the sealed microchannels, the liquid was capillary-drawn inside the channel while compressing the trapped air at the dead end. The filling process was bimodal as shown in Fig. B-5. It started with a high initial velocity which compressed the air, then, the liquid velocity decreased gradually due to air compressive backpressure and reached to an approximately constant value which gradually pushed the compressed air out from the porous PDMS.

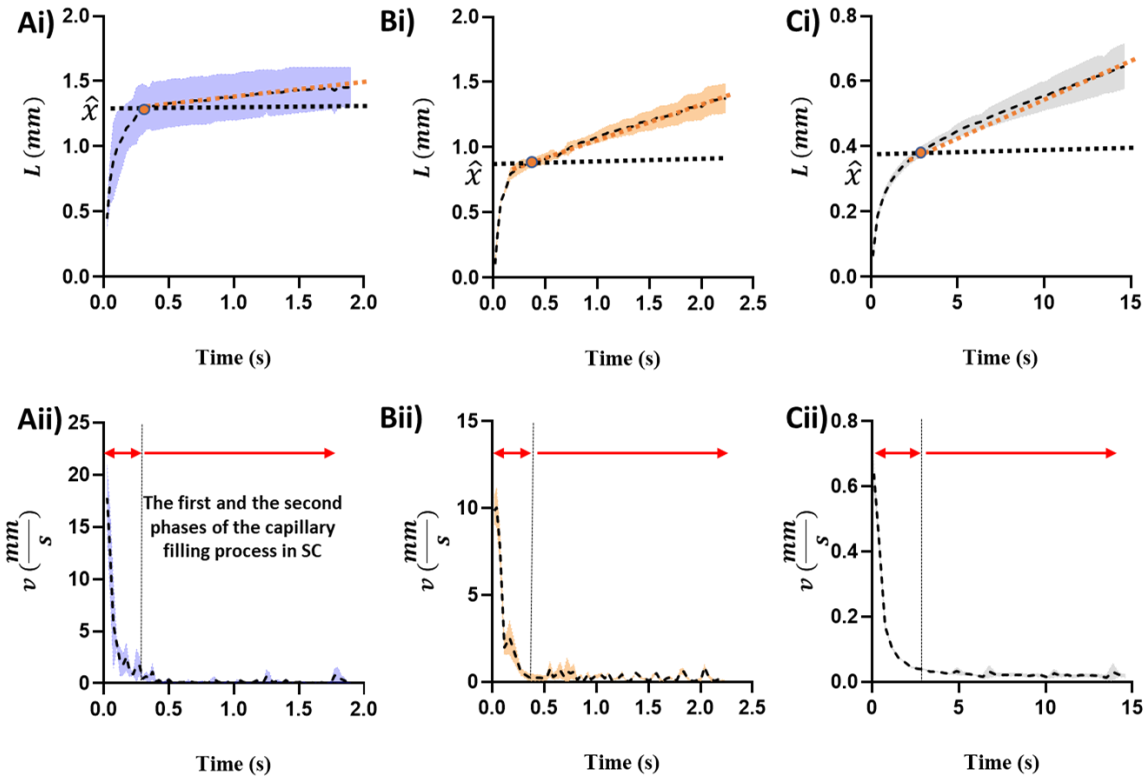

Figure B-5: Capillary filling process in the sealed microchannels (SC2) of the PVA-coated PDMS viscometer. The changes in the filling length (i) and liquid velocity (ii) are shown for (A) water, (B) 5cSt silicone oil, and (C) 20 cSt silicone oil. $\hat{x}$ shows the average filling length in the sealed microchannel where the liquid velocity reached a constant value. The first and second phases of capillary filling process in the sealed microchannel are shown with red arrows (Aii-Cii).

During the capillary filling process in the sealed microchannels, surface tension force is balanced by inertia, viscous, and trapped air backpressure forces. However, since in capillary pressure driven flows, the Reynolds number and Weber number are very low (i.e., $Re < 1$ and $We \ll 1$), we can neglect the inertial effect. Also, the velocity of the liquid in the sealed microchannel decreased quickly and the length of the liquid column before reaching to a constant velocity was relatively

small (Fig. B-5). Therefore, a negligible viscous force during the initial filling stages could be a reasonable assumption [313,314]. Considering the air backpressure force as the dominant resistive force against the surface tension force, Eq. (2) can be rewritten as:

$$P_{capillary} = P_{atm}(\frac{L_{sc}}{x} - 1) \quad \text{(B-5)}$$

where, L_{sc} is the length of the sealed microchannel and x is the filling length when the air backpressure force is equal to the capillary force. Here, x was calculated at the time when the velocity of liquid in the sealed microchannel decreased and reached to 5% of the maximum initial velocity. The average value for x is shown in Fig. B-5 as $\hat{x}$.

Capillary filling in sealed nano-and micro-channels made of gas impermeable materials (e.g., glass and silicone) has been previously studied [304,313]. It has been shown that the process at first resembles the capillary filling of open-end channels with x being proportional to t^{α}. The classical theory for capillary filling in gas impermeable sealed microchannels suggests that the fluid's filing length cannot exceed x [304,313]. However, Phan et al. [313] demonstrated that at the end of the filling process in nanochannels, the liquid menisci do not stop at the value predicted by the classical model. In fact, the liquid continues to fill the nanochannel with a constant filling rate at the second stage of the filling process. This was primarily due to the absorption and diffusion of gas molecules in the liquid in nanoscales which the classical model did not predict. We hypothesize that a similar phenomenon occurred for our gas permeable PDMS microchannels. Initially, the capillary pressure of the liquid sample was more than the air pressure inside the channel and moved the liquid forward with a high velocity. As the liquid moved forward, the air pressure inside the sealed channel increased against the capillary pressure; therefore, the velocity decreased. After the first stage of the filling, when the air backpressure force reached an amount almost equal to the capillary pressure, the trapped air gradually escaped through the PDMS walls to keep the air pressure constant while the liquid continued moving forward and filling the sealed channel. During this process, the surface tension force is close to the air backpressure force. Right before the velocity reached a constant value, the liquid column length (x) was used to calculate the capillary pressure as described in Eq. 5. In the future, the capillary filing process in microchannels made of gas permeable materials can be studied in more detail to develop theoretical models for this phenomenon.

B.4.3 Validation of the PVA-coated PDMS-based viscometer

We used water and two types of silicone oil with known viscosities to validate the performance of our viscometer, as shown in Table 1. The capillary pressure and vL product were calculated for calibration liquid ($P_{capillay,calib}$ and vL_{calib}) and main sample ($P_{capillay,sample}$ and vL_{sample}) as described earlier. Knowing the viscosity of DI water as the calibration fluid (μ_{calib}) we used Eq. B-4 to calculate the viscosity of sample (μ_{sample}). The average dynamic viscosity of samples was shown in Table. 1 for water and two types of silicone oil. These values compare favorably with the reference viscosity reported in the literature and company measurements using conventional viscometers [315,316] with a maximum error of 11.8% for 20 cSt silicone oil.

Table B-1. Dynamic viscosity of calibration fluids measured with the proposed viscometer

	Water	**5 cSt silicone oil**	**20 cSt silicone oil**
Reference viscosity (cP) [#]	0.89	4.56	19
Measured Viscosity (cP) with the presented viscometer	0.86 ± 0.04	4.81 ± 0.31	21.25 ± 0.37
Average Error (%)	3.4	5.5	11.8

[#] [315,316]

B.4.4 Hemolymph viscosity of *Drosophila melanogaster* larvae

Fig. B-6 shows the filling process in the open and sealed microchannels of the proposed viscometer for *Drosophila* hemolymph. Hemolymph had a behaviour similar to water and silicone oils. In the open microchannel, hemolymph had a high velocity at the beginning. As hemolymph moved forward, L increased while v gradually decreased (Fig. B-6A and 6B). The average $\hat{v}$ and vL values for larval hemolymph were 4.2 ± 0.31 mm/s and 196.1 ± 30.6 mm2/s, respectively (Fig. B-6B and 6C). These values were less than those of water and more than those of silicone oils. In the sealed microchannel, hemolymph was capillary-drawn inside the channel with a high initial velocity (Fig. B-6D). Then, hemolymph velocity gradually decreased to an approximately constant value while the liquid continued moving forward, similar to what was observed for water and silicone oils.

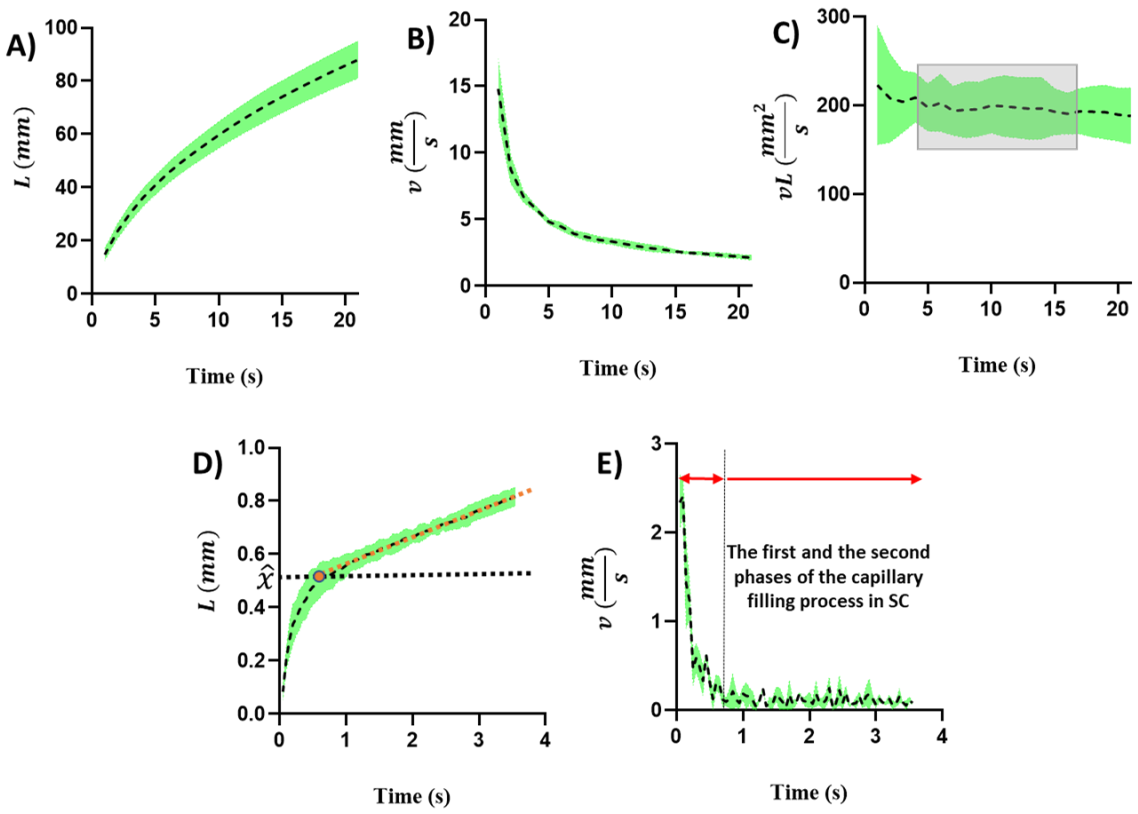

Figure B-6: Capillary filling process for Drosophila larval hemolymph in the open (A-C) and sealed (D-E) microchannels of the PVA-coated PDMS viscometer. The changes in the liquid column length (A and D), velocity (B and E), and the product of velocity and liquid column length (C) are shown for Drosophila larval hemolymph. The transparent rectangle in panels (C) shows the mid-60% time interval considered for averaging the vL product. $\hat{x}$ shows the average filling length in the sealed microchannel where the liquid velocity reached a constant value. The first and second phases of capillary filling process in the sealed microchannel are shown with red arrows (E).

Following the same strategy explained for water and silicone oil, *Drosophila* hemolymph viscometry was done using the PDMS-based capillary pressure driven viscometer. *Drosophila* larval hemolymph viscosity was calculated to be 1.34 ± 0.07 cP (Fig. B-7) which is ~50% more than the viscosity of water and ~51% lower than the viscosity of hornworm hemolymph at room temperature [296]. Of note, the hornworm viscosity measurement was conducted with a cone and plate viscometer as the insect was extremely larger than *Drosophila* larvae and extraction of enough hemolymph was doable for large insects. Also, the *Drosophila* larval hemolymph viscosity was ~5% lower than the viscosity of human blood plasma (1.413 cP at 37°C) [300].

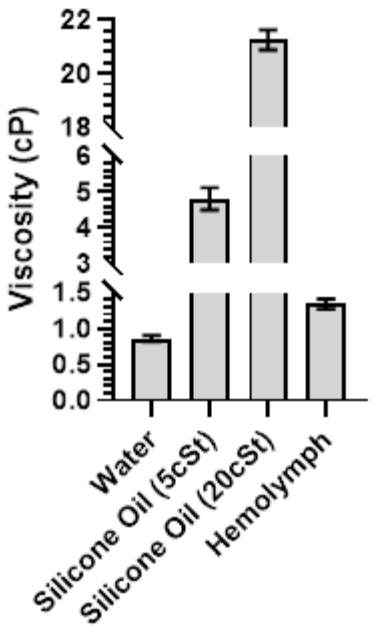

Figure B-7: Viscosity of different samples measured with the proposed PVA-coated PDMS based microfluidic viscometer.

Using dye angiography and optical coherence tomography (OCT), Choma et al. [288] estimated the intracardiac shear rate in *Drosophila* prepupae (one stage after third instar larvae) to be ~40–60 1/s. Due to the fact that *Drosophila* hemolymph viscosity had not been characterized by that time, they assumed that hemolymph had a viscosity similar to acellular human plasma at a comparable shear rate (~2.5 cP [317]). This assumption yielded a shear stress of ~1–2 dyne/cm^2 for *Drosophila* prepupae [288]. However, after calculating *Drosophila* hemolymph viscosity in our study and assuming that intracardiac shear rate of 3rd instar larvae is similar to prepupae, the estimated shear stress in [288] can be corrected to be ~0.5–1 dyne/cm^2.

Besides biological applications, knowing the hemolymph viscosity can address some technical challenges in studying hemolymph drop impact outcomes on aerodynamic surfaces [292]. Due to challenges associated with hemolymph extraction from small *Drosophila* and unknown physical properties, larger insects were used for such studies [292]. The reported value for *Drosophila* hemolymph viscosity can be used to prepare surrogate samples with water and glycerine with physical properties resembling *Drosophila* hemolymph. This can be used to understand the influence of viscosity on the classification of droplets impacting on aerodynamic surfaces with various wettability characteristic [318].

B.5 Conclusion

Viscosity measurement of small volume of liquids in the order of nano to microliters, e.g., insects' hemolymph, is challenging. Many microfluidic viscometers were developed to enable measuring rheological parameters of small volumes. Capillary pressure driven viscometers received many attentions because they are simple and do not need other components e.g., syringe pumps. The fabrication of microfluidic devices using PDMS soft lithography is simpler, cheaper, and less time consuming compared to other methods (e.g., silicone, glass, and plastic micromachining). However, PDMS is hydrophobic and gas permeable. These incompatible characteristics of PDMS hindered its use in fabrication of capillary pressure driven microchannels. Here, we adopted a microfluidic based viscosity measurement technique to determine the viscosity of *Drosophila* 3rd instar larval hemolymph. We changed the material from glass to PDMS to make it suitable for replica molding on photolithographically patterned or 3D-printted master molds. Subsequently, new steps were added in microfabrication and viscosity calculation to address the hydrophobicity and gas permeability of PDMS. We investigated the capillary filing process in open and sealed microchannels made of PVA-coated PDMS. Then, we validated the accuracy of our proposed viscosity measurement technique using viscosity-standard solutions. Finally, the *Drosophila* hemolymph viscosity was measured and reported for the first time. Also, the range of shear stress was estimated according to the hemolymph viscosity value and previously reported intracardiac shear rate in *Drosophila* prepupae. The proposed measurement technique can be used for various biological samples in other small organisms. The reported value for the viscosity of *Drosophila* larva can be used in many applications e.g., hemorheology, physiology, and aerospace for modeling hemolymph drop impact on airfoils.

C. Spearman's correlation coefficient

Table C-1: Spearman's correlation coefficient showing the strength and direction of relationship between the heart rate and arrhythmicity index for wild type and NP1029-GAL4:MTF1 larvae, (A) injected with 100 mM zinc chloride and (B) injected with 10 mM cadmium chloride (: $P < 0.05$)*

(A)	**2min-post injection**	**6min-post injection**	**10min-post injection**	**15min-post injection**
Wild type	-0.1744	-0.3438	-0.5501*	-0.5294*
MTF1	-0.2239	-0.1992	-0.1691	-0.1814
(B)	**2min-post injection**	**6min-post injection**	**10min-post injection**	**15min-post injection**
Wild type	0.2611	0.3437	0.3189	0.3529
MTF1	0.1621	0.1765	0.1744	0.2891

References

[1] B.H. Jennings, Drosophila-a versatile model in biology & medicine, Mater. Today. 14 (2011) 190–195. https://doi.org/10.1016/S1369-7021(11)70113-4.

[2] R.E. Kohler, Drosophila : A Life in the Laboratory, 26 (1993) 281–310.

[3] M.D. Adams, S.E. Celniker, R.A. Holt, C.A. Evans, J.D. Gocayne, P.G. Amanatides, S.E. Scherer, P.W. Li, R.A. Hoskins, R.F. Galle, others, The genome sequence of Drosophila melanogaster, Science (80-.). 287 (2000) 2185–2195.

[4] R.O. Flagg, Carolina Drosophila Manual, Carolina Biological Supply Company Burlington, 1988.

[5] M. Ashburner, others, Drosophila. A laboratory handbook., Cold spring harbor laboratory press, 1989.

[6] C. Ong, L.-Y.L. Yung, Y. Cai, B.-H. Bay, G.-H. Baeg, Drosophila melanogaster as a model organism to study nanotoxicity, Nanotoxicology. 9 (2015) 396–403.

[7] N. Piazza, R.J. Wessells, Chapter 5 - Drosophila Models of Cardiac Disease, in: K.T. Chang, K.-T. Min (Eds.), Anim. Model. Hum. Dis., Academic Press, 2011: pp. 155–210. https://doi.org/https://doi.org/10.1016/B978-0-12-384878-9.00005-4.

[8] A. Souidi, K. Jagla, Drosophila Heart as a Model for Cardiac Development and Diseases, Cells 2021, Vol. 10, Page 3078. 10 (2021) 3078. https://doi.org/10.3390/CELLS10113078.

[9] B. Rotstein, A. Paululat, On the Morphology of the Drosophila Heart, J. Cardiovasc. Dev. Dis. 3 (2016) 15. https://doi.org/10.3390/jcdd3020015.

[10] S.B. Diop, R. Bodmer, Drosophila as a model to study the genetic mechanisms of obesity-associated heart dysfunction, J. Cell. Mol. Med. 16 (2012) 966–971. https://doi.org/10.1111/j.1582-4934.2012.01522.x.

[11] E. Bier, R. Bodmer, Drosophila, an emerging model for cardiac disease, Gene. 342 (2004) 1–11. https://doi.org/https://doi.org/10.1016/j.gene.2004.07.018.

[12] D. Dulcis, R.B. Levine, Innervation of the heart of the adult fruit fly, Drosophila melanogaster, J. Comp. Neurol. 465 (2003) 560–578. https://doi.org/10.1002/CNE.10869.

[13] L. Bataillé, N. Colombié, A. Pelletier, A. Paululat, G. Lebreton, Y. Carrier, J.L. Frendo, A. Vincent, Alary muscles and thoracic alary-related muscles are atypical striated muscles involved in maintaining the position of internal organs, Development. 147 (2020). https://doi.org/10.1242/DEV.185645.

[14] K. Youssef, P. Bayat, A.R. Peimani, S. Dibaji, P. Rezai, Miniaturized Sensors and Actuators for Biological Studies on Small Model Organisms of Disease, in: Environ. Chem. Med. Sensors, Springer, 2018: pp. 199–225. https://doi.org/10.1007/978-981-10-7751-7_9.

[15] L. Tian, S.A. Hires, T. Mao, D. Huber, M.E. Chiappe, S.H. Chalasani, L. Petreanu, J.

Akerboom, S.A. McKinney, E.R. Schreiter, C.I. Bargmann, V. Jayaraman, K. Svoboda, L.L. Looger, Imaging neural activity in worms, flies and mice with improved GCaMP calcium indicators, Nat. Methods. 6 (2009) 875.

[16] L. Liu, O. Yermolaieva, W.A. Johnson, F.M. Abboud, M.J. Welsh, Identification and function of thermosensory neurons in Drosophila larvae, Nat. Neurosci. 6 (2003) 267.

[17] M. Ghannad-Rezaie, X. Wang, B. Mishra, C. Collins, N. Chronis, Microfluidic chips for in vivo imaging of cellular responses to neural injury in Drosophila larvae, PLoS One. 7 (2012). https://doi.org/10.1371/journal.pone.0029869.

[18] A.S. Cooper, K.E. Rymond, M.A. Ward, E.L. Bocook, R.L. Cooper, Monitoring heart function in larval Drosophila melanogaster for physiological studies, J. Vis. Exp. (2009) 1596. https://doi.org/10.3791/1596.

[19] A. Zabihihesari, A. Khalili, A.J. Hilliker, P. Rezai, Open access tool and microfluidic devices for phenotypic quantification of heart function of intact fruit fly and zebrafish larvae, Comput. Biol. Med. 132 (2021) 104314. https://doi.org/10.1016/J.COMPBIOMED.2021.104314.

[20] S. Jiang, C.P. Teng, W.C. Puah, M. Wasser, K.Y. Win, M.Y. Han, Oral Administration and Selective Uptake of Polymeric Nanoparticles in Drosophila Larvae as an in Vivo Model, ACS Biomater. Sci. Eng. 1 (2015) 1077–1084. https://doi.org/10.1021/ACSBIOMATERIALS.5B00163/SUPPL_FILE/AB5B00163_SI_001.PDF.

[21] R. Ghaemi, P. Rezai, F.R. Nejad, P.R. Selvaganapathy, Characterization of microfluidic clamps for immobilizing and imaging of Drosophila melanogaster larva's central nervous system, Biomicrofluidics. 11 (2017). https://doi.org/10.1063/1.4984767.

[22] P. Füger, L.B. Behrends, S. Mertel, S.J. Sigrist, T.M. Rasse, Live imaging of synapse development and measuring protein dynamics using two-color fluorescence recovery after photo-bleaching at Drosophila synapses, Nat. Protoc. 2 (2007) 3285.

[23] R. Ardeshiri, L. Hosseini, N. Amini, P. Rezai, Cardiac screening of intact Drosophila melanogaster larvae under exposure to aqueous and gaseous toxins in a microfluidic device, RSC Adv. 6 (2016) 65714–65724. https://doi.org/10.1039/c6ra14159e.

[24] P.D. Sandstrom David J., Isoflurane Reduces Excitability of Drosophila Larval Motoneurons by Activating a Hyperpolarizing Leak Conductance, Anesthesiol. J. Am. Soc. Anesthesiol. 108 (2008) 434–446. https://doi.org/10.1097/ALN.0b013e318164cfda.

[25] D.J. Sandstrom, Isoflurane depresses glutamate release by reducing neuronal excitability at the Drosophila neuromuscular junction, J. Physiol. 558 (2004) 489–502. https://doi.org/10.1113/jphysiol.2004.065748.

[26] N. Hafer, P. Schedl, Dissection of Larval CNS in Drosophila Melanogaster, J. Vis. Exp. 128 (2006) 1899–1909. https://doi.org/10.3791/85.

[27] G.M. Whitesides, The origins and the future of microfluidics, Nature. 442 (2006) 368–373. https://doi.org/10.1038/nature05058.

[28] Y. Lee, G. Lee, M. Cho, J.-K. Park, Design criteria and standardization of a microfluidic cell culture system for investigating cellular migration, J. Micromechanics Microengineering. 29 (2019) 43003. https://doi.org/10.1088/1361-6439/ab0796.

[29] S. Mobini, Y.H. Song, M.W. McCrary, C.E. Schmidt, Advances in ex vivo models and lab-on-a-chip devices for neural tissue engineering, Biomaterials. 198 (2019) 146–166. https://doi.org/https://doi.org/10.1016/j.biomaterials.2018.05.012.

[30] A. Shanti, J. Teo, C. Stefanini, In Vitro Immune Organs-on-Chip for Drug Development: A Review, Pharmaceutics. 10 (2018). https://doi.org/10.3390/pharmaceutics10040278.

[31] W. Sun, Z. Luo, J. Lee, H.-J. Kim, K. Lee, P. Tebon, Y. Feng, M.R. Dokmeci, S. Sengupta, A. Khademhosseini, Organ-on-a-Chip for Cancer and Immune Organs Modeling, Adv. Healthc. Mater. 8 (2019) 1801363. https://doi.org/10.1002/adhm.201801363.

[32] A. Khalili, P. Rezai, Microfluidic devices for embryonic and larval zebrafish studies, Brief. Funct. Genomics. (2019). https://doi.org/10.1093/bfgp/elz006.

[33] K. Youssef, A. Tandon, P. Rezai, Studying Parkinson's Disease using Caenorhabditis elegans Models in Microfluidic Devices, Integr Biol. In press (2019) INTBIO-2018-038.R2.

[34] V. Sivagnanam, M.A.M. Gijs, Exploring Living Multicellular Organisms, Organs, and Tissues Using Microfluidic Systems, Chem. Rev. 113 (2013) 3214–3247. https://doi.org/10.1021/cr200432q.

[35] H. Hwang, H. Lu, Microfluidic tools for developmental studies of small model organisms - nematodes, fruit flies, and zebrafish, Biotechnol. J. 8 (2013) 192–205. https://doi.org/10.1002/biot.201200129.

[36] N. Brandenberg, M.P. Lutolf, Chapter 27 - Employing Microfluidic Devices to Induce Concentration Gradients, in: A. Vishwakarma, J.M. Karp (Eds.), Biol. Eng. Stem Cell Niches, Academic Press, Boston, 2017: pp. 429–442. https://doi.org/https://doi.org/10.1016/B978-0-12-802734-9.00027-5.

[37] S. Mondal, S.P. Koushika, Microfluidic Devices for Imaging Trafficking Events In Vivo Using Genetic Model Organisms, in: A.I. Ivanov (Ed.), Exocytosis and Endocytosis, Springer New York, New York, NY, 2014: pp. 375–396. https://doi.org/10.1007/978-1-4939-0944-5_26.

[38] B. Lin, A. Levchenko, Spatial Manipulation with Microfluidics, Front. Bioeng. Biotechnol. 3 (2015) 1–6. https://doi.org/10.3389/fbioe.2015.00039.

[39] Q. Wu, N. Kumar, V. Velagala, J.J. Zartman, Tools to reverse-engineer multicellular systems: case studies using the fruit fly, J. Biol. Eng. 13 (2019) 33. https://doi.org/10.1186/s13036-019-0161-8.

[40] A. V. Spirov, Microfluidics Approaches in Modern Developmental Biology, Russ. J. Dev. Biol. 49 (2018) 146–158. https://doi.org/10.1134/S1062360418030086.

[41] Y. Yan, L. Jiang, K.J. Aufderheide, G.A. Wright, A. Terekhov, L. Costa, K. Qin, W.T. Mccleery, J.J. Fellenstein, A. Ustione, J.B. Robertson, C.H. Johnson, D.W. Piston, M.S. Hutson, J.P. Wikswo, W. Hofmeister, C. Janetopoulos, A Microfluidic-Enabled Mechanical

Microcompressor for the Immobilization of Live Single- and Multi-Cellular Specimens, Microsc. Microanal. 20 (2014) 141–151. https://doi.org/10.1017/S1431927613014037.

[42] S. Mondal, S. Ahlawat, K. Rau, V. Venkataraman, S.P. Koushika, Imaging in vivo Neuronal Transport in Genetic Model Organisms Using Microfluidic Devices, Traffic. 12 (2011) 372–385. https://doi.org/10.1111/j.1600-0854.2010.01157.x.

[43] R.J. Wessells, R. Bodmer, Screening assays for heart function mutants in Drosophila, Biotechniques. 37 (2004) 58–66. https://doi.org/10.2144/04371ST01/ASSET/IMAGES/LARGE/FIGURE3.JPEG.

[44] R. Navawongse, D. Choudhury, M. Raczkowska, J.C. Stewart, T. Lim, M. Rahman, A.G.G. Toh, Z. Wang, A. Claridge-Chang, Drosophila learn efficient paths to a food source, Neurobiol. Learn. Mem. 131 (2016) 176–181. https://doi.org/10.1016/j.nlm.2016.03.019.

[45] A. Zabihihesari, A.J. Hilliker, P. Rezai, Fly-on-a-Chip: Microfluidics for Drosophila melanogaster Studies, Integr. Biol. 11 (2020) 425–443. https://doi.org/10.1093/intbio/zyz037.

[46] C.C. Chen, S. Zappe, O. Sahin, X.J. Zhang, M. Fish, M. Scott, O. Solgaard, Design and operation of a microfluidic sorter for Drosophila embryos, Sensors Actuators, B Chem. 102 (2004) 59–66. https://doi.org/10.1016/j.snb.2003.10.015.

[47] K. Chung, Y. Kim, J.S. Kanodia, E. Gong, S.Y. Shvartsman, H. Lu, A microfluidic array for large-scale ordering and orientation of embryos, Nat. Methods. 8 (2011) 171.

[48] B. Mishra, M. Ghannad-Rezaie, J. Li, X. Wang, Y. Hao, B. Ye, N. Chronis, C.A. Collins, Using Microfluidics Chips for Live Imaging and Study of Injury Responses in Drosophila Larvae, J. Vis. Exp. (2014) 1–15. https://doi.org/10.3791/50998.

[49] J.C.K. Leung, A.J. Hilliker, P. Rezai, An integrated hybrid microfluidic device for oviposition-based chemical screening of adult Drosophila melanogaster, Lab Chip. 16 (2016) 709–719. https://doi.org/10.1039/C5LC01517K.

[50] G. Vogler, R. Bodmer, Cellular Mechanisms of Drosophila Heart Morphogenesis, J. Cardiovasc. Dev. Dis. 2 (2015) 2–16. https://doi.org/10.3390/jcdd2010002.

[51] R. Bodmer, The gene tinman is required for specification of the heart and visceral muscles in Drosophila., Development. 118 (1993) 719–729.

[52] N. Azpiazu, M. Frasch, Tinman and bagpipe: Two homeo box genes that determine cell fates in the dorsal mesoderm of Drosophila, Genes Dev. 7 (1993) 1325–1340. https://doi.org/10.1101/gad.7.7b.1325.

[53] M.J. Wolf, H. Amrein, J.A. Izatt, M.A. Choma, M.C. Reedy, H.A. Rockman, Drosophila as a model for the identification of genes causing adult human heart disease, Proc. Natl. Acad. Sci. 103 (2006) 1394–1399.

[54] J. Na, L.P. Musselman, J. Pendse, T.J. Baranski, R. Bodmer, K. Ocorr, R. Cagan, A Drosophila Model of High Sugar Diet-Induced Cardiomyopathy, PLoS Genet. 9 (2013). https://doi.org/10.1371/journal.pgen.1003175.

[55] O. Anyagaligbo, J. Bernard, A. Greenhalgh, R.L. Cooper, The effects of bacterial endotoxin (LPS) on cardiac function in a medicinal blow fly (Phaenicia sericata) and a fruit fly (Drosophila melanogaster), Comp. Biochem. Physiol. Part C Toxicol. Pharmacol. 217 (2019) 15–24. https://doi.org/https://doi.org/10.1016/j.cbpc.2018.11.008.

[56] C.A. Malloy, K. Ritter, J. Robinson, C. English, R.L. Cooper, Pharmacological identification of cholinergic receptor subtypes on Drosophila melanogaster larval heart, J. Comp. Physiol. B. 186 (2016) 45–57.

[57] S. Dasari, R.L. Cooper, Direct influence of serotonin on the larval heart of Drosophila melanogaster, J. Comp. Physiol. B Biochem. Syst. Environ. Physiol. 176 (2006) 349–357. https://doi.org/10.1007/s00360-005-0058-3.

[58] E. Johnson, J. Ringo, N. Bray, H. Dowse, Genetic and Pharmacological Identification of Ion Channels Central to the Drosophila Cardiac Pacemaker, J. Neurogenet. 12 (1998) 1–24. https://doi.org/10.3109/01677069809108552.

[59] S. Bahadorani, A.J. Hilliker, Biological and Behavioral Effects of Heavy Metals in Drosophila melanogaster Adults and Larvae, J. Insect Behav. 2009 225. 22 (2009) 399–411. https://doi.org/10.1007/S10905-009-9181-4.

[60] G.G.E. Scudder, J. Meredith, The permeability of the midgut of three insects to cardiac glycosides, J. Insect Physiol. 28 (1982) 689–694. https://doi.org/10.1016/0022-1910(82)90147-0.

[61] S. Shugarts, L.Z. Benet, The Role of Transporters in the Pharmacokinetics of Orally Administered Drugs, Pharm. Res. 2009 269. 26 (2009) 2039–2054. https://doi.org/10.1007/S11095-009-9924-0.

[62] T. Huang, P. Kissinger, Liquid chromatographic determination of serotonin in homogenized dog intestine and rat brain tissue using a 2 mm id PEEK Column, Curr. Sep. 14 (1996) 114–119.

[63] P. Song, X. Dong, X. Liu, A microfluidic device for automated, high-speed microinjection of Caenorhabditis elegans, Biomicrofluidics. 10 (2016) 011912. https://doi.org/10.1371/journal.pbio.0060216.

[64] M. Nakajima, T. Hirano, M. Kojima, N. Hisamoto, N. Nakanishi, H. Tajima, M. Homma, T. Fukuda, Local Nano-injection of Fluorescent Nano-beads inside C. elegans based on Nanomanipulation, in: 2012 IEEE/RSJ Int. Conf. Intell. Robot. Syst., 2012: pp. 3241–3246.

[65] M.A. Choma, M.J. Suter, B.J. Vakoc, B.E. Bouma, G.J. Tearney, Physiological homology between Drosophila melanogaster and vertebrate cardiovascular systems, Dis. Model. Mech. 4 (2011) 411–420.

[66] E. Johnson, J. Ringo, H. Dowse, Modulation of Drosophila heartbeat by neurotransmitters, J Comp Physiol B. 167 (1997) 89–97.

[67] E. Zornik, K. Paisley, R. Nichols, Neural transmitters and a peptide modulate Drosophila heart rate, Peptides. 20 (1999) 45–51. https://doi.org/10.1016/S0196-9781(98)00151-X.

[68] N. Nikoh, A. Duty, G. Gibson, Effects of population structure and sex on association

between serotonin receptors and Drosophila heart rate, Genetics. 168 (2004) 1963–1974.

[69] L.T. Wasserthal, Drosophila flies combine periodic heartbeat reversal with a circulation in the anterior body mediated by a newly discovered anterior pair of ostial valves andvenous' channels, J. Exp. Biol. 210 (2007) 3707–3719.

[70] S.-Y. Guo, F.-T. Liao, M.-T. Su, C.-Y. Chang, H.-R. Su, J.-C. Huang, W.-C. Kuo, Semiautomatic and rapid quantification of heartbeat parameters in Drosophila using optical coherence tomography imaging, J. Biomed. Opt. 18 (2013) 26004.

[71] C.-Y. Lee, H.-J. Wang, J.-D. Jhang, I.-C. Cho, Automated drosophila heartbeat counting based on image segmentation technique on optical coherence tomography, Sci. Rep. 9 (2019) 1–9.

[72] Z. Dong, J. Men, Z. Yang, J. Jerwick, A. Li, R.E. Tanzi, C. Zhou, FlyNet 2.0: drosophila heart 3D (2D+ time) segmentation in optical coherence microscopy images using a convolutional long short-term memory neural network, Biomed. Opt. Express. 11 (2020) 1568–1579.

[73] S. Sénatore, V.R. Reddy, M. Sémériva, L. Perrin, N. Lalevée, Response to mechanical stress is mediated by the TRPA channel painless in the Drosophila heart, PLoS Genet. 6 (2010) e1001088.

[74] M. Fink, C. Callol-Massot, A. Chu, P. Ruiz-Lozano, J.C.I. Belmonte, W. Giles, R. Bodmer, K. Ocorr, A new method for detection and quantification of heartbeat parameters in Drosophila, zebrafish, and embryonic mouse hearts, Biotechniques. 46 (2009) 101–113.

[75] A. Cammarato, S. Ocorr, K. Ocorr, Enhanced assessment of contractile dynamics in Drosophila hearts, Biotechniques. 58 (2015) 77–80.

[76] M.P. Tarvainen, P.O. Ranta-aho, P.A. Karjalainen, An advanced detrending method with application to HRV analysis, IEEE Trans. Biomed. Eng. 49 (2002) 172–175. https://doi.org/10.1109/10.979357.

[77] D. Berh, A. Scherzinger, N. Otto, X. Jiang, C. Klämbt, B. Risse, Automatic non-invasive heartbeat quantification of Drosophila pupae, Comput. Biol. Med. 93 (2018) 189–199. https://doi.org/10.1016/j.compbiomed.2017.12.017.

[78] S. Motamedi-Fakhr, M. Moshrefi-Torbati, M. Hill, C.M. Hill, P.R. White, Signal processing techniques applied to human sleep EEG signals—A review, Biomed. Signal Process. Control. 10 (2014) 21–33.

[79] R. Sameni, G.D. Clifford, A review of fetal ECG signal processing; issues and promising directions, Open Pacing. Electrophysiol. Ther. J. 3 (2010) 4.

[80] S. Bahadorani, S. Mukai, D. Egli, A.J. Hilliker, Overexpression of metal-responsive transcription factor (MTF-1) in Drosophila melanogaster ameliorates life-span reductions associated with oxidative stress and metal toxicity, Neurobiol. Aging. 31 (2010) 1215–1226. https://doi.org/10.1016/j.neurobiolaging.2008.08.001.

[81] D. Egli, A. Selvaraj, H. Yepiskoposyan, B. Zhang, E. Hafen, O. Georgiev, W. Schaffner, Knockout of "metal-responsive transcription factor" MTF-1 in Drosophila by homologous

recombination reveals its central role in heavy metal homeostasis, EMBO J. 22 (2003) 100–108. https://doi.org/10.1093/emboj/cdg012.

[82] A.S. Cooper, K.E. Rymond, M.A. Ward, E.L. Bocook, R.L. Cooper, Drosophila melanogaster for Physiological Studies, J. Vis. Exp. (2009) 1–7. https://doi.org/10.3791/1596.

[83] B. Rotstein, A. Paululat, On the Morphology of the Drosophila Heart, J. Cardiovasc. Dev. Dis. 3 (2016) 15. https://doi.org/10.3390/jcdd3020015.

[84] A. Zabihihesari, A.J. Hilliker, P. Rezai, Localized microinjection of intact Drosophila melanogaster larva to investigate the effect of serotonin on heart rate, Lab Chip. (2020) 343–355. https://doi.org/10.1039/C9LC00963A.

[85] A. Zabihihesari, S. Parand, A.B. Coulthard, A. Molnar, A.J. Hilliker, P. Rezai, An In-Vivo Microfluidic Assay Reveals Cardiac Toxicity of Heavy Metals and the Protective Effect of Metal Responsive Transcription Factor (Mtf-1) in Drosophila Model, SSRN Electron. J. (2022) 1–33. https://doi.org/10.2139/SSRN.4028275.

[86] A. Zabihihesari, S. Parand, A.J. Hilliker, P. Rezai, MICROFLUIDICS FOR MEASURING DROSOPHILA HEMOLYMPH VISCOSITY, in: 25th Int. Conf. Miniaturized Syst. Chem. Life Sci., Palm Springs, 2021: pp. 377–378.

[87] S. Zabihihesari, Alireza Parand, A.J. van Wijngaarden, Ellen Coulthard, Alistair B Hilliker, R. Pouya, MICROFLUIDIC-BASED CARDIAC TOXICITY ASSAY TO INVESTIGATE THE ROLE OF METAL RESPONSIVE TRANSCRIPTION FACTOR (MTF-1) IN A DROSOPHILA HEART MODEL, in: 25th Int. Conf. Miniaturized Syst. Chem. Life Sci., Palm Springs, 2021: pp. 377–378.

[88] A. Zabihihesari, A.J. Hilliker, P. Rezai, Microfluidic-based anesthetic-free microinjection of intact Drosophila larva to investigate the effect of serotonin on heartrate, in: 23rd Int. Conf. Miniaturized Syst. Chem. Life Sci. MicroTAS 2019, 2019: pp. 396–397.

[89] A. Zabihihesari, T. Akbar, A.J. Hilliker, P. Rezai, IN-VIVO CARDIOVASCULAR SCREENING MODEL USING A MICROFLUIDIC DEVICE FOR LOCALIZED MICROINJECTION INTO INTACT DROSOPHILA MELANOGASTER LARVAL HEART TUBE, in: Twenty Second Int. Conf. Miniaturized Syst. Chem. Life Sci. (MTAS 2018), Kaohsiung, Taiwan, 2018.

[90] A. Zabihihesari, A.J. Hilliker, P. Rezai, A Microfluidic Device for Localized Microinjection into Intact Drosophila melanogaster Larval Heart Tube, in: Ontario-on-a-Chip TOeP Symp., Toronto, Canada, 2018: pp. 1–2.

[91] J. Bilen, N.M. Bonini, Drosophila as a Model for Human Neurodegenerative Disease, (2005). https://doi.org/10.1146/annurev.genet.39.110304.095804.

[92] J. van de Leemput, Z. Han, Drosophila, a powerful model to study virus-host interactions and pathogenicity in the fight against SARS-CoV-2, Cell Biosci. 11 (2021) 1–9. https://doi.org/10.1186/S13578-021-00621-5/FIGURES/2.

[93] B. Egger, L. Van Giesen, M. Moraru, S.G. Sprecher, In vitro imaging of primary neural cell culture from Drosophila, Nat. Protoc. 8 (2013) 958–965.

https://doi.org/10.1038/nprot.2013.052.

[94] L. Van Giesen, G.L. Neagu-Maier, J.Y. Kwon, S.G. Sprecher, A microfluidics-based method for measuring neuronal activity in Drosophila chemosensory neurons, Nat. Protoc. 11 (2016) 2389–2400. https://doi.org/10.1038/nprot.2016.144.

[95] K.G. Hales, C.A. Korey, A.M. Larracuente, D.M. Roberts, Genetics on the Fly: A Primer on the Drosophila Model System, Genetics. 201 (2015) 815 LP – 842. https://doi.org/10.1534/genetics.115.183392.

[96] C. Cytokinesis, N. Ingression, Dynamic Analyses of Drosophila, Science (80-.). 322 (2008) 1546–1550. https://doi.org/10.1126/science.1167094.

[97] Y. Wang, Z. Khan, M. Kaschube, E.F. Wieschaus, Differential positioning of adherens junctions is associated with initiation of epithelial folding, Nature. 484 (2013) 390–393. https://doi.org/10.1038/nature10938.Differential.

[98] R. Tomer, K. Khairy, F. Amat, P.J. Keller, Quantitative high-speed imaging of entire developing embryos with simultaneous multiview light-sheet microscopy, Nat. Methods. 9 (2012) 755–763. https://doi.org/10.1038/nmeth.2062.

[99] U. Krzic, S. Gunther, T.E. Saunders, S.J. Streichan, L.H. Hufnagel, Multiview light-sheet microscope for rapid in toto imaging, Nat. Methods. 9 (2012) 730–736. https://doi.org/10.1038/nmeth.2064.

[100] M.M. Witzberger, J.A.J. Fitzpatrick, J.C. Crowley, J.S. Minden, End-on imaging: A new perspective on dorsoventral development in Drosophila embryos, Dev. Dyn. 237 (2008) 3252–3259. https://doi.org/10.1002/dvdy.21752.

[101] J.S. Kanodia, R. Rikhy, Y. Kim, V.K. Lund, R. DeLotto, J. Lippincott-Schwartz, S.Y. Shvartsman, Dynamics of the Dorsal morphogen gradient, Proc. Natl. Acad. Sci. 106 (2009) 21707–21712. https://doi.org/10.1073/pnas.0912395106.

[102] K. Chung, Y. Kim, J.S. Kanodia, E. Gong, S.Y. Shvartsman, H. Lu, A microfluidic array for large-scale ordering and orientation of embryos, Artic. Nat. Methods. 8 (2011). https://doi.org/10.1038/Nmeth.1548.

[103] Y. Goyal, T.J. Levario, H.H. Mattingly, S. Holmes, S.Y. Shvartsman, H. Lu, Parallel imaging of *Drosophila* embryos for quantitative analysis of genetic perturbations of the Ras pathway, Dis. Model. Mech. 10 (2017) 923–929. https://doi.org/10.1242/dmm.030163.

[104] O. Grimm, V.S. Zini, Y. Kim, J. Casanova, S.Y. Shvartsman, E. Wieschaus, Torso RTK controls Capicua degradation by changing its subcellular localization, Development. 139 (2012) 3962–3968.

[105] E.M. Lucchetta, J.H. Lee, L.A. Fu, N.H. Patel, R.F. Ismagilov, Dynamics of Drosophila embryonic patterning network perturbed in space and time using microfluidics, 434 (2005). https://doi.org/10.1038/nature03461.1.

[106] E.M. Lucchetta, M.S. Munson, R.F. Ismagilov, Characterization of the local temperature in space and time around a developing Drosophila embryo in a microfluidic device, Lab Chip. 6 (2006) 185–190. https://doi.org/10.1039/b516119c.

[107] E.M. Lucchetta, M.E. Vincent, R.F. Ismagilov, A precise Bicoid gradient is nonessential during cycles 11--13 for precise patterning in the Drosophila blastoderm, PLoS One. 3 (2008) e3651.

[108] G.T. Dagani, K. Monzo, J.R. Fakhoury, C. Chen, J.C. Sisson, X. Zhang, Microfluidic self-assembly of live Drosophila embryos for versatile high-throughput analysis of embryonic morphogenesis, (2007) 681–694. https://doi.org/10.1007/s10544-007-9077-z.

[109] Z. Bai, H. Bao, Y. Yuan, X. Yang, Y. Xi, M. Wang, Real-time observation of perturbation of a Drosophila embryo's early cleavage cycles with microfluidics, Anal. Chim. Acta. 982 (2017) 131–137. https://doi.org/10.1016/j.aca.2017.05.024.

[110] Z. Wang, S.C. Oppegard, D.T. Eddington, J. Cheng, Effect of localized hypoxia on Drosophila embryo development, PLoS One. 12 (2017) 1–16. https://doi.org/10.1371/journal.pone.0185267.

[111] K. Chung, Y. Kim, J.S. Kanodia, E. Gong, S.Y. Shvartsman, H. Lu, A microfluidic array for large-scale ordering and orientation of embryos, Nat. Methods. 8 (2011) 171–176. https://doi.org/10.1038/nmeth.1548.

[112] T.J. Levario, C. Zhao, T. Rouse, S.Y. Shvartsman, H. Lu, An integrated platform for large-scale data collection and precise perturbation of live Drosophila embryos, Sci. Rep. 6 (2016) 1–12. https://doi.org/10.1038/srep21366.

[113] D. Casso, F.-A. Ramírez-Weber, T.B. Kornberg, GFP-tagged balancer chromosomes for Drosophila melanogaster, Mech. Dev. 88 (1999) 229–232. https://doi.org/10.1016/S0925-4773(99)00174-4.

[114] W.A. Bonner, H.R. Hulett, R.G. Sweet, L.A. Herzenberg, Fluorescence Activated Cell Sorting, Rev. Sci. Instrum. 43 (1972) 404–409. https://doi.org/10.1063/1.1685647.

[115] D. Wlodkowic, K. Khoshmanesh, J. Akagi, D.E. Williams, J.M. Cooper, Wormometry-on-a-chip: Innovative technologies for in situ analysis of small multicellular organisms, Cytom. Part A. 79 A (2011) 799–813. https://doi.org/10.1002/cyto.a.21070.

[116] R. Pulak, Techniques for analysis, sorting, and dispensing of C. elegans on the COPAS^{TM} flow-sorting system, in: C. Elegans, Springer, 2006: pp. 275–286.

[117] J.G.P. Thompson, P. Schedl, R. Pulak, Sex-specific GFP-expression in Drosophila embryos and sorting by Copas flow cytometry technique, in: 45th Annu. Drosoph. Res. Conf. Washington, DC, 2004: pp. 24–28.

[118] M.S. Halfon, S. Gisselbrecht, J. Lu, B. Estrada, H. Keshishian, A.M. Michelson, New fluorescent protein reporters for use with the Drosophila Gal4 expression system and for vital detection of balancer chromosomes, Genesis. 34 (2002) 135–138.

[119] E.E.M. Furlong, D. Profitt, M.P. Scott, Automated sorting of live transgenic embryos, Nat. Biotechnol. 19 (2001) 153.

[120] W. Wang, X. Liu, D. Gelinas, B. Ciruna, Y. Sun, A fully automated robotic system for microinjection of zebrafish embryos, PLoS One. 2 (2007). https://doi.org/10.1371/journal.pone.0000862.

[121] J. Shapiro, Mobile genetic elements, Elsevier, 2012.

[122] M.S. Cheers, C.A. Ettensohn, Rapid Microinjection of Fertilized Eggs, in: Dev. Sea Urchins, Ascidians, Other Invertebr. Deuterostomes Exp. Approaches, Academic Press, 2004: pp. 287–310. https://doi.org/https://doi.org/10.1016/S0091-679X(04)74013-3.

[123] D. Delubac, C.B. Highley, M. Witzberger-Krajcovic, J.C. Ayoob, E.C. Furbee, J.S. Minden, S. Zappe, Microfluidic system with integrated microinjector for automated Drosophila embryo injection, Lab Chip. 12 (2012) 4911–4919. https://doi.org/10.1039/c2lc40104e.

[124] R. Ghaemi, P. Arefi, A. Stosic, M. Acker, Q. Raza, J. Roger Jacobs, P.R. Selvaganapathy, A microfluidic microinjector for toxicological and developmental studies in Drosophila embryos, Lab Chip. 17 (2017) 3898–3908. https://doi.org/10.1039/C7LC00537G.

[125] E.K. Paluch, C.M. Nelson, N. Biais, B. Fabry, J. Moeller, B.L. Pruitt, C. Wollnik, G. Kudryasheva, F. Rehfeldt, W. Federle, Mechanotransduction: use the force(s), BMC Biol. 13 (2015) 47. https://doi.org/10.1186/s12915-015-0150-4.

[126] E. Farge, Mechanical induction of Twist in the Drosophila foregut/stomodeal primordium, Curr. Biol. 13 (2003) 1365–1377.

[127] A.Z. Shorr, U.M. Sönmez, J.S. Minden, P.R. LeDuc, High-throughput mechanotransduction in Drosophila embryos with mesofluidics, Lab Chip. 19 (2019) 1141–1152. https://doi.org/10.1039/C8LC01055B.

[128] W.J. Polacheck, R. Li, S.G.M. Uzel, R.D. Kamm, Microfluidic platforms for mechanobiology, Lab Chip. 13 (2013) 2252–2267. https://doi.org/10.1039/C3LC41393D.

[129] C. Schmied, P. Tomancak, Sample preparation and mounting of Drosophila embryos for multiview light sheet microscopy, in: Drosophila, Springer, 2016: pp. 189–202.

[130] P.J. Keller, Imaging morphogenesis: technological advances and biological insights, Science (80-.). 340 (2013) 1234168.

[131] J. Huisken, J. Swoger, F. Del Bene, J. Wittbrodt, E.H.K. Stelzer, Optical sectioning deep inside live embryos by selective plane illumination microscopy, Science (80-.). 305 (2004) 1007–1009.

[132] R. McGorty, H. Liu, D. Kamiyama, Z. Dong, S. Guo, B. Huang, Open-top selective plane illumination microscope for conventionally mounted specimens, Opt. Express. 23 (2015) 16142–16153.

[133] A.D. Pilling, D. Horiuchi, C.M. Lively, W.M. Saxton, Kinesin-1 and Dynein are the primary motors for fast transport of mitochondria in Drosophila motor axons, Mol. Biol. Cell. 17 (2006) 2057–2068.

[134] G. Vogler, K. Ocorr, Visualizing the beating heart in Drosophila, JoVE (Journal Vis. Exp. (2009) e1425.

[135] I. Heemskerk, T. Lecuit, L. LeGoff, Dynamic clonal analysis based on chronic in vivo imaging allows multiscale quantification of growth in the Drosophila wing disc, Development. 141 (2014) 2339–2348.

[136] K.E. Miller, J. DeProto, N. Kaufmann, B.N. Patel, A. Duckworth, D. Van Vactor, Direct observation demonstrates that Liprin-$α$ is required for trafficking of synaptic vesicles, Curr. Biol. 15 (2005) 684–689.

[137] A.R. Chaudhury, R. Insolera, R. Der Hwang, Y.W. Fridell, C. Collins, N. Chronis, On chip cryo-anesthesia of Drosophila larvae for high resolution in vivo imaging applications, Lab Chip. 17 (2017) 2303–2322. https://doi.org/10.1039/c7lc00345e.

[138] N.H. Badre, M.E. Martin, R.L. Cooper, The physiological and behavioral effects of carbon dioxide on Drosophila melanogaster larvae, Comp. Biochem. Physiol. Part A Mol. Integr. Physiol. 140 (2005) 363–376. https://doi.org/https://doi.org/10.1016/j.cbpb.2005.01.019.

[139] D. Cevik, M. Acker, P. Arefi, R. Ghaemi, J. Zhang, P.R. Selvaganapathy, I. Dworkin, J.R. Jacobs, Chloroform and desflurane immobilization with recovery of viable Drosophila larvae for confocal imaging, J. Insect Physiol. 117 (2019) 103900. https://doi.org/https://doi.org/10.1016/j.jinsphys.2019.103900.

[140] H.A. MacMillan, M. Nørgård, H.J. MacLean, J. Overgaard, C.J.A. Williams, A critical test of Drosophila anaesthetics: Isoflurane and sevoflurane are benign alternatives to cold and CO2, J. Insect Physiol. 101 (2017) 97–106. https://doi.org/https://doi.org/10.1016/j.jinsphys.2017.07.005.

[141] S. Mondal, S. Ahlawat, S.P. Koushika, Simple Microfluidic Devices for in vivo Imaging of C. elegans, Drosophila and Zebrafish, J. Vis. Exp. (2012) 1–9. https://doi.org/10.3791/3780.

[142] R. Ghaemi, P. Rezai, B.G. Iyengar, P.R. Selvaganapathy, Microfluidic devices for imaging neurological response of Drosophila melanogaster larva to auditory stimulus, Lab Chip. 15 (2015) 1116–1122. https://doi.org/10.1039/C4LC01245C.

[143] G. Si, J.K. Kanwal, Y. Hu, C.J. Tabone, J. Baron, M. Berck, G. Vignoud, A.D.T. Samuel, Structured Odorant Response Patterns across a Complete Olfactory Receptor Neuron Population, Neuron. 101 (2019) 950–962. https://doi.org/https://doi.org/10.1016/j.neuron.2018.12.030.

[144] R. Ardeshiri, P. Rezai, Lab-on-chips for manipulation of small-scale organisms to facilitate imaging of neurons and organs, Proc. Annu. Int. Conf. IEEE Eng. Med. Biol. Soc. EMBS. 2016-Octob (2016) 5749–5752. https://doi.org/10.1109/EMBC.2016.7592033.

[145] C.D. AU - Nichols, J. AU - Becnel, U.B. AU - Pandey, Methods to Assay Drosophila Behavior, JoVE. (2012) e3795. https://doi.org/doi:10.3791/3795.

[146] J.W. Gargano, I. Martin, P. Bhandari, M.S. Grotewiel, Rapid iterative negative geotaxis (RING): a new method for assessing age-related locomotor decline in Drosophila, Exp. Gerontol. 40 (2005) 386–395. https://doi.org/https://doi.org/10.1016/j.exger.2005.02.005.

[147] M.B. Sokolowski, Foraging strategies ofDrosophila melanogaster: A chromosomal analysis, Behav. Genet. 10 (1980) 291–302. https://doi.org/10.1007/BF01067774.

[148] A.-H. Pool, K. Scott, Feeding regulation in Drosophila, Curr. Opin. Neurobiol. 29 (2014) 57–63. https://doi.org/https://doi.org/10.1016/j.conb.2014.05.008.

[149] A. Eriksson, M. Raczkowska, R. Navawongse, D. Choudhury, J.C. Stewart, Y.L. Tang, Z. Wang, A. Claridge-Chang, Neuromodulatory circuit effects on Drosophila feeding behaviour and metabolism, Sci. Rep. 7 (2017) 8839.

[150] D. Kim, M. Alvarez, L.M. Lechuga, M. Louis, Species-specific modulation of food-search behavior by respiration and chemosensation in Drosophila larvae, Elife. 6 (2017) 1–23. https://doi.org/10.7554/eLife.27057.

[151] O. Rota-Stabelli, M. Blaxter, G. Anfora, Drosophila suzukii, Curr. Biol. 23 (2013) R8--R9.

[152] D.J. Panagopoulos, A. Karabarbounis, L.H. Margaritis, Effect of GSM 900-MHz mobile phone radiation on the reproductive capacity of Drosophila melanogaster, Electromagn. Biol. Med. 23 (2004) 29–43.

[153] R.F. Rockwell, J. Grossfield, Drosophila: Behavioral Cues for Oviposition, Am. Midl. Nat. 99 (1978) 361–368.

[154] T.A. Markow, O. O'Grady, Reproductive ecology of Drosophila, Funct. Ecol. 22 (2008) 747–759. https://doi.org/10.1111/j.1365-2435.2008.01457.x.

[155] J.C.K. Leung, R.W. Taylor-Kamall, A.J. Hilliker, P. Rezai, Agar-polydimethylsiloxane devices for quantitative investigation of oviposition behaviour of adult Drosophila melanogaster, Biomicrofluidics. 9 (2015) 34112. https://doi.org/10.1063/1.4922737.

[156] D.M. Panchision, H.-L. Chen, F. Pistollato, D. Papini, H.-T. Ni, T.S. Hawley, Optimized flow cytometric analysis of central nervous system tissue reveals novel functional relationships among cells expressing CD133, CD15, and CD24, Stem Cells. 25 (2007) 1560–1570.

[157] E. Molnár, Long-term potentiation in cultured hippocampal neurons, Semin. Cell Dev. Biol. 22 (2011) 506–513. https://doi.org/https://doi.org/10.1016/j.semcdb.2011.07.017.

[158] P.-A. Salmand, M. Iché-Torres, L. Perrin, Tissue-specific cell sorting from Drosophila embryos: Application to gene expression analysis, Fly (Austin). 5 (2011) 261–265. https://doi.org/10.4161/fly.5.3.16509.

[159] P.J. Hollenbeck, J.R. Bamburg, Comparing the properties of neuronal culture systems: a shopping guide for the cell biologist, Methods Cell Biol. 71 (2003) 1–16.

[160] L.-J. Wu, Y. Lu, T.-L. Xu, A novel mechanical dissociation technique for studying acutely isolated maturing Drosophila central neurons, J. Neurosci. Methods. 108 (2001) 199–206. https://doi.org/https://doi.org/10.1016/S0165-0270(01)00404-6.

[161] L.D. Jager, C.-M.A. Canda, C.A. Hall, C.L. Heilingoetter, J. Huynh, S.S. Kwok, J.H. Kwon, J.R. Richie, M.B. Jensen, Effect of enzymatic and mechanical methods of dissociation on neural progenitor cells derived from induced pluripotent stem cells, Adv. Med. Sci. 61 (2016) 78–84. https://doi.org/10.1016/j.advms.2015.09.005.

[162] L. Wallman, E. Åkesson, D. Ceric, P.H. Andersson, K. Day, O. Hovatta, S. Falci, T. Laurell, E. Sundström, Biogrid—a microfluidic device for large-scale enzyme-free dissociation of stem cell aggregates, Lab Chip. 11 (2011) 3241–3248.

[163] B. Patra, Y.-H. Chen, C.-C. Peng, S.-C. Lin, C.-H. Lee, Y.-C. Tung, A microfluidic device for uniform-sized cell spheroids formation, culture, harvesting and flow cytometry analysis, Biomicrofluidics. 7 (2013) 54114.

[164] G.M. Walker, M.S. Ozers, D.J. Beebe, Insect Cell Culture in Microfluidic Channels, Biomed. Microdevices. 4 (2002) 161–166. https://doi.org/10.1023/A:1016088128057.

[165] L. Jiang, R. Kraft, L.L. Restifo, Y. Zohar, Dissociation of brain tissue into viable single neurons in a microfluidic device, IEEE Int. Conf. Nano/Molecular Med. Eng. NANOMED. 2016-June (2016) 29–32. https://doi.org/10.1109/NANOMED.2015.7492500.

[166] L. Van Giesen, L. Hernandez-Nunez, S. Delasoie-Baranek, M. Colombo, P. Renaud, R. Bruggmann, R. Benton, A.D.T. Samuel, S.G. Sprecher, Multimodal stimulus coding by a gustatory sensory neuron in Drosophila larvae, Nat. Commun. 7 (2016) 1–10. https://doi.org/10.1038/ncomms10687.

[167] E.R. Liman, Y. V Zhang, C. Montell, Peripheral coding of taste, Neuron. 81 (2014) 984–1000.

[168] C. Beck, T. Singh, A. Farooqi, T. Venkatesh, M. Vazquez, Controlled microfluidics to examine growth-factor induced migration of neural progenitors in the Drosophila visual system, J. Neurosci. Methods. 262 (2016) 32–40. https://doi.org/10.1016/j.jneumeth.2015.12.012.

[169] Q. Kong, R.A. Able, V. Dudu, M. Vazquez, A Microfluidic Device to Establish Concentration Gradients Using, J. Biomech. Eng. 132 (2019) 1–9. https://doi.org/10.1115/1.4002797.

[170] C.E. Narciso, N.M. Contento, T.J. Storey, D.J. Hoelzle, J.J. Zartman, Release of Applied Mechanical Loading Stimulates Intercellular Calcium Waves in Drosophila Wing Discs, Biophys. J. 113 (2017) 491–501. https://doi.org/10.1016/j.bpj.2017.05.051.

[171] M. Morel, D. Bartolo, J.-C. Galas, M. Dahan, V. Studer, Microfluidic stickers for cell- and tissue-based assays in microchannels, Lab Chip. 9 (2009) 1011–1013. https://doi.org/10.1039/B819090A.

[172] M. Levis, N. Kumar, E. Apakian, C. Moreno, U. Hernandez, A. Olivares, F. Ontiveros, J.J. Zartman, Microfluidics on the fly: Inexpensive rapid fabrication of thermally laminated microfluidic devices for live imaging and multimodal perturbations of multicellular systems, Biomicrofluidics. 13 (2019) 24111. https://doi.org/10.1063/1.5086671.

[173] T. Schwerte, D. Überbacher, B. Pelster, Non-invasive imaging of blood cell concentration and blood distribution in zebrafish Danio rerio incubated in hypoxic conditions in vivo, J. Exp. Biol. 206 (2003) 1299–1307. https://doi.org/10.1242/jeb.00249.

[174] T. Schwerte, R. Fritsche, Understanding cardiovascular physiology in zebrafish and Xenopus larvae: the use of microtechniques, Comp. Biochem. Physiol. Part A Mol. Integr. Physiol. 135 (2003) 131–145. https://doi.org/https://doi.org/10.1016/S1095-6433(03)00044-8.

[175] R.J. Wessells, E. Fitzgerald, J.R. Cypser, M. Tatar, R. Bodmer, Insulin regulation of heart function in aging fruit flies, Nat. Genet. 36 (2004) 1275–1281.

[176] J. Robbins, R. Aggarwal, R. Nichols, G. Gibson, Genetic variation affecting heart rate in Drosophila melanogaster, Genet. Res. (Camb). 74 (1999) 121–128.

[177] G. Paternostro, C. Vignola, D.-U. Bartsch, J.H. Omens, A.D. McCulloch, J.C. Reed, Age-associated cardiac dysfunction in Drosophila melanogaster, Circ. Res. 88 (2001) 1053–1058.

[178] H. Mönck, D. Toppe, E. Michael, S. Sigrist, V. Richter, D. Hilpert, D. Raccuglia, M. Efetova, M. Schwärzel, A new method to characterize function of the Drosophila heart by means of optical flow, J. Exp. Biol. 220 (2017) 4644–4653.

[179] A.S. Forouhar, J.R. Hove, C. Calvert, J. Flores, H. Jadvar, M. Gharib, Electrocardiographic characterization of embryonic zebrafish, Annu. Int. Conf. IEEE Eng. Med. Biol. - Proc. 26 V (2004) 3615–3617. https://doi.org/10.1109/iembs.2004.1404016.

[180] K.L. Yozzo, G.M. Isales, T.D. Raftery, D.C. Volz, High-content screening assay for identification of chemicals impacting cardiovascular function in zebrafish embryos, Environ. Sci. Technol. 47 (2013) 11302–11310. https://doi.org/10.1021/es403360y.

[181] J. Ohn, M. Liebling, In vivo, high-throughput imaging for functional characterization of the embryonic zebrafish heart, Proc. - Int. Symp. Biomed. Imaging. (2011) 1549–1552. https://doi.org/10.1109/ISBI.2011.5872696.

[182] Mutations affecting the formation and function of the cardiovascular system.pdf, (n.d.).

[183] C. Papaefthimiou, G. Theophilidis, An in vitro method for recording the electrical activity of the isolated heart of the adult Drosophila melanogaster, Vitr. Cell. Dev. Biol. 37 (2001) 445–449.

[184] K. Ocorr, N.L. Reeves, R.J. Wessells, M. Fink, H.-S.V. Chen, T. Akasaka, S. Yasuda, J.M. Metzger, W. Giles, J.W. Posakony, others, KCNQ potassium channel mutations cause cardiac arrhythmias in Drosophila that mimic the effects of aging, Proc. Natl. Acad. Sci. 104 (2007) 3943–3948.

[185] T.J. Hamilton, A. Morrill, K. Lucas, J. Gallup, M. Harris, M. Healey, T. Pitman, M. Schalomon, S. Digweed, M. Tresguerres, Establishing zebrafish as a model to study the anxiolytic effects of scopolamine, Sci. Rep. 7 (2017) 1–9. https://doi.org/10.1038/s41598-017-15374-w.

[186] R. Raghunathan, M. Singh, M.E. Dickinson, K. V. Larin, Optical coherence tomography for embryonic imaging: a review, J. Biomed. Opt. 21 (2016) 1. https://doi.org/10.1117/1.jbo.21.5.050902.

[187] E. De Luca, G.M. Zaccaria, M. Hadhoud, G. Rizzo, R. Ponzini, U. Morbiducci, M.M. Santoro, ZebraBeat : A flexible platform for the analysis of the cardiac rate in zebrafish embryos, Sci. Rep. 4 (2014) 1–13. https://doi.org/10.1038/srep04898.

[188] P.K. Chan, C.C. Lin, S.H. Cheng, Noninvasive technique for measurement of heartbeat regularity in zebrafish (Danio rerio) embryos, BMC Biotechnol. 9 (2009) 11.

[189] X. Lin, V.W.T. Li, S. Chen, C.Y. Chan, S.H. Cheng, P. Shi, Autonomous system for cross-organ investigation of ethanol-induced acute response in behaving larval zebrafish,

Biomicrofluidics. 10 (2016). https://doi.org/10.1063/1.4946013.

[190] C. Pylatiuk, D. Sanchez, R. Mikut, R. Alshut, M. Reischl, S. Hirth, W. Rottbauer, S. Just, Automatic zebrafish heartbeat detection and analysis for zebrafish embryos, Zebrafish. 11 (2014) 379–383. https://doi.org/10.1089/zeb.2014.1002.

[191] E. Puybareau, D. Genest, E. Barbeau, M. Léonard, H. Talbot, An automated assay for the assessment of cardiac arrest in fish embryo, Comput. Biol. Med. 81 (2017) 32–44. https://doi.org/10.1016/j.compbiomed.2016.12.007.

[192] R. Peravali, J. Gehrig, S. Giselbrecht, D.S. Lütjohann, Y. Hadzhiev, F. Müller, U. Liebel, Automated feature detection and imaging for high-resolution screening of zebrafish embryos, Biotechniques. 50 (2011) 319–324. https://doi.org/10.2144/000113669.

[193] K. Ocorr, M. Fink, A. Cammarato, S.I. Bernstein, R. Bodmer, Semi-automated optical heartbeat analysis of small hearts, JoVE (Journal Vis. Exp. (2009) e1435.

[194] M.H. Malone, N. Sciaky, L. Stalheim, K.M. Hahn, E. Linney, G.L. Johnson, Laser-scanning velocimetry: A confocal microscopy method for quantitative measurement of cardiovascular performance in zebrafish embryos and larvae, BMC Biotechnol. 7 (2007) 1–11. https://doi.org/10.1186/1472-6750-7-40.

[195] S. Krishna, K. Chatti, R.R. Galigekere, Automatic and Robust Estimation of Heart Rate in Zebrafish Larvae, IEEE Trans. Autom. Sci. Eng. 15 (2018) 1041–1052. https://doi.org/10.1109/TASE.2017.2705240.

[196] A. Khalili, P. Rezai, Microfluidic devices for embryonic and larval zebrafish studies, Briefings Funct. Genomics,. (2019) 1–14.

[197] A. Khalili, E. van Wijngaarden, G.R. Zoidl, P. Rezai, Multi-phenotypic and bi-directional behavioral screening of zebrafish larvae, Integr. Biol. 12 (2020) 211–220. https://doi.org/10.1093/intbio/zyaa016.

[198] L.A. White, J.M. Ringo, H.B. Dowse, Effects of deuterium oxide and temperature on heart rate in Drosophila melanogaster, J. Comp. Physiol. B. 162 (1992) 278–283.

[199] B. Risse, S. Thomas, N. Otto, T. Löpmeier, D. Valkov, X. Jiang, C. Klämbt, FIM, a novel FTIR-based imaging method for high throughput locomotion analysis, PLoS One. 8 (2013) e53963.

[200] J. Gierten, C. Pylatiuk, O.T. Hammouda, C. Schock, J. Stegmaier, J. Wittbrodt, J. Gehrig, F. Loosli, Automated high-throughput heartbeat quantification in medaka and zebrafish embryos under physiological conditions, Sci. Rep. 10 (2020) 1–12. https://doi.org/10.1038/s41598-020-58563-w.

[201] C.P. Kang, H.C. Tu, T.F. Fu, J.M. Wu, P.H. Chu, D.T.H. Chang, An automatic method to calculate heart rate from zebrafish larval cardiac videos, BMC Bioinformatics. 19 (2018) 1–10. https://doi.org/10.1186/s12859-018-2166-6.

[202] E. Puybareau, H. Talbot, M. Léonard, Automated heart rate estimation in fish embryo, 5th Int. Conf. Image Process. Theory, Tools Appl. 2015, IPTA 2015. (2015) 379–384. https://doi.org/10.1109/IPTA.2015.7367171.

[203] W.H. Frishman, P. Grewall, Serotonin and the heart, Ann. Med. 32 (2000) 195–209.

[204] H. Sternbach, The serotonin syndrome, Am J Psychiatry. 148 (1991) 705–713.

[205] J. Breuer, R. Meschig, H.W. Breuer, G. Arnold, Effects of serotonin on the cardiopulmonary circulatory system with and without 5-HT2-receptor blockade by ketanserin., J. Cardiovasc. Pharmacol. 7 (1985) S64--6.

[206] E. Belougne-Malfatti, O. Aguejouf, F. Doutremepuich, C. Doutremepuich, Action of neurotransmitters: acetylcholine, serotonin, and adrenaline in an experimental arterial thrombosis induced by oxygen free radicals, Thromb. Res. 88 (1997) 435–439.

[207] C.G. Missouris, F.P. Cappuccio, E. Varsamis, J.L. Barron, N.D. Markandu, G.A. MacGregor, others, Serotonin and heart rate in hypertensive and normotensive subjects, Am. Heart J. 135 (1998) 838–843.

[208] M. Jaishankar, T. Tseten, N. Anbalagan, B.B. Mathew, K.N. Beeregowda, Toxicity, mechanism and health effects of some heavy metals, Interdiscip. Toxicol. 7 (2014) 60. https://doi.org/10.2478/INTOX-2014-0009.

[209] P.B. Tchounwou, C.G. Yedjou, A.K. Patlolla, D.J. Sutton, Heavy Metals Toxicity and the Environment, 101 (2012) 1–30. https://doi.org/10.1007/978-3-7643-8340-4.

[210] G.A. Lamas, F. Ujueta, A. Navas-Acien, Lead and Cadmium as Cardiovascular Risk Factors: The Burden of Proof Has Been Met, J. Am. Heart Assoc. 10 (2021) 18692. https://doi.org/10.1161/JAHA.120.018692.

[211] P. M, E. I, B. H, H. L, K. J, Blood cadmium and plasma zinc measurements in acute myocardial infarction., Eur. J. Cardiol. 9 (1979) 379–391. https://europepmc.org/article/med/456396 (accessed July 25, 2021).

[212] M. Tellez-Plaza, M.R. Jones, A. Dominguez-Lucas, E. Guallar, A. Navas-Acien, Cadmium Exposure and Clinical Cardiovascular Disease: a Systematic Review, Curr. Atheroscler. Rep. 15 (2013). https://doi.org/10.1007/S11883-013-0356-2.

[213] M.C. Houston, Role of mercury toxicity in hypertension, cardiovascular disease, and stroke, J. Clin. Hypertens. 13 (2011) 621–627. https://doi.org/10.1111/J.1751-7176.2011.00489.X.

[214] P. Richter, O. Faroon, R.S. Pappas, Cadmium and Cadmium/Zinc Ratios and Tobacco-Related Morbidities, Int. J. Environ. Res. Public Heal. 2017, Vol. 14, Page 1154. 14 (2017) 1154. https://doi.org/10.3390/IJERPH14101154.

[215] J. Nriagu, others, Zinc toxicity in humans, Sch. Public Heal. Univ. Michigan. (2007) 1–7.

[216] L. Cai, X.-K. Li, Y. Song, M.G. Cherian, Essentiality, Toxicology and Chelation Therapy of Zinc and Copper, Curr. Med. Chem. 12 (2005) 2753–2763. https://doi.org/10.2174/092986705774462950.

[217] N. R, Copper deficiency and heart disease: molecular basis, recent advances and current concepts, Int. J. Biochem. Cell Biol. 29 (1997) 1245–1254. https://doi.org/10.1016/S1357-2725(97)00060-5.

[218] D. J, M. DM, H. RL, Cardiac ultrastructural and electrophysiological abnormalities in

postweanling copper-restricted and copper-repleted rats in the absence of hypertrophy, J. Nutr. 122 (1992) 1566–1575. https://doi.org/10.1093/JN/122.7.1566.

[219] A.J. Crawford, S.K. Bhattacharya, Excessive intracellular zinc accumulation in cardiac and skeletal muscles of dystrophic hamsters, Exp. Neurol. 95 (1987) 265–276. https://doi.org/10.1016/0014-4886(87)90137-3.

[220] H. RM, Y. J, Particulate matter in the atmosphere: which particle properties are important for its effects on health?, Sci. Total Environ. 249 (2000) 85–101. https://doi.org/10.1016/S0048-9697(99)00513-6.

[221] U.P. Kodavanti, M.C. Schladweiler, P.S. Gilmour, J.G. Wallenborn, B.S. Mandavilli, A.D. Ledbetter, D.C. Christiani, M.S. Runge, E.D. Karoly, D.L. Costa, S. Peddada, R. Jaskot, J.H. Richards, R. Thomas, N.R. Madamanchi, A. Nyska, The role of particulate matter-associated zinc in cardiac injury in rats, Environ. Health Perspect. 116 (2008) 13–20. https://doi.org/10.1289/EHP.10379.

[222] G. V, L. U, S. W, The taste of heavy metals: gene regulation by MTF-1, Biochim. Biophys. Acta. 1823 (2012) 1416–1425. https://doi.org/10.1016/J.BBAMCR.2012.01.005.

[223] C. P, P. JC, C. LC, R. AM, Metallothionein: the multipurpose protein, Cell. Mol. Life Sci. 59 (2002) 627–647. https://doi.org/10.1007/S00018-002-8454-2.

[224] G. C, H. R, G. O, M. KH, L. P, B. H, M. S, A. A, S. W, Embryonic lethality and liver degeneration in mice lacking the metal-responsive transcriptional activator MTF-1, EMBO J. 17 (1998) 2846–2854. https://doi.org/10.1093/EMBOJ/17.10.2846.

[225] S. Bahadorani, A.J. Hilliker, Biological and Behavioral Effects of Heavy Metals in Drosophila melanogaster Adults and Larvae, J. Insect Behav. 22 (2009) 399–411. https://doi.org/10.1007/s10905-009-9181-4.

[226] P. Engel, N.A. Moran, The gut microbiota of insects – diversity in structure and function, FEMS Microbiol. Rev. 37 (2013) 699–735. https://doi.org/10.1111/1574-6976.12025.

[227] M.D. Abràmoff, P.J. Magalhães, S.J. Ram, Image processing with ImageJ, Biophotonics Int. 11 (2004) 36–42.

[228] A.G. Gaonkar, Interfacial tensions of vegetable oil/water systems: effect of oil purification, J. Am. Oil Chem. Soc. 66 (1989) 1090–1092.

[229] Y. Kitamura, K. Kizu, T. Takahashi, Breakup of relatively low-concentrated O/W emulsion jets, Can. J. Chem. Eng. 63 (1985) 244–249.

[230] K.G. Ormerod, O.K. LePine, P.S. Abbineni, J.M. Bridgeman, J.R. Coorssen, A.J. Mercier, G.J. Tattersall, Drosophila development, physiology, behavior, and lifespan are influenced by altered dietary composition, Fly (Austin). 11 (2017) 153. https://doi.org/10.1080/19336934.2017.1304331.

[231] J. Geiser, R.C. De Lisle, G.K. Andrews, The Zinc Transporter Zip5 (Slc39a5) Regulates Intestinal Zinc Excretion and Protects the Pancreas against Zinc Toxicity, PLoS One. 8 (2013) e82149. https://doi.org/10.1371/JOURNAL.PONE.0082149.

[232] J. Lee, W.J. Yu, J. Song, C. Sung, E.J. Jeong, J.S. Han, P. Kim, E. Jo, I. Eom, H.M. Kim, J.T. Kwon, K. Choi, J. Choi, H. Kim, H. Lee, J. Park, S.M. Jin, K. Park, Developmental toxicity of intravenously injected zinc oxide nanoparticles in rats, Arch. Pharm. Res. 39 (2016) 1682–1692. https://doi.org/10.1007/S12272-016-0767-Z/TABLES/6.

[233] S. Amara, I. Ben Slama, I. Mrad, N. Rihane, W. Khemissi, L. El Mir, K. Ben Rhouma, H. Abdelmelek, M. Sakly, Effects of zinc oxide nanoparticles and/or zinc chloride on biochemical parameters and mineral levels in rat liver and kidney, Hum. Exp. Toxicol. 33 (2014) 1150–1157. https://doi.org/10.1177/0960327113510327.

[234] G. Kazantzis, W.J. Hanbury, The induction of sarcoma in the rat by cadmium sulphide and by cadmium oxide., Br. J. Cancer. 20 (1966) 190. https://doi.org/10.1038/BJC.1966.22.

[235] S.-M. Chen, S. Phuagkhaopong, C. Fang, J.C.C. Wu, Y.-H. Huang, P. Vivithanaporn, H.-H. Lin, C.-Y. Tsai, Dose-Dependent Acute Circulatory Fates Elicited by Cadmium Are Mediated by Differential Engagements of Cardiovascular Regulatory Mechanisms in Brain, Front. Physiol. 0 (2019) 772. https://doi.org/10.3389/FPHYS.2019.00772.

[236] Y. Xu, W. Wang, L. Ma, X. Cui, I. Lynch, G. Wu, Acute toxicity of Zinc Oxide nanoparticles to silkworm (Bombyx mori L.), Chemosphere. 259 (2020) 127481. https://doi.org/10.1016/J.CHEMOSPHERE.2020.127481.

[237] T.J. Ragan, A.P. Bailey, A.P. Gould, P.C. Driscoll, Volume determination with two standards allows absolute quantification and improved chemometric analysis of metabolites by NMR from submicroliter samples, Anal. Chem. 85 (2013) 12046–12054.

[238] M. Desai-Shah, A.R. Papoy, M. Ward, R.L. Cooper, Roles of the Sarcoplasmic/Endoplasmic reticulum Ca2+-ATPase, plasma membrane Ca2+-ATPase and Na+/Ca2+ exchanger in regulation of heart rate in larval Drosophila, Open Physiol. J. 3 (2010) 16.

[239] S.M. Ahmad, Conserved signaling mechanisms in Drosophila heart development, Dev. Dyn. 246 (2017) 641–656.

[240] N.J. Curtis, J.M. Ringo, H.B. Dowse, Morphology of the pupal heart, adult heart, and associated tissues in the fruit fly, Drosophila melanogaster, J. Morphol. 240 (1999) 225–235.

[241] M.K. Goel, P. Khanna, J. Kishore, Understanding survival analysis: Kaplan-Meier estimate, Int. J. Ayurveda Res. 1 (2010) 274–278. https://doi.org/10.4103/0974-7788.76794.

[242] C. Malloy, J. Sifers, A. Mikos, A. Samadi, A. Omar, C. Hermanns, R.L. Cooper, Using optogenetics to assess neuroendocrine modulation of heart rate in Drosophila melanogaster larvae, J. Comp. Physiol. A. 203 (2017) 791–806.

[243] J. Men, J. Jerwick, P. Wu, M. Chen, A. Alex, Y. Ma, R.E. Tanzi, A. Li, C. Zhou, Drosophila preparation and longitudinal imaging of heart function in vivo using Optical Coherence Microscopy (OCM), JoVE (Journal Vis. Exp. (2016) e55002.

[244] L. Ma, A. Bradu, A.G. Podoleanu, J.W. Bloor, Arrhythmia caused by a Drosophila tropomyosin mutation is revealed using a novel optical coherence tomography instrument, PLoS One. 5 (2010) e14348.

[245] K. Sláma, R. Farkaš, Heartbeat patterns during the postembryonic development of Drosophila melanogaster, J. Insect Physiol. 51 (2005) 489–503.

[246] I. Miguel-Aliaga, H. Jasper, B. Lemaitre, Anatomy and Physiology of the Digestive Tract of Drosophila melanogaster, Genetics. 210 (2018) 357. https://doi.org/10.1534/GENETICS.118.300224.

[247] A. Zabihihesari, A. Khalili, A.J. Hilliker, P. Rezai, Open access tool and microfluidic devices for phenotypic quantification of heart function of intact fruit fly and zebrafish larvae, Comput. Biol. Med. 132 (2021) 104314. https://doi.org/10.1016/j.compbiomed.2021.104314.

[248] Y. Yang, Y. Yu, R. Zhou, Y. Yang, Y. Bu, The effect of combined exposure of zinc and nickel on the development of zebrafish, J. Appl. Toxicol. 41 (2021) 1765–1778. https://doi.org/10.1002/JAT.4159.

[249] M. Küçüko\uglu, U.S. Binokay, A.B. PEKMEZEKMEK, The effects of zinc chloride during early embryonic development in zebrafish (Brachydanio rerio), Turkish J. Biol. 37 (2013) 158–164.

[250] S. Marchán, M.S. Davies, S. Fleming, H.D. Jones, Effects of copper and zinc on the heart rate of the limpet Patella vulgata L., Comp. Biochem. Physiol. Part A Mol. Integr. Physiol. 123 (1999) 89–93. https://doi.org/10.1016/S1095-6433(99)00043-4.

[251] R. Zhang, M. Wang, X. Chen, C. Yang, L. Wu, Combined toxicity of microplastics and cadmium on the zebrafish embryos (Danio rerio), Sci. Total Environ. 743 (2020) 140638. https://doi.org/10.1016/J.SCITOTENV.2020.140638.

[252] A. V. Hallare, M. Schirling, T. Luckenbach, H.R. Köhler, R. Triebskorn, Combined effects of temperature and cadmium on developmental parameters and biomarker responses in zebrafish (Danio rerio) embryos, J. Therm. Biol. 30 (2005) 7–17. https://doi.org/10.1016/J.JTHERBIO.2004.06.002.

[253] M. Wold, M. Beckmann, S. Poitra, A. Espinoza, R. Longie, E. Mersereau, D.C. Darland, T. Darland, The Longitudinal Effects of Early Developmental Cadmium Exposure on Conditioned Place Preference and Cardiovascular Physiology in Zebrafish, Aquat. Toxicol. 191 (2017) 73. https://doi.org/10.1016/J.AQUATOX.2017.07.017.

[254] J.P. Phillips, A.J. Hilliker, Genetic Analysis of Oxygen Defense Mechanisms in Drosophila Melanogoster, Adv. Genet. 28 (1990) 43–71. https://doi.org/10.1016/S0065-2660(08)60523-4.

[255] P. Calap-Quintana, J. González-Fernández, N. Sebastiá-Ortega, J.V. Llorens, M.D. Moltó, Drosophila melanogaster Models of Metal-Related Human Diseases and Metal Toxicity, Int. J. Mol. Sci. 2017, Vol. 18, Page 1456. 18 (2017) 1456. https://doi.org/10.3390/IJMS18071456.

[256] D. P, S. S, R. GR, Studies on cadmium toxicity in plants: a review, Environ. Pollut. 98 (1997) 29–36. https://doi.org/10.1016/S0269-7491(97)00110-3.

[257] G.K. Andrews, Regulation of metallothionein gene expression by oxidative stress and metal ions, Biochem. Pharmacol. 59 (2000) 95–104. https://doi.org/10.1016/S0006-

2952(99)00301-9.

[258] X. W, L. Q, C. L, W. Z, F. W, Stable overexpression of human metallothionein-IIA in a heart-derived cell line confers oxidative protection, Toxicol. Lett. 188 (2009) 70–76. https://doi.org/10.1016/J.TOXLET.2009.03.007.

[259] A. Nandi, D.K. Chowdhuri, Cadmium mediated redox modulation in germline stem cells homeostasis affects reproductive health of Drosophila males, J. Hazard. Mater. 402 (2021) 123737. https://doi.org/10.1016/J.JHAZMAT.2020.123737.

[260] M. Alaraby, B. Annangi, A. Hernández, A. Creus, R. Marcos, A comprehensive study of the harmful effects of ZnO nanoparticles using Drosophila melanogaster as an in vivo model, J. Hazard. Mater. 296 (2015) 166–174. https://doi.org/10.1016/J.JHAZMAT.2015.04.053.

[261] S. El Kholy, J.P. Giesy, Y. Al Naggar, Consequences of a short-term exposure to a sub lethal concentration of CdO nanoparticles on key life history traits in the fruit fly (Drosophila melanogaster), J. Hazard. Mater. 410 (2021) 124671. https://doi.org/10.1016/J.JHAZMAT.2020.124671.

[262] F.A. Al-Momani, A.M. Massadeh, Effect of Different Heavy-Metal Concentrations on Drosophila melanogaster Larval Growth and Development, 108 (2005).

[263] S. Bahadorani, A.J. Hilliker, Biological and Behavioral Effects of Heavy Metals in Drosophila melanogaster Adults and Larvae, J. Insect Behav. 22 (2009) 399–411. https://doi.org/10.1007/S10905-009-9181-4.

[264] J. Leung, R. Taylor-Kamall, A. Hilliker, P. Rezai, Agar-Polydimethylsiloxane Devices for Quantitative Investigation of Oviposition Behaviour of Adult Drosophila melanogaster., Biomicrofluidics. 9 (2015) 15096.

[265] J. Leung, A. Hilliker, P. Rezai, An Integrated Hybrid Microfluidic Device for Oviposition-based Chemical Screening of Adult Drosophila melanogaster, Lab Chip. 16 (2016) 709–719.

[266] S. Yin, Q. Qin, B. Zhou, Functional studies of Drosophila zinc transporters reveal the mechanism for zinc excretion in Malpighian tubules, BMC Biol. 2017 151. 15 (2017) 1–12. https://doi.org/10.1186/S12915-017-0355-9.

[267] E. Tuncay, A. Bilginoglu, N.N. Sozmen, E.N. Zeydanli, M. Ugur, G. Vassort, B. Turan, Intracellular free zinc during cardiac excitation–contraction cycle: calcium and redox dependencies, Cardiovasc. Res. 89 (2011) 634–642. https://doi.org/10.1093/CVR/CVQ352.

[268] S. Choi, X. Liu, Z. Pan, Zinc deficiency and cellular oxidative stress: prognostic implications in cardiovascular diseases, Acta Pharmacol. Sin. 2018 397. 39 (2018) 1120–1132. https://doi.org/10.1038/aps.2018.25.

[269] D. Brugger, W.M. Windisch, Short-term subclinical zinc deficiency in weaned piglets affects cardiac redox metabolism and zinc concentration, J. Nutr. 147 (2017) 521–527. https://doi.org/10.3945/JN.116.240804.

[270] P. Liu, S. Wang, Z. Chang, L. Li, H. Xing, W.F. Dong, Combined toxicity of silica nanoparticles and cadmium chloride on the cardiovascular system of zebrafish (Danio rerio)

larvae, Comp. Biochem. Physiol. Part C Toxicol. Pharmacol. 239 (2021) 108895. https://doi.org/10.1016/J.CBPC.2020.108895.

[271] C.B. Rohde, F. Zeng, R. Gonzalez-Rubio, M. Angel, M.F. Yanik, Microfluidic system for on-chip high-throughput whole-animal sorting and screening at subcellular resolution, Proc. Natl. Acad. Sci. U. S. A. 104 (2007) 13891–13895. https://doi.org/10.1073/PNAS.0706513104/SUPPL_FILE/06513MOVIE1.AVI.

[272] A.S. Joshi, A.D. Alegria, B. Auch, K. Khosla, J.B. Mendana, K. Liu, J. Bischof, D.M. Gohl, S.B. Kodandaramaiah, Multiscale, multi-perspective imaging assisted robotic microinjection of 3D biological structures, Proc. Annu. Int. Conf. IEEE Eng. Med. Biol. Soc. EMBS. (2021) 4844–4850. https://doi.org/10.1109/EMBC46164.2021.9630858.

[273] M. Deubel, G. Von Freymann, M. Wegener, S. Pereira, K. Busch, C.M. Soukoulis, Direct laser writing of three-dimensional photonic-crystal templates for telecommunications, Nat. Mater. 2004 37. 3 (2004) 444–447. https://doi.org/10.1038/nmat1155.

[274] F.P.W. Melchels, J. Feijen, D.W. Grijpma, A review on stereolithography and its applications in biomedical engineering, Biomaterials. 31 (2010) 6121–6130. https://doi.org/10.1016/J.BIOMATERIALS.2010.04.050.

[275] O.A. Mohamed, S.H. Masood, J.L. Bhowmik, Optimization of fused deposition modeling process parameters: a review of current research and future prospects, Adv. Manuf. 3 (2015) 42–53. https://doi.org/10.1007/S40436-014-0097-7/TABLES/2.

[276] US20200001063A1 - Anti-clogging and anti-adhesive micro-capillary needle with enhanced tip visibility - Google Patents, (n.d.). https://patents.google.com/patent/US20200001063A1/en (accessed April 10, 2022).

[277] P.L. Kastritis, A.M.J.J. Bonvin, On the binding affinity of macromolecular interactions: daring to ask why proteins interact, J. R. Soc. Interface. 10 (2013). https://doi.org/10.1098/RSIF.2012.0835.

[278] T. Tsutamoto, A. Wada, H. Sakai, C. Ishikawa, T. Tanaka, M. Hayashi, M. Fujii, T. Yamamoto, T. Dohke, M. Ohnishi, H. Takashima, M. Kinoshita, M. Horie, Relationship Between Renal Function and Plasma Brain Natriuretic Peptide in Patients With Heart Failure, J. Am. Coll. Cardiol. 47 (2006) 582–586. https://doi.org/10.1016/J.JACC.2005.10.038.

[279] T.P. Velavan, C.G. Meyer, The COVID-19 epidemic, Trop. Med. Int. Heal. 25 (2020) 278. https://doi.org/10.1111/TMI.13383.

[280] F. Krammer, SARS-CoV-2 vaccines in development, Nat. 2020 5867830. 586 (2020) 516–527. https://doi.org/10.1038/s41586-020-2798-3.

[281] M.S. Ramadan, L. Bertolino, R. Zampino, E. Durante-Mangoni, D. Iossa, M.P. Ursi, F. D'Amico, A. Karruli, M. Ramadan, R. Andini, M. Bernardo, G. Ruocco, G. Dialetto, F.E. Covino, S. Manduca, A. Della Corte, M. De Feo, S. De Vivo, M.L. De Rimini, N. Galdieri, Cardiac sequelae after coronavirus disease 2019 recovery: a systematic review, Clin. Microbiol. Infect. 27 (2021) 1250. https://doi.org/10.1016/J.CMI.2021.06.015.

[282] F. Nainu, D. Rahmatika, T. Bin Emran, H. Harapan, Potential Application of Drosophila

melanogaster as a Model Organism in COVID-19-Related Research, Front. Pharmacol. 11 (2020) 1415. https://doi.org/10.3389/FPHAR.2020.588561/BIBTEX.

[283] S. Yang, M. Tian, A.N. Johnson, SARS-CoV-2 protein ORF3a is pathogenic in Drosophila and causes phenotypes associated with COVID-19 post-viral syndrome, BioRxiv. (2020). https://doi.org/10.1101/2020.12.20.423533.

[284] J. yi Zhu, J.G. Lee, J. van de Leemput, H. Lee, Z. Han, Functional analysis of SARS-CoV-2 proteins in Drosophila identifies Orf6-induced pathogenic effects with Selinexor as an effective treatment, Cell Biosci. 11 (2021) 1–13. https://doi.org/10.1186/S13578-021-00567-8/FIGURES/6.

[285] S.C. Piyankarage, H. Augustin, Y. Grosjean, D.E. Featherstone, S.A. Snippy, Hemolymph Amino Acid Analysis of Individual Drosophila Larvae, Anal. Chem. 80 (2008) 1201–1207. https://doi.org/10.1021/AC701785Z.

[286] C. Géminard, E.J. Rulifson, P. Léopold, Remote control of insulin secretion by fat cells in Drosophila, Cell Metab. 10 (2009) 199–207. https://doi.org/10.1016/J.CMET.2009.08.002.

[287] G. Lee, J.H. Park, Hemolymph Sugar Homeostasis and Starvation-Induced Hyperactivity Affected by Genetic Manipulations of the Adipokinetic Hormone-Encoding Gene in Drosophila melanogaster, Genetics. 167 (2004) 311–323. https://doi.org/10.1534/GENETICS.167.1.311.

[288] M.A. Choma, M.J. Suter, B.J. Vakoc, B.E. Bouma, G.J. Tearney, Physiological homology between Drosophila melanogaster and vertebrate cardiovascular systems, Dis. Model. Mech. 4 (2011) 411–420. https://doi.org/10.1242/dmm.005231.

[289] K. Krishnan, R. Robison, E. Tetteh, E. Loth, T. Farrell, J. Crouch, D. Berry, Characterization of insect residue on an aerodynamic leading edge, 8th AIAA Atmos. Sp. Environ. Conf. (2016). https://doi.org/10.2514/6.2016-3445.

[290] D. Carter, E. Loth, Insect Residue Height for Different Coatings and Conditions, (2018). https://doi.org/10.2514/6.2018-0313.

[291] E.J. Siochi, N.S. Eiss, D.R. Gilliam, J.P. Wightman, A fundamental study of the sticking of insect residues to aircraft wings, J. Colloid Interface Sci. 115 (1987) 346–356. https://doi.org/10.1016/0021-9797(87)90049-X.

[292] A. Milionis, K. Ghokulla Krishnan, E. Loth, Hemolymph drop impact outcomes on surfaces with varying wettability, Appl. Surf. Sci. 345 (2015) 36–43. https://doi.org/10.1016/J.APSUSC.2015.02.185.

[293] H.A. MacMillan, B.N. Hughson, A high-throughput method of hemolymph extraction from adult Drosophila without anesthesia, J. Insect Physiol. 63 (2014) 27–31.

[294] A. Hiroyasu, D.C. DeWitt, A.G. Goodman, Extraction of hemocytes from Drosophila melanogaster larvae for microbial infection and analysis, J. Vis. Exp. JoVE. (2018).

[295] A.F. Payam, W. Trewby, K. Vo\"\itchovsky, Simultaneous viscosity and density measurement of small volumes of liquids using a vibrating microcantilever, Analyst. 142 (2017) 1492–1498.

[296] M.C. Kenny, M.N. Giarra, E. Granata, J.J. Socha, How temperature influences the viscosity of hornworm hemolymph, J. Exp. Biol. 221 (2018).

[297] S. Gupta, W.S. Wang, S.A. Vanapalli, Microfluidic viscometers for shear rheology of complex fluids and biofluids, Biomicrofluidics. 10 (2016) 043402. https://doi.org/10.1063/1.4955123.

[298] S. Kim, K.C. Kim, E. Yeom, Microfluidic method for measuring viscosity using images from smartphone, Opt. Lasers Eng. 104 (2018) 237–243. https://doi.org/10.1016/J.OPTLASENG.2017.05.016.

[299] Y.J. Kang, S.Y. Yoon, K.H. Lee, S. Yang, A Highly Accurate and Consistent Microfluidic Viscometer for Continuous Blood Viscosity Measurement, Artif. Organs. 34 (2010) 944–949. https://doi.org/10.1111/J.1525-1594.2010.01078.X.

[300] N. Srivastava, R.D. Davenport, M.A. Burns, Nanoliter viscometer for analyzing blood plasma and other liquid samples, Anal. Chem. 77 (2005) 383–392.

[301] J.M.K. Ng, I. Gitlin, A.D. Stroock, G.M. Whitesides, Components for integrated poly(dimethylsiloxane) microfluidic systems, (n.d.). https://doi.org/10.1002/1522-2683(200210)23:20.

[302] J. Friend, L. Yeo, Fabrication of microfluidic devices using polydimethylsiloxane, Biomicrofluidics. 4 (2010) 026502. https://doi.org/10.1063/1.3259624/1.3259624.MM.ORIGINAL.V1.MOV.

[303] T. Trantidou, Y. Elani, E. Parsons, O. Ces, Hydrophilic surface modification of PDMS for droplet microfluidics using a simple, quick, and robust method via PVA deposition, Microsystems \& Nanoeng. 3 (2017) 1–9.

[304] E.W. Washburn, The Dynamics of Capillary Flow, Phys. Rev. 17 (1921) 273. https://doi.org/10.1103/PhysRev.17.273.

[305] R. Lucas, Ueber das Zeitgesetz des kapillaren Aufstiegs von Flüssigkeiten, Kolloid-Zeitschrift. 23 (1918) 15–22. https://doi.org/10.1007/BF01461107.

[306] S. Bahadorani, S. Mukai, D. Egli, A.J. Hilliker, Overexpression of metal-responsive transcription factor (MTF-1) in Drosophila melanogaster ameliorates life-span reductions associated with oxidative stress and metal toxicity, Neurobiol. Aging. 31 (2010) 1215–1226. https://doi.org/10.1016/J.NEUROBIOLAGING.2008.08.001.

[307] D. Bodas, C. Khan-Malek, Formation of more stable hydrophilic surfaces of PDMS by plasma and chemical treatments, Microelectron. Eng. 83 (2006) 1277–1279. https://doi.org/10.1016/J.MEE.2006.01.195.

[308] S.H. Tan, N.T. Nguyen, Y.C. Chua, T.G. Kang, Oxygen plasma treatment for reducing hydrophobicity of a sealed polydimethylsiloxane microchannel, Biomicrofluidics. 4 (2010). https://doi.org/10.1063/1.3466882.

[309] J. Bacharouche, H. Haidara, P. Kunemann, M.F. Vallat, V. Roucoules, Singularities in hydrophobic recovery of plasma treated polydimethylsiloxane surfaces under non-contaminant atmosphere, Sensors Actuators A Phys. 197 (2013) 25–29.

https://doi.org/10.1016/J.SNA.2013.04.003.

[310] H.T. Kim, O.C. Jeong, PDMS surface modification using atmospheric pressure plasma, Microelectron. Eng. 88 (2011) 2281–2285. https://doi.org/10.1016/J.MEE.2011.02.084.

[311] D. Bodas, C. Khan-Malek, Hydrophilization and hydrophobic recovery of PDMS by oxygen plasma and chemical treatment—An SEM investigation, Sensors Actuators B Chem. 123 (2007) 368–373. https://doi.org/10.1016/J.SNB.2006.08.037.

[312] H. Hillborg, M. Sandelin, U.W. Gedde, Hydrophobic recovery of polydimethylsiloxane after exposure to partial discharges as a function of crosslink density, Polymer (Guildf). 42 (2001) 7349–7362. https://doi.org/10.1016/S0032-3861(01)00202-6.

[313] V.N. Phan, N.T. Nguyen, C. Yang, P. Joseph, L. Djeghlaf, D. Bourrier, A.M. Gue, Capillary Filling in Closed End Nanochannels, Langmuir. 26 (2010) 13251–13255. https://doi.org/10.1021/LA1010902.

[314] M. Radiom, • W K Chan, • C Yang, Á.W.K. Chan, Á.C. Yang, Capillary filling with the effect of pneumatic pressure of trapped air, 9 (2010) 65–75. https://doi.org/10.1007/s10404-009-0527-1.

[315] W. Wagner, H.-J. Kretzschmar, International Steam Tables, Int. Steam Tables. (2008). https://doi.org/10.1007/978-3-540-74234-0.

[316] E. Castillo-Orozco, A. Davanlou, P.K. Choudhury, R. Kumar, Droplet impact on deep liquid pools: Rayleigh jet to formation of secondary droplets, Phys. Rev. E - Stat. Nonlinear, Soft Matter Phys. 92 (2015) 053022. https://doi.org/10.1103/PHYSREVE.92.053022/FIGURES/14/MEDIUM.

[317] P.W. RAND, E. LACOMBE, H.E. HUNT, W.H. AUSTIN, Viscosity of normal human blood under normothermic and hypothermic conditions, Https://Doi.Org/10.1152/Jappl.1964.19.1.117. 19 (1964) 117–122. https://doi.org/10.1152/JAPPL.1964.19.1.117.

[318] Y.H. Yeong, J. Burton, E. Loth, I.S. Bayer, Drop impact and rebound dynamics on an inclined superhydrophobic surface, Langmuir. 30 (2014) 12027–12038. https://doi.org/10.1021/LA502500Z.

[319] W.Y. Chen, J.A.C. John, C.H. Lin, C.Y. Chang, Molecular Cloning and Developmental Expression of Zinc Finger Transcription Factor MTF-1 Gene in Zebrafish, Danio rerio, Biochem. Biophys. Res. Commun. 291 (2002) 798–805. https://doi.org/10.1006/BBRC.2002.6517.

[320] Q. Tan, L. Brunetti, M.W.C. Rousseaux, H.-C. Lu, Y.-W. Wan, J.-P. Revelli, Z. Liu, M.A. Goodell, H.Y. Zoghbi, Loss of Capicua alters early T cell development and predisposes mice to T cell lymphoblastic leukemia/lymphoma, Proc. Natl. Acad. Sci. 115 (2018) E1511--E1519. https://doi.org/10.1073/pnas.1716452115.

[321] W. Driever, C. Nüsslein-Volhard, The bicoid protein determines position in the Drosophila embryo in a concentration-dependent manner, Cell. 54 (1988) 95–104. https://doi.org/https://doi.org/10.1016/0092-8674(88)90183-3.

[322] A. Zabihihesari, S. Parand, A.B. Coulthard, A. Molnar, A.J. Hilliker, P. Rezai, An In-Vivo Microfluidic Assay Reveals Cardiac Toxicity of Heavy Metals and the Protective Effect of Metal Responsive Transcription Factor (Mtf-1) in Drosophila Model, SSRN Electron. J. (2022). https://doi.org/10.2139/SSRN.4028275.